SISSA

Scuola
Internazionale
Superiore di
Studi Avanzati

PHYSICS AREA – PhD COURSE IN ASTROPARTICLE PHYSICS

DOCTORAL THESIS

Beyond General Relativity: Modified Theories and Non-Singular Black Holes

CANDIDATE:

Francesco Di Filippo

ADVISOR:

Prof. Stefano Liberati

ACADEMIC YEAR 2019 – 2020

ii

Abstract

Einstein's general relativity is an extremely elegant and successful theory. Recent observations coming from the LIGO/VIRGO collaboration as well as from the Event Horizon Telescope give us the possibility to perform precision test of general relativity in regimes never tested before. Even though all the current observations are in perfect agreement with the predictions of general relativity, there are several reasons to study extensions of the theory.

From the experimental point of view, we are forced to include a dark sector for the matter and energy content of the universe to explain the cosmological data. Whereas from a conceptual point of view, the theory is not perturbatively renormalizable, and it predicts the formation of spacetime singularities.

This thesis studies possible modifications of general relativity both considering specific theories of modified gravity and implementing a model independent approach.

In the first part of the thesis, we study a specific class of modified theory of gravity which has the peculiarity of propagating the same number of degrees of freedom of general relativity. The existence of these theories apparently challenges the distinctive role of general relativity as the unique non-linear theory of massless spin-2 particles. However, we provide strong evidence that these theory are actually equivalent to general relativity in vacuum.

In the second part of the thesis, we focus on the problem of black hole singularities which are unavoidably present in general relativity. However, it is reasonable to assume that there will be a mechanism preventing their formation in a full theory of quantum gravity. Without specifying any theory of quantum gravity or the nature of such mechanism, simply assuming a minimal set of kinematical constraints, we classify and study the properties of non-singular spacetime with a trapping horizon. Contrary to what one might expect, the set of regular geometries that arises is remarkably limited. Furthermore we show that it is very difficult to construct a self consistent geometry without any long range effect. This give us further motivation to study the phenomenology of non-singular black holes. To this end, we provide a set of parameters describing the deviations from classical black holes, and we review the possible observational channels that can measure or constrain them.

Contents

Publication list

This thesis is based on the following list of publications.

P1 R. Carballo Rubio, F. Di Filippo, S. Liberati.
Minimally modified theories of gravity: a playground for testing the uniqueness of general relativity.
JCAP **06** (2018), 026, (2018), arXiv:1802.02537.

P2 R. Carballo Rubio, F. Di Filippo, S. Liberati, C. Pacilio, M. Visser.
On the viability of regular black holes.
JHEP **07** (2018), 023, arXiv:1805.02675.

P3 R. Carballo Rubio, F. Di Filippo, S. Liberati, M. Visser.
Phenomenological aspects of black holes beyond general relativity.
Phys. Rev. D **98** (2018) no.12, 124009, arXiv:1809.08238.

P4 R. Carballo Rubio, F. Di Filippo, N. Moynihan.
Taming higher-derivative interactions and bootstrapping gravity with soft theorems.
JCAP **10** (2019), 030, arXiv:1811.08192.

P5 R. Carballo Rubio, F. Di Filippo, S. Liberati, M. Visser.
Opening the Pandora's box at the core of black holes.
Class. Quant. Grav. **37** (2020) no.14, 145005, arXiv:1908.03261.

P6 R. Carballo Rubio, F. Di Filippo, S. Liberati, M. Visser.
Geodesically complete black holes.
Phys. Rev. D **101** (2020), 084047, arXiv:1911.11200.

P7 R. Carballo Rubio, F. Di Filippo, S. Liberati, M. Visser.
Causal hierarchy in modified gravity.
Preprint, arXiv:2005.08533.

Introduction

General relativity represents a very elegant theory from a conceptual point of view and a very successful one from the experimental side. Thanks to the recent observations coming from the LIGO/VIRGO collaboration [1, 2, 3, 4, 5, 6] as well as from the Event Horizon Telescope [7, 8, 9, 10, 11, 12], we have the possibility to perform precision test of general relativity in regimes never tested before. Remarkably, the outcomes of all these observations are in perfect agreement with the prediction of general relativity.

Regardless of the phenomenological success, there are good reasons to study modifications of the theory. From an experimental point of view, cosmological data cannot be explained within general relativity only with the matter and the energy that we observe. The most simple explanation is given by the ΛCDM model where one adds two addiional "dark" cosmological fluids: a pressurless dust and a cosmological constant, avoiding any modification of the gravitational interaction. Nonetheless, it is also possible to explain the cosmological data without introducing dark matter and dark energy, but by modifying general relativity. This possibility is reinforced by the fact the ΛCDM is not free from problems. For instance, there is a naturalness problem for the value of the cosmological constant which is very different from the one which can be naively estimated [13] and different measurements of the Hubble constant at different redshifts lead to values in tension with each other [14].

Even stronger reasons to modify general relativity come from theoretical arguments. General relativity predicts the formations of spacetime singularities. In 1939 Oppenheimer and Snyder studied the gravitational collapse of a spherically symmetric ball of pressureless dust [15], obtaining that the endpoint of the collapse is a singular black hole. However, it was widely believed that the formation of the singularity was simply due to the highly idealized scenario and that a realistic collapse would not end up with the formation of a black hole. In fact, something similar happens in Newtonian gravity, where a spherically symmetric collapse produces a region of infinite density , but an arbitrary small amount of angular momentum will prevent the formation of such a region. While preliminary results appeared to confirm this possible resolution of singularities [16], Penrose's 1965 singularity theorem [17] proved them as the natural end points of general relativity. This theorem states that if a trapped region is formed, the spacetime cannot be geodesically complete, implying that there must exist at least one geodesic ending in a Cauchy horizon or in a singularity. If we assume that the spacetime is globally hyperbolic, there cannot be any Cauchy horizon, and thus a singularity has

to form. Subsequent results extended the theorem to cosmological scenarios [18] and got rid of the global hyperbolicity assumption [19] showing that in general relativity singularities are going to be unavoidably present both as an endpoint in gravitational collapse and in cosmology.

A possible approach to accept the presence of singularities in general relativity, is to assume that while the theory will unavoidably produce them, it will also always hide them as well. The precise mathematical formulation of this concept is given by the cosmic censorship conjecture [20]. There are two main non equivalent formulations of the conjecture that go by the names of the weak and strong cosmic censorship conjecture[1].

The *weak cosmic conjecture* states that all singularities are shielded behind an event horizon. This condition ensures that observers far from the black hole have a well defined evolution within general relativity, and they are not influenced by singularities.

The *strong cosmic censorship conjecture* states that the maximally Cauchy development of the initial data is inextendible, meaning that if there are incomplete geodesics, they have to end up in a singularity and they cannot be extended beyond it.

It is easy to consider exact solutions in general relativity that are counterexamples to both the weak and the strong versions of the cosmic censorship, so the correct way to formulate these conjectures is to state that under generic initial conditions it is impossible to end up with any of the aforementioned solutions and spacetime evolves in a way to satisfy the conjectures.

Both versions of the censorship conjecture aim to ensure that the black hole singularities do not spoil the well-posedness of the initial value problem for observers that do not fall into the black hole. However, it is undeniable that the presence itself of a singularity is abhorrent from a physical point of view as we expect that the ultimate theory has to remain predictive for every observer, not just those outside a black hole. Therefore, it seems that some extension of general relativity is required for predicting the fate of observers that within black holes.

Finally, the last reasons we want to mention that tells us that general relativity cannot be the ultimate theory of gravity comes from the fact that when we express the general relativity in the standard quantum field theory formalism, the resulting quantum gravity theory is not perturbatively renormalizable [21, 22, 23]. It is often stated that this implies that the theory cannot be predictive in the UV as loops correction will introduce an infinite number of divergences that require an infinite number of free parameters to be tamed. This conclusion is a bit rushed, as it is, in principle, still possible to have a predictive theory in UV if all the coupling constants flow in a fixed point making the theory asymptotically safe and non-perturbatively renormalizable [24] (see also [25] for a recent overview). However, there is still no evidence that this is the case, and at the very least, we can conclude that a lot of work has to be done to understand the behavior of gravity at high energy.

All these problems may have a common solution. A full theory of quantum gravity will definitely become relevant in the final stages of gravitational collapse, and it is standard lore to believe that quantum gravity effects will prevent the formation of the singularity. Furthermore, it is possible that the quantum gravity theory will have an

---

[1]Note that, despite the name, the strong cosmic conjecture is not mathematically stronger as it does not imply the weak cosmic conjecture.

effective field theory description in the low energy limit that can have some difference from general relativity in cosmological scenario and that could, hopefully, explain the cosmological data without the introduction of the dark sector, hence resolving the issues associated with it.

Having established that there are good reasons to modify general relativity, we need to understand how to do that. The conceptually simplest way to proceed would be to pick a candidate for a quantum theory of gravity and study its predictions to understand if it is able to address the problems of general relativity. However, such an approach can be very difficult in practice.

In this thesis we are going to focus on two complementary approaches to look for deviation from general relativity. We are first going to consider a specific class of modified theory of gravity, and, after that, the thesis will focus on an agnostic approach directly tackling one of the open problems of general relativity, *i.e.,* the singularity problem.

Specific modified theory approach

In order to consider a modified theory of gravity, we face the problem that there are many different ways to modify general relativity and we need a guiding principle to choose which type of modification we want to consider. General relativity possesses a number of properties that make it unique, and we need to decide which of these properties we want to relax and which ones we want to keep. In four dimensions, Lovelock's theorem [26] singles out general relativity as the only diffeomorfism invariant theory that propagates only two degrees of freedom. Recent attempts to evade the conclusions of the theorem [27] turned out to be unsuccessful (see, *e.g.* [28]).

In chapter 1, we are going to study a class of theories that relax the assumption of invariance under the diffeomrfism group, but that keeps unchanged the number of degrees of freedom. We will provide strong evidence that, in vacuum, these theories are actually general relativity written terms of non standard variables. However, coupling with matter can break the equivalence.

Agnostic approach

The rest of the thesis focuses on the problem of black hole singularities. It would be an interesting line of investigation to understand whether the minimally modified theories that we have studied could resolve some of the issues with the black hole singularities. In fact, the equivalence of the theories in vacuum tells us that the singular black solution of general relativity will also be present in the minimally modified theory. However, the difference in the matter sector may change the dynamics of a gravitational collapse and could, in principle, avoid the consequences of Penrose's theorem and avoid the formation of the singularities.

While this analysis would definitely be very interesting, the results would be specific to a given theory and a given matter coupling. Therefore without a strong motivation to single out one specif modified gravity theory, in the rest of the thesis, we have addressed the problem of hole singularities in a model independent way, which allows us to obtain less stringent but much more generic results. To set the stage, in chapter 2, we study

what type of requirement we have to impose to the spacetime in order to have a well defined notion of causality in a generic modified theory of gravity.

With the knowledge we have acquired, simply giving a minimal set of assumptions without specifying any particular theory, in chapter 3, we provide a classification of non-singular spacetime with a trapping horizon. To this end, we study the properties of four classes of geometry and, using Penrose singularity theorem as a guidance, we prove that the most generic non-singular spacetime is given by a combination of these four classes. The analysis is carried in spherical symmetry, but the language we use is well suited to address less symmetric configuration. In fact, most of the results can be trivially extended to a more realistic scenario.

The classification is performed on purely geometrical grounds. While from the mathematical point of view all the geometries are perfectly fine, in chapter 4, we study the viability of these geometries as solutions to the singularity problem once that some physically motivated ingredients are added. Such ingredients include the presence of perturbations and the compatibility with semiclassical physics. We show that there is no safe option, meaning that the classes of geometries that can very closely mimic a black hole are plagued by self consistency issues, and it is not easy to make them viable.

This gives us a strong motivation to study the possible phenomenological signature. In chapter 5, we discuss the possible phenomenological channels to detect or constrain deviations from classical black holes. We also provide a set of phenomenological parameters to systematically parametrize the room that is still available for black holes alternatives.

Appendices

The appendices contain information that is propaedeutic for the discussion in the various chapters of the thesis. App. A contains the proof that the minimally modified theory of gravity discussed in chapter 1 recover the Poincaré group in the linear limit of the theory. App. B contains a brief review of the most important aspects of the spinor helicity formalism. App. C contains the proof of some conditions for the absence of curvature singularity that have been used in chapter 3. Finally, App. D contains some interesting properties of the regular black hole geometries that we have considered in different stages throughout the thesis.

Chapter 1

Minimally modified theories of gravity

General relativity posses a number of properties that make it a very simple and elegant theory. To study a specific modification of general relativity, we have to decide which properties of the theory we want to keep and which ones we want to relax. In this chapter, we are going to study a class of theories introduced in [29] where the guiding principle is to keep unchanged the number of degrees of freedom propagating in the gravitational sector.

This is not a trivial task as, in four dimensions, Lovelock theorem singles out general relativity as the only diffeomorphism invariant gravitational theory that propagates only two degrees of freedom.

These theories avoid the conclusion of Lovelock theorem by relaxing the assumption of invariance under the full diffeomorphism group. The basic fields that are used in order to construct these theories are the 3-dimensional metric h_{ij}, the lapse N and the shift N^i. While this corresponds to the familiar ADM decomposition in general relativity, in which the spacetime metric reads

$$\mathrm{d}s^2 = -N^2\mathrm{d}t^2 + h_{ij}(\mathrm{d}x^i + N^i\mathrm{d}t)(\mathrm{d}x^j + N^j\mathrm{d}t), \tag{1.1}$$

in [29] the action is modified and it is given by

$$S = \int \mathrm{d}t\,\mathrm{d}^3x\sqrt{h}NF(K_{ij}, R_{ij}, \nabla_i, h_{ij}, t) \tag{1.2}$$

where $K_{ij} = (\partial_t h_{ij} - \nabla_i N_j - \nabla_j N_i)/(2N)$ and R_{ij} are the extrinsic curvature and the Ricci tensor of the constant-t hypersurfaces, respectively, and ∇_i is the covariant derivative compatible with the induced metric h_{ij}. In this class of theories the authors study which conditions have to be satisfied by the function F for the theory to propagates only two degrees of freedom.

A central question is whether or not these theories are equivalent to general relativity. It is possible that, in spite of being apparently different, these are however, physically equivalent (but are expressed in terms of a non-standard choice of variables). As we will see, clarifying this point has its subtleties due to the non-linear nature of general relativity. Before starting our analysis, let us explain what we mean with equivalence of theories and why we believe that it is worth analyzing this problem. In

order to do so, the starting point is the action of general relativity written in the ADM decomposition

$$S = \int dt\, d^3x \sqrt{h} N \left(R + K_{ij}K^{ij} - K^2 \right). \tag{1.3}$$

Now we can perform a field redefinition to obtain a theory which is off-shell different from general relativity as the action, and the guage groups are different, but which is completely equivalent to general relativity on-shell. Provided that the field redefinition is linear in the lapse, we would obtain an action of the form of Eq. (1.2) which will, therefore, belong to the class of theories with two degrees of freedom identified in [29]. It is therefore crucial to understand if some of the theories found are genuinely new theories.

Of course, one possible way to establish the equivalence of these theories would be to find a field redefinition that maps them back to general relativity. In practice, this is a very difficult task, so we are going to follow a different approach. We are going to compare on-shell tree level scattering amplitudes of graviton with the value they assume in general relativity. The chapter is mainly based on reference **P1**, and it is organized as follows. In Sec. 1.1, starting directly with the Hamiltonian picture, we will discuss the non-linear algebra of constraints as well as their linearization (focusing on the recovery of the Poincaré group in the linear limit) of a certain set of theories that includes some of the particular examples given in [29]. Then, in Sec. 1.2, we will connect the results obtained in the Hamiltonian perspective with the analysis of the Lagrangian formulation of a broad set of theories, illustrating that theories that recover the Poincaré group in the linear limit describe gravitons (massless spin-2 particles) in this limit. This observation, and the fact that the 3-point amplitudes of gravitons in these examples are the same as in general relativity (as shown in detail), represent a strong hint that these theories are classically equivalent to general relativity. This conclusion is strengthened with the analysis of n-point amplitudes for $n \geq 4$, using on-shell techniques. In Sec. 1.4 we consider, as a counterpoint, two examples of theories that are not equivalent to general relativity: in one of them the algebra of constraints does not reproduce the Poincaré algebra in the linear limit and, in the other one, gravitons display modified dispersion relations (and additional degrees of freedom can arise due to radiative corrections). The last part of this chapter, Sec. 1.5, deals with additional issues that come up when couplings to matter are introduced.

1.1   A class of Hamiltonian theories

As a way to illustrate in a simpler way the main result in [29], and make the present discussion self-consistent, let us consider a class of Hamiltonian theories that are in principle structurally different from general relativity, but that still contain two local degrees of freedom. While not encompassing all the possible theories found in [29], this is however a large enough set to represent a convenient framework for our discussion (let us note that, in particular, it includes general relativity as a particular case).

The class of theories we introduce in this section are constructed from the variables $\{N, N^i, h_{ij}\}$ and their conjugated momenta $\{\pi_N, \pi_i, \pi^{ij}\}$, and are defined by the

Hamiltonian

$$H = \int d^3x \left(N\mathcal{H} + N^i \mathcal{D}_i + \lambda_N \pi_N + \lambda^i \pi_i \right), \tag{1.4}$$

where

$$\mathcal{H} = \sqrt{h}\, F(R + \lambda \Pi/h), \qquad \mathcal{D}_i = -2\nabla_j \pi^j_{\ i}. \tag{1.5}$$

Here $\Pi = \pi_{ij}\pi^{ij} - \pi^2/2$ (where $\pi = \pi^{ij}h_{ij}$).

General relativity corresponds to the choice of the function $F(x) = x$ and $\lambda = 1$, namely $\mathcal{H} = \sqrt{h}R + \Pi/\sqrt{h}$. For general relativity, we can easily identify the familiar expressions that appear in the so-called Hamiltonian and diffeomorphism constraints.

In all these theories, λ_N and λ^i are Lagrange multipliers that enforce the primary constraints

$$\pi_N = 0, \qquad \pi_i = 0, \tag{1.6}$$

which in turn induce the secondary constraints

$$\mathcal{H} = 0, \qquad \mathcal{D}_i = 0. \tag{1.7}$$

In the particular case of general relativity, the latter correspond to the Hamiltonian and diffeomorphism constraints, respectively. We will keep using this nomenclature for any theory with total Hamiltonian given by Eq. (1.4).

As in general relativity, a great deal of information is encoded in the off-shell algebra of Poisson brackets of these constraints. Following the usual practice, let us define the smeared constraints

$$\mathcal{H}[\alpha] = \int \mathrm{d}^3x\, \alpha\mathcal{H}, \qquad \mathcal{D}[\alpha^i] = \int \mathrm{d}^3x\, \alpha^i \mathcal{D}_i. \tag{1.8}$$

Where α and α^i are arbitrary functions.
From an explicit computation, it follows that

$$\begin{aligned}
\{\mathcal{H}[\alpha], \mathcal{H}[\beta]\} &= \mathcal{D}\left[\lambda F'(R + \lambda\Pi/h)^2 h^{ij} \left(\beta\partial_j\alpha - \alpha\partial_j\beta\right)\right], \\
\{\mathcal{D}[\alpha^i], \mathcal{H}[\alpha]\} &= \mathcal{H}\left[\mathcal{L}_{\alpha^i}\alpha\right], \\
\{\mathcal{D}[\alpha^i], \mathcal{D}[\beta^j]\} &= \mathcal{D}\left[\mathcal{L}_{\alpha^i}\beta^j\right].
\end{aligned} \tag{1.9}$$

Note that $F'(x)$ denotes the derivative of $F(x)$ with respect to its single argument x. Several observations can be made:

- The algebra is closed and all the constraints are first class, which leaves $(20 - 2 \times 8)/2 = 2$ degrees of freedom. In other words, all these theories satisfy the conditions discussed in [29].

- The algebra obtained is a slight modification of the usual Dirac algebra of general relativity [30]. In particular, the only difference appears in the bracket between Hamiltonian constraints, where the structure function inside the Hamiltonian constraint is different; let us recall that for general relativity one has $\lambda F'(R + \lambda\Pi/h)^2 = 1$. Let us mention that similar modifications have been observed to occur in loop quantum gravity [31, 32, 33, 34, 35, 36], which makes part of our discussion below of possible interest for these studies (note that, however, signature change [37, 38] is not structurally allowed in the theories we are considering in this section).

In summary, we have a large class of theories that contain two degrees of freedom, the same as general relativity, but which seem to be structurally different from the latter theory. In particular, the off-shell algebra is different from the usual Dirac algebra. One may jump to the conclusion that these theories are different from general relativity. But is this true?

Before diving into this question, let us make a remark that will be important later: the value of λ can be changed arbitrarily by a positive multiplicative factor. This can be noticed by considering the field redefinition

$$\pi^{ij} \to \kappa\pi^{ij}, \qquad\qquad N^i \to N^i/\kappa, \qquad\qquad (1.10)$$

with $\kappa \in \mathbb{R}$ a constant. It is straightforward to check that the combination $N^i\mathcal{D}_i$ is invariant under this rescaling, so that diffeomorphism constrain is unchanged, but that the Hamiltonian constraint becomes

$$\mathcal{H} = \sqrt{h}\, F\left(R + \lambda k^2 \Pi/h\right) = \sqrt{h}\, F\left(R + \lambda'\Pi/h\right), \qquad\qquad (1.11)$$

with $\lambda' = \lambda\kappa^2$. Hence, it is possible to change the absolute value of $|\lambda|$ arbitrarily; note however that its sign cannot be modified by this redefinition. So, being always possible to set $\lambda = \pm 1$, it is $F(x) \neq x$ the real difference with general relativity.

1.1.1   Poincaré algebra

As a first partial answer to the question asked at the end of the previous section, we now show that in the flat spacetime limit, the Poincaré algebra is recovered in all these theories. As it is mentioned, for instance, in [33, 34, 39], the Poincaré algebra can be obtained as a subalgebra of the off-shell algebra of constraints (1.9) by considering the Minkowski spacetime (i.e., $N = 1$, $N^i = 0$ and $h_{ij} = \delta_{ij}$) and looking to the transformations generated by the Hamiltonian and momentum constraints associated with the linear functions

$$\alpha = \delta\mu^0 + x_i\delta\omega^{i0}, \qquad\qquad \alpha^i = \delta\mu^i + x_j\delta\omega^{ji}. \qquad\qquad (1.12)$$

Restricting to Minkowski spacetime, the algebra of constraints (1.9) reads

$$\begin{aligned}
\{\mathcal{H}[\alpha], \mathcal{H}[\beta]\} &= \mathcal{D}\left[\lambda F'(0)^2\delta^{ij}\left(\beta\partial_j\alpha - \alpha\partial_j\beta\right)\right], \\
\left\{\mathcal{D}[\alpha^i], \mathcal{H}[\alpha]\right\} &= \mathcal{H}\left[\mathcal{L}_{\alpha^i}\alpha\right], \\
\left\{\mathcal{D}[\alpha^i], \mathcal{D}[\beta^j]\right\} &= \mathcal{D}\left[\mathcal{L}_{\alpha^i}\beta^j\right].
\end{aligned} \qquad\qquad (1.13)$$

We can now exploit the observation, made at the end of the previous section, that the absolute value of λ can be changed arbitrarily in order to write the algebra [assuming $F'(0) \neq 0$] in the form

$$\begin{aligned}
\{\mathcal{H}[\alpha], \mathcal{H}[\beta]\} &= \mathcal{D}\left[\theta\delta^{ij}\left(\beta\partial_j\alpha - \alpha\partial_j\beta\right)\right], \\
\left\{\mathcal{D}[\alpha^i], \mathcal{H}[\alpha]\right\} &= \mathcal{H}\left[\mathcal{L}_{\alpha^i}\alpha\right], \\
\left\{\mathcal{D}[\alpha^i], \mathcal{D}[\beta^j]\right\} &= \mathcal{D}\left[\mathcal{L}_{\alpha^i}\beta^j\right],
\end{aligned} \qquad\qquad (1.14)$$

where $\theta = \pm 1$. The value $\theta = 1$ corresponds to general relativity, while $\theta = -1$ to Euclidean general relativity (see, e.g., [40] and references therein). These expression

of the algebra reduces to the Poincaré algebra once we restrict the functions α, α^i, β and β^i to be of the form of Eq. (1.12) (for completeness, this is shown in App. A). This implies that all these theories contain either the Poincaré algebra or its Euclidean counterpart.

1.2 A class of Lagrangian theories

In the previous sections we have worked with a class of Hamiltonian theories that display an arbitrary function $F(x)$ of a particular combination of the variables in the phase space, but that still contain the same number of degrees of freedom as general relativity. We have illustrated that for all these theories [satisfying a non-degeneracy condition $F'(0) \neq 0$], the Poincaré algebra is recovered in a suitable (standard) limit of the non-linear algebra of constraints. This is a first indication that even if these theories may seem different from general relativity, this may be an artifact of the way in which these are constructed, and at the end of the day these may turn out to be physically equivalent to the latter.

A clear possibility is that these theories could be obtained from the usual Hamiltonian formulation of general relativity by means of a non-linear field redefinition. However, this is fairly difficult to show in general, unless one is able to find by inspection the particular field redefinition that does the job (which, in any case, would not be a systematic approach). Hence, a different strategy is needed in order to learn more about these theories and their relation to general relativity. In particular, in this section we pick up a specific theory among the Hamiltonian theories previously studied, and switch to its Lagrangian formulation in order to illustrate a number of important features. The subsequent discussion is not limited to this particular theory but applies to a large class of Lagrangian theories, as detailed in Sec. 1.2.4. However, we will use this particular example in order to motivate the different steps in the analysis. This class of Lagrangian theories is not necessarily in one-to-one correspondence with the class of Hamiltonian theories discussed in Sec. 1.1, although we expect that the results below will be shared by all these Hamiltonian theories, as we have shown that the Poincaré algebra is recovered in all of them.

For a generic function $F(x)$, it is not easy to find the corresponding Lagrangian. However, one of the Lagrangian examples given in [29] leads precisely to a Hamiltonian of the form given in Eq. (1.4). These authors call this theory "square root gravity", which is defined by the Lagrangian density

$$\mathcal{L} = \sqrt{h} N \left(M^4 \sqrt{(c_1 + c_2 \mathcal{K})(c_3 + c_4 R)} - c_5 \right). \tag{1.15}$$

Here, M and $\{c_n\}_{n=1}^5$ are real constants with the appropriate dimensions, and $\mathcal{K} = K_{ij}K^{ij} - K^2$. It is worth mentioning that in the $c_1 = c_3 = c_5 = 0$ case, the Baierlein-Sharp-Wheeler action [41] is recovered (see also [42]).

The associated Hamiltonian is

$$\mathcal{H} = \sqrt{h} \left(-M^4 \sqrt{c_1 c_4} \sqrt{R - \frac{4}{c_2 c_4} \frac{\Pi}{h} + \frac{c_3}{c_4}} + c_5 \right). \tag{1.16}$$

It is therefore clear that this theory belongs to the class introduced in Sec. 1.1, with $F(x) = -M^4\sqrt{c_1 c_4}\sqrt{x + c_3/c_4} + c_5$ and $\lambda = -4/c_2 c_4$. In particular, from our discussion above it follows that: (i) this theory contains two degrees of freedom (as discussed as well in [29]), and (ii) if the constants are chosen such that Minkowski spacetime is a solution, these two degrees of freedom in h_{ij} carry a representation of the Poincaré group. These two features (satisfied by all the Hamiltonian theories introduced before) suggest strongly that these two degrees of freedom must correspond to the usual two polarizations of the gravitational field in linearized general relativity. Let us show this explicitly in the following.

1.2.1　Linearized field equations

Before linearizing the field equations, let us remark that not all the constants in Eq. (1.15) are independent. If we consider a constant rescaling of the lapse,

$$N \longrightarrow \zeta N, \tag{1.17}$$

with $\zeta \in \mathbb{R}^+$, then Eq. (1.15) becomes

$$\mathcal{L} = \zeta\sqrt{h}N\left(M^4\sqrt{(c_1 + c_2\mathcal{K}/\zeta^2)(c_3 + c_4 R)} - c_5\right). \tag{1.18}$$

This Lagrangian is real when evaluated on a Minkowski spacetime if and only if $c_1 c_3 > 0$. Moreover, it is always possible to choose $\zeta^2 = |c_2 c_3/c_1 c_4|$ and rescale M^4 and c_5 accordingly so that (1.18) becomes

$$\mathcal{L} = \sqrt{h}N\left(M^4\sqrt{(1 + \theta c_4\mathcal{K}/c_3)(1 + c_4 R/c_3)} - c_5\right), \tag{1.19}$$

with $\theta = \pm 1$. Hence, we see that the coefficients in front of $\mathcal{K}$ and R inside the square root can be chosen to be the same, up to a sign; this sign is related to the Euclidean or Lorentzian character of the theory, so we will choose in the following $\theta = 1$ which corresponds to the Lorentzian sector.

Let us consider an expansion of the Lagrangian (1.19) such that $N \longrightarrow 1 + N$ and $h_{ij} \longrightarrow \delta_{ij} + h_{ij}$; alternatively,

$$g_{\mu\nu} = \eta_{\mu\nu} + h_{\mu\nu}, \tag{1.20}$$

where $h_{00} = N$ and $h_{0i} = \delta_{ij}N^j$. In practice, we can arrange the different orders in $h_{\mu\nu}$ in terms of the different orders in $\sqrt{h}N$ and the curvature scalars $\mathcal{K}$ and R. Let us choose c_5 requiring that there is no term proportional to $\sqrt{h}N$ only, namely $c_5 = M^4$ (otherwise we would have to consider a non-zero cosmological constant, which however does not change the physical results).

Renaming $c = c_4/c_3$ and taking into account that $\mathcal{K}$ is at least of second order in $h_{\mu\nu}$, while R is of first order, Eq. (1.19) can be expanded as

$$\mathcal{L} = cM^4\sqrt{-g}\left\{(\mathcal{K} + R) - \frac{c}{4}R^2\right\} + \dots \tag{1.21}$$

where the dots indicate higher orders in $h_{\mu\nu}$ (that is, cubic and higher-order terms, which will be dealt with in Secs. 1.2.3 and 1.3, respectively).

The combination $\mathcal{K} + R$ can be recognized as the 4-dimensional Ricci scalar (up to a boundary term); hence this part of the Lagrangian leads to the Fierz-Pauli Lagrangian $\mathcal{L}_{\text{FP}}$ at lowest order in $h_{\mu\nu}$. For the quadratic term in R, we just need to recall (e.g., [43]) that $R^{(0)} = 0$ and $R^{(1)} = \partial_i \partial_j h^{ij} - \partial_i \partial^i h^j_j$, so that (the overall multiplicative constant is irrelevant)

$$\frac{1}{cM^4}\mathcal{L} = \mathcal{L}_{\text{FP}} - \frac{c}{4}(\partial_i \partial_j h^{ij} - \partial_i \partial^i h^j_j)^2. \tag{1.22}$$

This action is invariant under the linear diffeomorphisms characteristic of Fierz-Pauli theory,

$$h_{\mu\nu} \to h_{\mu\nu} + \partial_{(\mu}\xi_{\nu)}. \tag{1.23}$$

On the other hand, the equations of motion are given by

$$\Box h_{\mu\nu} - \partial_\mu \partial^\rho h_{\rho\nu} - \partial_\nu \partial^\rho h_{\rho\mu} + \eta_{\mu\nu}\partial_\rho \partial_\sigma h^{\rho\sigma} - \eta_{\mu\nu}\Box h + \partial_\mu \partial_\nu h$$
$$- c\left(\partial_i \partial_j \partial_k \partial_l h^{kl} - \partial_i \partial_j \Delta \tilde{h} - \delta_{ij}\partial_k \partial_l \Delta h^{kl} + \delta_{ij}\Delta^2 \tilde{h}\right)\delta^i_\mu \delta^j_\nu = 0. \tag{1.24}$$

In this equation, we have defined $\Box = \partial_\mu \partial^\mu$, $\Delta = \partial_i \partial^i$, and $\tilde{h} = h^j_j$. In particular, the $\mu = \nu = 0$ component of the field equations is the same as in Fierz-Pauli theory, and takes the form

$$\Box h_{00} + 2(\partial_0)^2 h_{00} + 2\partial_0 \partial^i h_{i0} + (\partial_0)^2 h_{00} - 2\partial_0 \partial^i h_{i0} - \partial_i \partial_j h^{ij} + \Box h + (\partial_0)^2 h = 0, \tag{1.25}$$

which can be arranged simply as

$$\Delta \tilde{h} - \partial_i \partial_j h^{ij} = 0. \tag{1.26}$$

This equation implies, as in Fierz-Pauli theory, that in the absence of matter it is possible to choose the so-called transverse and traceless gauge (e.g., [44]). Using the spatial diffeomorphisms, it is possible to choose a gauge in which $\partial_j h^{ij} = 0$, but then Eq. (1.26) reduces to $\Delta \tilde{h} = 0$, which is the necessary and sufficient condition that allows the residual gauge transformations to gauge away the spatial trace $\tilde{h}$. Alternatively, the linearized field equations (1.24) reduce to the Fierz-Pauli equations; to show this it is not even necessary to pick up a specific gauge, but rather to realize that Eq. (1.26) directly implies that the term proportional to c in Eq. (1.24) vanishes, so that Eq. (1.24) is written as

$$\mathcal{O}^{\mu\nu,\alpha\beta}h_{\alpha\beta} = 0, \tag{1.27}$$

where

$$\mathcal{O}^{\mu\nu,\alpha\beta} = \eta^{\mu(\alpha}\eta^{\beta)\nu}\Box - \eta^{\nu(\alpha}\partial^{\beta)}\partial^\mu - \eta^{\mu(\alpha}\partial^{\beta)}\partial^\nu + \eta^{\mu\nu}\partial^\alpha \partial^\beta - \eta^{\mu\nu}\eta^{\alpha\beta}\Box - \eta^{\alpha\beta}\partial^\mu \partial^\nu. \tag{1.28}$$

In summary, we have shown that the two degrees of freedom described by the theory with Lagrangian (1.15) correspond, in the linear limit, to the two usual polarizations of gravitons. This result is not accidental, as we knew in advance that linearizing the algebra of constraints of this theory leads to the Poincaré group. That the tensor field h_{ij} transforms in the usual way under Poincaré transformations, combined with the fact that it encodes only two degrees of freedom, does not leave much wiggle room (the discussion above is not needed in order to realize this, but it is a nice explicit illustration of this general assertion).

1.2.2 Propagator

Aside from the on-shell properties of the linearized field equations, the form of the propagator will be important in order to analyze the non-linear interactions. The propagator is an off-shell quantity, and therefore may show differences without necessarily implying the existence of physical differences. Let us start by writing the field equations (1.24) in momentum space, and in the form of Eq. (1.27); i.e., in terms of the operator

$$
\begin{aligned}
& \mathcal{O}^{\mu\nu,\alpha\beta} + c\delta_i^\mu \delta_j^\nu \delta_k^\alpha \delta_l^\beta \left(p^i p^j p^k p^l - \boldsymbol{p}^2 p^i p^j \delta^{kl} - \boldsymbol{p}^2 p^k p^l \delta^{ij} + \boldsymbol{p}^4 \delta^{ij}\delta^{kl} \right) \\
& = \mathcal{O}^{\mu\nu,\alpha\beta} + c\delta_i^\mu \delta_j^\nu \delta_k^\alpha \delta_l^\beta \left(p^i p^j - \boldsymbol{p}^2 \delta^{ij} \right) \left(p^k p^l - \boldsymbol{p}^2 \delta^{kl} \right) \\
& = \mathcal{O}^{\mu\nu,\alpha\beta} + c\mathcal{A}^{\mu\nu}\mathcal{A}^{\alpha\beta},
\end{aligned}
\tag{1.29}
$$

where $\mathcal{O}^{\mu\nu,\alpha\beta}$ is the operator that appears in the field equations of Fierz-Pauli theory. The factorization property of the terms proportional to c is quite important in what follows below. Let us recall that the field equations (1.24) are invariant under linearized diffeomorphisms (1.23). This implies that, as in Fierz-Pauli theory, we need to partially fix the gauge redundancy in order to be able to find the propagator. In order to keep the discussion as close as possible to the Fierz-Pauli case, let us fix the de Donder gauge $\partial_\mu h^{\mu\nu} = \partial^\nu h/2$ [45, 46]. Let us recall that, in this gauge,

$$
\mathcal{O}^{\mu\nu,\alpha\beta} = \frac{p^2}{2}(\eta^{\mu\alpha}\eta^{\nu\beta} + \eta^{\nu\alpha}\eta^{\mu\beta} - \eta^{\mu\nu}\eta^{\alpha\beta}).
\tag{1.30}
$$

The inverse of this operator $\mathcal{F}_{\alpha\beta\rho\sigma}$, namely the quantity that verifies

$$
\mathcal{O}^{\mu\nu,\alpha\beta}\mathcal{F}_{\alpha\beta\rho\sigma} = \frac{1}{2}(\delta_\rho^\mu \delta_\sigma^\nu + \delta_\sigma^\mu \delta_\rho^\nu),
\tag{1.31}
$$

is given by

$$
\mathcal{F}_{\alpha\beta\rho\sigma} = \frac{1}{2p^2}(\eta_{\alpha\sigma}\eta_{\beta\rho} + \eta_{\alpha\rho}\eta_{\beta\sigma} - \eta_{\alpha\beta}\eta_{\sigma\rho}).
\tag{1.32}
$$

The differential operator in the field equations (1.24) has however a more complex expression, so its inverse has additional terms. We cannot use directly Eq. (1.29), as we need to impose the de Donder gauge, which in particular implies constraints between h_{ij} and h_{00}. It is not difficult to show that the relevant expression to analyze is given by

$$
\mathcal{O}^{\mu\nu,\alpha\beta} + c\mathcal{O}^{\mu\nu,00}\mathcal{O}^{00,\alpha\beta}.
\tag{1.33}
$$

Note that the only difference with respect to Eq. (1.29) is that the differential operator $\mathcal{A}^{\mu\nu}$ is identified with $\mathcal{O}^{00,\mu\nu}$ in the de Donder gauge, which can be obtained from Eq. (1.30). The problem of finding the inverse of the differential operator (1.33) is a variant of the simpler calculation of the photon propagator in quantum electrodynamics (e.g., [47]); for completeness, all the necessary details are given in the following.

A detailed inspection of the problem suggests the ansatz

$$
\mathcal{D}_{\alpha\beta\rho\sigma} = \mathcal{F}_{\alpha\beta\rho\sigma} + cB(p)\mathcal{W}_{\alpha\beta}\mathcal{W}_{\rho\sigma},
\tag{1.34}
$$

where $B(p)$ is a function of p^2 and $\mathcal{W}_{\rho\sigma}$ is defined using Eq. (1.31), namely

$$
\mathcal{W}_{\rho\sigma} = p^2 \mathcal{O}^{\alpha\beta,00}\mathcal{F}_{\alpha\beta\rho\sigma} = p^2 \delta_\rho^0 \delta_\sigma^0.
\tag{1.35}
$$

This tensor satisfies

$$\mathcal{O}^{\mu\nu,\alpha\beta}\mathcal{W}_{\alpha\beta} = p^2\mathcal{O}^{\mu\nu,00} = p^2\mathcal{A}^{\mu\nu}. \tag{1.36}$$

We can write therefore

$$[\mathcal{O}^{\mu\nu,\alpha\beta} + c\,\mathcal{O}^{\mu\nu,00}\mathcal{O}^{00,\alpha\beta}][\mathcal{F}_{\alpha\beta\rho\sigma} + cB(p)\mathcal{W}_{\alpha\beta}\mathcal{W}_{\rho\sigma}] =$$

$$= \mathcal{O}^{\mu\nu,\alpha\beta}\mathcal{F}_{\alpha\beta\rho\sigma} + c\mathcal{O}^{\mu\nu,\alpha\beta}B(p)\mathcal{W}_{\alpha\beta}\mathcal{W}_{\rho\sigma} + c\mathcal{O}^{\mu\nu,00}\mathcal{O}^{00,\alpha\beta}\mathcal{F}_{\alpha\beta\rho\sigma}+$$

$$+c^2B(p)\mathcal{O}^{\mu\nu,00}\mathcal{O}^{00,\alpha\beta}\mathcal{W}_{\alpha\beta}\mathcal{W}_{\rho\sigma} \tag{1.37}$$

$$= \mathcal{O}^{\mu\nu,\alpha\beta}\mathcal{F}_{\alpha\beta\rho\sigma} + cp^2B(p)\mathcal{O}^{\mu\nu,00}\mathcal{W}_{\rho\sigma} + \tfrac{c}{p^2}\mathcal{O}^{\mu\nu,00}\mathcal{W}_{\rho\sigma}+$$

$$+c^2B(p)\mathcal{O}^{\mu\nu,00}\mathcal{O}^{00,\alpha\beta}\mathcal{W}_{\alpha\beta}\mathcal{W}_{\rho\sigma}.$$

In order to write the last identity we have used Eqs. (1.35) and (1.36). Imposing the equivalent of Eq. (1.31), we can solve for $B(p)$ as

$$B(p) = -\frac{1}{p^2(p^2 + c\mathcal{O}^{00,\alpha\beta}\mathcal{W}_{\alpha\beta})}. \tag{1.38}$$

We just have to evaluate

$$\mathcal{O}^{00,\alpha\beta}\mathcal{W}_{\alpha\beta} = p^2\mathcal{O}^{00,00} = \frac{p^4}{2}, \tag{1.39}$$

in order to obtain the full propagator

$$\mathcal{D}_{\alpha\beta\rho\sigma} = \mathcal{F}_{\alpha\beta\rho\sigma} - \frac{c}{1 + cp^2/2}\delta^0_\alpha\delta^0_\beta\delta^0_\rho\delta^0_\sigma. \tag{1.40}$$

We see that the propagator is not the same as in Fierz-Pauli theory, which is reasonable as off-shell equivalence is not guaranteed (nor needed in order to show physical equivalence). However, the propagator is still a function of the covariant combination of p^2 only and, for large p^2, its behavior is the same as in Fierz-Pauli theory, namely $1/p^2$. These features will be of importance later, in Sec. 1.3.
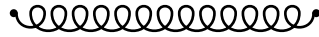

Figure 1.1: The propagator is a function of p^2 with a leading dependence $1/p^2$.

1.2.3 On-shell 3-point amplitudes

Let us now consider the next order in the perturbative expansion of Eq. (1.19):

$$\mathcal{L} = cM^4\sqrt{-g}\left\{(\mathcal{K} + R) + cR^2 + c\mathcal{K}R + c^2R^3\right\} + \dots \tag{1.41}$$

where again we are omitting terms, which this time are at least of fourth order in $h_{\mu\nu}$. The first piece, proportional to $\sqrt{-g}(\mathcal{K} + R)$, leads to the usual 3-point amplitudes. On the other hand, the additional terms contain the new interaction vertices

$$\sqrt{-g}\, R^2 = [R^{(1)}]^2 - \frac{1}{2}h[R^{(1)}]^2 + 2R^{(1)}R^{(2)} + ...$$
$$\sqrt{-g}\, \mathcal{K}R = \mathcal{K}^{(2)}R^{(1)} + ...$$
$$\sqrt{-g}\, R^3 = [R^{(1)}]^3 + ... \tag{1.42}$$

But we have shown that Eq. (1.26) is satisfied at the linear level, which implies

$$R^{(1)} = \partial_i\partial_j h^{ij} - \Delta\tilde{h} = 0. \tag{1.43}$$

Note that this quantity above is precisely the $\mu = \nu = 0$ component of the field equations (1.27), $\mathcal{O}^{00,\alpha\beta}h_{\alpha\beta} = 0$, up to a sign. Therefore, if just one of the legs of the 3-point amplitude is on-shell, the contributions coming from the $[R^{(1)}]^3$ vertex vanish identically; no differences from general relativity can result from these vertices. Moreover, noting that $R^{(1)} = -\mathcal{O}^{00,\alpha\beta}h_{\alpha\beta}$ appears in all the 3-point vertices in Eq. (1.42), if follows that this observation extends to all these vertices when all the external particles are on-shell (i.e., when the amplitude is on-shell).
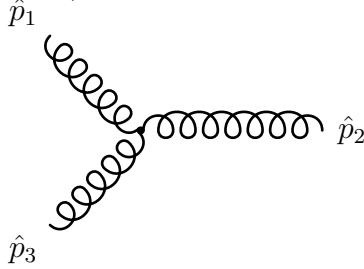
Figure 1.2: The on-shell 3-point amplitudes (of complex momenta) are the same as in general relativity. As discussed in the next section, these are the building blocks for constructing on-shell n-point amplitudes of real momenta for $n \geq 4$, which makes this equivalence fundamental for our discussion.

Let us recall that 3-point amplitudes of massless particles become trivial on-shell [48, 49]. However, if the momenta of the external particles are considered to be complex, this is no longer the case [50] (see also [51]). This allows to write expressions for the 3-point on-shell amplitudes which are non-zero for complex momenta, but become trivial for real momenta. The argument above following which the contributions from the non-covariant interaction vertices (e.g., $[R^{(1)}]^3$) vanish if the external legs are on-shell, applies as well to complex momenta. Hence, we can conclude that the on-shell 3-point amplitudes (of complex momenta) for the theory with Lagrangian density (1.19) are the same as in general relativity.

1.2.4 Interlude, the most general theories compatible with these results

The results in Secs. 1.2.1, 1.2.2 and 1.2.3 are not particular to the theory with Lagrangian density (1.15). We have made this observation above, but we would like to

show it more explicitly at this point in the discussion. Let us consider the Lagrangian density

$$\mathcal{L} = \sqrt{-g}\, G(\mathcal{K}, R), \tag{1.44}$$

where $G(\mathcal{K}, R)$ is a function of $\mathcal{K}$ and R, satisfying the conditions derived in [29] so that the theory contains two local degrees of freedom. It is interesting to note that Eq. (1.44) is general enough to include all the explicit examples constructed in [29]. This function can be expanded around Minkowski spacetime as

$$\left.\frac{\partial\mathcal{L}}{\partial R}\right|_{R=\mathcal{K}=0} R + \left.\frac{\partial\mathcal{L}}{\partial\mathcal{K}}\right|_{R=\mathcal{K}=0}\mathcal{K} + \frac{1}{2}\left.\frac{\partial^2\mathcal{L}}{\partial\mathcal{K}\partial R}\right|_{R=\mathcal{K}=0} R\,\mathcal{K} + \frac{1}{2}\left.\frac{\partial^2\mathcal{L}}{\partial R^2}\right|_{R=\mathcal{K}=0} R^2 + \frac{1}{6}\left.\frac{\partial^3\mathcal{L}}{\partial R^3}\right|_{R=\mathcal{K}=0} R^3 + ... \tag{1.45}$$

Unless $\partial\mathcal{L}/\partial R|_{R=\mathcal{K}=0} = 0$ or $\partial\mathcal{L}/\partial\mathcal{K}|_{R=\mathcal{K}=0} = 0$, it is always possible to perform field redefinitions (constant rescalings) as we have done previously in order to reconstruct the 4-dimensional Ricci scalar up to an irrelevant boundary term. We have then an expansion in $\mathcal{K}$ and R that is precisely of the form that has been used in Secs. 1.2.1, 1.2.2 and 1.2.3, so that the results of these sections equally apply to all the theories with Lagrangian (1.44) (implying, in particular, the equivalence of the linearized field equations and 3-point amplitudes with that of general relativity). Let us note that $\partial\mathcal{L}/\partial\mathcal{K}|_{R=\mathcal{K}=0}$ must be non-zero in order to have a kinetic term for the field $h_{\mu\nu}$, so the only possibility to avoid this general result within this family is considering theories in which $\partial\mathcal{L}/\partial R|_{R=\mathcal{K}=0} = 0$. We analyze this case separately in Sec. 1.4.1, showing that this kind of theory does not even contain gravitons at the linearized level, which raises doubts about whether or not these describe gravitational theories (and is also disastrous from an observational perspective).

1.3 Higher orders in the perturbative expansion

Up to now, we have shown that the theory defined by the Lagrangian density in Eq. (1.15) is equivalent to general relativity for its two lowest orders: at the linear level the field equations are equivalent to that of Fierz-Pauli theory, and at first order in the interactions, the 3-point amplitudes are the same as in general relativity. Moreover, we have discussed that the latter property is an unavoidable consequence of the former in all theories of the fairly general form (1.44). Armed with this knowledge, we can use now a battery of results from on-shell scattering amplitudes in order to obtain non-trivial information about the higher orders in the perturbative expansion. The goal of this section is simple: we know that theories of the form (1.44) that satisfy $\partial\mathcal{L}/\partial R|_{R=\mathcal{K}=0} \neq 0$ and $\partial\mathcal{L}/\partial\mathcal{K}|_{R=\mathcal{K}=0} \neq 0$ have the same polarizations of the gravitational field at the linear level and the same 3-point amplitudes as general relativity; in this section we study whether or not this equivalence holds for n-point amplitudes with $n \geq 4$.

In order to achive our goal, we will have to take a detour from our previous discussion in terms of Hamiltonian and Lagrangian mechanics and consider a language which is more powerful in order to deal with the perturbative structure of non-linear theories. This language is that of scattering amplitudes in quantum field theory, in its modern incarnation using spinor-helicity variables which are specially suited for the description of massless particles. Some of these ingredients are briefly reviewed in App. B in order to make the discussion reasonably self-contained.

We have studied on-shell 3-point amplitudes in Sec. 1.2.3. However, for the purposes of this section, we will need to take into account some properties of the off-shell 3-point vertices of the actions with Lagrangian density (1.44). The most important observation is that, while in general relativity any interaction vertex only contains two powers of momenta, the theories (1.44) do not verify this requirement. In particular, from the last line in Eq. (1.42) we can read that off-shell 3-point vertices can have up to 6 powers of the (spatial) momenta. This feature forbids applying previous uniqueness results [52, 53, 54, 55] that use an extension of the Britto-Cachazo-Feng-Witten (BCFW) relations [56, 57] but assume that interaction vertices are at most quadratic in the momenta (that higher-derivative interaction vertices are problematic is well-known [58]). Technically, this follows from the necessity of showing that contributions from Feynman diagrams remain bounded for large (complex) momenta; that vertices may contain higher powers of momenta spoil the bounds that can be obtained for the quadratic case. The most virulent behavior comes from off-shell 3-point vertices with 6 powers of the momenta, namely the ones in the last line of Eq. (1.42). However, these contributions can only come from internal vertices, as we have shown in Sec. 1.2.3 that these vertices vanish when at least one of the legs stitched to it is on-shell.

Let us start with the n-point amplitude of n gravitons with the same helicity, $A_n(1^+2^+...n^+)$, or just with the helicity of one graviton flipped, $A_n(1^-2^+...n^+)$. In general relativity these amplitudes vanish for any value of n. There is a simple argument to show that this must be the case by counting the powers of momenta in Feynman diagrams (see, e.g., Sec. 2.7 in [48]). The argument boils down to the observation that this amplitude can be non-zero only if vertices contribute at least with $2n$ powers of the momenta that can be contracted with the $2n$ polarization vectors (B.13) and (B.14) of external gravitons [no powers of the momenta can be provided by propagators, which is true both in general relativity and in the theories analyzed here; recall Eq. (1.40)]. If this is not the case, at least two of these polarization vectors will be contracted with each other, and this combination can be shown to be zero up to a gauge transformation, implying that the overall amplitude vanishes. While it is impossible to obtain these $2n$ powers of the momenta in the case of general relativity (and, in general, for any theory in which interaction vertices are quadratic in the momenta), here we have to be more careful with the interaction vertices containing higher powers of momenta. However, the potentially most virulent behavior, coming from the $[R^{(1)}]^3$ off-shell 3-point vertex in Eq. (1.42), turns out to be innocuous as the corresponding 6 powers of the momenta cannot be coupled to the polarization vectors of external particles. Taking a look at Eq. (1.43), we see that the first part can be gauged away (off-shell), while the second one contributes with a factor $p_i p^i$ that has no free indices to be contracted with the indices of polarization vectors. Alternatively, in the de Donder gauge, $R^{(1)}$ is simply proportional to the scalar p^2. The remaining 3-point vertices $\mathcal{K}^{(2)}R^{(1)}$ and $R^{(2)}R^{(1)}$ only have 2 powers of the momenta that can be contracted with the ϵ_+^μ, which leads to the same maximum number of momenta as in general relativity. Let us therefore turn our attention to 4-point vertices, from which $[\mathcal{K}^{(2)}]^2$ and $[R^{(2)}]^2$ display the worst behavior, with a p^4 dependence. However, counting the number of vertices in the corresponding Feynman diagrams (see App. B) shows that in this case the maximum possible number of momenta is $2n - 4 < 2n$. Therefore, we conclude that

$$A_n(1^+2^+...n^+) = A_n(1^-2^+...n^+) = 0, \qquad \forall n \geq 3. \tag{1.46}$$

This is a quite non-trivial statement that is characteristic of general relativity as well as Yang-Mills theories. This implies that, in order to have a non-zero amplitude, we need to flip the helicity of at least two gravitons (which leads to the so-called maximally helicity violating –MHV– amplitudes [59]).

In order to deal with the MHV amplitudes $A_n(1^-2^-3^+...n^+)$ and other possibly non-vanishing amplitudes, we need to resort to more sophisticated arguments. As reviewed briefly in App. B, the most powerful argument to deal with these amplitudes involves complexifying the external momenta in order to construc n-point amplitudes $A_n(1^-2^-3^+...n^+)$ from $n-1$-amplitudes evaluated on complex momenta. This recursive procedure is valid as long as certain technical conditions are satisfied by the complexification of the n-point amplitude $A_n(1^-2^-3^+...n^+)$ [48]. There are different ways in which the complexification can be done. The one that we want to study was considered in the App. A of [53] (see also [54]) in order to obtain what these authors call the "auxiliary" recursion relations. This particular complex extension represents the optimal choice in general relativity, and therefore it will be also the optimal choice here, as the only change in the present discussion is the behavior of interaction vertices with the momenta. Note that we cannot apply directly the conclusions of these authors, as the theories we are interested in have interaction vertices which are not quadratic in the momenta.

Without loss of generality, let us consider an amplitude in which $N \geq n/2$ external legs have positive helicity; the case in which there is a larger number of external legs with negative helicity is completely parallel. If $s \in [1, N]$ labels all the external legs with positive helicity, and t marks a single external leg with negative helicity, we define the complex extension

$$\hat{p}_s = p_s + zq_s, \qquad \hat{p}_t = p_t - z\sum_{s=1}^{N} q_s, \qquad (1.47)$$

where $z \in \mathbb{C}$ and $\{q_s\}_{s=1}^{N}$ are complex vectors verifying certain requirements [48].

To show the validity of the recursion relations, let us exploit the fact that it is a sufficient condition that all Feynman diagrams contributing to a given amplitude vanish asymptotically for large $|z|$. Taking into account that Feynman diagrams are just the multiplication of diverse elements (external legs, interaction vertices and propagators), we just need to understand how these different elements scale with $|z|$:

- $N+1$ external particles are shifted (that is, their momenta are complexified) such that their polarization tensors constructed from Eqs. (B.13) and (B.14) give each a leading contribution $1/|z|^2$.

- All propagators in Eq. (1.40) are shifted (this property that depends only on the topology of the relevant Feynman diagrams was shown in [53]) and therefore contribute with a $1/|z|$ factor each.

- Vertices behave as $|z|^k$. Internal (i.e., off-shell) 3-point vertices display 6 powers of the spatial momenta instead of being just quadratic in the covariant momenta, which suggests a $|z|^6$ dependence. However, a careful inspection shows (as discussed in Secs. 1.2.2 and 1.2.3) that these off-shell vertices are proportional in the

de Donder gauge to the covariant combination $(p^2)^3$, which means that these also scale as $|z|^3$. A similar comment applies to internal vertices that contain $R^{(1)}$.

Putting all these elements together, for Feynman diagrams involving only k-point vertices the leading z dependence goes like

$$A_n(z) \propto \left(z^{-2}\right)^{N+1} \left(z^{-1}\right)^p \left(z^k\right)^v, \qquad (1.48)$$

where the first multiplicative factor is the contribution from the polarization tensors of the shifted external legs, p is the number of propagators and v is the number of vertices. For k-point vertices one has (App. B)

$$p = \frac{n-k}{k-2}, \qquad\qquad v = \frac{n-2}{k-2}. \qquad (1.49)$$

The recursion relations can be valid only if $A_n(z) \propto z^w$ with $w < 0$ (which in general relativity is always satisfied [53]). This leads to the inequality

$$N > \frac{(k-1)n - (3k-4)}{2(k-2)}. \qquad (1.50)$$

It is straightforward to show that the most stringent of these conditions is obtained for $k = 3$, which implies that interaction vertices with $k \geq 4$ only give subleading contributions to the asymptotic behavior on $|z|$ of Feynman diagrams.

Overall, this leads to the main results of this section, together with Eq. (1.46):

- $n = 4$ and $n = 5$: all amplitudes $A_n(1^{h_1}2^{h_2}...n^{h_n})$ can be constructed from 3-point amplitudes and are therefore the same as in general relativity.

- $n \geq 6$: the MHV amplitude $A_6(1^-2^-3^+4^+5^+6^+)$ is the same as in general relativity. This argument does not fix the form of $A_6(1^-2^-3^-4^+5^+6^+)$ or any of the remaining n-point amplitudes with $n > 6$ that are not already contained in Eq. (1.46).

In summary, we have applied state-of-the-art techniques of on-shell scattering amplitudes in order to calculate a sequence of scattering amplitudes which would be otherwise extremely difficult (and time-consuming) to calculate. This illustrates that on-shell techniques can be used in order to understand the physical content of modified gravity theories. The information extracted in this way (see Fig. 1.3) is quite interesting, as it uncovers unexpected cancellations of the additional (non-relativistic) interaction vertices, and strengthens the possibility that these theories are equivalent to general relativity. In particular, we have determined that differences might arise only for 6-point amplitudes [in the $A_6(1^-2^-3^-4^+5^+6^+)$ amplitude] or higher.

Let us stress that this does not necessarily imply that it is likely that there will be differences. It is ubiquitous in the study of on-shell scattering amplitudes that unexpected cancelations occur, so that terms that may seemingly give additional contributions leave no trace. In fact, we already know that these kinds of cancellations indeed happen for the theories analyzed here. For instance, in the amplitudes $A_4(1^{h_1}2^{h_2}3^{h_3}4^{h_4})$ the contributions coming from the additional (i.e., not present in general relativity) 4-point

vertices $[\mathcal{K}^{(2)}]^2$ and $[R^{(2)}]^2$ cancel identically. A similar observation follows for arbitrary $A_n(1^{h_1}2^{h_2}...n^{h_n})$ for $n \leq 5$, and applies to all the possible interaction vertices that are involved in these amplitudes, including the most virulent $[R^{(1)}]^3$. This even applies to $A_n(1^+2^+...n^+)$ and $A_n(1^-2^+...n^+)$ for arbitrary values of n. It is not unreasonable to think that these cancellations will keep taking place for the remaining tree-level amplitudes, but that the on-shell arguments used here are not powerful enough to show this. Reaching a definitive conclusion is not possible at the moment; it may be that some generalization of these arguments will be successful, or additional calculations might uncover a counterexample. But we certainly think this is an interesting question that deserves further study.

$$(1.51)$$

Figure 1.3: One of the results in this section is that the $A_4(1^{h_1}2^{h_2}3^{h_3}4^{h_4})$ is constructible from on-shell 3-point amplitudes of complex momenta using recursion relations, which in particular implies equivalence to general relativity at this particular order in the perturbative expansion. As in general relativity, this means that 4-point vertices carry no physical information, but are present in order to guarantee off-shell gauge invariance. This result is remarkable as it extends this observation from the 4-point vertices $\mathcal{K}^{(4)}$ and $R^{(4)}$ of general relativity, to include also $[\mathcal{K}^{(2)}]^2$ and $[R^{(2)}]^2$. Moreover, we have shown that perturbative equivalence with general relativity holds for $A_n(1^{h_1}2^{h_2}...4^{h_4})$ up to $n = 5$ no matter the helicity configuration, and for selected configurations when $n > 5$.

Before finishing this section, let us point out that the BCFW shift is not the only possible way to extend the momenta in the complex plane. A different possibility is given by

$$p_s \longrightarrow \hat{p}_s = p_s(1 - a_s\,z), \qquad (1.52)$$

where $z \in \mathbb{C}$ as before and the constants a_s are such to satisfy the momentum constraint

$$\sum_{i=1}^{n} \hat{p}_i = z \sum_{i=1}^{n} a_i p_i = 0. \qquad (1.53)$$

When $z = 1/a_s$ one of the external particle becomes soft and it is possible to use the soft theorem in order to get information on the scattering amplitude A_n (see, e.g. [60]). This type of shift has been used in **P4** where it was shown that, although the shift can be useful to prove the equivalence of the scattering matrices of two theories when the BCFW fails (for instance it was possible to prove the equivalence of the scattering matrices of general relativity and unimodular gravity), it does not provide useful information in the study of the theories discussed in this thesis.

1.4   Genuinely different theories

In the previous sections we have used different probes of large classes of theories and found no evidence of differences with respect to general relativity. It would be interesting to find theories that still satisfy the conditions in [29] ensuring that the number of degrees of freedom is the same as general relativity, but that are manifestly different from general relativity. In this section we analyze two kinds of theories that fall within this category, discussing their main properties and, in particular, their pathologies.

1.4.1   Theories with no gravitons

As already noticed in [29], theories that do not contain the 3-dimensional Ricci tensor R_{ij} in the Lagrangian density describe automatically two degrees of freedom . In particular, for theories of the form (1.44) this would imply $\partial \mathcal{L}/\partial R = 0$. The simplest example of this kind of theory is given by

$$\mathcal{L} = \sqrt{h} N \, \mathcal{K}. \tag{1.54}$$

Let us now show that this theory is clearly inequivalent to general relativity, by looking at its Hamiltonian formulation: the momenta are given by

$$\pi^{ij} = 2 \left(K^{ij} - K h^{ij} \right) \frac{1}{2} \sqrt{h}, \qquad \pi_N = 0, \qquad \pi_i = 0, \tag{1.55}$$

and the total Hamiltonian takes the usual form

$$H = \int d^3 x \left(N \mathcal{H} + N^i \mathcal{D}_i + \lambda_N \pi_N + \lambda^i \pi_i \right), \tag{1.56}$$

but with

$$\mathcal{H} = \frac{\Pi}{\sqrt{h}}. \tag{1.57}$$

The secondary constraints are again $\mathcal{H} = 0$ and $\mathcal{D}_i = 0$. The main difference lies now in the algebra of constraints, which takes the form

$$\begin{aligned}
\{\mathcal{H}[\alpha], \mathcal{H}[\beta]\} &= 0, \\
\{\mathcal{D}[\alpha^i], \mathcal{H}[\alpha]\} &= \mathcal{H} \left[\mathcal{L}_{\alpha^i} \alpha \right], \\
\{\mathcal{D}[\alpha^i], \mathcal{D}[\beta^j]\} &= \mathcal{D} \left[\mathcal{L}_{\alpha^i} \beta^j \right].
\end{aligned} \tag{1.58}$$

Note the difference with respect to Eq. (1.9): the first bracket is identically vanishing. This has clear physical implications, which can be noticed for instance recalling our discussion in Sec. 1.1.1 and App. A: even if the theory describes two degrees of freedom, at linear level these excitations do not carry a representation of the Poincaré group (not even in some kind of low-energy limit). For instance, in the theory analyzed in this section, time translations and boosts commute, as well as two boosts (in the Poincaré group, these commutators will be proportional to spatial translations and rotations, respectively). Therefore, these theories are escaping equivalence with general relativity, but at the price of modifying drastically even the linear properties of the theory (i.e., not describing gravitons at the linear level).

In particular, it is not clear if it is legitimate to call these theories "gravitational" theories [29]. The linear excitations in this theory do not satisfy a wave equation, which would imply that there are no gravitational waves and therefore contradicts observational facts. This is a reasonable outcome, which shows that tampering with the very properties of the carrier of the gravitational force generally has drastic physical consequences.

1.4.2 Theories with a modified dispersion relation for gravitons

The previous example is interesting from a theoretical perspective but is, in some sense, too trivial. In this section we consider a class of examples that are more interesting physically. In some sense these examples are complementary to the ones in the previous section: instead of considering a Lagrangian density that does not depend on R_{ij}, let us consider Lagrangian densities that are obtained by adding a piece that is independent from K_{ij} (and also the lapse N). As shown in a brief section at the end of the paper [29], adding this term renders the Hamiltonian constraint second class, but it also introduces a tertiary constraint. Therefore, the number of degrees of freedom does not change even if the way the counting is performed is changed. This class of examples was also found in [61]. Phenomenological consequences for some of these theories (and extensions) are studied in [62]. Here, we focus on the effects that these kind of terms have when added to the Einstein-Hilbert action; our conclusions stated below do not depend on this specific choice of starting point. For concreteness, let us consider

$$\mathcal{L} = \sqrt{h}N(\mathcal{K} + R) + \ell^2\sqrt{h}\,R_{ij}R^{ij}, \tag{1.59}$$

where ℓ is a constant with dimensions of length.

Let us now obtain the form of the field equations. The first piece in Eq. (1.59) leads to the usual Fierz-Pauli equations, so we will focus on the second piece, for which we need to recall (e.g., [43]) that $R_{ij}^{(1)} = (\Delta h_{ij} - \partial_i\partial^k h_{kj} - \partial_j\partial^k h_{ki} + \partial_i\partial_j\tilde{h})/2$, so that the corresponding contribution to the field equations is proportional to

$$\frac{1}{2}\left(\delta_i^k\delta_j^l\Delta - 2\delta_i^k\partial_j\partial^l + \delta_{ij}\partial^k\partial^l\right)\left(\Delta h_{kl} - \partial_k\partial^m h_{ml} - \partial_l\partial^m h_{mk} + \partial_k\partial_l\tilde{h}\right)\delta_\mu^i\delta_\nu^j. \tag{1.60}$$

We can see that the additional term describe higher-derivative corrections to the purely spatial components of the Fierz-Pauli equations, similarly to what happened in the square root gravity, Eq. (1.24). However, in the square root gravity these contributions were identically vanishing. Here we will see that the same does not apply.

First of all, let us recall that, as in the square root gravity, the $\mu = \nu = 0$ component of the field equations is given by Eq. (1.26). This, in turn, implies that the trace of Eq. (1.60) vanishes on-shell: it is given by

$$\begin{aligned}&\frac{1}{2}\left(\delta^{kl}\Delta + \partial^k\partial^l\right)\left(\Delta h_{kl} - \partial_k\partial^m h_{ml} - \partial_l\partial^m h_{mk} + \partial_k\partial_l\tilde{h}\right)\\&= \frac{3}{2}\Delta(\Delta\tilde{h} - \partial_i\partial_j h^{ij}) = 0.\end{aligned} \tag{1.61}$$

We can therefore:

- Impose the de Donder gauge $\partial^\mu \bar{h}_{\mu\nu} = 0$, where $\bar{h}_{\mu\nu} = h_{\mu\nu} - \eta_{\mu\nu} h/2$.

- Exploit the $\mu = 0$, $\nu = 0$ and $\mu = 0$, $\nu = i$ components of the field equations to gauge away the $\bar{h}_{00}$ and $\bar{h}_{0i}$ components of the gravitational field.

- Use the trace of the field equations, $\Box \bar{h} = 0$, to fix completely the residual gauge freedom setting $\bar{h} = 0$.

This implies that the field equations can be written simply as

$$\Box h_{ij} + \ell^2 \Delta^2 h_{ij} = 0. \tag{1.62}$$

This is a quite interesting equation that implies that this theory describes gravitons (with two degrees of freedom), but with modified dispersion relations. At least at low energies (measured in terms of the scale ℓ), the usual Lorentz-invariant picture is recovered. This suggests that these theories are interesting alternatives to general relativity that reduce to the latter at low energies.

However, there is a feature of the theories which include "potential" terms in the 3-dimensional Ricci tensor R_{ij} that must be kept in mind. The inclusion of this kind of potential term independent of the lapse N and the extrinsic curvature K_{ij} changes drastically the nature of the constraints of the theory. First of all, the form of the Hamiltonian and diffeomorphism constraints is unchanged. However, the Hamiltonian constraint is not automatically preserved by evolution, and an additional constraint must be added in order to ensure its preservation. This, in turn, implies that the Hamiltonian constraint is second class. Hence, the only remaining gauge symmetries are spatial diffeomorphisms. But here is where the trouble lies: instead of the very combination

$$\mathcal{K} = K_{ij} K^{ij} - K^2, \tag{1.63}$$

that appears in the Lagrangian density (1.59) and is characteristic of general relativity, spatial diffeomorphisms can only select the combination

$$K_{ij} K^{ij} - \mu K^2, \tag{1.64}$$

with μ an arbitrary constant; this is for instance a well-known observation in the framework of Hořava-Lifshitz gravity [63]. Equally well-known in this framework (e.g., [64]) is the fact that a theory with a Lagrangian density linear in the combination just above can only contain two degrees of freedom if and only if $\mu = 1$; for different values of this parameter, an additional degree of freedom (a scalar graviton) appears. Let us stress that the same result follows from our analysis in Sec. 1.1; one of the features that guarantees that the theories analyzed in that section (and also the ones in Sec. 1.4.1) contain only two degrees of freedom is that $\mu = 1$ for them [equivalently, the momenta π^{ij} enter through the combination Π in Eq. (1.5)].

In summary, including potential terms such as $\sqrt{h}\, R_{ij} R^{ij}$ in Eq. (1.59) generally makes the Hamiltonian constraint second class and therefore leaves spatial diffeomorphisms as the only gauge symmetries of the theory. As a consequence, it is not possible to guarantee that the value of μ is protected against radiative corrections, and therefore that these theories do not acquire additional degrees of freedom in this way [65].

Hence, the theory may describe instead two polarizations of the gravitational field with modified dispersion relation, and an additional scalar graviton.[1]

1.5 Coupling to matter

Our analyses above have been restricted to theories which only include the gravitational field. In this last section we include matter fields (for simplicity, a scalar field). This is motivated due to two reasons. The first one is that any realistic theory of gravity must include matter. The second one is that in [29] the authors study Friedmann-Lemaître-Robertson-Walker solution in the square root gravity studied in Sec. 1.2 and find that the corresponding equations are genuinely different than the ones obtained in general relativity. This may suggest that, even if the square root gravity may be equivalent to general relativity in vacuum, differences might be unavoidable when couplings to matter are included. However, we think that one must be careful before jumping into this conclusion, as many subtleties arise in the procedure of coupling matter in these alternative theories.

1.5.1 Algebra of constraints for minimal coupling

Let us come back to our starting point, namely the Hamiltonian theories introduced in Sec. 1.1, and include a scalar field in the system as the simplest possible representation of matter fields. The Lagrangian density for the scalar field is given by

$$\mathcal{L}^\phi = \sqrt{-g}\left[g^{\mu\nu}\nabla_\mu\phi\nabla_\nu\phi + V(\phi)\right], \tag{1.65}$$

where $V(\phi)$ is the potential. In order to obtain the form of the Hamiltonian let us recall that, in the ADM decomposition, the components of the metric are given by

$$g^{00} = -\frac{1}{N^2} \qquad g^{0i} = \frac{N^i}{N^2}, \qquad g^{ij} = h^{ij} - \frac{N^i N^j}{N^2}. \tag{1.66}$$

Taking also into account that $\sqrt{-g} = -N\sqrt{h}$, it follows that

$$\mathcal{L}^\phi = -\frac{1}{2}\sqrt{h}\left[-\frac{1}{N}\partial_0\phi\partial_0\phi + 2\frac{N^i}{N}\partial_0\phi\nabla_i\phi + N\,h^{ij}\nabla_i\phi\nabla_j\phi - \frac{N^i N^j}{N}\nabla_i\phi\nabla_j\phi + V(\phi)\right], \tag{1.67}$$

so that the scalar field Hamiltonian is given by (P is the conjugate momentum of ϕ):

$$H^\phi = \int d^3x\, N\left(\frac{1}{2}\frac{P^2}{\sqrt{h}} + \frac{1}{2}\sqrt{h}h^{ij}\nabla_i\phi\nabla_j\phi + \sqrt{h}V(\phi)\right) + PN^i\nabla_i\phi. \tag{1.68}$$

If we define

$$\mathcal{H}^\phi = \frac{1}{2}\frac{P^2}{\sqrt{h}} + \frac{1}{2}\sqrt{h}h^{ij}\nabla_i\phi\nabla_j\phi + \sqrt{h}V(\phi), \qquad \mathcal{D}_i^\phi = P\nabla_i\phi, \tag{1.69}$$

---

[1]Note that, even if $\mu = 1$ is not protected under radiative corrections, the extra scalar mode may be suppressed in the infrared if $\mu = 1$ is an infrared fixed point. Some examples of this behavior, in the framework of Hořava-Lifshitz gravity, are given in [66, 67].

the total (gravity plus matter) Hamiltonian becomes

$$H_{\mathrm{T}} = \int d^3x \, N(\mathcal{H} + \mathcal{H}^\phi) + N^i(\mathcal{D}_i + \mathcal{D}_i^\phi) + \lambda_N \pi_N + \lambda^i \pi_i. \tag{1.70}$$

The primary constraints are again

$$\pi_N = 0, \qquad\qquad \pi_i = 0, \tag{1.71}$$

while the subsequent secondary constraints are given by

$$\mathcal{H}_{\mathrm{T}} = \mathcal{H} + \mathcal{H}^\phi = 0, \qquad\qquad (\mathcal{D}_{\mathrm{T}})_i = \mathcal{D}_i + \mathcal{D}_i^\phi = 0. \tag{1.72}$$

In order to obtain the off-shell algebra of constraints satisfied, it is convenient to evaluate first the following brackets: first of all the Poisson brackets involving the gravitational and matter sectors of the Hamiltonian constraint,

$$\{\mathcal{H}[\alpha], \mathcal{H}[\beta]\} = \mathcal{D}[F'^2 h^{ij}(\alpha\nabla_j\beta - \beta\nabla_j\alpha)]$$
$$\{\mathcal{H}[\alpha], \mathcal{H}^\phi[\beta]\} = -\int d^3x \, \frac{\lambda}{2\sqrt{h}}\left(\frac{\pi P^2}{\sqrt{h}} - \pi V(\phi) + \sqrt{g}\pi^{ij}\nabla_i\phi\nabla_j\phi\right),$$
$$\{\mathcal{H}^\phi[\alpha], \mathcal{H}^\phi[\beta]\} = \mathcal{D}^\phi[h^{ij}(\alpha\nabla_j\beta - \beta\nabla_j\alpha)]. \tag{1.73}$$

For the diffeomorphism constraint, one has

$$\{\mathcal{D}[\alpha^i], \mathcal{D}[\beta^j]\} = \mathcal{D}\left[\mathcal{L}_{\alpha^i}\beta^j\right],$$
$$\{\mathcal{D}[\alpha^i], \mathcal{D}^\phi[\beta^j]\} = 0,$$
$$\{\mathcal{D}^\phi[\alpha^i], \mathcal{D}^\phi[\beta^j]\} = \mathcal{D}^\phi\left[\mathcal{L}_{\alpha^i}\beta^j\right]. \tag{1.74}$$

Lastly, the brackets involving the different sectors of the Hamiltonian and diffeomorphism constraints are

$$\{\mathcal{D}[\alpha^i], \mathcal{H}[\alpha]\} = \mathcal{H}[\mathcal{L}_{\alpha^i}\alpha],$$
$$\{\mathcal{D}[\alpha^i], \mathcal{H}^\phi[\alpha]\} = \int d^3x \left\{\frac{1}{2}\frac{P^2}{\sqrt{h}}\nabla_i\alpha^i - \frac{1}{2}\sqrt{h}\nabla_k\phi\nabla^k\phi\nabla_i\alpha^i + \sqrt{h}\nabla_i\phi\nabla_j\phi\nabla^i f\alpha^j - \sqrt{h}V(\phi)\nabla_i\alpha^i\right\},$$
$$\{\mathcal{D}^\phi[\alpha^i], \mathcal{H}[\alpha]\} = 0,$$
$$\{\mathcal{D}^\phi[\alpha^i], \mathcal{H}^\phi[\alpha]\} = \int d^3x \left\{-\frac{P\alpha}{\sqrt{h}}\nabla_i\left(P\alpha^i\right) + \sqrt{h}\nabla_i\left(\alpha\nabla^i\phi\right)\alpha^j\nabla_j\phi - \sqrt{h}\frac{\partial V(\phi)}{\partial\phi}\alpha\alpha^i\nabla_i\phi\right\}. \tag{1.75}$$

Combining these equations, it is now easy to write the off-shell algebra of constraints:

$$\{\mathcal{H}_{\mathrm{T}}[\alpha], \mathcal{H}_{\mathrm{T}}[\beta]\} = \mathcal{D}\left[\lambda F'^2(R + \lambda\Pi/h)h^{ij}(\beta\partial_j\alpha - \alpha\partial_j\beta)\right] + \mathcal{D}^\phi\left[h^{ij}(\beta\partial_j\alpha - \alpha\partial_j\beta)\right],$$
$$\{\mathcal{D}_{\mathrm{T}}[\alpha^i], \mathcal{H}_{\mathrm{T}}[\alpha]\} = \mathcal{H}_{\mathrm{T}}\left[\mathcal{L}_{\alpha^i}\alpha\right],$$
$$\{\mathcal{D}_{\mathrm{T}}[\alpha^i], \mathcal{D}_{\mathrm{T}}[\beta^j]\} = \mathcal{D}_{\mathrm{T}}[\mathcal{L}_{\alpha^i}\beta^j]. \tag{1.76}$$

The only change in the off-shell algebra of constraints (1.76) with respect to the vacuum case appears in the Poisson bracket $\{\mathcal{H}_{\mathrm{T}}[\alpha], \mathcal{H}_{\mathrm{T}}[\beta]\}$. That this Poisson bracket is no longer proportional to any of the primary constraints (1.71) or secondary constraints (1.72) implies the existence of a tertiary constraint

$$\lambda F'^2 \mathcal{D}_i + \mathcal{D}_i^\phi = 0. \tag{1.77}$$

This is an independent combination of the two sectors of the diffeomorphism constraint $(\mathcal{D}_{\mathrm{T}})_i = 0$. Therefore we take as independent constraints

$$(\mathcal{D}_{\mathrm{T}})_i = 0, \qquad \mathcal{D}_i^\phi = 0. \tag{1.78}$$

The constrain $\mathcal{D}_i^\phi = P \partial_i \phi = 0$ does however not satisfy the regularity conditions [68] that are needed in order to proceed with the standard counting of degrees of freedom. As explained in [68], the matrix obtained by taking the derivatives of the constraint with respect to the variables in the phase space must have constant rank on the constraint surface.

Therefore, we have to choose either $P = 0$ or $\partial_i \phi = 0$. Let us discuss each of these cases separately:

- $P = 0$: first of all, consistency with the dynamical evolution implies

$$\{P, H_{\mathrm{T}}\} = \{P, \mathcal{H}^\phi[N] + \mathcal{D}^\phi[N^i]\} = \sqrt{h} \partial_i (N \partial^i \phi) - \sqrt{h} N \frac{\partial V}{\partial \phi} = 0. \tag{1.79}$$

This leads to a quaternary constraint, the smeared version of which reads

$$\mathcal{C}[\mu] = \int \mathrm{d}^3 x \sqrt{h} \, \mu \left[\partial_i (N \partial^i \phi) - N \frac{\partial V}{\partial \phi} \right]. \tag{1.80}$$

The complete Hamiltonian is therefore given by

$$H_{\mathrm{T}} = \int d^3 x \, N(\mathcal{H} + \mathcal{H}^\phi) + N^i (\mathcal{D}_i + \mathcal{D}_i^\phi) + \lambda_N \pi_N + \lambda^i \pi_i + \lambda_P P + \lambda_\mathcal{C} \mathcal{C}. \tag{1.81}$$

From all the constraints, $\mathcal{H} + \mathcal{H}^\phi$, π_N, P and $\mathcal{C}$ are second-class constraints. This implies that the phase space is 5-dimensional, similarly to what happens in Hořava-Lifshitz gravity [69, 70]. Therefore ϕ cannot describe standard matter degrees of freedom.

- $\phi - f(t) = 0$: we impose this form of the constraint (instead of $\partial_i \phi = 0$) in order to ensure a more direct matching between the constraints and the degrees of freedom removed. Again, consistency with the dynamical evolution implies

$$-\dot{f} + \{\phi, H_{\mathrm{T}}\} = -\dot{f} + \frac{NP}{\sqrt{h}}, \tag{1.82}$$

where $\dot{f} = \mathrm{d}f/\mathrm{d}t$. Similarly to the previous situation, these two additional constraints, together with $\mathcal{H} + \mathcal{H}^\phi$ and π_N, are second-class constraints. The counting of degrees of freedom is therefore the same as in the example just above.

Summarizing, coupling a scalar field in a minimal way can only be consistent if the scalar field is constrained. Therefore, this scalar field cannot be used to describe standard matter. Introducing an unconstrained scalar field would only be possible at the cost of explicitly breaking the symmetries of the gravitational action, hence exciting additional degrees of freedom (let us note that something similar would happen if a scalar field is coupled to general relativity in a way that diffeomorphism invariance is not preserved.).

This result would apply to any kind of field that is minimally coupled. Therefore, in order to compare these theories with general relativity coupled to matter (or to explore their possible phenomenological consequences), first of all one must find how to couple consistently matter to these theories in a way that no constraints have to be satisfied by the matter fields. In the two next sections we discuss briefly two attempts at achieving this.

1.6   Conclusions

In this chapter, we have presented a comprehensive analysis of the class of theories found in [29], which are characterized by the fact that these contain the same number of degrees of freedom as general relativity. We have used a battery of techniques in order to gain an intuition of the physical meaning of the existence of these theories. First of all we need to count the number of degrees of freedom using the Hamiltonian analysis. Once we know that there are only 2 degrees of freedom, we can use the Lagrangian formulation of the theory expanding around Minkowskii spacetime to study the linear polarization state of the graviton and the three point function. This analysis shows that, while the theory is apparently Lorentz breaking, the polarization state and the three point function are Lorentz covariant and equal to the general relativity counterpart. This feature allows us to construct the spinor helicity variables in the standard way and to use the recursion relation to construct higher order point function. This shows how intertwined the three steps of our analysis are as each step could not be applied without the previous one.

Our main conclusion is that these results strengthen the view that general relativity is a unique theory that is not easily deformed. This claim follows from a combination of results:

- There are certainly examples that are manifestly different from general relativity (as explained in Sec. 1.4). However, these examples entail profound deviations from general relativity; either these are too trivial to describe gravity and experimentally excluded, or it is not clear if these really have only two degrees of freedom, as it does not seem possible to ensure that the removal of additional degrees of freedom is protected under radiative corrections.

- The most interesting theories would exhibit the same linearized properties of general relativity (perhaps at low energy), but would include non-linear deviations from the latter. The formalism developed in [29] is general enough to encompass these theories, and we have studied in Secs. 1.1 and 1.2 quite general families of theories that would seemingly fall into this category. However, every attempt to show differences with respect to general relativity has only demonstrated the existence of unexpected cancellations that eventually dissipate the possible sources of these differences. This has been shown to occur on-shell, both at the linear and non-linear level.

Our analysis agrees with the one present in [71] where the author from a different perspective obtains the same result. These conclusions do not imply that the class of theories found in [29] is not interesting. On the contrary, we think that the results by

these authors provide a convenient framework in which a series of new questions about the possibility of deforming general relativity can be formulated.

Furthermore, the equivalence of the theories only holds in vacuum and matter can break it. As we have shown, it is not consistent to use minimal coupling, and in [71] it has been shown that there are consistent ways to couple matter, which can also break the equivalence with general relativity. While it is not clear if this would simply be equivalent to consider general relativity with non minimally coupled matter, working with a modified theory can provide a guiding principle in the choice of a matter coupling that would otherwise seem unnatural in general relativity. It has been shown, for instance, that one example of minimally modified theory has very interesting cosmological consequences [72].

The main focus of this thesis is the study of black holes, specifically we try to get insight toward the resolution of the singularity problem. Given that black holes are vacuum solutions of general relativity, we already know that the family of minimally modified theories possess singular solutions. Anyway, it is still an open and interesting question of whether these solutions will unavoidably be reached in the dynamical evolution of the theory as it happens in general relativity. It other words, we still do not know is the differences in the matter sector of the theory could prevent the formation of singularities or if there is a singularity theorem also in these theories. This possibility will be addressed in future works.

Chapter 2

Causal hierarchy beyond general relativity.

Working with a specific theory has many advantages as it allows you to have full control over the model. However, in this case, the range of applicability of the results is limited to the theory under consideration. In what follows we will try to be as much model independent as possible. In this chapter we are going to study the requirements that causality conditions can impose on the manifold in a generic theory of modified gravity.

In general relativity there is a is well-established standard causal hierarchy, key elements of which are chronology, causality, strong causality, stable causality, and global hyperbolicity. Here we investigate how to extend this causal hierarchy depending on the extra structure (such as: multiple metrics, aether fields, modified dispersion relations, Hořava-like gravity, parabolic propagation, etcetera) that the modified theory can have. This chapter contains some of the results of **P7**.

2.1 The standard general relativity causal hierarchy

In general relativity one can invoke a well-established hierarchy of causality conditions which is explained in detail both at a pedagogical level [73, 19] and at a more formal level [74].
Let us briefly review these definitions as our goal is to extend them to a more generic framework. The two more basic levels of the causal hierarchy are:

- **Chronology condition**: There are no closed timelike curves.

- **Causality condition**: There are no closed non-spacelike curves.

The absence of closed timelike curves is needed to forbid time travel. Closed null curves are less problematic, but it is usually possible to deform a null closed curve in order to construct a timelike closed curve [74] and, even when this is not possible, we can imagine to slightly perturb the manifold to end up with a closed timelike curve. For this reasons, it is desirable to forbid closed null curves as well.
Strong causality is the next step in the usual hierarchy. There are more than one way to characterize strong causality (see **P7**). The simplest one is the following: For

any point x there is an open set U such that any causal curve that starts at x and then leaves U cannot ever re-enter U. What that means is that not only closed causal curve are forbidden, but also that non-spacelike curves cannot return arbitrary close to their starting point.

The set of causality conditions we have introduced so far ensures the absence of pathologies in the spacetime we are considering. Given that we are interested in theories where the spacetime is a dynamical object, we can always perform a small perturbation of our spacetime. Therefore we may also want to rule out those spacetimes that are arbitrary close to violating the hierarchy of causality conditions above. To this end, we construct a partial ordering on the space of Lorentzian metrics $\mathbb{L}(M)$ by saying that one metric $[\hat{g}]_{ab}$ is "wider" than another second metric $[g]_{ab}$, denoted $[\hat{g}]_{ab} > [g]_{ab}$, if all non-spacelike vectors in the second metric are strictly timelike in the first metric. This partial ordering can be used to define open intervals in the set of all Lorentzian metrics, and these open intervals can be used to define a *sub-basis* for a topology on the set of Lorentzian metrics one can define on the spacetime manifold — this topology is called the interval topology and, for our purposes, it behaves as the typical C^0 open topology (different metrics become close to each other when their metric coefficients in some prescribed set of coordinates are close, even if their derivatives are not). For the discussion in the next section it will be important to keep in mind that, being a partial order, not every pair of metrics need to be comparable.

With this in mind, the next step in the hierarchy, the **stable causality condition**, can be defined in at least 3 equivalent ways:

- There exists a global time function $\tau(x)$ whose gradient is everywhere timelike. (So, adopting $- + ++$ signature, the vector $-g^{ab}\nabla_b\tau$ is future-pointing timelike. This definition of stable causality implies that for any future-pointing timelike vector V^a one has $V^a\nabla_a\tau > 0$.)

- There is a metric wider than the physical metric such that the wider metric satisfies the chronology condition.

- There is an open set in the C^0 open topology on the set of all Lorentzian metrics which contains the physical metric and such that all of the metrics in that open set satisfy the chronology condition.

The second and the third statements are clearly equivalent as they are merely different ways of express the same physical concept. The proof that the first statement is equivalent to the other two is not trivial. While some discussion can be found in classical textbooks, see *e.g.* [73] for the equivalence between the first and second statement, or [19] for the equivalence between the first and third statement, some technical points are overlooked there and a for a complete proof we refer to [75].

Finally, the last step in the standard causal hierarchy, **global hyperbolicity**, can also be defined in at least 3 equivalent ways:

- (Causality condition) + (causal diamonds are compact).

- Wave equations with suitable initial data have unique solutions.

- The spacetime is foliated by spacelike Cauchy hypersurfaces.

For a technical discussion see references [75, 76]. We shall soon see that the last of these conditions, the existence of a foliation by suitably redefined and suitably modified Cauchy hypersurfaces, is one of the more straightforward causality conditions to work with once one steps far beyond standard general relativity.

2.2 Multi-metric frameworks

Perhaps the most straightforward extensions of the usual causal hierarchy occur in multi-metric frameworks. Multi-metric extensions of general relativity have a long and quite complicated history — over the last decade one of the key examples of this type of model has been the dRGT "massive gravity" models [77, 78, 79, 80], though earlier attempts go back several decades [81]. Central to all of these models are multiple Lorentzian metrics $\{[g_i]_{ab}\}_{i=1}^N$ (some dynamical, some possibly non-dynamical background metrics) interacting in various ways.[1]

To extend the usual causal hierarchy to such a multi-metric framework at minimum one would want to apply the usual causal hierarchy to *each* effective metric separately, *and* to demand that you cannot violate causality by switching metrics $[g_i]_{ab}$ part way through whatever physical process you are interested in. Perhaps the simplest way to formulate this is to redefine the notion of chronological/causal curves as follows:

(i) A piecewise chronological curve is one that can be split into connected segments each one of which is timelike with respect to at least one of the metrics $[g_i]_{ab}$.

(ii) A piecewise causal curve is one that can be split into connected segments each one of which is non-spacelike with respect to at least one of the metrics $[g_i]_{ab}$.

With these definitions in place we can immediately generalize the chronology and causality conditions in multi-metric framework as follows:

- **Piecewise chronology condition**: There are no closed piecewise chronological curves.

- **Piecewise causality condition**: There are no closed piecewise causal curves.

We can similarly modify the definitions of chronological/causal past/future, and the definitions of chronological/causal diamonds, so as to define strong causality in terms of piecewise timelike curves.

It is useful to break down the piecewise chronology/causality conditions above into equivalent conditions that are often simpler to work with:

- The piecewise chronology condition being satisfied by $\{[g_i]_{ab}\}_{i=1}^N$ is equivalent to each of the individual metrics $[g_i]_{ab}$ independently satisfying the chronology condition, plus the compatibility condition between all the pairs of metrics that $I_i^+(p) \cap I_j^-(p) = \emptyset$, $\forall i, j \in [1, ..., N]$.

---

[1]Instead of thinking of the $\{[g_i]_{ab}\}_{i=1}^N$ as a set, sometimes it will be useful to think about these metrics as an element $([g_1]_{ab}, ..., [g_N]_{ab})$ of $\mathbb{L}(M)^N$, the Cartesian product of N copies of $\mathbb{L}(M)$.

- The piecewise causality condition being satisfied by $\{[g_i]_{ab}\}_{i=1}^N$ is equivalent to each of the individual metrics $[g_i]_{ab}$ independently satisfying the causality condition, plus the compatibility condition between all the pairs of metrics that $J_i^+(p) \cap J_j^-(p) = \emptyset$, $\forall i, j \in [1, ..., N]$.

In the multi-metric framework, there are different possible definitions of **piecewise stable causality** which suitably generalize the usual notion of stable causality. For instance, working in terms of a global time function:

A_1 : Each of the individual metrics $[g_i]_{ab}$ is stably causal, and in addition there exists a global time function τ whose gradient is everywhere future-pointing with respect to all of the individual metrics $[g_i]_{ab}$. That is, all of the vector fields $[V_i]^a$ that are future-pointing and timelike with respect to the appropriate individual metric $[g_i]_{ab}$ must satisfy $[V_i]^a \nabla_a \tau > 0$.

Thence a piecewise chronological curve, having a tangent vector V^a that is timelike with respect to at least one of the individual metrics $[g_i]_{ab}$, must satisfy $V^a \nabla_a \tau > 0$, and so cannot be closed. Thence, this definition implies that all the future-pointing propagation cones must lie on the same side of the constant-τ hypersurfaces.

Furthermore, the two definitions that rely primarily on the existence of the partial order $>$ also generalize naturally, as one just needs to replace $\mathbb{L}(M)$ by $\mathbb{L}(M)^N$, the latter equipped with the product order:

A_2 : There is an element in $\mathbb{L}(M)^N$ wider than the physical metrics $([g_1]_{ab}, ..., [g_N]_{ab})$ such that it satisfies the piecewise causal condition.

A_3 : There is an open set in the C^0 open topology on the set $\mathbb{L}(M)^N$ which contains the physical metrics $([g_1]_{ab}, ..., [g_N]_{ab})$ and such that all the elements in that open set satisfy the piecewise causal condition.

One can then show that these definitions are equivalent (see **P7** for a proof of this statement).

There is an alternative way of proceeding in case the set $\{[g_i]_{ab}\}_{i=1}^N$ satisfies some additional requirements. If there exists a metric in the set $\{[g_i]_{ab}\}_{i=1}^N$ that is wider than the rest, or if there exists a metric $[g_{\text{wide}}]_{ab}$ in $\mathbb{L}(M)$ that is wider than all the elements $\{[g_i]_{ab}\}_{i=1}^N$ (that is, the propagation cone of $[g_{\text{wide}}]_{ab}$ contains the union of all the propagation cones of the individual $[g_i]_{ab}$), then we can apply the usual definitions of general relativity the metric $[g_{\text{wide}}]_{ab}$:

B_1 : There exists a global time function whose gradient is everywhere timelike with respect to $[g_{\text{wide}}]_{ab}$.

B_2 : There is a metric wider than $[g_{\text{wide}}]_{ab}$ such that the wider metric satisfies the causality condition.

B_3 : There is an open set in the C^0 open topology on the set of all Lorentzian metrics which contains the metric $[g_{\text{wide}}]_{ab}$ and such that all of the metrics in that open set satisfy the causality condition.

It is also important to notice that, if $[g_{\text{wide}}]_{ab}$ exists, piecewise chronological/causal curves for $\{[g_i]_{ab}\}_{i=1}^N$ are just ordinary chronological/causal curves of $[g_{\text{wide}}]_{ab}$.

Hence, we have two triplets of definitions $\{A_i\}_{i=1}^3$ and $\{B_i\}_{i=1}^3$ providing slightly different characterizations of stable causality, which are not equivalent in general. It is straightforward to realize that the equivalence between these triplets requires (at a minimum) the existence of $[g_{\text{wide}}]_{ab}$. However, there is a situation which, besides from making these two characterizations comparable from the perspective of logical implication, is interesting from a physical standpoint, namely when $\{[g_i]_{ab}\}_{i=1}^N$ is a totally ordered set with respect to $>$. Under this assumption, the two triplets are indeed equivalent, as shown in reference **P7**. Intuitively, one can see that the necessary condition mentioned above for these being equivalent is satisfied, as $\{[g_i]_{ab}\}_{i=1}^N$ being totally ordered implies that $[g_{\text{wide}}]_{ab}$ can be identified with the maximal element in $\{[g_i]_{ab}\}_{i=1}^N$.

When it comes to **global hyperbolicity** all of the 3 standard versions of this notion can easily be adapted to the multi-metric framework, although again there are two possible versions which are not fully equivalent in general:

C_1 : Causality condition + causal diamonds are compact; (use piecewise causal curves).

C_2 : For each individual metric $[g_i]_{ab}$ wave equations with suitable initial data have unique solutions.

C_3 : The spacetime is foliated by spacelike Cauchy hypersurfaces; where Cauchy now means spacelike with respect to each individual metric $[g_i]_{ab}$, and for each metric $[g_i]_{ab}$ the causal curves of that metric intersect the Cauchy surface once and once only.

Alternatively:

D_1 : Causality condition + causal diamonds are compact (use $[g_{\text{wide}}]_{ab}$).

D_2 : For the metric $[g_{\text{wide}}]_{ab}$ wave equations with suitable initial data have unique solutions.

D_3 : The spacetime is foliated by spacelike Cauchy hypersurfaces; where Cauchy now means spacelike with respect to the metric $[g_{\text{wide}}]_{ab}$, and the causal curves of that metric intersect the Cauchy surface once and once only.

These are the minimum requirements for reformulating the causal hierarchy in a multi-metric framework.

2.3 Infinite signal velocities

In some frameworks (for instance in Hořava gravity) we have that some of the modes propagates at infinite speed with respect to some aether covector field u_a (not at this stage necessarily hypersurface orthogonal). In this case:

- Define the analogue of chronological curves in terms of the tangent being future-pointing with respect to the aether, $t^a u_a < 0$. (No metric is required to establish this.)

- Define the analogue of causal curves in terms of the tangent being non-past-pointing with respect to the aether, $t^a u_a \leq 0$. (No metric is required to establish this.)

We shall first show that for infinite signal speeds sensible causal behaviour implies that the aether field has to be hypersurface orthogonal. We shall also show that for infinite signal speeds sensible causal behaviour implies that the aether field is unique.

2.3.1   Hypersurface orthogonality of the aether

To demonstrate the need for hypersurface orthogonality of the aether (in the presence of infinite signal velocity) suppose the the contrary — that aether is not hypersurface orthogonal, then its vorticity is nonzero: $\omega^a = \varepsilon^{abcd} u_b u_{[c,d]} \neq 0$. Pick any point p in the manifold and go to Riemann local coordinates, pointing u^a in the t direction, $(1, 0, 0, 0)$, and ω^a in the z direction, $(0, 0, 0, 1)$. Then

$$g_{ab} = \eta_{ab} + O([\delta x]^2); \qquad u_a = (-1; \omega y, -\omega x, 0) + O([\delta x]^2). \tag{2.1}$$

Here we note $|u|^2 = -1 + O([\delta x]^2)$ and $\omega^a = (0, 0, 0, \omega) + O([\delta x]^2)$.

Now in these coordinates consider the closed topologically circular curve

$$\mathcal{C}: \qquad x^a(\lambda) = \Big(0, r_* \cos(\theta(\lambda)), r_* \sin(\theta(\lambda)), 0\Big). \tag{2.2}$$

This curve has tangent vector

$$
\begin{aligned}
t^a(\lambda) &= \frac{dx^a(\lambda)}{d\lambda} \\
&= \Big(0, -r_* \sin(\theta(\lambda)), r_* \cos(\theta(\lambda)), 0\Big) \frac{d\theta}{d\lambda} \\
&= r_* \Big(0, -\sin(\theta(\lambda)), \cos(\theta(\lambda)), 0\Big) \frac{d\theta}{d\lambda}.
\end{aligned}
\tag{2.3}
$$

Meanwhile along this curve we have

$$u_a(\lambda) = \Big(-1; \omega r_* \sin(\theta(\lambda)), -\omega r_* \cos(\theta(\lambda)), 0\Big) + O(r_*^2). \tag{2.4}$$

Then

$$t^a u_a = -\omega \, r_*^2 \, \frac{d\theta}{d\lambda} + O(r_*^3). \tag{2.5}$$

As long as $\omega \neq 0$ we can choose r_* small enough to safely ignore the $O(r_*^3)$ term. Then choose the sign of $\frac{d\theta}{d\lambda}$ to be the same as the sign of ω and one has a closed chronological curve. Thus if $\omega \neq 0$ in the presence of infinite signal velocities the causal hierarchy fails at the very first step.

That is: to preserve the chronology condition in the presence of infinite signal speed the relevant aether field with respect to which infinite signal velocity is defined must have zero vorticity and so be hypersurface orthogonal. So we can set

$$u_a = -\frac{\nabla_a \tau}{||\nabla \tau||}. \tag{2.6}$$

2.3.2 Uniqueness of the aether field

Suppose now that we have two propagating modes, both with infinite signal speeds, but defined with respect to two distinct hypersurface orthogonal aether fields u_1^a and u_2^a. We want to show that $u_1^a = u_2^a$ if any sensible notion of causality is to survive. For the current argument it is good enough to work in flat Minkowski space. Pick any point p in spacetime and go to coordinates where $\frac{1}{2}(u_1^a + u_2^a)$ is pointing in the t direction, $(1, 0, 0, 0)$, and the spatial 3-vectors $(u_1)^i$ and $(u_2)^i$ are pointing in the $\pm x$ directions, $(\pm 1, 0, 0)$. Then for some $-1 < v < 1$ we have

$$g_{ab} = \eta_{ab}; \qquad (u_{1,2})_a = \gamma(-1; \pm v, 0, 0), \qquad (2.7)$$

where $\gamma = (1 - v^2)^{1/2}$ so that $|u_{1,2}|^2 = -1$.

Consider the closed circular curve

$$\mathcal{C}: \qquad x^a(\lambda) = \Big(0, r_* \cos(\theta(\lambda)), r_* \sin(\theta(\lambda)), 0\Big) \qquad (2.8)$$

with tangent vector

$$
\begin{aligned}
t^a(\lambda) &= \frac{dx^a(\lambda)}{d\lambda} \\
&= \Big(0, -r_* \sin(\theta(\lambda)), r_* \cos(\theta(\lambda)), 0\Big) \frac{d\theta}{d\lambda} \\
&= r_* \Big(0, -\sin(\theta(\lambda)), \cos(\theta(\lambda)), 0\Big) \frac{d\theta}{d\lambda}.
\end{aligned}
\qquad (2.9)
$$

Then

$$t^a(u_{1,2})_a = \pm \gamma \, v \, r_* \, \sin(\theta(\lambda)) \, \frac{d\theta}{d\lambda}. \qquad (2.10)$$

On each of the two half-circles $\theta \in (0, \pi)$ and $\theta \in (\pi, 2\pi)$ the curve will be chronological, $(t^a u_a < 0)$, with respect to either one or the other aether fields. At $\theta = 0$ and $\theta = \pi$ the curve is still causal ($t^a u_a \leq 0$, in fact $t^a u_a = 0$). But this means one has a closed causal curve with two chronological sections — so you can send messages into your own past. The only way to avoid this serious violation of the causality condition is to set $v = 0$, that is, for the two aether fields to coincide.

Causal structure

Hence in the presence of infinite signal velocities the preservation of even the most basic notions of causality implies that there is a global time function $\tau(x)$ whose normalized gradient (2.6) is unique and causally well-behaved in the sense described below:

- Define the analogue of chronological curves in terms of the tangent being future-pointing with respect to the global time function, $t^a \nabla_a \tau > 0$.

- Define the analogue of causal curves in terms of the tangent being non-past-pointing with respect to the global time function, $t^a \nabla_a \tau \geq 0$.

With these definitions there automatically are no closed chronological curves — thence a variant of the chronology condition is built into this formalism.

There *are* closed causal curves (infinite speed communication) but this is not a problem since by assumption there is a unique global time function to keep things under control. The presence of closed causal curves also implies that strong causality is violated.For infinite signal velocities stable causality needs significant revision. In fact there is certainly by construction no "wider" metric to deal with.)
Finally,the concept of global hyperbolicity needs significant revision and it needs to be replaced by some stronger requirement.

In fact we need to introduce the new concept of *global parabolicity*, which is now defined as demanding a foliation by (parabolic) Cauchy hypersurfaces (crossed by chronological curves once and once only). This implies in particular that for any point x we demand that $I^+(x) \cup I^-(x) \cup \tau^{-1}(x)$ is the entire spacetime, so that diffusion equations with suitable initial data (on any fixed but arbitrary slice of the preferred foliation) have unique solutions.

2.3.3   Universal horizons

Working in Hořava-like models (the key ingredients being the existence of a preferred foliation *and* infinite signal velocity) leads to a new concept — that of a *universal horizon* [82, 83, 84]; see also references [85, 86].
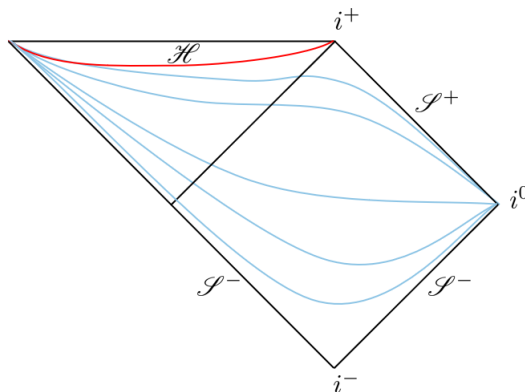

Figure 2.1: Carter–Penrose diagram describing a universal horizon. The diagram shows several constant-chronon hyper-surfaces, (leaves of the preferred foliation), with the red line depicting the universal horizon.

The most basic form of universal horizon arises in static and spherically symmetric situations iff the gradient of the chronon is anti-parallel to the gradient of the radial coordinate, $\nabla_a \tau = -\chi^2 \nabla_a r$. They also appear in slowly rotating black hole solutions in Hořava gravity [87]. If this happens, then for any chronological curve the tangent vector, by definition satisfying $t^a \nabla_a \tau > 0$, also satisfies $t^a \nabla_a r < 0$. Thus all chronological curves are trapped and forced to move "inwards". Thence the universal horizon is a constant chronon hypersurface, (a leaf of the preferred foliation), that is simultaneously a constant r hypersurface. See figure 2.1.

To properly define "static" one also needs to have a metric g_{ab} available, in order to map the Killing vector into a covector, $K_a = g_{ab} K^b$, to which one can apply the hypersurface orthogonality constraint. One also needs the metric to define the notion of the Killing vector being timelike (sufficiently far away from the black hole region). Under these conditions the static Killing vector is 4-orthogonal to ∇r, and so the universal horizon can equally well be defined by $K^a \nabla_a \tau = 0$, see [85]. Moreover since the static Killing vector is hypersurface orthogonal it induces a natural "Killing time" coordinate, t, in terms of which we have $K_a \propto \nabla_a t$. So at the universal horizon one has $g^{ab} \nabla_a \tau \nabla_b t = 0$; that is, gradients of the "chronon time" and "Killing time" are 4-orthogonal (note however that $\nabla_a t$ is spacelike inside the Killing horizon).

Because one has a Lorentzian metric g_{ab} available, one can introduce the usual notions of i^-, i^0, and i^+, and also $\mathscr{I}^\pm$. Asymptotically, as one moves "outwards" on the constant chronon hypersurface corresponding to the universal horizon one must approach i^+. (This is not what one would naively expect in "normal" situations, an asymptotic approach to i^0. See figure 2.1. This observation can be modified to develop a general definition of universal horizon.)

A generic condition for defining a universal horizon is that it is a constant-chronon leaf of the preferred spacetime foliation that contains i^+. So a universal horizon would not be a Cauchy hypersurface, since causal curves that intersect $\mathscr{I}^+$ would not necessarily intersect the universal horizon. In contrast, under "normal" conditions constant-chronon leaves of the preferred spacetime foliation asymptote to i^0; so they would be Cauchy hypersurfaces. This compatible with the constructions developed in [85].

Now is the universal horizon a Cauchy horizon? This depends, very delicately, on precise technical definitions. The key thing about Cauchy horizons is that something odd is happening to the "initial data" needed to define time-evolution into the future. Is there something odd with universal horizons? One issue is this: Since i^+ lies on the universal horizon, then anything outside the universal horizon can influence physics at i^+. But then given the assumed infinite signal speeds used to define the universal horizon, *anything anywhere* in the domain of outer communication can influence physics anywhere on the universal horizon. This is certainly odd behaviour.

More precisely — the leaves of the preferred foliation before formation of the universal horizon all asymptote to i^0, and so to get a well-defined Cauchy problem at worst one needs to impose some regularity condition at spacelike infinity i^0. In contrast, after the universal horizon forms one needs new extra "initial data" (corresponding to some regularity condition at future timelike infinity i^+) in order to set up a well-defined Cauchy problem. It is in this precise technical sense that the universal horizon can be considered to be a Cauchy horizon.

There are various ways of rephrasing this in a more formal manner. For instance: If x lies on a universal horizon then $J^-(x) = J^-(i^+)$. Furthermore, if the event x precedes formation of the universal horizon, then $x \in I^-(i^+)$ and $\mathscr{I}^+ \subset I^+(x)$. The overall message is clear: Preferred foliations combined with infinite signal speeds lead to unusual but internally consistent notions of causal hierarchy.

2.4   Conclusions

The framework we have developed above allows one to mathematically extend the usual Lorentzian causal hierarchy to multi-metric spacetimes, Einstein-aether models, Hořava-like spacetimes, modified dispersion relations, and parabolic PDEs. The key dividing point in the analysis is whether the signal velocity is finite or infinite. When the signal speed is finite, a variant of the usual general relativistic causal hierarchy can be formulated. When the signal speed is infinite, a significantly modified causal hierarchy must be formulated in terms of a global time function (chronon). Preserving even minimal notions of causality in the presence of infinite signal velocity requires the aether field to be both unique and hypersurface orthogonal, leading us to introduce the notion of global parabolicity. Either case provides a logically coherent framework for dealing with "superluminal" signalling while still maintaining a consistent approach to causality.

For every scenario that we have considered, global hyperbolicity is a necessary condition for a well defined notion of causality, even if in some cases it is not a sufficient conditions and stronger constraints have to be imposed. For this reason, in the next chapter, where we are going to study the singularity problem with the minimum possible number of assumption, we will assume that the manifold is globally hyperbolic.

Chapter 3

Geodesically complete black holes

In this chapter we will adopt an agnostic approach and look directly where the deviations from general relativity may arise. This means that instead of focusing on a particular modified theory, we are going to directly look at the problem of the black hole singularities, which is expected to be resolved once that quantum gravity effects are taken into account. This will allow us to obtain less stringent but more general results. We will not impose any particular quantization scheme of the gravitational field and, using Penrose's singularity theorem as guidance, which tells us that singularities are inevitable in general relativity under specific conditions imposed on matter fields, we will perform a systematic analysis of the possible non-singular spacetimes with a trapping horizon. Such analysis will be blind to the dynamics (classical, semi-classical, or quantum) of a specific theory and will only assume a minimal set of kinematical requirements. This feature makes our analysis quite general and applicable to any theory of quantum gravity that satisfies the aforementioned kinematical requirements in a certain regime, and virtually to any theory of modified gravity. It is possible to schematically divide Penrose's theorem into two part: In the first part of the theorem, the weak energy condition and the Einstein fields equations together with geodesic completeness are used in order to prove the existence of a focusing point (see Fig. 3.1), then, considerations of a purely geometrical nature are used in order to prove that the existence of a focusing point is actually incompatible with the topology of spacetime [17]. Hence, in order to understand the possible geometries that follow from the violation of either the weak energy condition or the Einstein fields equations, we just need to categorize in geometric terms the possible ways in which the focusing point can be avoided. This chapter is based on reference **P6**, and it is organized as follows. In Sec. 3.1 we briefly review the original Penrose singularity theorem and explain in depth the rationale of our analysis. In Sec. 3.2, we explain the geometrical setting that we will be using and prove some results that will be important for the subsequent discussion. Our main results are formalized in Sec. 3.3, where we categorize and discuss the possible geometries. Finally Sec. 3.4 contains a brief discussion of our main conclusions.
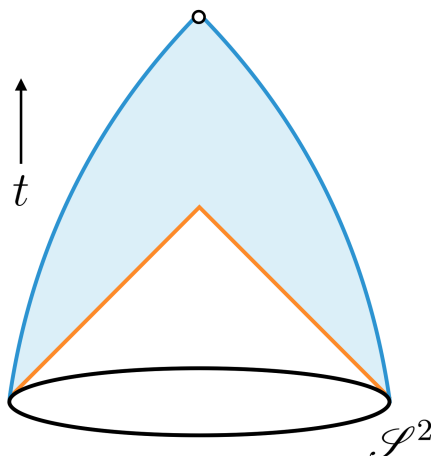
Figure 3.1: Pictorial representation of the formation of a focusing point. Such a focusing point is not compatible with the topology of spacetime.

3.1   Avoiding singularities: Beyond Penrose's theorem

Penrose's singularity theorem [17], and its modern variants and extensions (see for instance [88]), demonstrates that once a trapped surface $\mathscr{S}^2$ is formed, then in some region of spacetime contained in the causal future $J(\mathscr{S}^2)$ of $\mathscr{S}^2$, one of the following must hold in order to avoid a spacetime singularity (more precisely, to avoid that the spacetime is geodesically incomplete.):

(a) The weak energy condition is violated.

(b) The Einstein field equations do not hold.

(c) Pseudo-Riemannian geometry does not provide an adequate description of spacetime.

(d) Global hyperbolicity breaks down.

These options span a huge space of possibilities that are very difficult (if not impossible) to describe exhaustively. Our goal is to gain a complete understanding of the information that pseudo-Riemannian geometry may contain about theories that go beyond general relativity, and regularize the singularities of the latter. Accordingly, we will work in a framework where we *ab initio* impose the minimal conditions that:

(1) Pseudo-Riemannian geometry provides an effective description of spacetime;

(2) The spacetime is globally hyperbolic.[1]

---

[1]Note that Penrose's theorem also assumes that the Cauchy surface is non-compact. As explained in [89] the non-compact assumption can be relaxed by assuming the existence of at least one future inextendible curve from the Cauchy surface $\mathscr{C}^3$ which does not intersect the causal future of the trapping surface. We implicitly assume that this is realized, as it corresponds to the very physically reasonable assumption that there exists at least one observer which does not fall into the collapsing star;

(3) The spacetime is geodesically complete;

(4) There are no curvature singularities.[2]

On the other hand, we will accept that both (a) and (b) in Penrose's list of possibilities can take place, perhaps simultaneously. We will see that the geometric structure assumed in (1), (2), (3) and (4) above is tight enough to leave only a handful of possibilities.

Among this assumptions, the first one is arguably the most controversial one. It is reasonable to think that in a theory of quantum gravity spacetime may lose its smoothness in certain situations, so that a description in terms of differentiable manifolds breaks down. Anyway, if this happens in a bounded region, it seems always possible to devise a classical geometry that matches the physical one at the boundary of this non-classical region; while one does not expect this effective classical description to provide a precise description of the non-classical regime, it may capture some of the relevant physics of the transition through this region.

Even more importantly, advances in frameworks such as loop quantum gravity, loop quantum cosmology and asymptotic safety show that a description in terms of an effective metric provides a good approximation in many situations [94, 95, 96, 97, 98, 99], so that, for a large sector of initial conditions for the quantum state of the system, the description in terms of differentiable manifolds remains meaningful throughout dynamical evolution. Whether these initial conditions are relevant to describe physical situations of interest in black holes (where several technical issues remain to be solved [100, 101, 102]) is unclear at the moment but, regardless of this issue, we think that there is no question that effective descriptions in terms of differentiable manifolds can provide useful illustrations of the physics at play.

Finally, it might be useful to study the difficulties that arise trying the regularize the spacetime while maintaining pseudo Riemannian geometry even if this description breaks down in some region of spacetime, as the analysis can provide insight on where this description has to break down.

The other assumptions on our list are less debatable. Once that we have accepted that pseudo-Riemannian geometry provides a good description of the spacetime, we need to impose some causality requirements on the manifold. As discussed in chapter 2, global hyperbolicity might not be enough to guarantee a regular causal structure beyond general relativity, but it is definitely a necessary condition.

Finally, conditions (3) and (4) are simply two different (and non equivalent) ways to impose the absence of singularities.

Let us note that some of these assumptions have been widely used in previous explorations of singularity regularization in black holes [103, 104, 105, 106, 107, 108, 109, 110, 111, 112, 113, 114, 115]; however, it is worth remarking that global hyperbolicity is violated in static regular black holes (we will discuss this explicitly in due course). What makes our approach novel, and more powerful, is that all these works assume additional postulates in order to select specific realizations of non-singular spacetimes, while here we want to provide a complete catalogue of possibilities based only on geometric notions. Our study can be understood as a supplement to Penrose's theorem

---

[2]It is worth mentioning the existence of works in the literature in which assumption (2) holds but this one is dropped, such as [90, 91, 92, 93].

that goes a step beyond and characterizes all the spherically symmetric geometries that avoid the formation of focusing points while satisfying (1–4) above.

3.2 Geometric setting

Let us start with some geometric preliminaries. We will be dealing with a 4-dimensional and globally hyperbolic spacetime $\mathscr{M}$, with $t : \mathscr{M} \to \mathbb{R}$ a global time function and $\mathscr{C}^3$ a Cauchy surface. Additionally, our spacetimes of interest describe the collapse of a regular distribution of matter from a given initial Cauchy surface with topology $\mathbb{R}^3$. It is important to note that this fixes the topology of all the Cauchy hypersufaces of entire manifold as our assumptions are incompatible with topology change [116, 117, 118]. It is also useful to restrict the initial discussion to spherically symmetric spacetimes, postponing for future works the discussion of the more general setting in which this assumption is dropped. Let us recall the standard property that the isometry group of a spherically symmetric spacetime permits to identify a foliation in 2-spheres S^2. Furthermore, spherical symmetry allows us to prove the following auxiliary result:

Proposition 1: Under the assumptions (1–4) above, the entire manifold $\mathscr{M}$ can be covered with a single coordinate chart in which all points $p \in \mathscr{M}$ are labelled using double null coordinates (associated with radial null geodesics) and two angular coordinates.

Proof: Due to the existence of a local light-cone structure and the dimensionality of $\mathscr{M}$, through every point p in the manifold there are exactly two future-directed radial null geodesics (which we will call in the following left-going and right-going) and two past-directed radial null geodesics (their continuation to the past of p). Global hyperbolicity implies that either the two future-directed or the two past-directed causal curves through p must intersect $\mathscr{C}^3$. As there are only two such geodesics for each p, we can use these (together with the two angular coordinates on the unit 2-sphere) in order to label all points in spacetime, as long as these labels are unique. In order to show that these labels are unique, let us demonstrate that any situation in which these are not unique is inconsistent with our assumptions. For two points $p, q \in \mathscr{M}$, with $p < q$, let us define their causal diamond $\mathscr{D}(q, p)$ as the intersection between the causal future of p and the causal past of q, namely $\mathscr{D}(q, p) = J^-(q) \cap J^+(p)$ (for fixed values of the angular coordinates). If the two radial null geodesics crossing at p and intersecting $\mathscr{C}^3$ also cross at q, the boundary of $\mathscr{D}(q, p)$ is smooth except at the points p and q; in other words, the sides of the diamond are smoothed, as each of them are identified with segments of a left-going and right-going radial null geodesic, respectively. This smoothing implies the existence of at least two points in the boundary of $\mathscr{D}(q, p)$ in which the light cones in the corresponding tangent spaces are degenerate, as Σ^2 is simply connected. Let us consider for instance the side of the diamond generated by the left-going radial null geodesic; it is clear that there exist right-going null geodesics that cross the former at two points, but also other right-going null geodesics without crossing points (this is also true for smaller segments of the left-going radial null geodesic). Smoothness implies the existence of an intermediate right-going radial null geodesic that is tangent to the segment of the corresponding left-going radial null geodesic at one point at least; the light cone at this point would be then degenerate. ∎

The areas of the 2-spheres preserved by rotations are geometric invariants which, in
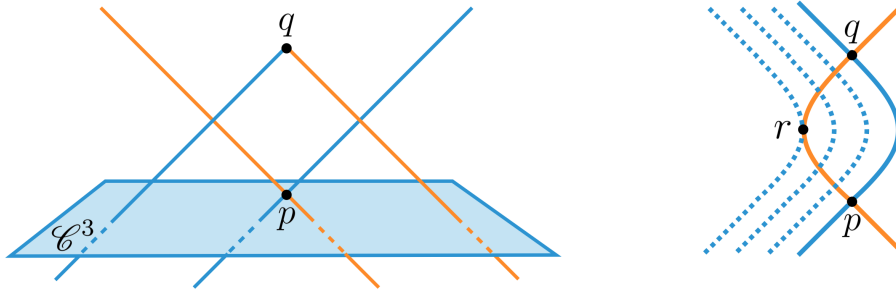
Figure 3.2: *On the left:* Left-going and right-going radial null geodesics that can be used to label two points p and q in spacetime, and the corresponding causal diamond. *On the right:* The curved lines between p and q illustrate the hypothetical situation discussed in **Proposition 1**, where the sides of the causal diamond are smoothed. The dashed lines mark some additional radial null geodesics, illustrating that the light-cone structure of spacetime becomes degenerate on two points along these sides (for graphical simplicity we are just including one of these points, $r \in \mathscr{M}$).

turn, provide a suitable definition for the radial coordinate r in these spacetimes. We will often use the coordinates (v, r) and (u, r) (in the following, we omit the angular coordinates) instead of (u, v). For instance, in the former case we always write the line element, without loss of generality, as

$$\mathrm{d}s^2 = -e^{-2\phi(v,x)}F(v,x)\mathrm{d}v^2 + 2e^{-\phi(v,x)}\mathrm{d}v\mathrm{d}x + r^2(v,x)\mathrm{d}\Omega^2, \qquad (3.1)$$

where $\mathrm{d}\Omega^2$ is the line element on the unit 2-sphere. The function $r(v, x)$ may be, for v fixed, bijective. In this case, we can perform a change of coordinates in order to write

$$\mathrm{d}s^2 = -e^{-2\phi(v,r)}F(v,r)\mathrm{d}v^2 + 2e^{-\phi(v,r)}\mathrm{d}v\mathrm{d}r + r^2\mathrm{d}\Omega^2. \qquad (3.2)$$

Even if $r(v, x)$ for v fixed does not provide a bijective relation between r and x, we can always find open subsets in the domain of $r(v, x)$ in which a bijective relation exists. Hence, we would at worst have different coordinate charts in each of which the line element has the form given above in Eq. (3.2), covering different regions of spacetime.

As in Penrose's theorem, we will assume the existence of a spacelike trapped surface $\mathscr{S}^2$, defined using the null vector fields that are normal to it. Due to the dimensionality of $\mathscr{M}$ and $\mathscr{S}^2$, and the spacelike character of the latter, there are two independent (future-directed) normal null vectors at each point of $\mathscr{S}^2$, that we will call $\boldsymbol{l}$ (outgoing null normal) and $\boldsymbol{k}$ (ingoing null normal). If h_{ab} is the 2-metric induced on $\mathscr{S}^2$, we can define the expansions along these vector fields as

$$\theta^{(\boldsymbol{X})} = \frac{1}{\sqrt{h}}\,\mathcal{L}_{\boldsymbol{X}}\sqrt{h} = h^{ab}\nabla_a X_b, \qquad \boldsymbol{X} \in \{\boldsymbol{l}, \boldsymbol{k}\}, \qquad (3.3)$$

where $\mathcal{L}_{\boldsymbol{X}}$ is the Lie derivative along $\boldsymbol{X}$, $h = \det(h_{ab})$ and $\boldsymbol{\nabla}$ is the 4-dimensional covariant derivative. The expansion $\theta^{(\boldsymbol{X})}$ measures the local change in the area of $\mathscr{S}^2$

under a local deformation along the vector field $\boldsymbol{X}$. Then, a trapped surface is defined by the conditions

$$\theta^{(\boldsymbol{k})} < 0, \qquad\qquad \theta^{(\boldsymbol{l})} < 0. \tag{3.4}$$

This definition connects naturally with quasi-local characterizations of the boundary of black holes. Although for the discussion in this chapter we only need the existence of a trapped surface, it is worth keeping in mind that the geometries that we will be analyzing display the same quasi-local properties as a black hole only for finite (in some cases very large) periods of time, but without necessarily sharing their global properties, or other features such as the existence of spacetime singularities. The study of these quasi-local properties has been a very active area of research during the last two decades and there are many published works [119, 120, 121, 122, 123, 124, 125, 126, 127, 128, 129], as well as several reviews [130, 131, 132] available. One of these quasi-local concepts is that of a *future outer trapping horizon* [120]: a 3-dimensional hypersurface $\mathscr{H} = \bigcup_{t \in \mathbb{R}} \mathscr{S}_t$ of $\mathscr{M}$ that is foliated by closed and spacelike 2-dimensional surfaces $\mathscr{S}_t$ satisfying $\theta^{(\boldsymbol{k})} < 0$ and $\theta^{(\boldsymbol{l})} = 0$, which can be understood as the limiting (or marginal) case of a trapped surface. There is the additional condition $\mathscr{L}_{\boldsymbol{k}} \theta^{(\boldsymbol{l})} < 0$ which guarantees that the spacetime around the horizon $\mathscr{H}$ has the quasi-local structure associated with the outer horizon of a black hole [120], in contradistinction to the inner horizon that appears in charged and rotating black holes. In particular, this third condition implies the existence of trapped surfaces arbitrarily close (from inside) to the marginally trapped surface which, again, is the main ingredient that we need for our discussion.

3.3   Taxonomy of non-singular geometries

We are now almost in position to formulate our central thesis, but before doing so, we still need to demonstrate another auxiliary result:

Proposition 2: If a congruence of outgoing radial null geodesics has a focusing point at a finite affine distance $\lambda = \lambda_0$, then $\theta^{(\boldsymbol{l})}\big|_{\lambda = \lambda_0} = -\infty$.

Proof: Let us recall that the expansion $\theta^{(\boldsymbol{l})}$ measures the rate of change of the element of area that is normal to the congruence of outgoing null geodesics [133], namely

$$\theta^{(\boldsymbol{l})} = \frac{1}{\delta A^{(\boldsymbol{l})}} \frac{\mathrm{d}}{\mathrm{d}\lambda} \delta A^{(\boldsymbol{l})}, \tag{3.5}$$

where $\delta A^{(\boldsymbol{l})}$ is the cross-sectional area of the congruence and λ the affine parameter along the congruence. If we choose the available freedom in the definition of the affine parameter so that $\lambda = 0$ corresponds to $\mathscr{S}^2$, we then have

$$\ln\left(\frac{\delta A^{(\boldsymbol{l})}\big|_{\lambda=\lambda_0}}{\delta A^{(\boldsymbol{l})}\big|_{\lambda=0}} \right) = \int_0^{\lambda_0} \mathrm{d}\lambda\, \theta^{(\boldsymbol{l})}(\lambda). \tag{3.6}$$

By construction, the quantity $\delta A^{(\boldsymbol{l})}\big|_{\lambda=0}$ is finite and positive. If there is a focusing point at $\lambda = \lambda_0$, $\delta A^{(\boldsymbol{l})}\big|_{\lambda=\lambda_0} = 0$, and the logarithm goes to infinitely negative values. Using the bound

$$\left| \int_0^{\lambda_0} \mathrm{d}\lambda\, \theta^{(\boldsymbol{l})}(\lambda) \right| \leq \lambda_0 \sup_{\lambda \in [0,\lambda_0]} \left| \theta^{(\boldsymbol{l})}(\lambda) \right|, \tag{3.7}$$
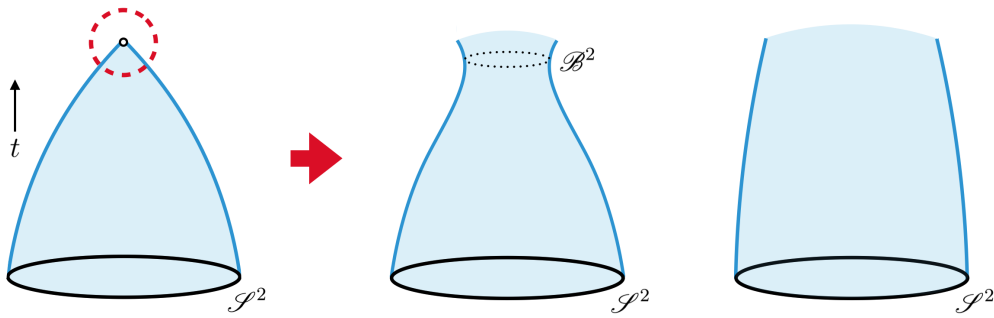
Figure 3.3: In order to avoid that the spacetime is geodesically incomplete, the space-time geometry must be modified in the surroundings of the focusing point in Penrose's theorem, so that either a defocusing point is created at a finite affine distance (thus also creating the 2-surface $\mathscr{B}^2$) or infinite affine distance, or the focusing point is displaced to infinite affine distance. The figure in the right is compatible with the two last cases. Note that ingoing radial null geodesics are not included in this picture, as these can display different behaviors that are analyzed in detail in the text.

it follows that the expansion $\theta^{(l)}(\lambda_0)$ must be divergent (and negative). ∎

The converse statement is also true but less immediate to prove. Indeed, if the expansion $\theta^{(l)}$ is divergent and negative, then the transverse area $A^{(l)}$ becomes zero, leading to focusing points; a proof of this statement can be found in [73, Sec. 9.3]. Thus, following Penrose's theorem and under conditions (1), (2), and (3) as defined in Sec. 3.1, in order to avoid that the spacetime is geodesically incomplete we need to modify the spacetime geometry in the vicinity of the focusing point, either creating a defocusing point or displacing the focusing point to infinite affine distance (see Fig. 3.3). The expansion $\theta^{(l)}(\lambda)$ must then remain finite for all the possible values of $\lambda \in [0, \infty)$ (where we are again identifying again $\lambda = 0$ with $\mathscr{S}^2$ without loss of generality).

The limiting situation in which the focusing point is displaced to infinite affine distance will be shown later to be still singular, although due to curvature invariants blowing up instead of geodesic incompleteness, thus violating our condition (4) in Sec. 3.1. Hence, we can anticipate that, in practice, the most interesting geometries are those with a defocusing point at $\lambda = \lambda_{\text{defocus}}$, where λ_{defocus} can be either finite or infinite. In terms of the behavior of $\theta^{(l)}(\lambda)$ we can distinguish three possibilities, as the outgoing expansion can either remain negative but finite (thus having no defocusing points), vanish asymptotically for infinite affine distance (whether or not there are defocusing points depends on the convergence properties of the integral of the expansion), or vanish at a finite affine distance (thus having a defocusing point at a finite affine distance). These three possibilities can be further characterized taking into account the behavior of congruences of ingoing null geodesics that intersect the outgoing ones for these values of λ and, in particular, their expansion $\theta^{(k)}$ at the intersection points. The intersection between ingoing and outgoing null geodesics will take place at a radius $r = R_{\text{defocus}}$, so we will denote the corresponding value of the ingoing expansion by $\bar{\theta} := \theta^{(k)}\big|_{r=R_{\text{defocus}}}$.

It is then convenient to use a label with three entries $\left(\lambda_{\text{defocus}}, R_{\text{defocus}}, \bar{\theta} \gtrless 0\right)$ in order to characterize these possibilities, with the first entry being the value of the affine parameter for which $\theta^{(l)}(\lambda)$ vanishes, the second entry being the value of the radius where the expansion vanishes or, if the latter does not vanish, its $\lambda \to \infty$ limit, and the third entry being the sign of the expansion $\theta^{(k)}$ of the ingoing null geodesic that intersects the outgoing one at the very same value of the radius.

Using these labels, there are 8 possibilities: $(\lambda_0, R_0, \bar{\theta} < 0)$, $(\lambda_0, R_0, \bar{\theta} \geq 0)$, $(\infty, R_\infty, \bar{\theta} < 0)$, $(\infty, R_\infty, \bar{\theta} \geq 0)$, $(\infty, 0, \bar{\theta} < 0)$, $(\infty, 0, \bar{\theta} \geq 0)$, $(\emptyset, 0, \bar{\theta} < 0)$, $(\emptyset, 0, \bar{\theta} \geq 0)$, where $\emptyset$ means that there is no value of λ for which the expansion $\theta^{(l)}(\lambda)$ vanishes. Let us describe these possibilities in more detail (a flowchart of this classification is provided in Fig. 3.14):

Case A - Defocusing point at a finite affine distance, $\lambda_{\text{defocus}} = \lambda_0$:

   A.I: $(\lambda_0, R_0, \bar{\theta} < 0)$: The expansion $\theta^{(l)}$ vanishes and changes sign at a finite affine distance $\lambda = \lambda_0$ or, in terms of the radius, at a value $R_0 > 0$ of the radial coordinate along the congruence of outgoing radial null geodesics at $\lambda = \lambda_0$ (namely, the radius of $\mathscr{B}^2$ in Fig. 3.3). On the other hand, the expansion of the intersecting ingoing radial null geodesics remains negative until (and including) λ_0, so that $\theta^{(k)}\big|_{r=R_0} < 0$.

   A.II: $(\lambda_0, R_0, \bar{\theta} \geq 0)$: The only difference with respect to the previous case is that the expansion of the intersecting ingoing radial null geodesics does not remain negative, $\theta^{(k)}\big|_{r=R_0} \geq 0$.

Case B - Defocusing point at an infinite affine distance, $\lambda_{\text{defocus}} = \infty$:

   B.I: $(\infty, R_\infty, \bar{\theta} < 0)$: The expansion $\theta^{(l)}$ vanishes in the limit $\lambda \to \infty$, in a manner such that the integral in Eq. (3.6) is convergent. The corresponding asymptotic value of the radial coordinate for radial outgoing null geodesics is $R_\infty > 0$. The expansion of the intersecting ingoing radial null geodesics remains negative, so that $\theta^{(k)}\big|_{r=R_\infty} < 0$.

   B.II: $(\infty, R_\infty, \bar{\theta} \geq 0)$: The only difference with respect to the previous case is that the expansion of the intersecting ingoing radial null geodesics does not remain negative, $\theta^{(k)}\big|_{r=R_\infty} \geq 0$.

   B.III: $(\infty, 0, \bar{\theta} < 0)$: The expansion $\theta^{(l)}$ vanishes in the limit $\lambda \to \infty$, in a manner such that the integral in Eq. (3.6) is divergent. Thus, the radial coordinate vanishes asymptotically along these geodesics (in other words, there is an asymptotic focusing point). The expansion of the intersecting ingoing radial null geodesics remains negative, so that $\theta^{(k)}\big|_{r=R_\infty} < 0$.

   B.IV: $(\infty, 0, \bar{\theta} \geq 0)$ The only difference with respect to the previous sub-case is that the expansion of the intersecting ingoing radial null geodesics does not remain negative, $\theta^{(k)}\big|_{r=R_\infty} \geq 0$.

Case C - No defocusing point, $\lambda_{\text{defocus}} = \emptyset$:

C.I: $(\emptyset, 0, \bar{\theta} < 0)$: The expansion $\theta^{(l)}$ remains negative in the limit $\lambda \to \infty$, which in particular implies that the integral in Eq. (3.6) is divergent. Thus, the radial coordinate vanishes asymptotically along these geodesics. The expansion of the intersecting ingoing radial null geodesics remains negative, so that $\theta^{(k)}\big|_{r=R_\infty} < 0$.

C.II: $(\emptyset, 0, \bar{\theta} \geq 0)$: The only difference with respect to the previous sub-case is that the expansion of the intersecting ingoing radial null geodesics does not remain negative, $\theta^{(k)}\big|_{r=R_\infty} \geq 0$.

It is important to keep in mind that, in practical terms, sub-cases B.III and C.I fall into the same category, as both of these situations can be understood as the limiting case in which the focusing point is pushed to an infinite affine distance along outgoing null geodesics. The same comment applies to cases B.IV and C.II, that only differ from the previous sub-cases (B.III and C.I) in the behaviour of $\theta^{(k)}$. Hence, when discussing these cases later, we will do it simultaneously.

In the following five sections we discuss in detail the geometric properties of each of the classes of geometries associated with the different cases defined above describing the behavior of outgoing null geodesics. One must keep in mind that these are not mutually exclusive cases, but that at least one of them must be satisfied (for each outgoing null geodesic crossing the region with trapped surfaces) in order to avoid the manifold being geodesically incomplete or not globally hyperbolic. The continuity of the spacetime manifold implies the existence of other trapped surfaces in an open neighborhood around $\mathscr{S}^2$, and we will consider the simplifying assumption that different outgoing null geodesics stemming from these other trapped surfaces belong to the same case (so that neither of the remaining cases can hold). This will allow us to better understand the geometric implications behind each of these cases; moreover, this is not a restrictive assumption. It simply means that we have to consider the set of geometries arising from this analysis as a kind of minimal complete set, in the sense that any possible geometry can be obtained combining the features found in this set.

Case A.I: Evanescent horizons, $(\lambda_0, R_0, \bar{\theta} < 0)$

As indicated above, in analyzing this case we will assume that all outgoing radial null geodesics stemming from trapped surfaces (as well as the intersecting ingoing radial null geodesics) display the same qualitative behavior. We will proceed similarly for the analysis of the other cases. In the current case, this implies the existence of a set of points $r = R_0(u)$ where the expansion $\theta^{(l)}$ vanishes. On the other hand, each ingoing radial null geodesic defines a slice of spacetime that is associated with a constant value of v. We can therefore identify the values of v associated with each $R_0(u)$ through a function $v(R_0(u))$. Let us start with a result constraining the form of this function:

Proposition 3: There must exist $2k$ (with $k \geq 1$) open intervals in the domain of $v(R_0)$ where the latter is bijective and the inverse function $R_0(v)$ exists, which is strictly increasing in half of them and strictly decreasing in the remaining intervals.[3]

---

[3]In reference **P6** this proposition is slightly different as we state that there are $2k+1$ (with $k \geq 0$) open intervals. The contradiction is only apparent as in reference **P6** we decided not to consider the region given by the initial trapping horizon while that region is counted here.

Proof: In spherically symmetric and globally hyperbolic spacetimes, outgoing radial null geodesics cannot cross (otherwise, the light-cone structure of spacetime would be degenerate at the crossing point; see **Proposition 7** below). In a slice of constant v, outgoing radial null geodesics that have a greater value of r have a smaller value of u. This implies that the function $R_0(u)$ must be strictly decreasing in order to avoid crossing points between different outgoing radial null geodesics. On the other hand, we show in App. C that the number of points in a slice of constant v where $\theta^{(l)}$ vanishes and changes sign must be even in order to ensure the regularity of curvature invariants. If there are only two such points for all values of v (the first one corresponding to the future outer trapping horizon), the function $v(R_0)$ is bijective and we can find its inverse $R_0(v)$. That this function must be either strictly increasing or decreasing follows from the strictly decreasing nature of $R_0(u)$. In the more general situation, there are open intervals in the domain of $v(R_0)$ around the $2k$ points where $\theta^{(l)}$ vanishes where $v(R_0)$ is bijective. ∎

Even if the proposition above reduces the number of possibilities, but we can reduce them even further using the regularity conditions derived in App. C:

Proposition 4: The function $R_0(v)$ defined over the innermost open subset of the domain of $v(R_0)$ where the latter is bijective must be strictly increasing in order to avoid curvature singularities at $r = 0$.
Proof: If $R_0(v)$ defined over the innermost open subset where $v(R_0)$ is bijective is strictly decreasing, the only possibility that is compatible with the assumption that all points in $R_0(v)$ are reached in finite affine distance along some outgoing radial null geodesic is that $R_0(v)$ eventually vanishes. The point in which this function vanishes must be reached in finite affine distance along a specific outgoing radial null geodesic, in order to avoid stepping into another of the cases discussed in Sec. 3.3, namely the case $(\infty, R_\infty, \bar{\theta} < 0)$ (this applies both to the particular choice $R_\infty = 0$, but also to the situation in which $\partial R_0(v)/\partial v$ vanishes asymptotically so that $R_0(v)$ tends to a finite value). This implies the existence of a curvature singularity that is reached in finite affine distance along this specific outgoing radial null geodesic, as follows from our arguments in App. C. The argument is straightforward if one takes a slice of constant v that reaches $r = 0$ simultaneously with $r = R_0(v)$, and notices that the necessary condition of an even number of zeros of $\theta^{(l)}$ for $r > 0$ is not satisfied. ∎

Propositions 3 and 4 imply that there must exist at least a portion of the submanifold in which $\theta^{(l)}$ vanishes such that $v(R_0)$ is invertible and $R_0(v)$ is strictly increasing. Interestingly, these portions correspond to future inner trapping horizons, as defined by Hayward [120]:

Proposition 5: Whenever $v(R_0)$ is invertible and $R_0(v)$ strictly increasing, the corresponding subset of the hypersurface in which $\theta^{(l)}$ vanishes is a spacelike future inner trapping horizon.
Proof: Following the definition in [120], a future inner trapping horizon is a hypersurface foliated by marginally trapped surfaces, on which $\theta^{(l)} = 0$ and $\mathscr{L}_k \theta^{(l)} > 0$. We just need to show that the second property is satisfied. However, this is just a corollary of the previous proposition and the structure of zeros of $\theta^{(l)} = 0$ in a slice of constant v that is necessary to avoid curvature singularities which, as discussed in App. C, must have $\mathscr{L}_k \theta^{(l)} < 0$ for the zeros in the odd positions where (with first one corresponding
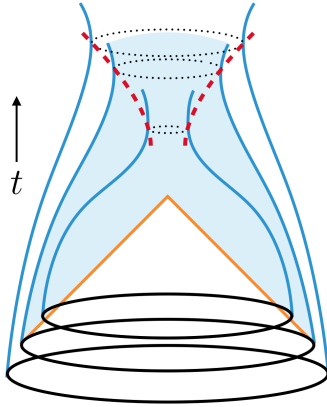
Figure 3.4: Determination of the position of the future inner trapping horizon (red dashed line), taking into account different trapped surfaces in the neighborhood of $\mathscr{S}^2$ and tracking the corresponding outgoing null geodesics. In this case the future inner trapping horizon is spacelike.

to the future outer trapping horizon), and $\mathscr{L}_{\boldsymbol{k}}\theta^{(\boldsymbol{l})} > 0$ for the zeros in the even positions. Regarding the spacelike character of the hypersurface $r = R_0(v)$, this just follows from the observation that this hypersurface lies outside the local light cone defined by outgoing and ingoing radial null geodesics. Indeed, let us consider a specific outgoing radial null geodesic reaching the point $\lambda = \lambda_0$ in which its expansion vanishes, and the ingoing radial null geodesic that crosses the same point towards smaller values of the radius, and therefore lies inside the mentioned outgoing radial null geodesic after the crossing point. As outgoing radial null geodesics cannot cross, $r = R_0(v)$ must lie outside the same outgoing radial null geodesic, and therefore outside the local light cone. ∎

In a similar way it can be proved that the region where $R_0(v)$ is strictly decreasing correspond to an outer horizon.

Let us now put all these pieces together in order to understand the global structure that is associated with the local geometric elements discussed in this section. In the following, $\mathscr{T}^3$ will denote the set of marginally trapped spheres (so that $\theta^{(\boldsymbol{l})} = 0$):

Proposition 6: $\mathscr{T}^3$ is a smooth compact submanifold only if the function $v(R_0)$ is not bijective, so that its domain contains at least two open subsets where the inverse $R_0(v)$ exists.

Proof: Let us assume that $v(R_0)$ is bijective in all its domain of definition, so that its inverse $R_0(v)$ is strictly increasing and defines the (evolving) position of a future inner trapping horizon, as a consequence of propositions 4 and 5. In this situation, outgoing radial null geodesics stemming from trapped surfaces must intersect the trajectory of the future inner trapping horizon $r = R_0(v)$. These outgoing radial null geodesics, being inside the trapped region, have crossed before the future outer trapping horizon. Hence, all such geodesics must intersect $\mathscr{T}^3$ twice. If $\mathscr{T}^3$ is compact, there will always exist a "tangent" outgoing radial null geodesic intersecting $\mathscr{T}^3$ only once (this is the limiting case in between the geodesics with two crossings and the geodesics with no crossings).

The alternative is that $\mathscr{T}^3$ is not compact, so that there is no outgoing radial null geodesic that intersects it only once (alternatively, one can take the limit in which this single intersection point is reached in infinite affine distance). In the compact case, both trapping horizons (inner and outer) will merge at the point where the "tangent" outgoing radial geodesic meets $\mathscr{T}^3$. Given that the position of the future inner trapping horizon is a strictly increasing function of the radial coordinate, $\mathscr{T}^3$ cannot be smooth at this point, displaying a cusp instead. ∎

The simplest situation compatible with the proposition above leads to the Penrose diagram depicted in Fig. 3.5 (more complicated situations just contain more outer and inner horizons). The topology of $\mathscr{T}^3$ is $S^1 \times S^2$, and the domain of the function $v(R_0)$ has two subsets where an inverse exists. In one of these subsets (associated with the top quadrant on the left diagram in Fig. 3.6), the function $R_0(v)$ is strictly increasing, so that this portion of $\mathscr{T}^3$ is identified with the expanding future inner trapping horizon. On the other hand, the right quadrant on the left diagram in Fig. 3.6 indicates the region in $\mathscr{T}^3$ in which $R_0(v)$ is decreasing, which is then identified as the shrinking future outer trapping horizon. Thus, the Penrose diagram depicted in Fig. 3.5 describes the formation and disappearance of a black hole that remains non-singular throughout its dynamical evolution, as forced by our assumptions.
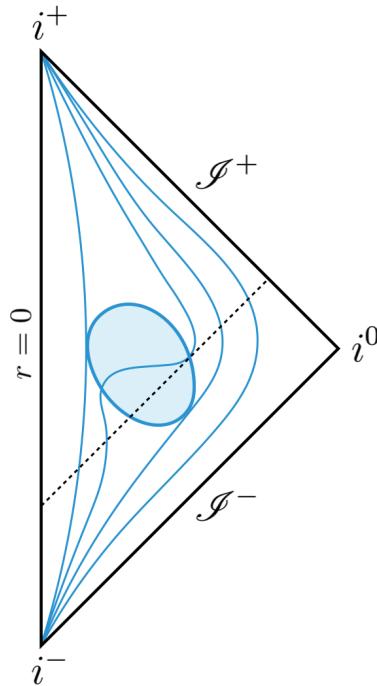

Figure 3.5: Penrose diagram of the formation and dissapearance of a geodesically-complete black hole. The submanifold $\mathscr{T}^3$ is the boundary of the shaded region. The dashed line is an outgoing radial null geodesic, while the remaining curved lines mark the hypersurfaces of constant radius r.

Our discussion does not assume any specific dynamical laws for either gravity or matter sectors which, in particular, implies that the disappearance of the black hole
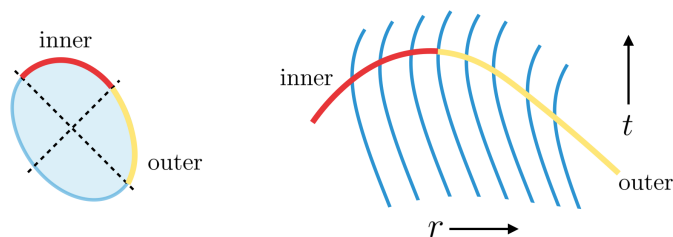
Figure 3.6: Structure of the inner and outer future trapping horizons in the simplest spacetime that contains the ingredients in this section. To the best of our knowledge, the first explicit discussion of this structure was provided in [106]. *On the left:* the boundary of the top quadrant (red line) corresponds to the strictly increasing branch of $R_0(v)$, while the boundary of the right quadrant (yellow line) corresponds to the strictly decreasing branch of $R_0(v)$. *On the right:* another perspective on the evolution of horizons, in which the hypersurfaces of constant r are vertical lines and time flows in the upward direction.

does not need to be linked with the emission of Hawking radiation. In other words, black hole evaporation would correspond to selecting specific geometries, with certain features and time scales, within the class that we have obtained as the result of our purely geometric analysis (moreover, it is important to keep in mind that we are not tracing explicitly the evolution of matter). For instance, an alternative to black hole evaporation that shares the same Penrose diagram was given in [134]. It is also possible that $\mathscr{T}^3$ is not simply connected, but is composed of disconnected regions. Also, if one demands time-reversal symmetry, there must be a region of anti-trapped surfaces, and the corresponding spacetime describes the transition between a black hole and a white hole [135, 136, 137, 138] (see Fig. 3.8).
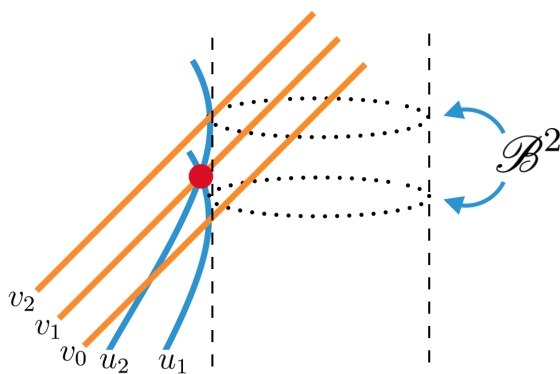

Figure 3.7: Different coordinate patches that are relevant for our discussion on the avoidance of crossing points between outgoing radial null geodesics (the red dot in this figure). The straight lines at 45 degrees represent ingoing radial null geodesics.

Let us now show that the explicit assumption in the above discussion that there cannot be crossing points between two outgoing radial null geodesics is, in fact, a consequence of global hyperbolicity, starting with a detailed discussion of the case in which $R_0(v)$ is a constant function:

Proposition 7: A spacetime in which $R_0(v)$ is a constant function cannot be globally hyperbolic.

Proof: That there cannot be crossing points between two outgoing radial null geodesics having $\theta^{(l)}\big|_{r=R_0} = 0$ does not imply that these geodesics cannot have the same value of the radial coordinate for the corresponding values of their affine parameters. The (weaker) consequence that follows is that the one-to-one correspondence between the value of the radial coordinate and spheres in spacetime must break down, such that a given value of the radial coordinate does not uniquely identify a single sphere. We can try, of course, to use the set of null coordinates (u, v) (in order to construct a complete set of coordinates we have to consider the angular coordinates as well, but it is not necessary to consider them explicitly). However, we shall now show that the geodesics reaching $r = R_0$ exit the spacetime region that can be covered with the (u, v) coordinate patch. Indeed, let us assume that both spheres (located at the red dot in Fig. 3.7) can be covered with the (u, v) patch. Then, one sphere will be labeled by the specific values (u_1, v_1), while the other sphere will be associated with (u_2, v_1). This would imply that the $u = u_1$ and $u = u_2$ geodesics must intersect $v = v_1$ at points that are identified with different values of the affine parameter along the latter ingoing radial null geodesic. However, this is in contradiction with Fig. (3.7), as one can consider an open subset of the manifold around the red dot and follow the evolution of the affine parameter along the ingoing radial null geodesic in this subset (so that it must be the same for the two points labelled with different values of u). Given that null coordinates always exist locally, the second sphere must be labelled by a radial ingoing null geodesic that cannot cross the Cauchy surface $\mathscr{C}^3$. Hence, the spacetime is not globally hyperbolic. ∎

Even if the proposition above is valid for $R_0(v)$ being a constant function, it is straightforward to see that a similar comment regarding the lack of global hyperbolicity in the presence of would-be intersection points applies to generic functions $R_0(v)$, as the argument above does not depend on the form of $R_0(v)$, but only on the interplay between different coordinate patches at the would-be intersection points. It is also worth stressing that the local behavior around these points may seem odd, but it is in fact ubiquitous in attempts of constructing non-singular black holes (we will discuss this in more detail in the corresponding cases below). The only difference is that our discussion is general enough to accommodate generic dynamical situations, while the well-known cases in the literature with Cauchy horizons are typically eternal black holes.

While we have so far focused on the minimal setting that just requires the existence of a single trapped region, as depicted in figure 3.5, note that there are models proposed in the literature that present additional features while still belonging in this class. For instance, see Fig. 3.8 for a sketch of a situation in which there is a bounce and subsequent formation of an additional anti-trapped region [135, 136, 137].
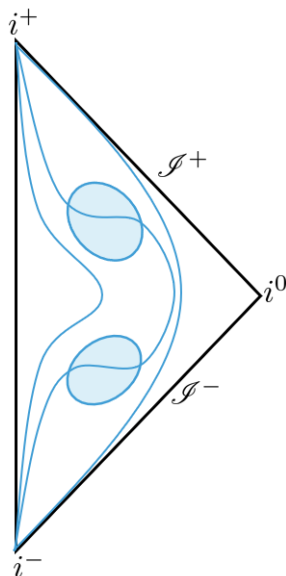
Figure 3.8: After the disappearance of the trapped region, an anti-trapped region is formed. This situation describes a bounce from a black hole like geometry to a white hole like geometry. Situations in which a recollapse takes place [135, 136] can be described by a sequence of trapped and anti-trapped regions.

Case A.II: One-way hidden wormholes $(\lambda_0, R_0, \bar{\theta} \geq 0)$

Characterizing this class is simpler than for the previous one. We just need to take into account that there exists an ingoing radial null geodesic that starts with a negative value of the expansion, that eventually vanishes and becomes positive. That both expansions (outgoing and ingoing) vanish, although in different regions in spacetime, is characteristic of dynamical wormhole throats [139, 140]. In fact, we can show the following proposition:

Proposition 8: There exists a hypersurface $r(u, v) = R_0$ where the radial coordinate has a local minimum.

Proof: The value of the radial coordinate along the outgoing radial null geodesic stemming from $\mathscr{S}^2$ (see the right panel in Fig. 3.9) must reach a minimum at $r = R_0$. Let us now study the intersections between outgoing and ingoing radial null geodesics, in similar terms as we did before the intersection of two outgoing radial null geodesics. Instead of dealing with a single intersection between outgoing radial null geodesics, in this case we deal with double intersections between outgoing and ingoing radial null geodesics (Fig. 3.9). This is also forbidden in spherical symmetry, as it would imply that two different points would be associated with the same values of (null) coordinates. In fact, as in the previous case, both coordinate sets (u, r) and (v, r) cannot be used to go through the points in which the expansion of ongoing and ingoing null geodesics, respectively, vanishes. However, the main difference with respect to the previous case is that the splitting of the second intersection point can be well described in the (u, v) coordinates, as illustrated graphically in Fig. 3.9, but at the price of creating two different hypersurfaces in spacetime corresponding to the same value of the radius
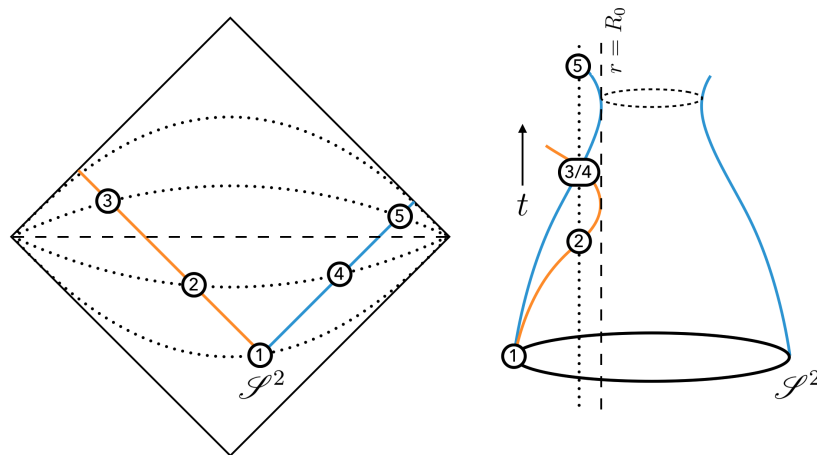
Figure 3.9: Part of the Penrose diagram of a static wormhole inside a future outer trapping horizon, corresponding to the quadrant containing the throat of the wormhole. The straight dashed line indicates the line of constant r with the minimum value of the latter, while the dotted lines are also lines of constant r but associated with with greater values. Two radial null geodesics, ingoing and outgoing, depart from the crossing point 1. The ingoing geodesic crosses the point 2 with a value of the radius corresponding to the would-be crossing point 3, reaches $r = R_0$ (which is the same for both ingoing and outgoing geodesics due to the wormhole being static), and bounces back until reaching what looks like a second crossing point 3. However, as illustrated by the Penrose diagram, there is no actual crossing, as the outgoing geodesic would be when having this same radius at point 4 of spacetime. That is, the right-hand figure, being based on using the r coordinate as primary, is misleading – exactly because the r coordinate is double-valued in this class of spacetimes.

(along the points 2, 4 and 3, 5 in the figure, respectively). Hence, when other trapped surfaces (and the corresponding outgoing radial null geodesics) in the neighborhood of $\mathscr{S}^2$ are considered, it follows that there must be a hypersurface $r(u, v) = R_0$ in which the radial coordinate has a local minimum. ∎
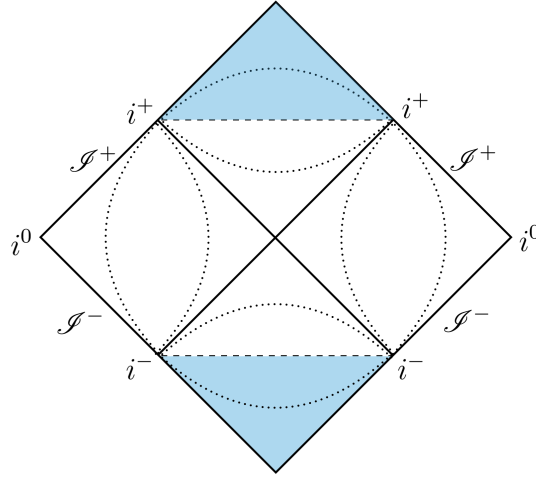

Figure 3.10: Dashed lines are lines of minimum radius $r = R_0$ (corresponding to $\mathscr{B}^2$ in Fig. 3.3). Dotted lines are lines of constant radius. The shaded regions indicate points in the manifold that cannot be covered with either the (u, r) or (v, r) coordinate systems.

This situation generally corresponds to a one-way (hidden) dynamical wormhole [140], except for the limiting case $\theta^{(k)}\big|_{\lambda=\lambda_0} = 0$ which describes a static wormhole [139]. It is important to keep in mind that these are not wormholes in the most common sense of this term, as the throats are inside a future outer trapping horizon.

Case B.I: Everlasting horizons $(\infty, R_\infty, \bar{\theta} < 0)$

This situation can be obtained as the $\lambda_0 \to \infty$ limit of $(\lambda_0, R_0, \bar{\theta} < 0)$. The toroidal topology of the horizons in the latter case is deformed so that outgoing radial null geodesics never reach the second point (along their trajectories) in which $\theta^{(l)}$ vanishes. The corresponding Penrose diagram, provided in Fig. 3.11, is a variation of the Penrose diagram in Fig. 3.5. In physical terms, the diagram in Fig. 3.11 is an intermediate situation between a static regular black hole and Fig. 3.5, in which outgoing radial null geodesics do not reach either $r = 0$ or $r = \infty$ (after crossing the future inner trapping horizon), but rather an intermediate radius $r = R_\infty(u)$. The corresponding black hole is always growing and never disappears; any process that describes the partial evaporation or total disappearance of the black hole must involve some outgoing radial null geodesics satisfying the conditions characteristic of the case $(\lambda_0, R_0, \bar{\theta} < 0)$ studied above.

Another issue that is worth clarifying is the asymptotic $(\lambda \to \infty)$ behavior of the lines of constant radial coordinate in the trapped region which, as depicted in Fig. 3.11,
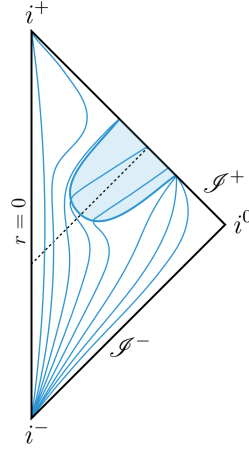
Figure 3.11: A geodesically-complete black hole that forms during gravitational collapse but never disappears, and without the formation of a Cauchy horizon.

become null asymptotically. This can be seen to be a consequence of $\theta^{(l)}$ vanishing in the limit $\lambda \to \infty$, which implies that the function $F(v,r)$ in Eq. (3.2) vanishes as well (see App. C for explicit expressions), and so does the line element on the lines of constant radial coordinate,

$$\mathrm{d}s^2\big|_{r=r_0} = -e^{-2\phi(v,r)}F(v,r)\mathrm{d}v^2. \tag{3.8}$$

Case B.II: Asymptotic hidden wormholes $(\infty, R_\infty, \bar{\theta} \geq 0)$

Similarly as the case just above, this situation can be understood as the $\lambda_0 \to \infty$ limit of a previously discussed case, namely $(\lambda_0, R_0, \bar{\theta} \geq 0)$, which described a wormhole. Hence, this kind of geometry corresponds to an asymptotically cylinder-like geometry. This is easiest to realize for the static case $\lim_{\lambda \to \infty} \theta^{(k)} = 0$, in which the radius of the cylinder is given by the size of the corresponding surface $\mathscr{B}^2$ (which is at infinite affine distance). The Penrose diagram would be given by Fig. 3.10 but removing the shaded regions. In the dynamical situation, we would have a "half-wormhole" where the second universe has been discarded and the throat pushed out to infinite affine distance along outgoing radial null geodesics.

Cases B.III, B.IV, C.I and C.II: Curvature singularities, $(\infty, 0, \bar{\theta} < 0)$, $(\emptyset, 0, \bar{\theta} < 0)$, $(\infty, 0, \bar{\theta} \geq 0)$ and $(\emptyset, 0, \bar{\theta} \geq 0)$

These four situations are sufficiently similar that we can analyze them simultaneously, with only slight differences due to the different behavior of the expansion of ingoing radial null geodesics. In fact, their main feature is that outgoing radial null geodesics reach $r = 0$. It is straightforward to show that this is not compatible with the regularity of curvature invariants, provided we maintain all our assumptions (such as geodesic completeness). Outgoing radial null geodesics reach $r = 0$ in an infinite affine distance but, generally, ingoing null geodesics will reach $r = 0$ (as there is no wormhole throat in

this case) in finite affine distance. At the same time, there is no future inner trapping horizon (in other words, a second point in which $\theta^{(l)}$ vanishes) which, following the discussion in Sec. C, is a necessary condition to ensure regularity at $r = 0$. Hence, these cases lead to a curvature singularity at infinite affine distance along outgoing null geodesics, but generally finite affine distance along ingoing null geodesics for instance. In other words, we have seen in the discussion of the cases above that, in order to avoid a curvature singularity at $r = 0$, one needs either a wormhole structure (a minimum value of the radial coordinate that prevents reaching $r = 0$) or a future inner trapping horizon. As the geometries studied in this item contain by construction none of these, these must be singular (if global hyperbolicity is maintained).
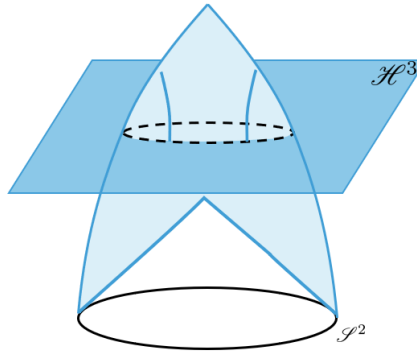

Figure 3.12: Static regular black holes evade Penrose's theorem due to the introduction of a Cauchy horizon (here represented as the horizontal plane) before the focusing point is reached, which allows the focusing point to be regular in these geometries.

It is always possible to violate the assumption of global hyperbolicity in Penrose's theorem (which is also one of the four conditions behind our analysis) in order to avoid being singular. Interestingly, geometries that appear often in the literature belong to this case. Even if the focusing point in these situations is reached generically in finite affine distance, this point in the discussion is a natural placement of these well-known geometries describing static regular black holes [103, 104, 105, 106, 107, 108, 109, 110, 111, 112, 113, 114, 115]. As shown graphically in Fig. 3.12 , these geometries do not evade Penrose's theorem by avoiding the formation of focusing points, but rather by introducing a Cauchy horizon before this focusing point is reached by outgoing geodesics. For completeness, we also provide in Fig. 3.13 the Penrose diagram of the corresponding eternal geometries. Static regular black holes correspond to the limiting situation in which the expansion $\theta^{(k)}$ associated with the ingoing radial null geodesics crossing $\mathscr{C}^3$ vanishes along the Cauchy horizon (in these spacetimes, there are ingoing radial null geodesics that intersect the trapped outgoing radial null geodesics while having $\theta^{(k)}$, but only in the region beyond the Cauchy horizon). One may think that it should be possible to devise situations in which $\theta^{(k)}$ actually changes sign without violating global hyperbolicity. However, these situations would always involve two intersections between outgoing and ingoing radial null geodesics which, due to the lack of wormhole throats in this situation ($r = 0$ is reached by outgoing radial null geodesics

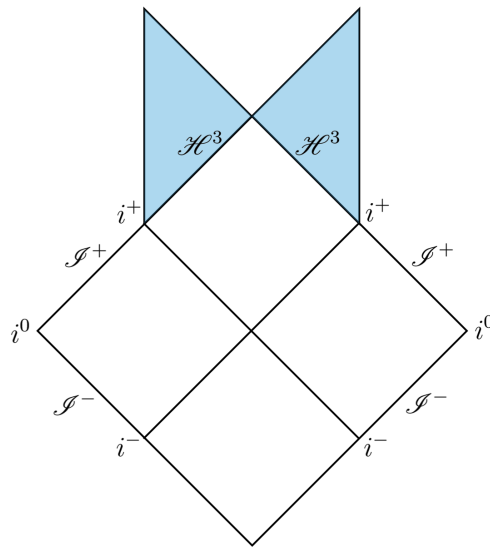by construction), implies the lack of global hyperbolicity.

Figure 3.13: Penrose diagram that can represent different kinds of (eternal) black holes, from charged to rotating black holes, but also regular black holes in which the central singularity has been removed. The colored quadrants on the left and on the right represent respectively the regions which are covered by the (v, r) patch but not with the (u, r) patch, and by the (u, r) patch but not with the (v, r) patch. These are particular examples of spacetimes that are not globally hyperbolic, following our general discussion in this section. The complete Penrose diagram is obtained by stacking indefinitely the section represented here. Our discussion in this chapter is more general, as it does not require that the diagram is not symmetric as this one (this symmetry is a consequence of the eternal nature of the black holes represented in this diagram).

3.4 Conclusions

We have studied in completely general terms the possible spherically symmetric geometries describing geodesically-complete black holes. Beside geodesic completeness, we have also demanded global hyperbolicity (so that it is reasonable to think that these geometries can be obtained through dynamical evolution) and the absence of curvature singularities.

Remarkably, we have found that purely geometric considerations are enough to strongly constrain the allowed class of spacetimes. Using our classification, we were able to identify four classes of geometries, that can either be taken as they are or be combined, in order to yield the most general spherically symmetric spacetime satisfying our requirements (1–4). Figure 3.14 summarizes the classification that we have provided and the different viable classes of geometries.
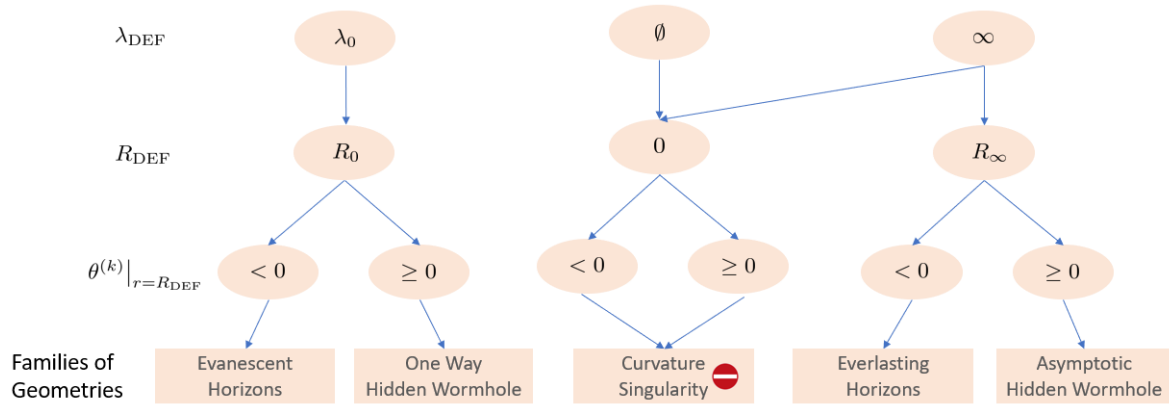
Figure 3.14: The table summarizes the classes of the allowed geometries. The most general geometry is given by a combination of the geometries in the table.

The first class corresponds to geometries in which the defocusing of outgoing null geodesics is placed at a finite value of the affine parameter and for a finite value of the radial coordinate, whereas ingoing null geodesics do not have a defocusing point. This class of geometries is associated with a geodesically-complete black hole that disappears in finite time, which we call an "evanescent regular black hole". Note that we are carefully avoiding the use of "evaporation"; our geometric analysis does not provide any hint about the dynamical process behind the disappearance of the black hole. Such process could either be Hawking radiation or some other process taking place in shorter time scales, for instance the proposed transition to a white hole;

The second class differs from the first one due to the value of the expansion parameter of ingoing null geodesics, which is non-negative at the point in which the defocusing point for the outgoing geodesics. We have discussed that this implies the existence of something closely resembling a wormhole throat. We refer to these geometries as "one-way hidden wormholes" to stress the fact that the throat is inside a trapped region.

The last two classes can be understood as the limit of $\lambda_{\text{defocus}} \to \infty$ of the previous two cases. The difference between these two classes is once again the value of the expansion parameter of ingoing null geodesics. If the expansion is negative, then we have an "everlasting regular black hole". If the expansion parameter is asymptotically zero or positive, we would get an "asymptotic hidden wormhole" which would again be non-traversable and now involve a one-way trip to the edge of spacetime.

We can see that the set of possibility is quite limited. In the next chapter we are going to constrain it even more as we will discuss some self consistency requirement that will allow us to question the viability of specific realizations of some of the geometries discussed in this chapter.

Chapter 4

On the viability of non-singular black holes

In the previous chapter we have discussed a geometrical classification of non-singular spacetimes with a trapping horizon. We have obtained the very interesting result that the most general spacetime can be classified within one of the four classes we have studied or it is a combination of them. In other words, there are very few possible non-singular configuration.

These families of spacetimes can be understood as effective descriptions of the evolution of non-singular black holes, sharing some qualitative properties but still displaying quantitative differences that can be described in terms of parametric and functional degrees of freedom. In this chapter, we want to highlight that the effective description in terms of these spacetimes would only be meaningful if displaying a satisfactory level of selfconsistency. Of course, the lack of knowledge of the specific dynamics that may yield these spacetimes implies a degree of uncertainty about some fine details of these models. However, this does not prevent extracting certain conclusions that, if formulated carefully enough, would remain robust regardless of this uncertainty.

In particular, we will see in Sec. 4.1 that it is very difficult to have a consistent model of evanescent or everlasting horizon geometry unless the lifetime of the object is very short. In Sec. 4.2 we will study the self consistency issues that affects the one way and the asymptotic hidden wormholes geometries. Finally, in Sec. 4.3 we will discuss the implications of our conclusions. The content of this chapter is based on **P2**, **P5** and **P6**.

4.1 Evanescent horizons and everlasting horizons

In the previous chapter, we have seen that one of the most conservative possibilities to regularize the singularity consist in changing the geometry close to the would be singularity introducing an inner horizon.

The non-singular core in these geometries replaces a region in which the spacetime curvature takes Planckian values or larger, and therefore in which the classical dynamics is modified [104, 105], by a region in which curvature is bounded.

When doing so, it is possible to leave the geometry outside the outer horizon unchanged, obtaining an object completely indistinguishable from a black hole. The geometry will certainly deviate from the one corresponding to a black hole when the outer

and inner horizon merge, but this could happen after a very long time[1]. Given the possible absence of phenomenological signatures, it is impossible to device any experiment able to rule out this possibility from a observational point of view and it is crucial to address the self consistency of the model. We will see that the inner horizon has an unstable nature which casts serious concerns regarding the self consistency of the model.

4.1.1   Time independent geometry

The geometries in the classes of evanescent horizons or everlasting horizons are characterized by the formation and eventual disappearance of an outer and an inner horizon. Therefore, the geometry has to be time dependent. In fact, as already discussed is Sec. 3.3, by explicitly looking at the Penrose diagram of a static regular black hole reported in Fig. 4.1 (see also [112]), it is immediate to see that a static regular black hole do not belong to any of the classes discussed in the previous chapter and the conclusion of the Penrose theorem are avoided by violating global hyperbolicity. This class of geometry are therefore actually outside our classification as one of the hypothesis is not satisfied. Anyway, it is convenient to start the analysis by considering a static configuration which will approximate the time dependent geometry if the evolution is slow enough. We will explicitly introduce the time dependence in Sec. 4.1.3.

Without loss of generality, the geometry of a static and spherically symmetric regular black hole can be written as

$$ds^2 = -e^{-2\phi(r)}F(r)dt^2 + \frac{dr^2}{F(r)} + r^2(d\theta^2 + \sin^2\theta\, d\phi^2). \tag{4.1}$$

where $\phi(r)$ and $F(r)$ are two real functions. When convenient, we will alternatively use the notation

$$F(r) = 1 - \frac{2m(r)}{r}. \tag{4.2}$$

The function $m(r)$ corresponds to the Misner–Sharp–Hernandez quasi-local mass [141, 142, 143]. Using the Einstein field equations, it is straightforward to see that the effective energy density associated with the geometry in Eq. (4.1) is given by $m'(r)/4\pi r^2$, where $m'(r) = dm(r)/dr$. This quantity can be finite at $r = 0$ if and only if $m(r)$ vanishes at least as r^3 in the limit $r \to 0$.

Hence, regularity at $r = 0$ requires $F(0) = 1$. On the other hand, asymptotic flatness enforces $\lim_{r\to\infty} F(r) = 1$. It follows (counting the multiplicity of the roots) that the function $F(r)$ must have an even number of zeros, with these zeros corresponding to different horizons. In the following we assume for simplicity that there are only two horizons, but all our results are independent of this assumption. The outer and inner horizons, respectively r_+ and r_-, are then defined by

$$F(r_\pm) = 0, \tag{4.3}$$

or equivalently by

$$r_\pm = 2m(r_\pm). \tag{4.4}$$

---

[1]For instance, we show in appendix D that if the only physical process at play is Hawking radiation the evaporation time is actually infinite and the evaporation start to differ from the general relativity counterpart only after an Hawking time $\tau \sim M^3$.
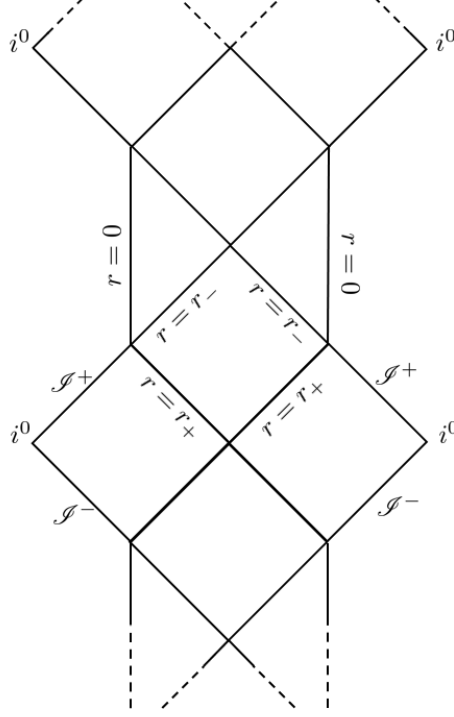
Figure 4.1: Penrose diagram for a static regular black hole. The spacetime is not globally hyperbolic as the inner horizon is a Cauchy horizon.

When studying the causal properties of the geometry, it is convenient to introduce the ingoing Eddington-Finkelstein coordinate v,

$$\mathrm{d}v = \mathrm{d}t + \frac{\mathrm{d}r}{e^{-\phi(r)}F(r)}, \tag{4.5}$$

in terms of which the line element (4.1) reads

$$\mathrm{d}s^2 = -e^{-2\phi(r)}F(r)\mathrm{d}v^2 + 2e^{-\phi(r)}\mathrm{d}r\mathrm{d}v + r^2(\mathrm{d}\theta^2 + \sin^2\theta\,\mathrm{d}\phi^2). \tag{4.6}$$

The outgoing Eddington-Finkelstein coordinate is instead given by $\mathrm{d}u = \mathrm{d}t - \mathrm{d}r/e^{-\phi(r)}F(r)$. For $m(r) = M$ and $\phi(r) = 0$, these expressions reduce to the standard ones in the Schwarzschild geometry.

Ingoing and outgoing radial null curves are determined respectively by the equations

$$\mathrm{d}v = 0, \tag{4.7}$$

and

$$\frac{\mathrm{d}r}{\mathrm{d}v} = \frac{e^{-\phi(r)}F(r)}{2}. \tag{4.8}$$

The Taylor expansion of Eq. (4.8) around $r = r_\pm$ is given by

$$\begin{aligned}
\frac{\mathrm{d}r}{\mathrm{d}v} &= \frac{e^{-\phi(r_\pm)}}{2}F'(r_\pm)\,(r - r_\pm) + \mathcal{O}(r - r_\pm) \\
&= -\frac{e^{-\phi(r)}}{2}\left(\frac{2m(r)}{r}\right)'\bigg|_{r=r_\pm}(r - r_\pm) + \mathcal{O}(r - r_\pm);
\end{aligned} \tag{4.9}$$

we see that the surface gravity at the outer and inner horizons are given by

$$\kappa_\pm = -\frac{e^{-\phi(r)}}{2} \left(\frac{2m(r)}{r}\right)' \bigg|_{r=r_\pm}. \tag{4.10}$$

In particular, $\kappa_+ > 0$ and $\kappa_- < 0$. As a consequence, at the outer horizon we have an exponential peeling of outgoing null rays,

$$\frac{\mathrm{d}(r - r_+)}{\mathrm{d}v} = |\kappa_+| \, (r - r_+) + \mathcal{O}(r - r_H), \tag{4.11}$$

while at the inner horizon we have an exponential focusing of outgoing null rays,

$$\frac{\mathrm{d}(r - r_-)}{\mathrm{d}v} = -|\kappa_-| \, (r - r_-) + \mathcal{O}(r - r_H). \tag{4.12}$$

4.1.2   Instability of the inner horizon

From the analysis of the previous section it seems that it is possible to replace the singularity with an inner horizon without changing the exterior geometry. This would imply that any quantum gravity effect will be confined within the trapping horizon and invisible to an external observer. Anyway we will now show that this picture is too simplistic due to the unstable nature of the inner horizon.

Such unstable nature is due to the exponential focusing of null rays and it was previously noticed, and thoroughly studied, in the different but related context of charged and rotating black holes. The main aspects were settled more than two decades ago [144, 145, 146, 147, 148, 149], though formal proofs of a number of technical aspects were only available later [150] (see also [151] for a review). In brief terms, the central conclusion of these works is that the inner horizon is unstable in the presence of both ingoing and outgoing perturbations, which are expected to exist in realistic collapse scenarios. While this is a classical instability, it is natural to expect the existence of semiclassical instabilities as well [152].

Let us start by explaining why it is natural to expect the existence of outgoing and ingoing perturbations in realistic scenarios. A regular black hole, being just a regularization of an ordinary black hole, would form after the gravitational collapse of a massive star. The star would emit radiation even after crossing the outer horizon (after this, the initially outgoing radiation is strongly lensed back to the collapsing star). On the other hand, there will be ingoing perturbations that come, for instance, from the backscattering of gravitational radiation. The process can be modelled following [148], where outgoing and ingoing perturbations are described in terms of null shells. This simplification allows to perform all necessary calculations analytically, and exploits the Dray–'t Hooft–Redmount (DTR) relation [153, 154]. Furthermore, despite its simplicity, this type of perturbation represent a good approximation of a real perturbation. In fact, we are exclusively interested in the geometry close to the inner horizon where, due to the intensive blueshift, the infalling waves are well described by the geometrical optic approximation.
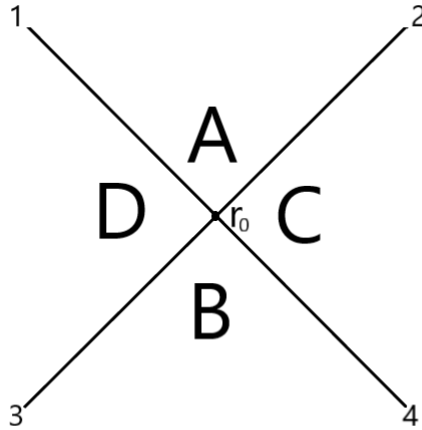
Figure 4.2: Schematic illustration of the physical process in consideration. Two null perturbations meet in a two surface of radius r_0 and divide the spacetime in four regions.

Derivation of the DTR relations

The analysis in this subsection is simply a more extended discussion of some aspect presented in [148]. However, as that work focus on general relativity, it is useful to carefully repeat the computation to explicitly show that the features we are interested in do not depend on the dynamics of general relativity as they descend directly from geometric notions.

The situation is schematically described in Fig. 4.2. We consider two perturbation described as an ingoing and an outgoing null shell Σ_3 and Σ_4 that intersect each other in a two surface S of radius r_0 and give rise to two other null shells Σ_1 and Σ_2, dividing the spacetime in four region. Let us denote the four regions A, B, C and D and the vectors tangent to the shells $l_{(i)}$. From our experience in general relativity, we know that this spacetime contains curvature singularities due to the presence of the thin shells [155]. However, these singularities have a clear physical interpretation as we know that they are due to the fact that we are attaching a finite energy to the shells, which are objects of zero width, and they would go away in a less idealized situation. However, we need to assume some regularity conditions on the spacetime that assure the absence of singularities without any physical interpretation. The first requirement leads to the Israel's first junction condition [155] which, on purely geometrical grounds, tell us that there is a well defined notion of induced metric on the shells σ_{ab}^i, meaning that projecting either four dimensional metric on the two side of each shell we obtain the same two dimensional metric.

Furthermore, we need to impose that the spacetime is well behaved on S (for instance we have to assume the absence of conical singularities). This implies that each point on S can be covered by a coordinate chart in which the metric is continuous and (piecewise) differentiable. Using this coordinates, we can derive a very useful relation. Due to fact

that to a given two surface embedded in a four dimensional spacetime there are only two orthogonal direction, we have that, at S, $l_{(3)}$ is parallel to $l_{(2)}$ and $l_{(4)}$ is parallel to $l_{(1)}$. So, for some constants α and β,

$$l^{\mu}_{(3)} = \alpha l^{\mu}_{(2)}, \qquad\qquad l^{\mu}_{(4)} = \beta l^{\mu}_{(1)}. \tag{4.13}$$

Given that we are never going to work in this particular coordinate chart, let us consider a coordinate invariant relation that trivially follows from Eq. (4.13)

$$\left(l_{(1)} \cdot l_{(2)}\right)\left(l_{(3)} \cdot l_{(4)}\right) = \left(l_{(1)} \cdot l_{(3)}\right)\left(l_{(2)} \cdot l_{(4)}\right). \tag{4.14}$$

This equality is going to be one of the key relations for our analysis.
An important role will also be played by the trace of the extrinsic curvature

$$\sigma^{ab}_{(i)} K^{(i)}_{ab} = \sigma^{ab}_{(i)} \mathscr{L}_{l_{(i)}} \sigma^{(i)}_{ab} = \sigma^{ab}_{(i)} l^{\alpha} \partial_{\alpha} \sigma^{(i)}_{ab} = \frac{2}{r} l^{\alpha}_{(i)} \partial_{\alpha} r, \tag{4.15}$$

where $\mathscr{L}$ denotes the Lie derivative and Latin indexes run from 1 to 2 while Greek indexes run from 0 to 3. The last step comes directly from the fact that we are considering spherical shells.

Due to the null nature of the shells, the orthogonal vector is also tangential to the shell and the extrinsic curvature is given by the tangential derivative of the metric along the shells. Therefore, the extrinsic curvature has to be continuous at the shell and it cannot depend on which region of spacetime is used in the computation. This would not be true if the shells were timelike as the extrinsic curvature would not be well defined and it would depend on the components of metric orthogonal to the shells which are different in the two side of the shells. We can rewrite Eq. (4.14) as

$$\frac{K^{(1)} K^{(2)} K^{(3)} K^{(4)}}{\left(l_{(1)} \cdot l_{(2)}\right)\left(l_{(3)} \cdot l_{(4)}\right)} = \frac{K^{(1)} K^{(2)} K^{(3)} K^{(4)}}{\left(l_{(1)} \cdot l_{(3)}\right)\left(l_{(2)} \cdot l_{(4)}\right)} \tag{4.16}$$

This may seem a triviality, but let us group the terms in a different way

$$\left(\frac{K^{(1)} K^{(2)}}{l_{(1)} \cdot l_{(2)}}\right)_A \left(\frac{K^{(3)} K^{(4)}}{l_{(3)} \cdot l_{(4)}}\right)_B = \left(\frac{K^{(1)} K^{(3)}}{l_{(1)} \cdot l_{(3)}}\right)_D \left(\frac{K^{(2)} K^{(4)}}{l_{(2)} \cdot l_{(4)}}\right)_C \tag{4.17}$$

where the index refer to the region of spacetime we need to use in order to evaluate the quantities in the bracket. Here it is clear why it is important that the extrinsic curvature is continuous across the shells.
Making use of the completeness relations

$$g^A_{\alpha\beta} = \sigma^{(1)}_{\alpha\beta} + \frac{l_{(1)\alpha} l_{(2)\beta}}{l_{(1)} \cdot l_{(2)}} + \frac{l_{(2)\alpha} l_{(1)\beta}}{l_{(1)} \cdot l_{(2)}}, \qquad g^B_{\alpha\beta} = \sigma^{(4)}_{\alpha\beta} + \frac{l_{(3)\alpha} l_{(4)\beta}}{l_{(3)} \cdot l_{(4)}} + \frac{l_{(4)\alpha} l_{(3)\beta}}{l_{(3)} \cdot l_{(4)}},$$

$$g^C_{\alpha\beta} = \sigma^{(2)}_{\alpha\beta} + \frac{l_{(2)\alpha} l_{(4)\beta}}{l_{(2)} \cdot l_{(4)}} + \frac{l_{(4)\alpha} l_{(2)\beta}}{l_{(2)} \cdot l_{(4)}}, \qquad g^D_{\alpha\beta} = \sigma^{(3)}_{\alpha\beta} + \frac{l_{(1)\alpha} l_{(3)\beta}}{l_{(1)} \cdot l_{(3)}} + \frac{l_{(3)\alpha} l_{(1)\beta}}{l_{(1)} \cdot l_{(3)}}, \tag{4.18}$$

and considering the coordinates charts in which the metrics in the four regions all take the form (4.1) (with different functions $F(r)$ and $\phi(r)$), from equations (4.15) and (4.17) we get that

$$F_A(r_0) F_B(r_0) = F_C(r_0) F_D(r_0). \tag{4.19}$$

This is the DTR relation that we are going to use in the following [153, 154, 148].

Mass inflation at the inner horizon

We are now in the position to discuss the phenomenon of mass inflation in the framework of regular black hole geometries.

We need to apply the DTR relation (4.19) with a background spacetime describing a regular black hole. The situation is schematically represented in the Penrose diagram of Fig. 4.3. We are interested in understanding the behavior of the system when the crossing point of the two shells is displaced along a null outgoing curve and approaches the inner horizon; that is, we will take a constant value $u = u_0$ (this value is arbitrary except for the condition that it lies inside the outer horizon), and modify the value of v, so that the crossing point describes a curve $r_0(v)|_{u=u_0}$.
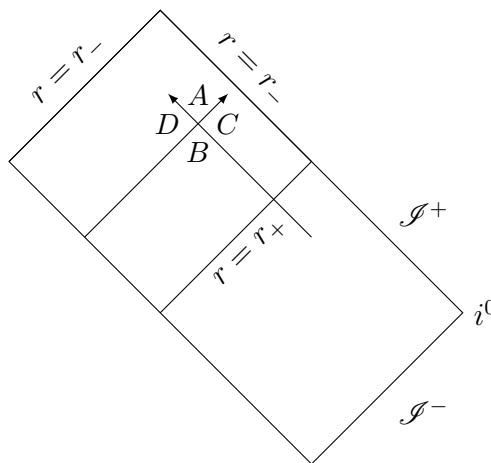
Figure 4.3: Schematic Penrose diagram of a regular black hole with concentric outgoing and ingoing null shells. The DTR relation is applied to the crossing point r_0 between outgoing and ingoing shells. The corresponding four spacetime regions A, B, C and D are depicted. We only depict the relevant quadrants of the maximally extended Penrose diagram present in Fig. 4.1

If we focus on a local neighbourhood around the crossing point r_0, Eq. (4.19) can be manipulated in order to obtain

$$m_A(r_0) = m_B(r_0) + m_{\text{in}}(r_0) + m_{\text{out}}(r_0) - \frac{2m_{\text{out}}(r_0)m_{\text{in}}(r_0)}{r_0 F_B(r_0)}, \qquad (4.20)$$

where we have $m_{\text{in}}(r_0) = m_C(r_0) - m_B(r_0)$, and also $m_{\text{out}}(r_0) = m_D(r_0) - m_B(r_0)$.

The first three terms on the right-hand side of Eq. (4.20) have a clear physical meaning: m_B measures the mass in the region inside both the ingoing and outgoing shells and, therefore, the original mass of the regular black hole before the ingoing shell is absorbed. This is moreover the region in which the coordinates (u, v) are defined. On the other hand, m_{in} and m_{out} are the mass of the ingoing and outgoing shells. These three contributions are finite, but the last contribution has to be analyzed carefully. The reason is that, as the point $r_0(v)|_{u=u_0}$ gets closer to the location of the inner

horizon, $F_B(r_0) \to 0$. This implies that, in order to understand the evolution of the system at late times, we need to understand the behavior with v of $m_{\mathrm{in}}(r_0(v)|_{u=u_0})$ and $F_B(r_0(v)|_{u=u_0})$ (note that m_{out} is constant along $u = u_0$):

a) *Behavior of* m_{in}: this quantity describes how the ingoing tails decay with v, and is determined by Price's law [156, 157, 158, 159, 160] to be given by a power law, namely

$$m_{\mathrm{in}}(r_0(v)|_{u=u_0}) \propto v^{-\gamma}, \tag{4.21}$$

where, for the purposes of the present discussion, it is enough to consider the lower bound $\gamma > 0$.

b) *Behavior of* F_B: this quantity vanishes on the inner horizon, but we need to determine how fast it approaches this value when we displace the point r_0 increasing the value of v along ingoing null curves. Along these trajectories Eq. (4.8) applies so that, close to the inner horizon, one has

$$\mathrm{d}v = \frac{2\mathrm{d}r}{e^{-\phi(r_-)}F'(r_-)(r - r_-)} + \mathcal{O}(r - r_H). \tag{4.22}$$

We just need to integrate this equation starting from some value of r greater than, but arbitrarily close to, r_-. Taking into account that $e^{-\phi(r_-)}F'(r_-) = 2\kappa_- = -2|\kappa_-|$, it follows that

$$F_B(r_0(v)|_{u=u_0}) \propto e^{-|\kappa_-|v}. \tag{4.23}$$

Combining these ingredients, we see that at late times ($v \gg 1/|\kappa_-|$), one has

$$m_A(r_0(v)|_{u=u_0}) \propto v^{-\gamma}e^{|\kappa_-|v}. \tag{4.24}$$

This is the equation that characterizes the phenomenon of mass inflation: the mass parameter in the region A grows exponentially, on a timescale determined by the surface gravity of the inner horizon. In other words, the inner horizon is unstable with a characteristic timescale $1/|\kappa_-|$ measured in the ingoing null coordinate v. This timescale is Planckian for most of the models in the literature (see Table D.1). Note that the proportionality constant in Eq. (4.24) is positive, which can be realized by recalling Eq. (4.20) and taking into account the signs of m_{out}, m_{in} and $F_B(r_0)$.

In the Reissner–Nordström metric, m_A is directly the physical mass in region A. However, in the geometries we are studying here, this would not be generally the case, although this does not change the meaning of Eq. (4.24). The reason is that m_A is always proportional to the mass M and, as a consequence, Eq. (4.24) can be directly translated into the unbounded growth of this parameter. In particular, on the inner horizon the function m_A is generically given by a positive numerical coefficient times M. This can be seen explicitly in the examples discussed in Table D.1.

4.1.3   Time dependent scenario

The analysis of the previous section refers to the static case. Now we discuss the generalization to the dynamical case as long as the evolution is slow enough. The
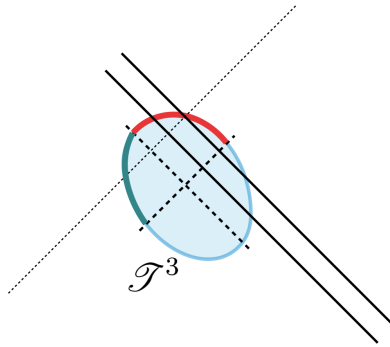
Figure 4.4: Detail of the trapped region for the regular black hole case and an outgoing radial null perturbation (dashed line) that intersects several ingoing radial null perturbations.

trapping region for the dynamical case is schematically depicted in Fig. 4.4 whereas the interesting sector of the Penrose diagram for the static case are depicted in Fig. 4.3.

It is clear that the two Penrose diagrams look very different from each other. Anyway, the main ingredient for mass inflation are unchanged. In fact, in both cases the g^{rr} component of the metric vanish at the inner horizon.

Hence, whenever the crossing points between outgoing and ingoing radial null perturbations are close (from inside) to the upper quadrant of $\mathscr{T}^3$ (the inner part in Fig. 4.4), we can calculate the mass in the different quadrants of spacetime defined by the two crossing shells, and integrate the resulting equations along the outgoing radial null geodesic describing the outgoing perturbation. As for the static case, it follows then that the mass in the quadrant that lies in the causal future of the crossing point grows exponentially with the value of v associated with the ingoing shell, being proportional to

$$e^{-|\bar{\kappa}_-|\Delta v}, \tag{4.25}$$

where $\bar{\kappa}_-$ is the average value on the interval Δv of the surface gravity of the future inner trapping, defined for the metric in Eq. (3.2) as

$$\kappa_-(v) = \frac{e^{-\phi(v,r)}}{2} \left.\frac{\partial F(v,r)}{\partial r}\right|_{r=R_0(v)}. \tag{4.26}$$

The only condition that is necessary in order to obtain Eq. (4.25) is that $R_0(v)$ remains roughly constant during the interval Δv, so that its variation can be neglected. Hence, there is an instability if the typical time scales of variation of $R_0(v)$ is much larger than $1/|\bar{\kappa}_-|$. This reasoning applies to the portion of the inner horizon in the right quadrant of Fig. 4.4, for which the intersection point of one ingoing and several outgoing null shell approaches the horizon in the future. A similar analysis can be performed for the other portion of the inner horizon in the left quadrant of Fig. 4.4, considering one outgoing and several ingoing null shells obtaining a instability exponentially growing in u with the same time scale $1/|\bar{\kappa}_-|$.

This means that short living geometry will be free from this instability. However unless the surface gravity value is fine-tuned, the natural value for the instability time scale is essentially given by the coordinate light-crossing time of the sphere $r = r_{\text{inner}}(v)$ which, in scenarios motivated by quantum gravity, is roughly the Planck time. Hence, this time scale is typically extremely short, if compared with the standard time scale associated with Hawking evaporation (that is cubic in the mass of the black hole). Of course, without a specific quantum gravity calculation it impossible to rule out the possibility for the surface gravity to assume a much lower value than the one naively expected. However, without this knowledge, and limiting our discussion to the effective description considered in this thesis (and other works dealing with regular black holes), the only possible way to deal with this instability is through extreme fine-tuning[2] of the properties of spacetime.

4.1.4   (Ir)relevance of the cosmological constant

So far we have not considered the presence of the cosmological constant for a very simple and intuitive reason. The instability is originated in a region of Planckian density where the role of the cosmological constant is completely negligible. Although this intuition is indeed correct, it seems contradicted by a series of work studying the instability of the inner horizon in general relativity for asymptotically De Sitter spacetimes in the context of the strong cosmic censorship [161, 162, 163, 164]. In these works the presence of a positive cosmological constant actually plays a crucial role and it still open the possibility that it may regularize the inner horizon of a Reissner-Nordström or Kerr black hole leading to the violation on the strong cosmic censorship conjecture. Let us pause from our discussion in order to understand why the cosmological constant is important in that situation and why the contradiction with our intuition is only apparent. While the geometry near the inner horizon is unchanged, the cosmological constant modifies the asymptotic geometry and the function $F(r)$ approaches

$$F(r) \sim 1 - \frac{2M}{r} - \frac{\Lambda}{3} r^2. \tag{4.27}$$

This results in a modification of the casual structure of spacetime as in addition to the inner and outer horizon we get an extra horizon, the cosmological horizon, approximately located at $r_c \sim \frac{\sqrt{3}}{\sqrt{\Lambda}}$. This, in turn, can effect the decay of the perturbation as the boundary conditions are modified and have to be imposed in the cosmological horizon rather then at spatial infinity.

As shown in [165, 166] the late time behavior of the perturbation in the presence of a cosmological constant does not follow the Price law (4.21) but it has an exponential decay.

$$m_{in} \propto e^{-\omega_I v} \tag{4.28}$$

where ω_I is the imaginary part of the least dumped quasinormal mode. Repeating the same steps leading to the mass inflation instability with this decay rate we would get

$$m_A(r_0(v)|_{u=u_0}) \propto e^{(|\kappa_-|-\omega_I)v}. \tag{4.29}$$

---

[2]That is, it is necessary to tune the order of magnitude dimensionless numbers to ensure that black holes can be long-lived.

Therefore, in the limit $v \to \infty$ the mass function m_A will go to zero if $\omega_I > |\kappa_-|$. This is why the relevance of the cosmological constant related to the fate of the strong cosmic censorship is an active area of research. Anyway, there are two reasons why Eq. (4.29) does not imply that the inner horizon is stable in our configuration. The first reason is that the most natural value for the surface gravity is given by the Planckian curvature. Therefore we expect $\omega_I < |\kappa_-|$. Anyway this is not a very satisfying solution. We could imagine to tune the surface gravity in order to obtain $\omega_I > |\kappa_-|$ and we would arrive at the conclusion that an arbitrary small cosmological constant is enough to regularize the inner horizon. To really understand why this conclusion is erroneous, we have to specify the meaning of "late time behavior".

In fact, the decay of the perturbation in an asymptotically de Sitter spacetime begin to differ from the one in an asymptotically flat spacetime only after a transient of time that is longer for smaller cosmological constant. From the physical point of view it is quite simple to understand why. If the cosmological constant is very small, the perturbation needs to reach a region of spacetime close enough to the cosmological horizon in order to manifest some difference with respect to the asymptotically flat spacetime. The late time behavior cannot start before this moment. Therefore we can estimate a lower bound for the time after which the dumping of the perturbation follow the law in Eq. (4.28) as the time needed to reach the cosmological horizon $v_c \sim r_c \sim \Lambda^{-1/2}$. So the dumping of the perturbation follows Price law for $v < v_c$, leading to

$$m_A \approx v^{-\gamma} e^{|\kappa_-| v}, \qquad v \lesssim \Lambda^{-1/2}. \tag{4.30}$$

This timescale is so huge that for generic initial condition the instability will be triggered well before the beginning of the exponential decay regime, showing that the cosmological constant in completely negligible for our discussion.

4.2 One way hidden wormholes and asymptotic hidden wormholes

The geometries belonging to the class of one way hidden wormhole do not have an inner horizon and, therefore, they are not plagued by the mass inflation instability. Anyway, the presence of a minimum radius poses problem concerning the topology of the spacetime. We will divide the discussion in two parts as the picture is similar but different for the one way hidden wormhole case and the asymptotic hidden wormhole case.

4.2.1 One way hidden wormhole

This class of geometry is characterized by a minimum radius throat. If the minimum of the radius is a global minimum than the topology of the Cauchy surfaces is $\mathbb{R} \times S^2$. Anyway, we want the spacetime to describe a gravitational collapse. This means that in a given initial Cauchy surface there is a regular distribution of matter implying that the topology of that surface is simply the topology of $\mathbb{R}^3$. As discussed in Sec. 3.2, topology change is not compatible with our assumption of global hyperbolicity which implies that all the Cauchy surfaces are homeomorphic with each other. Therefore, the

only possibility is that in any Cauchy surface the value of the radius $r = R_0$ is only a local minimum.

Therefore, the $r = R_0$ line, besides having a portion which is a minimum radius hypersurface (that is, the radius would be greater at both sides of the hypersurface), would have to reach both i^- and i^+. If we trace this $r = R_0$ line back to i^-, one goes continuously from a situation in which the radius is greater at both sides of this hypersurface to a situation in which the radius is greater on one side and smaller on the other one. Let us focus our attention on the side in which there is a transition from the radius being greater than its value on this hypersurface to becoming smaller, and take two points in these two regions. Along an arbitrary line connecting these two points, it is clear that, due to continuity, there is a point in which $r = R_0$ as well (which is not contained in the previous hypersurface). This argument can be repeated for all points on this side of the original $r = R_0$ hypersurface and arbitrarily close to the latter, which implies the existence of two $r = R_0$ that merge at some point. The metric cannot be analytical at this point. Also, the single $r = R_0$ line that remains after the merger must disappear (if we assume that it does not end up in i^0), which implies the existence of another point in which the metric is non analytic (see Fig. 4.5 for a sketch of the Penrose diagram in this situation).

Finally let us note that there is one last possibility that have been considered to make this class of geometries viable. It is simply possible that the geometry is not defined in the regions where it cannot analytic. This is exactly what happen in [167, 168, 169] where the authors provide a metric which locally describes an element of this class of geometries but which is not globally defined, *i.e.*, there are regions where an effective spacetime is not defined. This possibility lies outside our classification as we are assuming an everywhere defined metric, but it is a clear example of the fact that our analysis can provide useful insights also when this is not the case.

4.2.2   Asymptotic hidden wormhole

In the case of asymptotic hidden wormhole there is an extra consistency issue which is not easy to solve. This issue concern the consistency with semiclassical physics. Our analysis has a purely geometrical nature but we expect that the resulting geometry agrees with semiclassical physics and in particular with Hawking radiation. The asymptotic hidden wormhole class can be compatible with the existence of Hawking radiation if and only if the latter eventually switches off due to some unknown quantum gravity effect. Anyway, the switching off of Hawking radiation cannot be described using quantum field theory on the geometric backgrounds leading to remnants that have been discussed in complete generality in this thesis; this description must break down at some point, meaning that the effective description in terms of differentiable manifolds is no longer meaningful below a certain length scale. On the other hand, for these geometries there is an extra possibility to avoid the topology change. This possibility consist in the fact that the throat represent a spacelike boundary of the spacetime. This solution is only viable in the asymptotic hidden wormhole case as the boundary has to be reached only asymptotically for infinite value of the affine parameter in order to be consistent with geodesic completeness. The fact that the boundary is spacelike allows all the Cauchy hypersurfaces reach $r = 0$. Anyway, in practice, it is difficult to devise
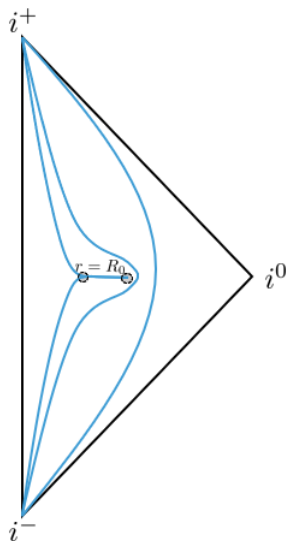
Figure 4.5: One-way hidden wormhole with some lines of constant r depicted. In order to avoid issues with topology change the metric must fail to be analytic in at least two points. Such points are encircled for clarity.

a geometry that realizes this configuration.

4.3 Conclusions

In this chapter we have studied the viability of the non-singular black hole solutions we have introduced in the previous chapter. In Fig. 4.6 we consider again the table present in Fig. 3.14 adding an extra line containing the information regarding the issues associated with each class of solution. The most immediate consequence of our analysis is that one cannot just naively assert that singularity regularization will solve the outstanding issues of black hole physics without introducing additional aspects that, after a thorough analysis, may lead to radical surprises for our theoretical and observational understanding of black holes. In fact, the remarkable result is that there is no fully "safe" option: all classes of geometries display internal inconsistencies (instabilities, topology change or incompatibilities with semiclassical physics), except for the particular case of evanescent black holes in short timescales. However, the timescales in the latter case are so short (of the order of the light-crossing time) that this possibility entails a complete rethinking of the concept of black hole. Indeed, a fast bounce would not be obviously at odds with observations only if the matter remains close enough to the would-be-horizon, or if this process constitutes a transient phase after which the object relaxes to a stable state (maybe horizonless to avoid the self-consistency issues of the other classes of geometries).

Let us stress that, although we have assumed an everywhere well defined geometry, our analysis is valuable also when this is not the case and it allows us to understand how to construct singularity regularization scenario that solves the self consistency issues raised in this chapter by allowing for region where an effective geometry cannot be
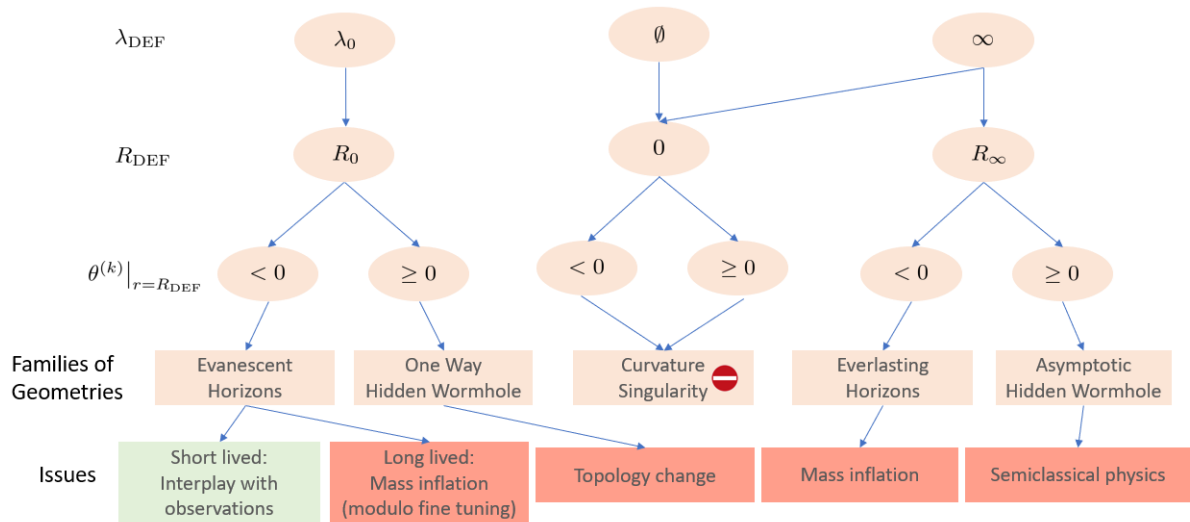
Figure 4.6: The table summarizes the classes of the allowed geometries and the issues associated with them.

defined. Interesting examples are constituted by the pictures studied in [167, 168, 169] where the geometry is defined almost everywhere but in a small region, a feature that allows these models to escape some of the self consistency issues raised here.

Finally, it is important to stress that, while the analysis was performed in spherical symmetry, the language we have used is well adapted to deal with the more realistic situation in which this simplifying assumption is lost. In fact, the only place in which spherical symmetry was explicitly used was to derive the conditions in Eq. C.2 which were necessary to prove the existence of an inner horizon for the classes of evanescent or everlasting horizon. A generalization of this result to the non spherically symmetric case would be enough to generalize the whole analysis.

Chapter 5

Phenomenology of non-singular black holes

After having discussed a geometrical classification of non-singular spacetimes in chapter 3 we have studied in detail their internal consistency in chapter 4. We have seen that the regularization schemes without possible phenomenological observation are very difficult to make self consistent. This gives us motivation to look into the possible observational windows that could discriminate between singular black holes and non-singular alternatives.

The discussion in this chapter is mainly based on **P4** and it is divided in two main parts. The first part consists of a brief review of the different scenarios that have been proposed in the literature in order to avoid theoretical problems that are inherent to classical and semiclassical black holes (e.g., the singularity or information loss problems), including a discussion about their collocation into the classes of geometries provided in chapter 3. The second part of the chapter focuses on the observational tests that are available to probe the structure of astrophysical black holes, with the goal of emphasizing how close we are to testing the existence of all the relevant mathematical elements of these objects as described by general relativity, and parametrizing the room that is still available for alternatives in terms of a set of phenomenological parameters. The meaning of these phenomenological parameters is illustrated by comparison with the scenarios described in Sec. 5.1.

5.1 A taxonomy of proposals

5.1.1 Regular black holes

The first class that we need to introduce is the one of regular black holes which has been discussed in detail in the previous chapter. As we have discussed, the main property of this type of geometry is that the singular core of a classical black hole spacetime is replaced by a smooth spacetime region. In order to make the curvature invariants finite everywhere, we are forced to introduce a inner horizon that pose stability issues. Therefore, the situation for this class of geometry can be summarized as follow:

- There might be small correction to the classical geometries in regions which are observationally available. However the existence of such deviation is not necessary

- The inner horizon is generically unstable and small perturbations can have large effect on the geometry.

Therefore, while we have discussed that it is difficult to make this geometry self consistent, we will see in the rest of the chapter that this model is very poor from a phenomenological point of view.

5.1.2   Bouncing geometries

Instead of focusing on the description of the regular geometries that may describe black holes once formed, let us now analyze in more detail the fate of one of the main actors in the formation process: matter. Black holes are formed from collapsing lumps of matter. It is therefore of utmost importance to understand the physical mechanisms that may prevent these lumps of matter from collapsing completely, resulting in a singularity, and the implications that follow.

In practical terms, we can divide the spacetime of a collapsing (spherically symmetric) distribution of matter in two regions: the external one, which is idealized as being vacuum, and the internal one which describes the interior of the collapsing matter. In the previous section we have been dealing mainly with the external geometry. However, the physics of the internal geometry is important as well, and in fact it might be the most important one regarding the regularization of the singularity [170].

The non-singular core of the regular black holes discussed above can be understood as the result of the tendency of matter towards collapsing, together with the existence of repulsive forces of quantum-mechanical nature that are triggered when Planckian curvatures are reached. However, from this perspective it seems unnatural that these two tendencies cancel exactly in order to stabilize the collapsing distribution of matter at a fixed radius no matter what the initial conditions are. Dynamically, it seems more natural to expect that the existence of a repulsive core would lead generally to bouncing geometries (while asymptotically stationary solutions with a small core may be reached for very particular values of the initial conditions).

This kind of bouncing behavior was first studied in [104, 105, 171, 172], but has been independently proposed more recently in scenarios inspired by emergent gravity [173, 135, 136] and loop quantum gravity [134, 137]. Regardless of the special details of each particular implementation of this idea, there are two aspects that are robust (see however [174, 175, 176, 177, 178, 179] and [180, 181] for alternative bouncing scenarios):

- *Timescale [182]:* concerning the timescale of a bounce of matter we need to separate the discussion in two cases. In the first case the timescale for the bounce (suitably defined in terms of the proper time of the relevant observers) is shorter than the (naive) evaporation time of the black hole,

$$\tau_{\rm B} < \tau^{(3)} \sim t_{\rm P}(M/m_{\rm P})^3 \tag{5.1}$$

Plausible values for this timescale are

$$\tau_{\rm B} = \tau^{(j)} \sim t_{\rm P}(M/m_{\rm P})^j, \qquad j = 1, 2. \tag{5.2}$$

These two values verify $\tau^{(j)} \ll \tau^{(3)}$. Let us note that these timescales are generally multiplied by logarithmic factors that have not been written explicitly but become

relevant for certain values of the parameters involved.

The second possibility is that the timescale scale of the bounce, in absence of Hawking radiation, would be larger than the timescale of the evaporation time of the black hole [169]. In this case the time evolution matches the one of a black hole evaporating in semiclassical gravity until it reaches Plankian size. Only at that point the physics responsible for the bounce becomes relevant and we have a bounce of a Plankian size blak hole into a white hole. We are not going to focus much on this possibility in the following as it is very poor from a phenomenological point of view due to the huge timescale of the process.

- *Modifications of the near-horizon geometry [135, 137]:* the external geometry of the spacetimes in which the bounce of the distribution of matter can be observed by external observers in the original asymptotic region must include modifications of the near-horizon geometry, even if the bounce of matter takes place much deeper inside the gravitational potential well (roughly, when the density of the radius of the collapsing structure is Planckian). The ultimate reason is that these geometries must interpolate between a black-hole-like geometry and a white-hole-like geometry. The only continuous way to define this interpolation involves modifications of the geometry up to a certain radius $r_\star > r_{\rm s}$, the value of which is typically constrained by $(r_\star - r_{\rm s}) \lesssim r_{\rm s}$. This point can be illustrated using Painlevé-Gullstrand coordinates:

$$\mathrm{d}s^2 = -\mathrm{d}t^2 + [\mathrm{d}r - fv(r)\mathrm{d}t]^2 + r^2\mathrm{d}\Omega^2, \tag{5.3}$$

where $f = \mp 1$ correspond to a black hole or a white hole in these coordinates, respectively, and $v(r) = \sqrt{r_{\rm s}/r}$. In order to modify the geometry continuously from one case to the other, a function $f(t, r)$ that interpolates between these values and which is nonzero at $r = r_{\rm s}$, is needed.

The shortest possible time for the bounce to take place is $\tau_{\rm B} = \tau^{(1)}$, as proposed originally in [173, 135, 136]. Another possibility, conjectured in [137, 183], has $\tau_{\rm B} = \tau^{(2)}$. The second timescale is small if compared with $\tau^{(3)}$, but is still quite large so that, for a black hole to be exploding today, it must be a primordial black hole (though with different mass than in the case of regular black holes for which the relevant timescale is assumed to be $\tau^{(3)}$). So far it does not seem possible to justify the timescale $\tau_{\rm B} = \tau^{(2)}$ through specific calculations such as the one in [183], while the timescale $\tau_{\rm B} = \tau^{(1)}$ arises in two independent calculations [172, 184].

Regarding possible observational channels, the second feature above (the modifications of the near-horizon geometry) might seem the most promising one at a first glance. Note that, in contraposition to regular black holes, these modifications are now a must. However, let us note that in the most natural scenarios, the modifications in these geometries are by construction $\mathscr{O}(1)$ only after the time $\tau_{\rm B}$.

This implies that, if we are probing the geometry with physical processes during an interval of time Δt (which could be, for instance, the time that an observed photon took to go through this region of the geometry), any cumulative effects due to these deviations from the classical geometries would be suppressed by the dimensionless quotient $\Delta t/\tau_{\rm B}$. For $\tau_{\rm B} = \tau^{(2)}$ this dimensionless number will be generally small. Hence, it is reasonable to think that, unless we are considering physical processes with typical

timescales comparable to the timescale of the bounce τ_{B}, it would be difficult to use these processes in order to learn about the geometry. It might be possible however that there exist non-trivial mechanisms that act to amplify the value of the number $\Delta t/\tau_{\mathrm{B}}$ when the latter is small, though at the moment this is just a conjecture. On the other hand, if one was able to perform experiments which monitor the evolution of the black hole during a time interval $\Delta t \sim \tau_{\mathrm{B}}$, the very end of the bounce process would be observable, which would certainly be more dramatic.

In consequence, in the absence of mechanisms that can compensate the small quotient $\Delta t/\tau_{\mathrm{B}}$, (looking for these amplification mechanisms would be an interesting exercise), the most promising observable feature of models with $\tau_{\mathrm{B}} = \tau^{(2)}$ is, again, the one associated with the end of the dynamical process; for regular black holes this was the evaporation process, but here is the very bounce of matter. The associated physics resides simply in the timescale τ_{B}, which for instance controls the typical size of the black holes for which these effects would be observable today.

Let us anyway assume that bounces with a timescale τ_{B} take place in nature. One is then forced to answer the question: what happens after the bounce? There are essentially two possibilities. One possibility is that the bounce releases all the available energy and matter such that the black hole dissipates completely. This would imply that black holes disappear in a timescale τ_{B}, which can be compatible with observations only if τ_{B} is large enough. This possibility is the one considered for instance in [185, 186] and, as we have discussed, from a phenomenological perspective the most promising observational opportunity is the detection of this cataclysmic event (see Sec. 5.3.5 for a more detailed discussion).

A second (and, arguably, more natural) possibility is that part of the energy content is released after the bounce, leaving a remnant that may again undergo renewed gravitational collapse [136, 184]. In this scenario, it may be possible that a different kind of horizonless equilibrium configuration is reached, so that the bounce itself (which may occur several times) would be just a transient. This second possibility is arguably more rich observationally, as both the transient phase with timescale roughly τ_{B} and the horizonless stable phase would have distinctive observational signatures which we shall now explore in the next section.

5.1.3   Quasi-black holes

In order to encompass different alternatives in the literature, let us define a static and spherically symmetric quasi-black hole in a rough way as a spacetime satisfying the following conditions: (i) the geometry is Schwarzschild above a given radius R that is defined to be the radius of the object, (ii) the geometry for $r \leq R$ is not Schwarzschild, and (iii) there are no event or trapping horizons. In other words, this kind of geometry is qualitatively similar to that of a relativistic star, but with a typical radius of the structure R that can be arbitrarily close to r_{s}, hence violating the isotropic-pressure Buchdahl-Bondi bound [187, 188] (let us note in passing that including pressure anisotropy permits one to attain more compact configurations that are not limited by the isotropic Buchdahl-Bondi bound [189].) In fact, in this section we consider objects that can be characterized as having a surface. Configurations that fall within the definition above but do not have a surface (wormholes) are described in the next

section.

There are several proposals in the literature for this kind of geometry (including gravastars [190, 191, 192], fuzzballs [193, 194], and black stars [195, 196]), but all of them present severe restrictions. In general terms, it is possible to prescribe (or derive from first principles [197]) this kind of geometry only when the outer geometry is that of non-rotating or slowly rotating black holes. Most importantly, there is virtually no knowledge about the dynamics of these objects; not only there are large gaps in the understanding of their possible formation mechanisms, but also of their behavior under other dynamical processes that they may undergo after formation. For instance, it is generally not clear how these objects interact with regular matter. There have been studies proposing Hawking radiation as the main ingredient to form these objects [198, 199, 200, 201, 202, 203], but these proposals share a number of problems (e.g., [204, 205, 206]) that raise substantial doubts about their validity. It is also worth stressing that quasi-black holes violate the assumptions of no-hair theorems (e.g., [207]), so that it is in principle possible that the external geometry is different than the Schwarzschild geometry in static (but not spherically symmetric) situations or the Kerr geometry in the rotating case. In particular, while in the static case such deviations are very strongly suppressed [208], this is no longer true for the rotating case [209].

If quasi-black holes are formed, this would require the existence of a transient before the system can settle down in this kind of configuration. The details of this transient are still largely unknown and would probably be rather complex, but in a first approach we can parametrize our ignorance in terms of another timescale, namely a relaxation timescale (in the bouncing scenario discussed above, this scale would be controlled by $\tau^{(1)}$, with logarithmic corrections depending on the values of certain parameters [182]). This timescale could also show up in other events such as, for instance, the merger of two of these objects. As emphasized above, it is not known whether or not it is possible that the result of the merger of two quasi-black holes is still a quasi-black hole. However, if this is the case, it is reasonable to assume that the final quasi-black hole state is reached after this relaxation timescale.

Aside from these transients, these objects are expected to lead to distinctive phenomenological signatures arising from interaction with light, matter and gravitational waves — due to the large modifications of the geometry starting at $r = R$. In particular, while black holes are perfectly absorptive, quasi-black holes do not necessarily satisfy this property (although there are again many uncertainties in this regard). Note, however, that any physical observable (i.e., a quantity that can be measured in an experiment) is expected to go back continuously to its value for a black hole in the limit in which $\mu \to 0$, where

$$\mu = 1 - \frac{r_{\mathrm{s}}}{R}. \tag{5.4}$$

This observation would seem to imply that, for extremely small μ, all observables should differ by very small amounts from the values they would take for a classical black hole (we can think about performing a Taylor expansion on the parameter μ). This depends, however, on the functional dependence of observables on μ. We will see that different observables display different behaviors (e.g., polynomial or logarithmic) with respect to μ.

In order to develop some intuition on the typical values of μ, let us make explicit the relation between μ and the distance between the surface and the would-be horizon.

For $\mu \ll 1$, and if the surface is at a proper radial distance $\ell \ll r_s$ from r_s, one has

$$\mu \simeq \frac{1}{4}\left(\frac{\ell}{r_s}\right)^2 \simeq 7 \times 10^{-78}\left(\frac{M_\odot}{M}\right)^2\left(\frac{\ell}{\ell_P}\right)^2. \tag{5.5}$$

It is illustrative to consider for instance $\ell \sim \ell_P$ and the mass corresponding to Sgr A*, $M = 4 \times 10^6\ M_\odot$, which yields $\mu \sim 10^{-91}$.

5.1.4   Wormholes

Wormholes are tunnels connecting different regions of spacetime and supported by large amounts of exotic matter or energy [210, 211, 212, 213, 191, 214]. The most interesting class of wormholes are the so-called traversable wormholes, that can be maintained open for enough time to allow geodesics to travel through them. Let us focus for simplicity on Morris-Thorne wormholes [215, 216]: time independent, non-rotating and spherically symmetric solutions of general relativity (with a suitable matter content) describing a bridge/passage between two asymptotically flat regions, not necessarily in the same universe. These objects are described by the metric

$$ds^2 = -e^{-2\phi(x)}dt^2 + dx^2 + r^2(x)d\Omega^2, \tag{5.6}$$

where $x \in (-\infty, +\infty)$ and one requires the absence of event horizons and metric components that are at least C^2 in x. Asymptotic flatness for $x \to \pm\infty$ requires

$$\lim_{x \to \pm\infty} \frac{r(x)}{|x|} = 1 \tag{5.7}$$

and

$$\lim_{x \to \pm\infty} \phi(x) = \Phi_\pm \in \mathbb{R}. \tag{5.8}$$

On the other hand, the radius at the wormhole throat is $r_0 = \min\{r(x)\}$, which can always be chosen to be at $x = 0$. The geometry (5.6) corresponds to flat spacetime, up to small corrections, far away from the throat. It is nevertheless possible to modify the external geometry so that it describes the gravitational field of a massive source, as in the Schwarzschild geometry [217, 218], or also to include rotation (e.g., [219]) which would be eventually necessary in order to describe realistic astrophysical black holes. Moreover, as in the case of quasi-black holes, the no-hair theorems do not directly apply to these objects, so that even in static situations it may be possible that higher multipoles take nonzero values.

   This metric is a solution of the (non-vacuum) Einstein equations that requires a stress-energy tensor that violates the null energy condition, which states the positivity of the product $T_{\mu\nu}k^\mu k^\nu$ for any null-like vector k^μ (this implies that the weak, strong and dominant energy conditions are violated as well [210, 220]). Hence, the matter and energy content that keeps the throat open cannot have standard properties. These exotic properties may find a justification in the quantum properties of matter, when the latter is described in terms of quantum fields. Quantum effects in curved backgrounds and, in particular, the polarization of the quantum vacuum, may provide the necessary stress-energy tensor to support wormholes [221, 222].

It is generally accepted that standard particles of matter and waves can cross traversable wormholes without experiencing appreciable interactions with the exotic matter opening the throat, although there is virtually no knowledge about the possible interactions between standard matter and the source of the wormhole geometry. Hence, here we will consider that the interior of wormholes is essentially transparent, but keeping in mind that a deeper analysis of this issue would be desirable. This assumption would be certainly more reasonable if the exotic matter inside the wormhole comes entirely from the polarization of the quantum vacuum. This traversability property (or, in other words, the lack of a physical surface) represents the main difference between wormholes and quasi-black holes as defined in the previous section. Aside from this difference, these two kinds of objects share several properties. In particular, most of (if not all) the uncertainties regarding the understanding of the dynamics of quasi-black holes and their formation mechanisms equally apply to wormholes.

5.1.5 From local to global classification on geometries.

At this point we have provided two different classification of non-singular geometries, one introduced in chapter 3 and the one introduced just now. We now want to provide a link between the two classifications and we are going to do so by analyzing one by one the geometries in chapter 3 and checking where they are placed in the classification just introduced. As we will see, there is no one to one link between the classes of geometry of the two classifications. This is not surprising as the classifications are based on very different aspects of the spacetime. The classification provided in chapter 3 is based on local properties of the geometry close to the trapping region. On the other side the classification just introduced is based on global properties of the geometries as seen from a asymptotic observer. Although the discussion of this section might be extracted from chapter 3, we include some key point here for convenience.

Evanescent horizon and everlasting horizon

Let us start from the class of evanescent horizons and everlasting horizon. These classes are characterized by the presence of an inner and a trapping horizon that merge at some point in the case of evanescent horizon or that reaches $\mathscr{S}^+$ in the case of everlasting horizon. The first possible global geometry associated to these classes is the one corresponding to a regular black hole which eventually evaporates leading to a spacetime without trapping horizon or which never disappears and either grows or stays stationary.

In the case of evanescent horizon there is another possibility which corresponds to a bouncing geometry. In this case the outer and the inner horizon are formed during the gravitational collapse and they disappear during the bounce. In this case, after the disappearance of the trapping region, an antitrapping region is formed (this possibility is depicted in Fig. 3.8) where the geometry is locally the one of a white hole. This is a clear example of how the same local properties at the trapping region correspond to two very different global geometries.

One-way hidden wormhole and asymptotic hidden wormhole

As the names suggest, one-way hidden wormholes and asymptotic hidden wormholes may correspond to a global geometry of a wormhole which can be traversed only in one direction as the throat is hidden beyond a trapping horizon[1]. Anyway, in this chapter we are mainly focused on traversable wormholes as they have a richer phenomenology. From the phenomenological point of view, this classes of geometries are more similar to regular black holes than to traversable wormholes.

As before, the one-way hidden wormhole can correspond to a bouncing geometry. In this case, matter bounces in the throat of the "wormhole" directly into an antitrapping region. As explained in Sec. 3.3 and depicted in Fig. 4.5, to realize this possibility the geometry cannot be defined everywhere.

Other geometries

Let us finally stress that the quasi-black hole and the traversable wormhole classes do not have any corresponding geometry in the classification of chapter 3 for the very simple reason that these classes do not posses a trapping region.

5.2 Phenomenological parametrization of deviations from general relativity

From the perspective of astrophysical observations using electromagnetic waves, black holes are regions in spacetime that can be detected only indirectly through their gravitational effects on matter surrounding them. This has changed with gravitational wave astronomy. However, observationally is not clear that these regions of spacetime correspond strictly to black holes in the sense of general relativity. This is a fundamental question regardless of the stance taken with respect to the different alternatives in Sec. 5.1. Only a detailed analysis of this question would make possible separating what is really known from the aspects that can be only inferred from (most of the time, partial) theoretical arguments.

In order to illustrate this point and make quantitative statements, let us introduce a set of phenomenological parameters encapsulating deviations from the behavior expected in general relativity. We will compare the physics associated with each of these parameters with the theoretical models reviewed in Sec. 5.1, and then consider how these parameters can be constrained observationally. These parameters are functions of the physical quantities characterizing the most general black hole geometry that is expected to be relevant for astrophysical scenarios, namely the Kerr geometry [223]: the mass M and the angular momentum J (that we do not deal explicitly with for simplicity). Let us start with two timescales:

1. *Lifetime*, τ_+: The timescale in which a black hole with mass M, in vacuum, disappears completely (due either to Hawking radiation, or some other effect).

---

[1]Note that in the case of asymptotic hidden wormholes case the throat is only reached asymptotically

2. *Relaxation*, τ_-: is the amount of time in which $\mathcal{O}(1)$ transient effects taking place after violent dynamical processes dissipate (formation of the black hole, merger, etc.). Typically this can be identified with the imaginary part of the lowest quasi-normal mode of the final-state system (e.g., [224]).

These two timescales describe the interval of time $t \in [\tau_-, \tau_+]$ in which the system is expected to be evolving slowly enough that it can maintain stable structural properties. Within this time interval, it is meaningful to define the following parameters:

3. *Size*, $R = r_s(1 + \Delta)$: Value of the radius below which the modifications to the classical geometry are $\mathcal{O}(1)$. We will use the more convenient parameter $\Delta \geq 0$. Note that this parameter is related to μ in Eq. (5.4) as $\mu = \Delta/(1+\Delta)$. For $\Delta \ll 1$ it follows that $\mu \simeq \Delta$, so that these two parameters can be used interchangeably.

4. *Absorption coefficient*, κ: Measures the fraction of the energy that is semi-permanently lost inside the region $r \leq R$. This can be due to the inelastic interaction with the horizonless object, when exciting internal degrees of freedom in the bulk, or simply due to its propagation into some other spacetime region (consider, for instance, a wormhole).

5. *Elastic reflection coefficient*, Γ: If there is a certain amount of energy falling onto the object and reaching $r = R$, this coefficient measures the portion that is reflected at $r \geq R$ due to elastic interactions (i.e., energy which is not absorbed and bounces back).

6. *Inelastic reflection coefficient*, $\tilde{\Gamma}$: Measures the portion of energy that is temporarily absorbed by the object and then re-emitted. That is, it measures the amount of energy that is inelastically reflected. It is related to κ and Γ by $\tilde{\Gamma} = 1 - \kappa - \Gamma$.

7. *Tails*, $\epsilon(t, r) \ll 1$: Modifications of the geometry that decay with radial distance, typically polynomial but possibly modulated by functions of compact support. Hence, there might be a maximum radius such that $\epsilon(t, r \geq r_\star) = 0$. In principle one would need to introduce a series of functions $\epsilon^J(t, r)$ to describe different decaying tails for different coefficients of the metric [225]. For $r_\star = \infty$ these tails would produce nonzero values of higher-order multipole moments (e.g., [207]).

These phenomenological parameters (and function) allow us to characterize our ignorance about the actual properties of astrophysical black holes: for a black hole in general relativity,

$$\begin{aligned} \tau_+ = \infty, \qquad & \tau_- \sim 10\,M, \qquad && \mu = 0, \\ \kappa = 1, \qquad & \Gamma = 0, \qquad && \epsilon(t, r) = 0. \end{aligned} \qquad (5.9)$$

Regarding the first parameter τ_+, we expect it to be at most $\tau_+ = \tau^{(3)}$ as defined in Eq. (5.1) due to Hawking radiation. But this is still infinite for any practical purposes for astrophysical black holes. The estimate for τ_- is obtained taking the inverse of the imaginary part of the lowest quasi-normal mode which governs the damping rate of perturbations [226, 227]. The rest of the parameters are unchanged in the semiclassical approximation. Hence testing the (semiclassical) black hole picture essentially means constraining the value of these parameters. The closer these parameters are to their

values in Eq. (5.9), the more confident we will be that astrophysical black holes are classical black holes (especially if we are able to discard some regions containing values associated with known theoretical models). The corresponding values for the various classes introduced in Sec. 5.1 are given in Table 5.1. In the rest of the chapter, we discuss the most stringent bounds that can be currently placed on these parameters.

It is always possible to introduce even more additional parameters or functional relations, such as frequency-dependent values of $\mu(\omega)$ and $\Gamma(\omega)$. However, in practical terms this just implies that we are including additional parameters that would provide more freedom to play with the observational data. The set we introduced above is minimal, but still interesting enough to give a detailed picture of the observational status of black holes. In practice, the only additional freedom that we will consider is the possibility that some of these coefficients are different for electromagnetic and gravitational waves.

Model	τ_-	τ_+	Δ	κ	Γ	$\tilde{\Gamma}$	$\epsilon(t,r)$
Classical black hole	$\sim 10M$	∞	0	1	0	0	0
Regular black hole	$\sim 10M$	U	0	1	0	0	MD
Bouncing geometries	MD	MD	0	1	0	0	$r_\star = \mathscr{O}(r_{\rm s})$
Quasi-black hole	MD/U	∞	> 0	MD/U	MD/U	$1 - \kappa - \Gamma$	U
Wormhole	U	∞	> 0	MD	$1 - \kappa$	0	U

Table 5.1: Values of the phenomenological parameters for the different classes of black hole mimickers. MD stands for Model Dependent and U for Unknown, whereas MD/U emphasizes that the quantity is model dependent but at the moment there is no particular model within the class that is able to predict specific values for the corresponding parameters.

5.3   Electromagnetic waves

The presence of dark distributions of mass that do not themselves emit electromagnetic radiation can be indirectly detected by their gravitational effects on the surrounding luminous matter. This has been traditionally the strategy followed in order to hunt for black holes in astronomical data. This electromagnetic radiation can also be used to probe the gravitational field around these dark distributions of mass and even constrain some of their surface properties. In this section we review the most powerful observations and reevaluate their strength on the basis of the parametrization introduced in Sec. 5.2 above.

5.3.1   Orbiting stars

The first kind of situation we shall consider can be idealized as a many-body system of compact distributions of matter that are interacting gravitationally, with at least one element that is not (appreciably) emitting electromagnetic radiation. The simplest possible configuration would be a binary system composed of a regular star and a dark

companion, an example of which is A0620-00 [228] (which is also the closest system of this kind to the solar system). The electromagnetic radiation coming from the luminous star can be used in order to deduce the mass of its companion through the so-called mass function [229, 230], which in the case of A0620-00 yields $6.60\pm0.25\ M_\odot$ [231]. This value is well above the maximum theoretically allowed mass for neutron stars [15, 232, 233]. While the mass parameter can be extracted, all the phenomenological parameters introduced in Sec. 5.2 remain virtually unconstrained (or weakly constrained if compared with other observations detailed below). Hence, observations of these binary systems of stellar-mass objects justify the existence of dark and compact distributions of matter that are not neutron stars, but not much more information about the intrinsic properties of these structures can be extracted.

The situation may improve if the mass of the dark object increases by several orders of magnitude, which would typically imply moving from a binary system to a many-body system. The larger number of luminous stars improves the statistics and therefore allows placing stronger constraints. On the one hand, there is only a single system of this kind that is accessible to current technology: the center of our own galaxy. Sagittarius A* (Sgr A*) is an astronomical radio source at the center of the Milky Way, which has long been considered to be the location of an astrophysical black hole [234]. On the other hand, this region has been extensively studied during more than two decades [235, 236, 237, 238, 239, 240], with the result that the trajectories of a large number of orbiting stars are known with excellent precision [241, 242]. A sizable portion of the claim that Sgr A* is a black hole comes in fact from these observations.

The main parameters which are fixed by these observations are the mass of Sgr A* and our distance from it. Precise values and errors can be found in the above references, but roughly these are given by $M = 4 \times 10^6\ M_\odot$ and $d = 8$ kpc, with errors of the order of 1%. The measure of the distance obtained from tracking these stars, which is based on the geometric method proposed in [243], is in good agreement with the results of other methods (e.g., [244]).

More interesting for the present discussion is the remark that these observations also constrain the size of Sgr A*, on the basis that these stars have been observed to travel freely without colliding with the central ultracompact object (UCO in the following). The values of the periastron in these orbits provide upper bounds to the value of R (equivalently, Δ). For the purposes of estimating the order of magnitude of this quantity, it is enough to consider the star S2 (also known as S0-2) [236, 237] which is one of the most precisely tracked. The periastron of S2 is 17 light hours, while the Schwarzschild radius of Sgr A* is 40 light seconds. Therefore,

$$\Delta \leq \mathscr{O}(10^3). \tag{5.10}$$

This first bound is a very crude bound which will be considerably tightened using other observational channels. Given that this kind of observation is essentially geometric in nature, the remaining phenomenological parameters that describe the physical intrinsic properties of the dark object remain unconstrained in practice. This continues to be true for more refined observations of the galactic center [245] that allow one to improve the constraint (5.10) by about three orders of magnitude. In the future it may however be possible to constrain the tails $\epsilon(t, r)$, though this would require gathering data for several stars with much shorter orbital periods [246], and which remain close enough

to Sgr A* [247, 248]. For instance, measurements of the redshift of S2, and their incompatibility with Newtonian mechanics, have been recently reported [249]. However, distinguishing effects beyond general relativity would require much higher precision.

5.3.2   Infalling matter close to the gravitational radius

Observations of stars orbiting UCOs at the center of galaxies are currently restricted to Sgr A* due purely to technological limitations, so that this constraint only applies to this particular astronomical source. Moreover, the distances involved in the orbits of the stars discussed in the previous section are large in comparison with the gravitational radius of the Sgr A*. However, another source of information comes from matter infalling on the UCO. It is reasonable to expect that processes involving matter in the surroundings of the gravitational radius constitute a better probe of the features of the CMO.

In order to describe these processes, we need to briefly review some aspects of the behavior of geodesics around the gravitational radius of the UCO that are caused by the strong gravitational fields in the near-horizon region. Both ingoing and outgoing geodesics are interesting phenomenologically, as the former describe the approach of particles and waves to the UCO, while the latter describe how and when the radiation produced in different processes escapes from the gravitational field of the UCO. We can just focus on null geodesics, given that these determine the boundaries of the lightcones in which timelike geodesics have to be contained. As is usually done in spherical symmetry, we can restrict attention to the $\theta = \pi/2$ plane without any loss of generality, and reduce the geodesic equation for trajectories $x^\mu(\lambda) = (t(\lambda), r(\lambda), \pi/2, \varphi(\lambda))$ to

$$\left(\frac{\mathrm{d}r}{\mathrm{d}\lambda}\right)^2 + \left(1 - \frac{2M}{r}\right)\frac{L^2}{r^2} = E^2. \tag{5.11}$$

The conserved quantities $E = (1 - 2M/r)\mathrm{d}t/\mathrm{d}\lambda$ and $L = r^2\mathrm{d}\varphi/\mathrm{d}\lambda$ correspond to the energy and angular momentum of the null geodesic. The derivation of these equations is described in most general relativity textbooks (see, for instance, [250]). The second term in the left-hand side of the equation above acts as an effective potential. Circular trajectories ($\mathrm{d}r/\mathrm{d}\lambda = 0$) can occur at maxima or minima of this effective potential, being respectively unstable or stable. It is straightforward to check from Eq. (5.11) that there is only one bound circular orbit, at

$$r_{\mathrm{ph}} = \frac{3}{2}r_{\mathrm{s}} = 3M. \tag{5.12}$$

The surface defined by $r = r_{\mathrm{ph}}$, known as the photon sphere, plays an important role in the discussions below.

Null geodesics that cross or reach the photon sphere have a maximum angular momentum $L_\star$ that can be directly evaluated from Eq. (5.11) by imposing the condition that $(\mathrm{d}r/\mathrm{d}\lambda)^2|_{r=r_{\mathrm{ph}}} \geq 0$,

$$L \leq L_\star = 3\sqrt{3}ME. \tag{5.13}$$

The main implication of the existence of this maximum angular momentum is that outgoing geodesics inside the photon sphere cannot cross the latter if $L > L_\star$. A similar comment applies to ingoing geodesics outside the photon sphere.
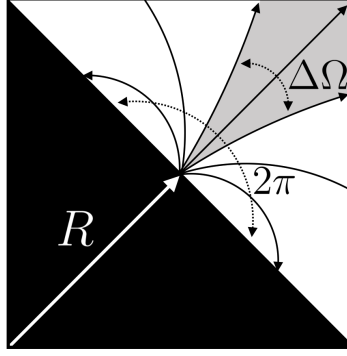
Figure 5.1: Only a fraction $\Delta\Omega/2\pi$ of geodesics emitted isotropically at a point on the surface $r = R$ can escape for ultra-compact configurations.

Let us now consider for instance an object with a surface at $r = R \leq r_{\mathrm{ph}}$ such that every point on the surface emits electromagnetic radiation isotropically in its local orthonormal frame $\{e_t^\mu, e_r^\mu, e_\theta^\mu, e_\varphi^\mu\}$. A fraction of these initially outgoing rays cannot reach the photon sphere, which means (see Fig. 5.1) that these will be strongly curved and will come back to the surface $r = R$ [251] (see also [252]). The escape angle $\vartheta_\star$ measured from the normal to the surface can be determined imposing the critical value $L = L_\star$ and calculating

$$\sin\vartheta_\star = \left. \frac{g_{\mu\nu}e_\varphi^\mu \mathrm{d}x^\nu/\mathrm{d}\lambda}{\sqrt{\left(g_{\mu\nu}e_\varphi^\mu\dfrac{\mathrm{d}x^\nu}{\mathrm{d}\lambda}\right)^2 + \left(g_{\mu\nu}e_r^\mu\dfrac{\mathrm{d}x^\nu}{\mathrm{d}\lambda}\right)^2}} \right|_{r=R,\,\theta=\pi/2,\,L=L_\star} \tag{5.14}$$

$$= \frac{L_\star}{ER}\sqrt{1 - \frac{2M}{R}}. \tag{5.15}$$

Here we have used $e_r^\mu = (0, \sqrt{1 - 2M/r}, 0, 0)$, and $e_\varphi^\mu = (0, 0, 0, 1/r)$, and we keep $\theta = \pi/2$ without loss of generality. The solid angle spanned by the cone of geodesics that escape from the sphere $r = R$ can be then calculated as

$$\Delta\Omega = \int_0^{2\pi} \mathrm{d}\varphi \int_0^{\vartheta_\star} \mathrm{d}\vartheta \sin\vartheta = 2\pi(1 - \cos\vartheta_\star) \tag{5.16}$$

$$= 2\pi \left[1 + \left(1 - \frac{3M}{R}\right)\sqrt{1 + \frac{6M}{R}}\right]. \tag{5.17}$$

In the limit $R \to r_{\mathrm{s}} = 2M$ (in which $\Delta \simeq \mu \ll 1$), one has

$$\frac{\Delta\Omega}{2\pi} = \frac{27}{8}\mu + \mathscr{O}(\mu^2). \tag{5.18}$$

Therefore, only a small fraction of the light emitted from the surface of the object will escape to infinity for ultracompact configurations. After this important remark, we can

study two different ways in which matter falls onto the UCO, namely the case in which stars collide with the UCO (triggering a "stellar disruption event" [253]) and the case in which the UCO is surrounded by an accretion disk.

Stellar disruption events

The physics associated with the possible collision of an orbiting star with the UCO gets quite complicated due to the existence of tidal forces. For a given pair, of star and UCO, there is a critical value of the radius r_T known as the Roche limit (or tidal radius), in which the internal forces holding the star together cannot endure the gravitational tidal forces, and the star is torn apart. A Newtonian estimate of the order of magnitude of this radius is $r_T \sim R_\star (M/M_\star)^{1/3}$, where $R_\star$ and $M_\star$ are the radius and the mass of the orbiting star, and M is the mass of the UCO [254]. For $M \gtrsim 10^7 M_\odot$ the tidal radius is very close to the Schwarzschild radius, therefore, tidal disruption events (TDE) happen in a region in which the Newtonian treatment is not sufficient and relativistic tidal forces must be taken into account [255], which is associated with the relativistic nature of the near-horizon orbits. Moreover, for $M \gtrsim 10^8 M_\odot$ (this value for the order of magnitude takes into account the relevant relativistic features), tidal forces are not strong enough, so that main-sequence stars are able to reach the Schwarzschild radius while keeping their integrity [256, 257].

That tidal disruption events (TDEs) have been observed for UCOs of $M \sim 10^6 M_\odot$ [258] leads to a first upper bound $r_s(1+\Delta) \leq r_T$ for these UCOs [253]. Taking as a reference $M_\star \sim M_\odot$ and $R_\star \sim R_\odot$, one obtains

$$\Delta \leq \mathcal{O}(10). \tag{5.19}$$

This improves by two order of magnitudes the bound (5.10) that applies to the same value of the mass, $M \sim 10^6 M_\odot$. But it is possible to do even better if we move to the range of masses between $M \sim 10^8 M_\odot$ and $M \sim 10^{10} M_\odot$, for which there are no TDEs and the descending star is allowed to continue its trip downwards and reach the radius $R = r_s(1+\Delta)$. The star would then crash into the surface, producing an envelope of debris that will radiate its energy away at the Eddington luminosity. The corresponding temperature at infinity is given by

$$T_\infty = \left(\frac{L_{\mathrm{Edd}}}{4\pi \sigma_{\mathrm{SB}} R^2}\right)^{1/4} \left(\frac{\Delta\Omega}{2\pi}\right)^{1/4}. \tag{5.20}$$

This is just the Stefan-Boltzmann law applied to the Eddington luminosity L_{Edd} integrated over the area of a sphere with radius R, and suppressed by the geometrical fraction $\Delta\Omega/2\pi$ of radiation that actually escapes to spatial infinity. The value of Eddington luminosity depends on the properties of the accreting matter but, in situations in which the two relevant parameters are the molecular mass m of the gas and the scattering cross-section σ between photons and gas particles, dimensional arguments lead to $L_{\mathrm{Edd}} \propto GMmc/\sigma$, where the proportionality factor should be taken to be 4π in order to obtain the usual result [259]. The Stefan-Boltzmann constant is $\sigma_{\mathrm{SB}} \simeq 5.67 \times 10^{-8} \mathrm{W\ m^{-2}\ K^{-4}}$. We refer to [253] for a detailed discussion of these aspects, while focusing the present discussion on the universal dependence of the equation above on the geometrical factor $\Delta\Omega/2\pi$.

If we combine Eqs. (5.18) and (5.20), we see that the temperature of the envelope of debris goes to zero as $\mu^{1/4}$. This makes harder to probe this phenomenon the more compact the UCO is. This feature is characteristic of inelastic processes in which some energy interacts with the surface of the UCO and is then radiated isotropically in the corresponding local reference frame, hence suffering the lensing effects described in Sec. 5.3.2.

This luminosity can be constrained using astronomical surveys, in particular the Pan-STARRS1 3π survey [260]. The larger the value of μ, the larger the luminosity, so that this analysis should lead to an upper bound on the value of μ. In order to do so, one needs additional information about the number of UCOs with a given mass and for a given value of redshift, and also an estimation of the number of stellar disruption events that would occur. The details of the distribution of the layer of debris around the UCO and, in particular, the position of the photosphere of this envelope, are also important. Taking into account all these details, the authors of [253] obtain a constraint $\mu \leq \mu_{\mathrm{UCO}} = 10^{-4}$ (we have just rounded off the value of the exponent). Note that the electromagnetic radiation is emitted from the photosphere, so that this observational channel is ultimately placing constraints on the size of the latter. We can remove the effect of the complex details regarding the thickness of the layer of debris by considering instead a very conservative bound derived from the fact that the radius of the UCO must certainly be smaller than the radius of the photosphere, namely $\mu \leq \mu_{\mathrm{ph}}$ where μ_{ph} measures the size of the photosphere. In order to do so, we just need to take into account that $\mu_{\mathrm{ph}}/\mu_{\mathrm{UCO}} \simeq \kappa_{\mathrm{T}} M_\star / 4\pi r_{\mathrm{s}}^2$ (see [253] for the derivation), with $\kappa_{\mathrm{T}} = 0.34 \times 10^{-3}$ m^2 kg^{-1} the Thomson opacity for solar metallicity, and $M_\star = \mathcal{O}(M_\odot)$. We can then write

$$\mu \leq 10^{-4} \frac{\kappa_{\mathrm{T}} M_\star}{4\pi r_{\mathrm{s}}^2} = \mathcal{O}(1) \times \left(\frac{10^8 M_\odot}{M} \right)^2 . \tag{5.21}$$

It is worth stressing that this bound still relies on a series of significant assumptions regarding the cosmological population of UCOs and the rate of stellar disruption events (and also an assumption that Δ does not depend explicitly on the mass of the UCO, an assumption which should be relaxed in future analyses). It should be therefore taken as a first estimate, and as a proof of principle that this kind of observation can be used to constrain the phenomenological parameters discussed here. More refined analysis and future observations would help to strengthen the accuracy of this bound.

Most importantly, Eq. (5.21) assumes that κ and Γ are both vanishing. The introduction of nonzero values for these two parameters has a significant impact on the discussion, with the left-hand side of Eq. (5.21) picking up factors that depend explicitly on these phenomenological parameters. The change in this equation is functionally equivalent to the change of the upper bound discussed in the next section, with the general outcome that the upper bound on μ becomes weaker for nonzero values of these parameters. We will show this explicitly in the discussion below, that includes naturally all the steps that are needed in order to take these parameters into account.

One last comment is that the factor that depends on $\Delta\Omega/2\pi$ in Eq. (5.20) is essential in order to avoid running into significantly problematic and wrong conclusions. Ignoring this factor and writing $T_\infty = (L_{\mathrm{Edd}}/4\pi\sigma_{\mathrm{SB}} R^2)^{1/4}$ would instead have resulted in an overestimate of the the outgoing flux of radiation by several orders of magnitude. It is clear that this would had led to stronger (but nevertheless flawed) constraints than

Eq. (5.21).

5.3.3   Accretion disks around supermassive black holes

The most stringent constraints on some of the phenomenological parameters come from the information about the average amount of infalling matter per unit of time onto UCOs. The value of this accretion rate $\dot{M}$ is generally more stable than the (much higher, but also more variable) accretion rate associated by the direct capture of an individual star, which are also much more sparse events. Estimations of the accretion rate for these objects depend on the physics of accretion disks [261, 262, 263], as the accretion rate is typically estimated from the luminosity of the disk. As we have done in the previous section, we will not discuss the model-dependent features behind these estimations. We will just assume that it is possible to obtain a measure of the order of magnitude of $\dot{M}$, focusing our discussion on the (already rich) physics that can be described in terms of $\dot{M}$ and our phenomenological parameters introduced previously. More accurate estimations of $\dot{M}$ would just permit to refine the observational bounds given below.

Let us start summarizing the main argument that has been invoked several times in the literature [264, 265, 266, 267, 268]. We can reduce this argument to its essentials by considering the system composed by the UCO and the accretion disk as a composite system in which energy is exchanged between its two components. The accretion rate $\dot{M}$ measures the energy that the accretion disk is pumping into the UCO. On the other hand, the quantity that is interesting in order to test the nature of the UCO is the energy that the UCO emits by itself, as this measures the reaction of the UCO to its interaction with the accretion disk. Ideally, one would like to disentangle the two fluxes of energy and measure independently the radiation emitted by the UCO. However, this is not yet observationally possible (and, as we discuss below, might be even impossible in practice due to its extreme faintness). Therefore, it is necessary to make additional assumptions in order to determine the properties of this outgoing energy flux:

1. *Thermality:* It was pointed out in [264, 265, 266] that the strong lensing of outgoing geodesics emitted at different points in the surface $r = R$ (a phenomenon that we have discussed in Sec. 5.3.2) implies that the surface reaches thermal equilibrium on a short timescale. This follows from the fact that different points of the surface are strongly coupled. Therefore, we can safely assume that the emitted radiation is thermal. This is correct for $\Delta \simeq \mu \ll 1$, which means that the arguments in this section hold only in these situations.

2. *Steady state:* The only parameter to be fixed after accepting the assumption above is the temperature T_∞ of the emitted radiation. The only possible model-independent argument to fix the power of the outgoing radiation is invoking conservation of energy and assuming that a steady state between the two components (UCO and accretion disk) has been reached, so that the two fluxes of energy carry the same amount of energy. This is a strong assumption that must be appropriately justified and that, as we see below, *fails* due to several competing effects.

If these two assumptions hold, then the emission of the UCO can be calculated: It is given by a thermal distribution with a temperature determined by the accretion

rate $\dot{M}$. For Sgr A*, this radiation should be bright in the infrared, but it has been shown [264, 265, 266, 267] that the emission of Sgr A* in the infrared is about 10^{-2} times this theoretical estimate (see [268] for the same argument applied to M87). The conclusions by these authors is that it is not possible that Sgr A* has a surface, and therefore that it must have a horizon. This is a very strong claim, as it would discard every possible value of Δ, except for $\Delta = 0$ which corresponds to a black hole. Even sub-Planckian values of Δ would be discarded. Let us now analyze in careful detail how this conclusion comes about — so to dispel any possible doubt concerning its robustness.

An obvious starting point for this revision are the two assumptions mentioned above. Indeed, as we show below, the Achilles' heel of this argument is the steady state assumption. This assumption is not valid for sufficiently compact UCOs; which leads to constraints on the maximum compactness of the object. This observation has been made only recently [253, 269]. It is worth mentioning that even recent reviews on this topic such as [234] still quote [264, 265, 266, 267, 268] as definitive evidence for the existence of event horizons, thus ignoring this loophole.[2] Our novel contribution to this discussion is the introduction (in terms of the phenomenological parameters defined in Sec. 5.2) of additional physical features that are expected to be relevant in realistic scenarios. As we discuss below, the introduction of these additional physical aspects make these constraints remarkably weaker.

Let us consider a simple calculation of the time at which steady state is reached (see figure 5.2). The initial configuration is given by an accretion disk that starts pumping energy into the UCO, the energy emission of the latter being negligible before accretion begins. We will start considering the most favorable case in which the UCO returns all the accreted energy as thermal radiation, and evaluate the timescale at which steady state can be achieved. Hence, the accretion rate onto the UCO is zero for $t < 0$ (this is just an irrelevant choice of the origin of time) and $\dot{M} \in \mathbb{R}$ for $t \in [0, T]$, where the timescale T is short enough so that the approximation of constant $\dot{M}$ is reasonable (more details below). For simplicity, we assume that all propagating energy is carried along null geodesics, and also restrict the discussion to spherically symmetric situations. The amount of energy emitted per unit time by the UCO, $\dot{E}$, is measured at the location of the accretion disk $r = R_{\text{disk}}$. Our goal is describing its evolution for $t \geq 0$. There are two effects to keep into account. First of all, the energy emitted $\dot{E}$ remains negligible until the first ingoing radial null geodesics can bounce back at the surface $r = R$ and return to the accretion disk. This time can be directly evaluated using the Schwarzschild metric as

$$T_{\text{bounce}} = 2 \left[R_{\text{disk}} - R + r_{\text{s}} \ln \left(\frac{R_{\text{disk}} - r_{\text{s}}}{R - r_{\text{s}}} \right) \right]. \qquad (5.22)$$

This timescale is divergent in the limit $R \to r_{\text{s}}$, or equivalently $\Delta \to 0$. However, the logarithmic behavior implies that even for extremely small, but strictly non-vanishing Δ, Eq. (5.22) would be at most $\mathcal{O}(10) \times r_{\text{s}}$. Hence, this timescale is essentially the light-crossing time of the UCO.

---

[2]It is perhaps worth stressing again that no local observation in space and time will be ever able to observe an event horizon, which is intrinsically a teleological notion. At most, observations will be able to confirm or exclude the existence of trapping horizons or other local definitions of the boundary of black holes. See, e.g., [270] for an extensive discussion of this point.
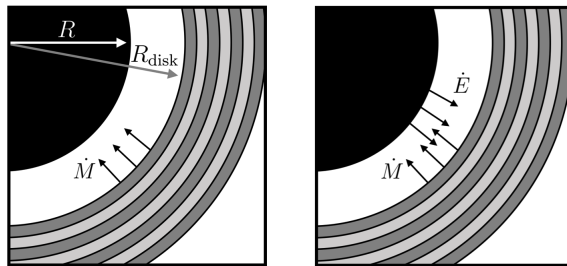
Figure 5.2: On the left: Initial state in which matter starts falling at a rate $\dot{M}$ from the accretion disk onto the UCO. On the right: steady state in which the energy emitted from the UCO and reaching the accretion disk is $\dot{E} = \dot{M}$.

This effect alone would delay the moment in which the steady state would be reached, but, given the logarithmic dependence, even sub-Planckian values for $R - r_{\mathrm{s}}$ would be ruled out. However, there is a second effect to keep into account. Outgoing null geodesics are strongly lensed, which implies that a fraction of them do not escape and fall again onto the surface of the UCO. This effect is unavoidable due to the inherently inelastic nature of the process that is necessary for thermalization to take place: the energy falling from the accretion disk is absorbed by the UCO in the first place, and then emitted. Even assuming spherical symmetry for the infalling energy, particles would not hit the surface and bounce back radially. On the contrary, this emission would be almost isotropic in a local frame at rest in the surface, thus implying that only a very small fraction of the initially absorbed energy contributes to $\dot{E}$. The remaining energy follows highly curved trajectories and is reabsorbed by the UCO in a timescale that can be calculated and is also controlled by its Schwarzschild radius, being $\mathscr{O}(10) \times r_{\mathrm{s}}$ at most. Then, a repetition of this process takes place, until eventually all the energy is radiated away.

In order to make the calculation tractable, let us follow the discussion in [252] and consider discrete intervals with their size given by the characteristic timescale $\tau_{\mathrm{s}} = \mathscr{O}(10) \times r_{\mathrm{s}}$, starting at $t = T_{\mathrm{bounce}}$. During each of these intervals, the mass that the accretion disk is ejecting into the UCO is given by $\dot{M}\tau_{\mathrm{s}}$. In the first interval after T_{bounce}, the amount of outgoing energy that reaches the accretion disk is given by the corresponding fraction of the first injection of energy,

$$E_1 = \frac{\Delta\Omega}{2\pi}\dot{M}\tau_{\mathrm{s}}. \tag{5.23}$$

During the second interval, one would get the same fraction of the energy corresponding to the second injection, plus a fraction of the remaining energy from the first injection:

$$
\begin{aligned}
E_2 &= \left[\frac{\Delta\Omega}{2\pi} + \frac{\Delta\Omega}{2\pi}\left(1 - \frac{\Delta\Omega}{2\pi}\right)\right]\dot{M}\tau_{\mathrm{s}} \\
&= E_1 + \left(1 - \frac{\Delta\Omega}{2\pi}\right)E_1. \tag{5.24}
\end{aligned}
$$

In general, one can show that

$$E_n = \sum_{k=1}^{n} \epsilon_k, \tag{5.25}$$

where the partial energies can be determined from the recurrence relation

$$\epsilon_{k+1} = \left(1 - \frac{\Delta\Omega}{2\pi}\right)\epsilon_k, \qquad k \geq 1, \tag{5.26}$$

with the seed $\epsilon_1 = E_1$ given in Eq. (5.23). Summing the geometric series, it follows then that

$$E_n = \frac{\Delta\Omega}{2\pi}\dot{M}\tau_{\text{s}} \sum_{k=0}^{n-1} \left(1 - \frac{\Delta\Omega}{2\pi}\right)^k = \dot{M}\tau_{\text{s}}\left[1 - \left(1 - \frac{\Delta\Omega}{2\pi}\right)^n\right]. \tag{5.27}$$

The accretion rate $\dot{M}$ is obtained dividing the mass accreted in each of these intervals by τ_{s}. Therefore, let us analogously define $\dot{E}_n = E_n/\tau_{\text{s}}$. When $\tau_s \ll T$, the timescale during which the accretion rate $\dot{M}$ is roughly constant, we can formally take the limit in which the size of the time intervals goes to zero and therefore $\dot{E}_n$ becomes a function of a continuous variable, $\dot{E}(t)$, which can be written in terms of the continuous variable $t \in [T_{\text{bounce}}, T]$ as

$$\frac{\dot{E}(t)}{\dot{M}} = 1 - \left(1 - \frac{\Delta\Omega}{2\pi}\right)^{(t - T_{\text{bounce}})/\tau_{\text{s}}}. \tag{5.28}$$

There are certain limits that are illustrative of the physics behind Eq. (5.28):

- In the limit $R \to r_{\text{ph}} = 3r_{\text{s}}/2$, one has $\Delta\Omega/2\pi \to 1$ [recall Eq. (5.17)]. This implies that $\dot{E} = \dot{M}$ identically for $R \geq r_{\text{ph}}$. This result is what one would expect if ignoring relativistic effects: for a regular star (neutron-star-like object or less dense), if the surface of the star emits instantly the absorbed energy, then after the time T_{bounce} the system reaches a steady state. It was this very same intuition originated in these astrophysical systems that led to the authors of the works [264, 265, 266] to assume that the steady state is reached in this same timescale for UCOs of arbitrary compactness (let us note, however, that in this limit the thermalization assumption would not hold).

- In the limit $R \to r_{\text{s}}$ ($\Delta \to 0$) one has $\dot{E}/\dot{M} \to 0$. This corresponds to the known astrophysical behavior of a black hole, in which a steady state cannot be achieved [264, 265, 266]. However, this limit is not abrupt, but proceeds in a continuous way: for $\Delta \simeq \mu \ll 1$, one has

$$\frac{\dot{E}}{\dot{M}} \simeq \mu(t - T_{\text{bounce}})/\tau_{\text{s}}. \tag{5.29}$$

In particular, there is a maximum value of $\dot{E}$ that is determined from the equation above when $t = T$ (if the accretion rate changes, the system would have to adapt to the new accretion rate and therefore the process of stabilization would restart).

The second limit above illustrates that relativistic lensing effects cannot be ignored for $\mu \ll 1$, and can indeed spoil the stabilization of the composite system into a steady state. In particular, for Sgr A* the typical timescale for the variation of its accretion rate is set by the Eddington timescale $T = Mc^2/L_{\text{Edd}} \simeq 3.8 \times 10^8$ yr. Hence, given that the emission of Sgr A* is at most 10^{-2} times that predicted under the steady state assumption [264], we can write

$$\left.\frac{\dot{E}}{\dot{M}}\right|_{t=T} \simeq \mu(T - T_{\text{bounce}})/\tau_{\text{s}} \leq \mathscr{O}(10^{-2}). \qquad (5.30)$$

Plugging the numbers into this equation, we obtain

$$\mu \simeq \Delta \leq \mathscr{O}(10^{-17}). \qquad (5.31)$$

In particular, we see that the steady state assumption is not valid if μ satisfies this constraint. In other words, this constraint would be the strongest statement that can be made using this method.

The same argument has been applied to the UCO in M87 [268] (although without taking into account the lensing of the geodesics in the near-horizon region), which is three orders of magnitude more massive than Sgr A* [271]. Taking into account the adjustments discussed in this section, we can find a constraint that is several orders of magnitude weaker than the one that applies to Sgr A*.

Non zero absorption coefficient. Even if the constraint (5.31) is considerably weaker than originally claimed, it is nevertheless an impressively strong constraints. Translating it into corresponding length scales it implies that it is possible to rule out the existence of a surface that emits all the absorbed energy as thermal radiation with a precision of 10^{-17} (in the coordinate distance r) on the size of the UCO. In terms of proper radial distances, this precision becomes smaller due to the Schwarzschild factor $\mu = 1 - r_{\text{s}}/R$, and is in fact roughly of a meter over a size of 10^9 m, which is impressive. Of course, this is still more than 70 orders of magnitude greater than $\Delta \sim \ell_{\text{P}}^2/r_{\text{s}}$ (corresponding to a proper radial distance of the order of the Planck length) which was originally thought to be ruled out by this argument.

Anyway, it is natural to expect that the surface of the UCO will not strictly have $\kappa = \Gamma = 0$. As we now show, the introduction of these parameters describing additional physics regarding the nature of the UCO has a huge impact in the discussion, with κ having the largest impact.

Intuitively, the reason for this is clear. Before escaping the gravitational field of the UCO, radiation undergoes several cycles of absorption (after being lensed back to the UCO) and emission. If $\kappa \neq 0$, in each of these cycles only a fraction $(1 - \kappa)$ of the absorbed energy is emitted. So, afterm many cycles the overall power of emitted radiation is strongly suppressed. Let us write explicitly the main equations for $\kappa \neq 0$, but for the moment let us keep $\Gamma = 0$. In order to get an intuition, as the situation is more cumbersome than it was for $\kappa = 0$ let us explicitly write down the energy which escapes at infinity after the firsts two time intervals. In the first time interval, the amount of outgoing energy that reaches the accretion disk is given by the fraction
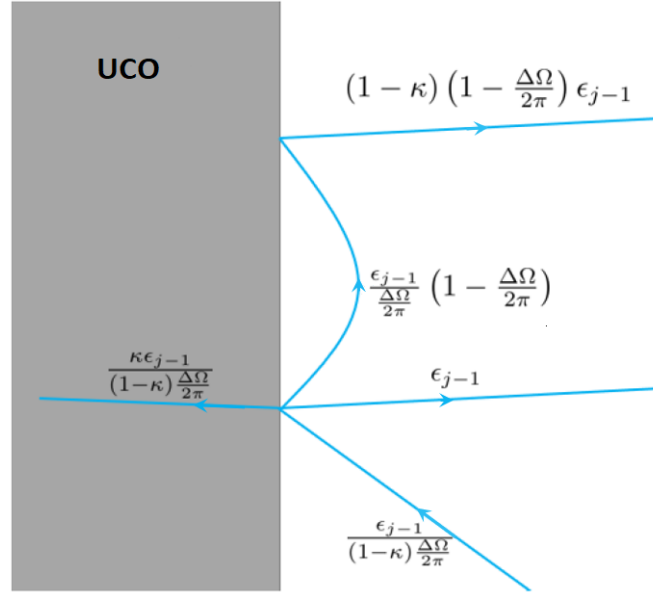
Figure 5.3: Schematic proof of Eq. (5.35). When some radiation hits the surface of the UCO a fraction $(1 - \kappa)\frac{\Delta\Omega}{2\pi}$ escapes, a fraction κ is absorbed and the rest will bounce back on the object.

of the first injection of energy which is not absorbed and which is emitted inside the escaping angle $\Delta\Omega$,

$$E_1 = (1 - \kappa)\frac{\Delta\Omega}{2\pi}\dot{M}\tau_S \tag{5.32}$$

For what concern the second interval, there is the same contribution but there is also a contribution coming from radiation that escapes after bouncing a second time on the surface.

$$
\begin{aligned}
E_2 &= (1 - \kappa)\frac{\Delta\Omega}{2\pi}\dot{M}\tau_S + (1 - \kappa)\frac{\Delta\Omega}{2\pi}\dot{M}\tau_S\left[1 - \left((1 - \kappa)\frac{\Delta\Omega}{2\pi}\right) - k\right] = \\
&= (1 - \kappa)\frac{\Delta\Omega}{2\pi}\dot{M}\tau_S + (1 - \kappa)\frac{\Delta\Omega}{2\pi}\dot{M}\tau_S\left[(1 - \kappa)\left(1 - \frac{\Delta\Omega}{2\pi}\right)\right].
\end{aligned}
\tag{5.33}
$$

In the square brackets we have the total energy minus the fraction of energy escaped after the first bounce and the fraction of energy absorbed in the first bounce. It is exactly this last contribution that makes a big difference with respect to the case $\kappa = 0$.

In general, the energy that reaches infinity after n time intervals is given by

$$E_n = \sum_{j=1}^{n} \epsilon_j \tag{5.34}$$

Where ϵ_j is the energy which escape after bouncing j times on the surface of the object. We note that $\epsilon_1 = (1 - \kappa)\frac{\Delta\Omega}{2\pi}\dot{M}\tau_S$ and (see Fig. 5.3)

$$\epsilon_j = (1 - \kappa)\left(1 - \frac{\Delta\Omega}{2\pi}\right)\epsilon_{j-1}. \tag{5.35}$$

So,

$$\epsilon_j = (1 - \kappa)^j \left(1 - \frac{\Delta\Omega}{2\pi}\right)^{j-1} \frac{\Delta\Omega}{2\pi} \dot{M}\tau_S. \tag{5.36}$$

Therefore, we have

$$\begin{aligned}
\frac{E_n}{\dot{M}\tau_S} &= \epsilon(1 - \kappa) \sum_{j=0}^{n-1} \left((1 - \kappa)^j \left(1 - \frac{\Delta\Omega}{2\pi}\right)^j\right) \\
&= \frac{\Delta\Omega}{2\pi} \frac{(1-\kappa)}{\kappa + \frac{\Delta\Omega}{2\pi}(1-\kappa)} \left(1 - (1 - \kappa)^n \left(1 - \frac{\Delta\Omega}{2\pi}\right)^n\right).
\end{aligned} \tag{5.37}$$

Going back to the continuum limit, and considering $\kappa \gg \tau_S/t$,

$$\frac{\dot{E}}{\dot{M}} = \frac{\Delta\Omega}{2\pi} \frac{(1 - \kappa)}{\kappa + \frac{\Delta\Omega}{2\pi}(1 - \kappa)}. \tag{5.38}$$

This result is very different from eq (5.28). First of all note that the time dependence has disappeared. This is because the system has reached a steady state. Anyway $\dot{E} \neq \dot{M}$ as part of the energy have been absorbed. In other words, as expected, the transfer of energy from surface degrees of freedom to bulk degrees of freedom strongly dampens the thermal emission from the surface of the UCO. Instead of Eq. (5.31), we obtain then the much weaker constraint

$$\frac{\mu}{\kappa} \leq \mathcal{O}(10^{-2}). \tag{5.39}$$

This equation can be understood as a lower bound on the value of κ that makes hard surfaces that would otherwise be excluded by Eq. (5.31) compatible with the available observational data.

Let us consider for instance the value $\mu = \mathcal{O}(10^{-7})$ that is 10 orders of magnitude greater than the constraint (5.31), which is valid only for $\kappa = 0$. From Eq. (5.39), we see that an absorption coefficient as small as

$$\kappa \geq \mathcal{O}(10^{-5}) \tag{5.40}$$

makes the existence of such surfaces compatible with observations.

It is also possible to obtain the equivalent of Eq. (5.38) for $\Gamma \neq 0$. The only difference is that the recurrence relation is in this case

$$\epsilon_{k+1} = \left[(1 - \kappa)\left(1 - \frac{\Delta\Omega}{2\pi}\right) + \Gamma\frac{\Delta\Omega}{2\pi}\right]\epsilon_k, \qquad k \geq 2, \tag{5.41}$$

and the seed of this relation is modified to

$$\epsilon_1 = (1 - \kappa - \Gamma)\frac{\Delta\Omega}{2\pi}\dot{M}r_s, \qquad \epsilon_2 = (1 - \kappa - \Gamma)\left(1 - \frac{\Delta\Omega}{2\pi}\right)\epsilon_1. \tag{5.42}$$

From these equations it is possible to check that a nonzero value of Γ further weakens these constraints, although this effect is not as pronounced as the one associated with the absorption coefficient κ given that it will not produce an exponential suppression

like the one in Eq. (5.38). For completeness, let us note that the analogue of Eq. (5.28) can be shown to be

$$\lim_{t \to \infty} \frac{\dot{E}}{\dot{M}} = \frac{(1 - \kappa - \Gamma)(1 - \Gamma)\Delta\Omega/2\pi}{\kappa + (1 - \kappa - \Gamma)\Delta\Omega/2\pi}. \tag{5.43}$$

We see that wormholes represent an extreme case from this perspective, as $\kappa + \Gamma = 1$ and therefore $\dot{E} = 0$ identically. Hence, wormholes cannot be tested as black hole alternatives using this particular observation channel. Finally, let us stress that the analysis is performed using spherical symmetry as a tool to simplify the calculation. Anyway, as shown in [272], a nonzero rotation parameter does not modify the order of magnitude estimation of this section unless the UCO is almost extremal.

Consistency constraints from accretion

Even in the best-case (but unphysical) scenario in which $\kappa = \Gamma = 0$, Eq. (5.31) should be improved by about 70 orders of magnitude in order to rule out well-motivated theoretical values of μ such as the one that follows from $\Delta \sim \ell_{\rm P}^2/r_{\rm s}$ and that can be obtained from Eq. (5.5). Such an improvement of observational data seems hardly realistic, thus suggesting that certain theoretical models are almost impossible to probe. The situation can only get worse if nonzero values of κ and Γ are allowed. However, it is possible that a better understanding of these ultracompact alternatives to black holes will uncover constraints that follow from their internal consistency and, in particular, from the laws governing their dynamical evolution (which are largely unknown at the moment). As stressed in Sec. 5.1, most alternative geometries such as the ones of quasi-black holes and wormholes are prescribed in static situations. The lack of a framework in which to deal with dynamical processes is highly unsatisfactory, and is arguably the main criticism that can be raised against these models on purely theoretical grounds.

One may expect that it would be difficult to reach model-independent conclusions, given that different models could display very different dynamical behavior. However, it has been shown recently [115] that certain model-independent dynamical considerations are restrictive enough to lead to a consistency relation that takes the form of a lower bound on μ. These model-independent considerations reduce essentially to the observation that the boundary (i.e., surface) of standard celestial objects evolves following causal trajectories in spacetime. Note that these trajectories need not correspond to actual moving particles, as this growth will be generally caused by the stacking or piling up of different particles of matter. But this growth is nevertheless driven by physical interactions, which must propagate in a causal manner. On the other hand, trapping horizons are known to be spacelike for standard accreting matter [120, 130]. There is a clear tension between these two different behaviors. This tension results into two possibilities: (i) the UCO is less compact than a given threshold, so that its surface can grow in a timelike (or at most, null) manner without forming trapping horizons, or (ii) the UCO is more compact than this threshold, hence developing trapping horizons in a given interval of time that can be calculated.

Option (i) translates into a consistency constraint that depends on the parameter μ and the particular model of accreting matter. In spherical symmetry and using the

Vaidya geometry, this consistency constraint can be obtained analytically [115],

$$\mu \geq \frac{4G\dot{M}}{c^3}.$$

(5.44)

Equivalently, we can write this as $\dot{M}c^2 \leq \mu P_{\mathrm{P}}/4$ where $P_{\mathrm{P}} = c^5/G$ is the Planck power, which may represent the maximum luminosity attainable in physical processes [273]. In more general situations this consistency constraint would take a different form, displaying for instance additional quantities such as the angular momentum of the UCO or the accreting matter. It would be necessary to extend this simple estimate in order to take into account these effects and obtain more precise constraints, although Eq. (5.44) can be used in order to extract some conclusions that are unlikely to be changed by these additional considerations. For instance, we can evaluate the lower bound above for Sgr A* using $\dot{M} \gtrsim 10^{-11}\ M_{\odot}\ \mathrm{yr}^{-1}$, which yields

$$\mu \geq \mathscr{O}(10^{-24}).$$

(5.45)

Recalling Eq. (5.5), this value corresponds to

$$\ell \gtrsim 1\ \mathrm{cm}.$$

(5.46)

This lower bound is strong enough in order to show for instance that quasi-black holes with $\ell \sim \ell_{\mathrm{P}}$, which have values of μ more than 60 orders of magnitude smaller, must develop trapping horizons during their lifetime. Let us stress that models for the formation of quasi-black holes through short-lived bouncing geometries involve the formation of trapping horizons for finite periods of time, that can be as short as $\tau \sim \tau^{(1)}$.

Contrary to the upper bounds analyzed above, Eq. (5.44) is not affected by the phenomenological parameters κ and Γ. Since it boils down to a statement about causality, the argument behind Eq. (5.44) depends only on the location of the region in which the interactions between the accreting matter and the UCO take place, and not on the particular details of this interaction.

The mechanism leading to this lower bound has also implications for gravitational waves, which are discussed in Sec. 5.4.2. The constraint 5.45 has a different nature respect to the other constraints presented in this chapter as there are a couple of assumption beyond it. First of all the analysis relies on the assumption that the interactions involved are local and causal in nature. This might not be the case if large quantum effects are involved in the stability of quasi-black holes given that, e.g., all of the energy conditions (including the dominant one) could be violated in these scenarios. Furthermore, even if the infalling matter causes the formation of a trapping horizon, nothing forbid the trapping horizon to disappear again after the flux of energy has been absorbed.

5.3.4   UCOs shadows

Any discussion regarding the observation of black holes via the EM channel would not be complete without mentioning the Event Horizon Telescope (EHT) collaboration which was able to directly detect the light coming from the black hole at the center of the M87 galaxy with an angular resolution of the order of the microarcsecond (μas)

thus being able to take an image of a black hole for the very first time [7, 8, 9, 10, 11, 12]. The image revealed the shadow of the UCO[3] that is associated with the photon sphere [274, 275, 276, 277, 278, 279] (although its size does not directly corresponds to the size of the latter due to lensing effects, and is weakly sensitive on its relative distance from the horizon).

This particular observation has received widespread attention in the astrophysics community, and it is often described as "imaging the event horizon of black holes" [280]. However, despite the fact that detecting the shadow is a truly remarkable achievement, the length scale that controls this phenomenon is not the Schwarzschild radius $r_{\rm s}$, but rather the much larger $r_{\rm ph} = 3r_{\rm s}/2$. The gap between these two distances is macroscopic, $r_{\rm ph} - r_{\rm s} = r_{\rm s}/2$. In other words, the observation was able to constrain an hypothetical boundary of the UCO within its photonsphere and to rule out some specific model which present $\mathcal{O}(1)$ modification of the geometry at photonsphere [12], but any object that is compact enough to have a photon sphere ($R < r_{\rm ph}$) should display the necessary physical characteristics to lead to a similar (and in most cases, indistinguishable) shadow. This has been recently stressed by several authors [281, 207, 282, 283, 284]. Furthermore, let us stress that the observation cannot improve on the constrain coming from Eq. 5.43 as EHT is blind to the frequency at which an hypothetical surface in thermal equilibrium should emit [12]. Overall, we can conclude that the existence of horizons cannot be decided only on the basis of the observations of the shadows of astrophysical black holes.

5.3.5 Bursts

The search for EM bursts has been claimed in the past as a possible strategy for detecting the outcome of bouncing geometries. Of course, if the previously discussed instability of regular black holes implies their conversion into bouncing solutions, the same observations will be relevant for constraining them. It is less clear if the possible conversion of regular black holes or short-lived bounces into quasi-black holes and wormholes would imply any transient burst and what it might depend on. It is natural to conjecture that, if these objects are the outcomes of a series of rapid bounces with short timescale $\tau^{(1)}$, high-energy quasi-periodic bursts with typical frequency $1/\tau^{(1)}$ should be expected [136]. However, without detailed models that describe, for instance, the damping of these oscillations, not much more can be said at the moment.

While what we said above holds in the case of short-lived bounces of typical timescale $\tau^{(1)}$, more complex is the case of long-lived bounces with $\tau = \tau^{(2)}$, for which several phenomenological studies have been performed in the literature [185, 186, 285, 286]. In this case no relevant signal is expected up to this timescale while two distinct components are predicted as being associated to the typical size of the exploding object (infrared component) and to the typical energy of the universe at the moment of its formation (ultraviolet component). If $\tau = \tau^{(2)}$, it is reasonably arguable that only primordial black holes, which formed in the early universe, would have the size and the lifetime for exploding soon enough so that we could observe the corresponding signals.

For primordial black holes whose lifetime is of the order of the Hubble time, it was

---

[3]It would probably be more appropriate to call it "silhouette" given that there is no physical surface on which the shadow is cast

shown that the infrared component of the signal could get up to the GeV scale and be peaked in the MeV, while the ultraviolet part of the burst is expected to be in the TeV range [285, 286]. If confirmed by more accurate modelling, this would place the search for the bursts associated to bouncing geometries within the realm of current high energy astrophysics experiments (provided that a sufficient number of primordial black holes is created in the early universe). Furthermore, the fact that bursts further away in redshift would correspond to less massive and more primordial objects implies that their higher peak frequency would partially compensate their higher cosmological redshift [286]. This is a peculiar behaviour that might be used a a signature for this kind of signals and might help distinguish them from other, more standard, astrophysical emissions.

With regards to our parameterization, it is clear that the detection of one of these bursts could be used to cast constraints on both $\tau_\pm$ (depending on the particular scenario), but would not tell us much about tails, $\epsilon(t, r)$.

5.4   Gravitational waves

The detection of gravitational waves in LIGO and VIRGO [1, 2, 3, 4, 5, 6] opens up additional possibilities for testing the properties of astrophysical black holes. One of the best sources of gravitational waves are mergers of compact objects: astrophysical black holes [1, 2, 3, 4, 5] or neutron stars [6]. The merger of compact objects releases abundant information about their nature, although part of it is difficult to extract due to the intrinsically nonlinear nature of the process. It is also interesting that, as discussed below, observations using electromagnetic and gravitational wave observations are complementary, in the sense that the different nature of the physical processes involving these forms of radiation makes the corresponding observational channels more sensible to (and therefore more suitable to measure) different phenomenological parameters. We will illustrate this point using the parametrization introduced in Sec. 5.2.

5.4.1   Coalescence of compact objects

The waveform produced in a merger can be roughly divided into three main parts: (i) the inspiral phase in which the two objects are far apart, (ii) the merging phase in which the two objects enter in direct contact, and (iii) the ringdown phase that describes the relaxation of the outcome of the merging phase. These three phases are defined by the different physical processes taking place; from a mathematical perspective, these phases are also characterized by the different techniques that are most appropriate for extracting the corresponding gravitational wave signatures.

- Inspiral phase:

  In the inspiral phase the two objects are far apart, so that Newtonian gravity can be used in order to describe this phase to a good approximation. Hence, as in the discussion of orbiting stars in Sec. 5.3.1, the details of the near-horizon geometry will not appreciably affect the evolution of the system in this phase. However, while in this phase, binary systems could still possibly display detectable differences with respect to a binary of black holes if the two objects have surfaces

instead of horizons (i.e., if $\Delta > 0$), due to the effects that the gravitational field of each of the two objects can have on the internal structure of its companion through the induced tidal forces. All known results regarding classical general relativity black holes are consistent with these objects having identically zero tidal deformability [287, 288, 289]. However, ultracompact configurations without horizons can be tidally deformed [290]. Moreover, if $\Gamma \neq 0$ the object would decrease its tidal heating (measured in terms of the amount of gravitational radiation that the object absorbs [291, 292]). It has been argued [293] (see also [294]) that both effects could be used in order to place upper bounds on the values of these two parameters Δ and Γ using data from the Laser Interferometer Space Antenna (LISA), with constraints on the value of Γ being the most promising ones. Soft fluctuations of the near-horizon geometry, given by tails $\epsilon(t, r)$ with compact support, can be also constrained using this part of the waveform [295].

- Merger:

  The dynamics in the merger phase is highly nonlinear, which renders most of the parameters in our phenomenological parametrization in Sec. 5.2 useless. In fact, virtually nothing is known about this nonlinear regime in theories beyond general relativity. It seems that this problem has to be addressed numerically and on a case-by-case basis. However, some of the models discussed in Sec. 5.1 could leave an imprint during this phase. In particular, short-lived bouncing geometries would disrupt the merger on timescales of the order of τ_-, perhaps leading to the formation of quasi-black holes as proposed in [136, 184]. This would create a distinctive periodic pattern [136, 170] that is similar to the (linear) phenomenon of gravitational wave echoes discussed in the next section, sharing the typical values of the timescale between subsequent echoes but being inherently nonlinear. For completeness, we also mention that horizonless configurations may also lead to electromagnetic afterglows in this phase [296, 297]. However, the strength of this emission is largely unknown, and also it is not clear how such a phenomenon would avoid being suppressed by the lensing discussed in Sec. 5.3.2.

- Ringdown:

  The ringdown part of the signal can again be described making used of a linear analysis, in terms of the so-called quasinormal modes [224]. The corresponding waveform is typically given by a linear combination of damped sinusoids. Shortly after the first detection of gravitational waves, a theoretical analysis [218] demonstrated explicitly that the form of this part of the signal is associated with the photon sphere at $r_{\mathrm{ph}} = 3r_{\mathrm{s}}/2$, and not the horizon. Hence, a similar comment as in Sec. 5.3.4 applies: testing the damping of the waveform does not allow drawing conclusions about the near-horizon geometry. However, if the object is not to compact, the presence of the surface can modify the ringdown (see, *e.g.* [298]) and, as discussed in the next section, for an UCO modifications of the near-horizon geometry may trigger new characteristic effects in the late-time ringdown.

5.4.2 Echoes in the late-time ringdown

After the relaxation of the object produced in the merger through the emission of grav-
itational waves, its properties could still leave imprints in the late-time gravitational-
wave signal. These imprints would be the result of the interaction of the gravitational
radiation, emitted previously, with the central object. As discussed in detail below,
for sufficiently compact situations a significant fraction of this gravitational radiation
is backscattered by the gravitational field of the central object, traveling back to and
interacting with the latter. The phenomenological parameter that control this late-time
behavior is the reflection coefficient Γ. For a black hole, $\Gamma = 0$, which means that all
backscattered radiation will disappear down its gravitational well. If $\Gamma \neq 0$, some of
this radiation would bounce back from the object and could be measured by distant
detectors.

Let us start with the simplest possible description of the main physics involved,
adding additional details progressively. The first element that must be discussed is the
mechanism that leads to the backscattering of the initially outgoing radiation [299].
This can be introduced by considering the propagation of test particles or waves in the
Schwarzschild geometry. For instance, the modes of a scalar field $\Phi(t, r, \theta, \varphi)$, in the
usual decomposition in spherical harmonics

$$\Phi(t, r, \theta, \varphi) = \sum_{l=0}^{\infty} \sum_{m=-l}^{l} \frac{\phi_{lm}(t, r)}{r} Y_{lm}(\theta, \varphi), \tag{5.47}$$

satisfy the wave equation

$$\left(-\frac{\partial^2}{\partial t^2} + \frac{\partial}{\partial r_*^2} - V_l \right) \phi_{lm}(t, r) = 0, \tag{5.48}$$

where r_* is the standard tortoise coordinate and

$$V_l = \left(1 - \frac{2M}{r} \right) \left(\frac{l(l+1)}{r^2} + \frac{2M}{r^3} \right) \tag{5.49}$$

is the Regge–Wheeler potential. This potential has a maximum in the vicinity of
$r_{\rm ph} = 3M$, with the deviation from this value controlled by $1/l$, and smaller the larger
the value of l. The radius $r_{\rm ph} = 3M$ marks also the location of the photon sphere (or
light ring), namely the innermost circular null geodesic that is stable (as discussed in
Sec. 5.3.2). Due to the existence of this maximum in the potential, outgoing waves
originated at $r < r_{\rm ph}$ will be backscattered. The fraction of backscattered radiation
can be calculated explicitly [300, 301, 302, 303]. Only objects that are compact enough
to have a photon sphere will display this phenomenon, and therefore we focus in the
following on these objects.

In the case of a black hole, the backscattered waves will be lost into the horizon.
However, for objects in which $\Gamma \neq 0$ and $\Delta \neq 0$, part of the incoming radiation will be
be reflected outwards. When crossing the photon sphere at $r_{\rm ph}$, part of this radiation
will escape and part will be backscattered. This leads to a periodic phenomenon that
would produce a series of "echoes" of the first event. Slightly modifying Eq. (5.22), the
characteristic timescale of this phenomenon is given by

$$T_{\rm echo} = 2M - 4M \ln(2\Delta) + T_{\rm int}, \tag{5.50}$$

where the first two terms on the right-hand side measure the time that a pointlike particle following a radial null geodesic takes to travel from $r_{\rm ph} = 3M$ and $R = r_{\rm s}(1+\Delta)$ and then from $R = r_{\rm s}(1+\Delta)$ to $r_{\rm ph} = 3M$, and $T_{\rm int}$ provides a measure of the time that the gravitational wave spends inside the central object (that is, in the region $r \leq R$).

The precise value of $T_{\rm int}$ depends on the particular model being used but, if one ignores the interaction between gravitational waves and the central object (which, as explained below, is most likely *not* consistent), this quantity is expected to be of the order of the light-crossing time or, equivalently, proportional to M (an explicit calculation is provided for instance in [304]). Then, for $\Delta \ll 1$ the leading order in Eq. (5.50) would be

$$T_{\rm echo} \simeq -4M \ln(\Delta). \tag{5.51}$$

This logarithmic behavior has been already discussed in Sec. 5.3.3. The amplitude of these echoes is proportional to the reflection coefficient Γ and also depends on the details of the barrier peaked around the photon sphere. Of course, the amplitude of subsequent echoes decreases monotonically, and a power-law for this decay has been found [301, 305].

The reader may have noticed that there seems to be an inconsistency between our treatment of electromagnetic waves in Sec. 5.3.2, and the treatment of gravitational waves in this section. More specifically, we are not bringing up the lensing that had to be taken into account in order to describe the behavior of electromagnetic waves. In other words, we are implying that gravitational waves are not affected by this lensing.

There are several aspects behind this assumption. The first one is that the processes involving electromagnetic waves have been assumed to be deeply inelastic, following our intuition about the interaction of light and matter in other systems. However, in the linear approximation used to describe gravitational wave echoes, it is assumed that gravitational waves interact elastically with the central object (we critically revise this assumption at the end of this section). If we accept this main difference it follows then, as long as we are analyzing waves with angular momentum below the critical value $L_\star$ derived in Sec. 5.3.2, that electromagnetic waves experience lensing effects while gravitational waves are unaffected.

Moreover, it is worth stressing that these two kinds of radiation have different wavelength, which determines whether or not the geometric optics approximation is reasonable. The gravitational waves produced in the merger of two compact objects into a central object of mass M have wavelengths that are comparable to the Schwarzschild radius of the central object [306] (of course, there is a distribution in wavelengths, or frequencies, around this typical scale). On the other hand, the electromagnetic waves relevant for our discussion in Sec. 5.3.2 have much shorter wavelengths. Hence, it is reasonable to describe the behavior of electromagnetic waves in these spacetimes within the geometric optics approximation, in which the strong lensing of lightlike geodesics by the gravitational field of the central object is unavoidable. As the gravitational waves of the wavelengths involved in the merger cannot be described in this approximation, they may circumvent the attraction of the central object and escape outwards even if having an angular momentum greater than $L_\star$, depending on the value of l (something that would lead to a grey-body feature of the gravitational wave spectrum). We think that this aspect is worth studying in detail.

Previous works (including [299, 301, 302, 307, 305]) have not analyzed this issue

explicitly, perhaps due to particular choices of initial conditions for gravitational radiation. In fact, it may be the case that phenomenologically reasonable values of L are below $L_\star$, hence preventing lensing to play any role in realistic scenarios. However, in order to deal with realistic situations one would also need to include the angular momentum of the central object, which would certainly change the value of $L_\star$.

On the other hand, let us recall that Eqs. (5.50) and (5.51) are strictly valid for null geodesics. Hence, it is assumed in the literature that the geometric optics approximation is indeed reasonable at least for the analysis of certain aspects of the problem, namely the evaluation of the characteristic timescale (5.51). The critical wavelength below which the geometric optics approximation can be used in order to describe the behavior of waves in the potential (5.49) is substantially larger than M for $\Delta \ll 1$ small enough; in fact, this critical wavelength is roughly given by Eq. (5.51). This restricts the wavelengths for which the discussion of the echoes provided above is consistent:

$$\lambda \ll |\ln \Delta| \times \mathscr{O}(M). \tag{5.52}$$

It is important to analyze the physics associated with this upper bound in more detail, in order to understand for instance how sharp it is. This is moreover relevant for modeling purposes, as Eq. (5.52) points out that the frequency content of the originally outgoing gravitational radiation will effectively experience a band-pass filter that selects the frequencies that would appear in the subsequent echoes. Moreover, waves with $L > L_\star$ may also experience a lower bound given by $M \lesssim \lambda$, although this is far from clear.

It is illustrative to use our parametrization in Sec. 5.2 in order to understand the kind of information that can be extracted from the search of echoes in gravitational wave events. The amplitude of gravitational wave echoes would be, following the discussion above, proportional to Γ. Hence, both the observation and non-observation of echoes can put constraints on the value of this parameter (this is, for instance, the main result in [308, 309]). The non-observation of echoes can only constrain this parameter and cannot say anything about the radius R or, alternatively, Δ. Of course, a positive detection of echoes could be used in order to determine the size of the central object, through the use of Eq. (5.51). The other two parameters which are relevant for the process are τ^+, which has to be greater than the characteristic timescale of echoes (this would place a very uninteresting lower bound on this quantity), and τ_- which has to be smaller (the consequences of this for theoretical models were analyzed in [310]).

The interest in this phenomenon has grown after tentative evidence for their existence in LIGO data was claimed [311, 312]. These works assume crude templates that are missing some of the details in the discussion above and in later works such as [301, 305], the importance of which for data analysis is not yet clear. Moreover, these claims are still controversial, although parts of the initial results have been corroborated by other groups [313, 314, 315, 316]. For completeness, let us also mention that qualitatively similar claims have been made about the binary neutron star merger GW170817 [317]. However, the latter analysis does not make any specific assumptions about the waveform of the echoes and just looks for periodicities. This opens the possibility of alternative explanations for these periodicities, as mentioned in the conclusions of [317] but also explored for instance in [318] and in Sec. 5.4.1 above in which it was stressed that short-lived bouncing geometries are also expected to lead to periodic patterns in the late-time part of gravitational wave signals.

Before ending this section, we want to stress that the discussion above neglects the (generally nonlinear) interaction between gravitational waves and the central object. In practical terms, the echo timescale is calculated in an approximation in which gravitational waves propagate in a fixed background, and the amplitude of the echoes is just proportional to the reflection coefficient Γ. This issue has been ignored in the literature, but here we want to highlight that this does not seem consistent and that this feature has fundamental implications for the existence (or not) of echoes.

Let us start by considering a toy model in the purely classical framework of general relativity, consisting of a perfectly reflecting ($\Gamma = 1$) and spherically symmetric mirror with radius $R = r_s(1+\Delta)$ enclosing a mass M, so that the geometry outside the mirror is Schwarzschild. We now consider an ingoing spherical shell of gravitational radiation, of which we just need to monitor the energy density; so that we will describe it in terms of pressureless null dust with uniform energy density. This ingoing radiation will be reflected by the mirror and will therefore travel outwards after interacting with the latter. However, the peeling of outgoing null geodesics leads to an accumulation of energy around the gravitational radius (see Fig. 5.4) For $\Delta \ll 1$ this accumulation of energy leads to the formation of trapping (and, in this classical setting, event) horizons even for an extremely modest amount of energy being received and reflected at the mirror [115]. Above a certain threshold in the power stored in the gravitational radiation, a black hole will form around the mirror and no radiation will escape to infinity.
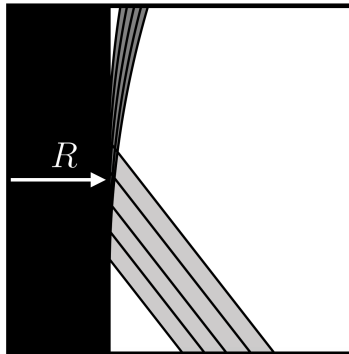

Figure 5.4: Exponential peeling of outgoing geodesics reflected at $r = R$. Even if the ingoing distribution of energy has low density (light gray region), the accumulation of geodesics around the gravitational radius produces high densities (dark gray region) that result in large backreaction effects on the background geometry.

The formation of a black hole in this toy model is intimately associated with the breakdown of the linear approximation for the gravitational waves propagating in the background geometry produced by the mirror, given that in the linear approximation these waves will always escape to infinity. Hence, this shows that one has to be careful when using the linear approximation to extract the features of echoes. The formation of a trapping horizon might be avoided if the nonlinear interactions between the ingoing gravitational waves and the central objects are considered. A model-independent outcome of these interactions has to be the expansion of the central object in order to avoid the formation of trapping horizons. This expansion of the object needs energy,

which can only be taken from the gravitational radiation. A straightforward application of the argument in [115] shows that the more compact the central object is, the larger is the fraction of the energy stored in the gravitational waves that has to be transferred through nonlinear interactions.[4] If most of the ingoing gravitational waves must interact and transfer their energy to the central object, it is likely that the reflection coefficient Γ will be extremely small, and therefore that there would be no echoes.

A similar argument for the importance of the non linear effects can be obtained by looking at the quasinormal modes of an ultracompact object. As seen in [320, 321] the imaginary part of the quasinormal modes goes to zero when the compactness approaches the black hole value. This implies that the linear perturbation are long lived and are likely to trigger non liner instabilities. This type of instability has been observed studying the perturbation of a quasi extremal Kerr black hole [322].

Of course, it is possible that the timescale of the instability is very long or that the nonlinear interactions with the central object are elastic and that the energy inside the central object is transferred back to the outgoing gravitational waves after their travel through its interior. In any case, these arguments show that previous theoretical analysis of this phenomenon are missing important details of the physics involved, which must be incorporated in order to arrive to a consistent picture. Therefore, we believe that a more detailed analysis is needed in order to determine whether the existence of echoes really is a robust theoretical prediction. Progresses along this line of research will be reported in future investigations.

Model	Stars (EM)	Accretion (EM)	Shadows (EM)	Bursts (EM)	Coalescence (GW)	Echoes (GW)
Regular black hole	$\epsilon(t,r)$	✗	✗	✗	✗	✗
Bouncing geometries	$\epsilon(t,r)$	✗	✗	✓	τ_- (short-lived)	
Quasi-black hole	$\epsilon(t,r)$	μ, Γ, κ	✗	✗	τ_-, μ, Γ	$\Gamma, [\mu]$
Wormhole	$\epsilon(t,r)$	✗ $(\Gamma + \kappa = 1)$	✗	✗	τ_-, Γ	$\Gamma, [\mu]$

Table 5.2: Parameters that can be possibly constrained or measured for the different classes of quantum-modified black holes and different observational channels. Square brackets are used in order to stress that μ can be measured using gravitational wave echoes only in the event of a positive detection (in other words, the non-observation of echoes places constraints on Γ only).

5.5   Conclusions

In this chapter we have studied and parametrized the possible theoretical alternatives to classical black holes and we have discussed the current status of the relevant observational constraints. We have classified the different alternatives into four classes:

---

[4]It is important to stress that it is clear that these interactions must be sufficiently exotic (see, e.g., [319] for a particular discussion) to avoid the formation of trapping horizons (in particular, it seems that these interactions must involve some kind of non-locality), although we will not insist on this point.

regular black holes, bouncing geometries, quasi-black holes and wormholes, and we have provided a set of phenomenological parameters that identify the key properties of each class. Both electromagnetic and gravitational wave observations can be used in order to constrain these parameters. Table 5.2 summarizes the parameters that can be measured or constrained with each of the different observational channels we have discussed.

The most promising observational channel using electromagnetic waves can only probe quasi-black holes. Eq. (5.39) represents the most stringent bound that electromagnetic observations can put on a combination of the parameters κ and μ (a similar relation including Γ can be derived). This provides an upper bound on the allowed values of μ that is generally weaker than the upper bound Eq. (5.31) that does not take into account the parameter κ (as in previous works in the subject). These constraints can become very weak for reasonable values of the parameters involved. We have also reviewed in Sec. 5.3.3 the existence of lower bounds on the parameter μ that can also be inferred from the observation of accretion disks around supermassive black holes. These lower bounds provide the most restrictive constraints on quasi-black holes and are insensitive to the parameters κ and Γ (albeit they do rely on the assumption of standard local interactions).

As with wormholes, testing regular black holes or long-lived bouncing geometries with electromagnetic observations seems hopeless during most of their extended lifetimes. The final stages in the evolution of these objects may be typically violent, which could lead to prompt emissions of electromagnetic radiation. Hence, quasi-black holes are arguably the most interesting scenarios from the perspective of electromagnetic observations, as they offer a number of phenomenological opportunities during all stages of their life cycle (that may involve transients characterized by short-lived bounces).

Regarding gravitational waves, we can conclude that the most promising theoretical scenarios from an observational perspective are quasi-black holes, wormholes, and short-lived bouncing geometries. The remaining theoretical scenarios, such as regular black holes, will be very difficult (if not impossible) to probe observationally in the near future, except perhaps for cataclysmic events that may lead to bursts of gravitational radiation (that can be associated, for instance, with long-lived bouncing geometries).

For these theoretical models, observational channels based on gravitational waves are mostly sensitive to the reflection coefficient Γ. This is due to the main difference with respect to electromagnetic radiation that is typically assumed: gravitational waves interact extremely weakly with standard matter. However, the lack of detailed knowledge of both the matter forming these objects and the possible nonlinear interactions of their gravitational fields with gravitational waves makes it impossible to assume at the moment that these objects will display an appreciable reflection coefficient. In any case, gravitational wave observations are starting to place constraints on this coefficient. These constraints will improve in the near future, thus providing valuable feedback for theoretical research. It is worth stressing that observational channels involving gravitational and electromagnetic waves are therefore complementary, thus providing a strong motivation for a multi-messenger approach to the problem.

108

General conclusions and outlook

In this thesis, we have investigated possible deviations from general relativity using different methods. In chapter 1, we have performed a systematic analysis of a specific class of minimally modified theories of gravity, which have the peculiarity of propagating the same degrees of freedom as general relativity. Our analysis required the interplay of many different techniques. In fact, both the Hamiltonian and the Lagrangian formulation of the theories were necessary in order to apply the spinor helicity formalism and show that the theories under consideration are actually general relativity in disguise. This does not mean that this class of theories is not interesting, as the equivalence holds in vacuum but can be broken by the matter content. In fact, as shown in [72], these theories can have interesting phenomenological aspects in cosmological scenarios.

The second part of the thesis approaches the problem of black hole singularity in a model independent way. In chapter 2, we have studied which type of constraint we need to impose on the spacetime in order to have a well posed notion of causality. We have extended the hierarchy of causality condition of general relativity to generic modified theories of gravity. In particular, for all the scenarios we have discussed, global hyperbolicity is always a necessary condition, even if in some cases it has to be replaced by some stronger condition (for instance we have seen that in the presence on a mode propagating at infinite speed, we have to assume the much stronger requirement of global parabolicity).

This knowledge was very important for the analysis of chapter 3, where we provide a complete classification of non-singular spacetime with trapping horizon. In fact, the key assumption of the analysis is that the spacetime has an effective description in terms of pseudo–Riemannian geometries. Once that we accept this property, in light of the results of the previous chapter, we know that the spacetime has to be global hyperbolic. With these assumptions and with the request of geodesic completeness and the absence of curvature singularities, we were able to introduce and study the properties of four classes of spacetimes: *evanescent horizon, everlasting horizon, one-way hidden wormhole* and *asymptotic hidden wormhole*. We have then proved that the most generic spacetime compatible with our hypothesis has to be a combination of these four classes. While the analysis was performed in spherical symmetry, most of the results can be immediately generalized to a less symmetric configuration. We have seen that some classes of geometries can mimic exactly a classical black hole from the point of view of an external observer while other classes are forced to have some

modification outside the trapping horizon. The geometrical analysis cannot provide insight on which of these two scenarios is more plausible nor on the timescale after which the modification leaks outside the trapping horizon in the second scenario.

Therefore, in chapter 4, we have added extra ingredients so to study the viability of the various solutions. We obtained the remarkable results that it is very difficult to obtain a well defined geometry without allowing for deviation with respect to classical black hole to arise in a short (typically Plankian) timescale.

The one way hidden wormhole and the asymptotic hidden wormhole geometries have problems due to the required topology change and their consistency with semiclassical physics, while the long lived evanescent horizon and the everlasting horizon geometries are generically unstable due to the presence of mass inflation instability. Therefore, the only model which is free from self consistency issue is the short lived evanescent black hole.

Among the various self consistency issues, mass inflation deserves special attention as it is a very general argument but it also present many subtleties that have to be interpreted correctly. It may appear counter intuitive that it is possible to prove the presence of an instability without specifying the dynamics of the theory. The reason why it was possible to use purely kinematical arguments is that we have only proved the existence of a linear instability, *i.e.*, we have shown that small perturbation has a huge impact on the geometry and the dynamical evolution is going to be highly non trivial, but it is not possible to predict what the outcome of this evolution would be. In general relativity, the instability of the inner horizon usually produces a singularity. However, in a full theory of quantum gravity, we expect that this will no longer be true and the backreaction will drive the time evolution to one of the other classes of geometry (maybe it will lead to a short lived evanescent horizon as that one is the only class free from pathologies).

Some possible frameworks for this analysis are given by asymptotic safety and loop quantum gravity as there are examples in which the theories regularize the singularity introducing an (unstable) inner horizon (see, *e.g.*, [97, 134]). These results are perfectly consistent as the works consider vacuum spacetimes without studying the interplay with perturbations. It is very interesting to note that these quantum theories of gravity tame the black hole singularity even if in idealized situations. The results in this thesis suggest that these analyses are actually incomplete, and the study of the backreaction of the perturbation in these frameworks will definitely be a non trivial but essential calculation.

The fact that it is not easy to write down a self consistent geometry without long range effect gives us strong motivation to look for phenomenological signatures of non singular black holes. In chapter 5, we parametrize the deviations from classical black holes with a set of phenomenological parameters and we analyze the possible observational channels that can be used to constrain them. Our geometrical analysis gives us strong motivations to believe that these phenomenological parameters differ from the one corresponding to classical black holes, but it cannot provide any inside on the scale of the differences. We have discussed that if such deviations arise at the Planck length (as expected by several models), than it is very difficult to observe them experimentally with the current technology due to the highly non linear behavior of the gravitational field close to the trapping horizon. We have also seen that different channels can probe

different parameters, thus underlying the need for a multi-messenger approach to the problem.

Let us finally stress that it is very interesting to analyze the interplay between our results and the logic behind the cosmic censorship conjecture. The cosmic censorship conjecture formalizes the intuition that whatever happens at the singularity does not influence the physics outside the event horizon. In this thesis, we have shown that, if a notion of spacetime in terms of pseudo–Riemannian manifold survives the regularization of the singularity, it is very difficult for this intuition to be correct, and that modifications are expected to percolate outside the horizon, regardless the fact that probing any deviation from classical black holes is very challenging from an experimental point of view. Of course, it is impossible to prove that singularity regularization will have long range effects as any analysis, including ours, has to make some assumptions. Anyway, we have shown that the geometries that do not have modifications outside the trapping horizon are very difficult to make self consistent. Therefore the main message of this thesis depends on the personal belief of the person reading it. If one strongly believes that quantum gravity will regularize the spacetime only deep inside the black hole, our analysis highlights some highly non trivial self consistency issues that a full theory of quantum gravity has to address. On the other hand, if one is open to the possibility that black hole spacetime can be modified by quantum effect also outside the trapped region, then our analysis constitutes a further motivation to look for such deviations.

Whatever is the reader opinion, the crucial point about this field is that we live in a new era of multi-messanger astronomy and very exiting times lie ahead towards our understanding of black holes and what they have to teach us about the final theory of gravity.

Appendix A

Extracting the Poincaré algebra

In this appendix we detail the calculations that permit to extract the Poincaré algebra from the non-linear algebra of Poisson brackets discussed in Sec. 1.1. We will do this calculation from scratch, as it is not easy to find it in the literature. First of all, let us note that the coefficients $\{\delta\mu^\alpha, \delta\omega^{\mu\nu}\}$ in Eq. (1.12) are the infinitesimal group parameters associated with the transformations of the Poincaré group, which act on the spacetime coordinates as

$$\delta x^\alpha = -\left(\delta\mu^\beta P_\beta + \delta\omega^{i0} L_{i0} + \frac{1}{2}\delta\omega^{ij} L_{ij}\right) x^\alpha. \tag{A.1}$$

This equation just sets the normalization of the elements of the algebra P_μ and $L_{\mu\nu}$ (note that greek indices are spacetime indices and latin indices are space indices), which will be needed in order to obtain the corresponding Poisson brackets.

Translations with translations

The simplest transformations are spacetime translations. If we consider $\alpha = \delta\mu^0$, $\alpha^i = 0$ and $\beta = 0$, $\beta^i = \delta\mu^i$, the only bracket in Eq. (1.14) that may not be trivial is given by

$$\{\mathcal{D}[\delta\mu^i], \mathcal{H}[\delta\mu^0]\} = \mathcal{H}[\mathcal{L}_{\delta\mu^i}\delta\mu^0] = 0, \tag{A.2}$$

where the last identity follows from the fact that $\delta\mu^0$ is independent of the position. This implies that the bracket between time and space translations is indeed trivial:

$$\{P_0, P_i\} = 0. \tag{A.3}$$

Something similar happens when choosing two time translations, or space translations $\alpha = \beta = 0$ and $\alpha^i = \delta^i_j$, $\beta^i = \delta^i_k$ with $j \neq k$. Hence we can write

$$\{P_\mu, P_\nu\} = 0. \tag{A.4}$$

Translations with boosts/rotations

Now let us consider a more interesting case, namely the bracket involving time translations and boosts. This situations corresponds to the choices $\alpha = \delta\mu^0$, $\alpha^i = 0$ and

$\beta = x_j \delta\omega^{j0}$, $\beta^i = 0$. The only non-trivial bracket in Eq. (1.14) is in this case

$$\{\mathcal{H}[\delta\mu^0], \mathcal{H}[x_j\delta\omega^{j0}]\} = \mathcal{D}[\theta\delta\mu^0\partial^i(x_j\delta\omega^{j0})] = \mathcal{D}[\theta\delta\mu^0\omega^{i0}]. \tag{A.5}$$

This equation implies that the bracket between the generator of time translations and boosts is proportional to a spatial translation:

$$\{P_0, L_{i0}\} \propto P_i. \tag{A.6}$$

But the very same equation can also be used to fix the proportionality constant: using the normalization of the generators given in Eq. (A.1), one must have (note that the minus sign below comes from the global minus sign in the definition of the infinitesimal transformations)

$$\delta\mu^0\omega^{i0}\{P_0, L_{i0}\} = -\theta\delta\mu^0\omega^{i0}P_i, \tag{A.7}$$

which implies (note that the infinitesimal parameters of the different transformations are arbitrary)

$$\{P_0, L_{i0}\} = -\theta P_i. \tag{A.8}$$

Let us now consider the following cases in less detail:

- $\alpha = \delta\mu^0$, $\alpha^i = 0$, $\beta = 0$, $\beta^i = x_j\delta\omega^{ji}$: the only non-trivial bracket is

$$\{\mathcal{D}[x_j\delta\omega^{ji}], \mathcal{H}[\delta\mu^0]\} = \mathcal{H}[\mathcal{L}_{x_j\delta\omega^{ji}}\delta\mu^0] = 0. \tag{A.9}$$

  This implies that the application of time translations and rotations is commutative, namely

$$\{P_0, L_{ij}\} = 0. \tag{A.10}$$

- $\alpha = 0$, $\alpha^i = \delta\alpha^i$, $\beta = x_j\delta\omega^{j0}$, $\beta^i = 0$: we have to evaluate

$$\{\mathcal{D}[\delta\mu^i], \mathcal{H}[x_j\delta\omega^{j0}]\} = \mathcal{H}[\mathcal{L}_{\delta\mu^i}x_j\delta\omega^{j0}] = \mathcal{H}[\delta\mu_i\omega^{i0}]. \tag{A.11}$$

  Hence

$$\{P_i, L_{j0}\} = -\delta_{ij}P_0. \tag{A.12}$$

- $\alpha = 0$, $\alpha^i = \delta\mu^i$, $\beta = 0$, $\beta^i = x_j\delta\omega^{ji}$: we have to evaluate

$$\{\mathcal{D}[\delta\mu^i], \mathcal{D}[x_k\delta\omega^{kj}]\} = \mathcal{D}[\mathcal{L}_{\delta\mu^i}(x_k\delta\omega^{kj})] = \mathcal{D}[\delta\mu_i\delta\omega^{ij}]. \tag{A.13}$$

  In this case we have to take into account the factor $1/2$ in Eq. (A.1). From the equation just above and (A.1) it follows that

$$\delta\mu^i\delta\omega^{kj}\{P_i, L_{kj}\} = 2\delta\mu_i\delta\omega^{ji}P_j. \tag{A.14}$$

  This last equation, together with the antisymmetric character of L_{jk}, leads uniquely to

$$\{P_i, L_{jk}\} = \delta_{ik}P_j - \delta_{ij}P_k. \tag{A.15}$$

Due to the explicit splitting between time and space in the Hamiltonian formulation, the Poincaré algebra appears naturally in a form that is not explicitly covariant. But it is straightforward to write Eqs. (A.8), (A.10), (A.12) and (A.15) in an explicitly covariant form. For $\theta = 1$ one obtains

$$\{P_\rho, L_{\mu\nu}\} = \eta_{\nu\rho}P_\mu - \eta_{\mu\rho}P_\nu, \tag{A.16}$$

while for $\theta = -1$ one has

$$\{P_\rho, L_{\mu\nu}\} = \delta_{\nu\rho}P_\mu - \delta_{\mu\rho}P_\nu. \tag{A.17}$$

Boosts/rotations with boosts/rotations

- Boosts with boosts; $\alpha = x_i \delta\omega^{i0}$, $N^i = 0$, $\beta = x_j \delta\bar{\omega}^{j0}$, $\beta^i = 0$:

$$\{\mathcal{H}[x_i\delta\omega^{i0}], \mathcal{H}[x_j\delta\bar{\omega}^{j0}] = \mathcal{D}[\theta x_k \delta\omega^{k0}\delta\bar{\omega}^{i0} - x_j\delta\bar{\omega}^{j0}\delta\omega^i]$$
$$= \mathcal{D}[\theta x_j(\delta\omega^{j0}\delta\bar{\omega}^{i0} - \delta\bar{\omega}^{j0}\delta\omega^{i0})]. \qquad (A.18)$$

This equation implies that

$$\delta\omega^{i0}\delta\bar{\omega}^{j0}\{L_{i0}, L_{j0}\} = -\frac{\theta}{2}L_{ji}(\delta\omega^{j0}\delta\bar{\omega}^{i0} - \delta\bar{\omega}^{j0}\delta\omega^{i0}) = -\theta\delta\bar{\omega}^{j0}\delta\omega^{i0}L_{ij}, \qquad (A.19)$$

namely

$$\{L_{i0}, L_{j0}\} = -\theta L_{ij}. \qquad (A.20)$$

- Boosts with rotations; $\alpha = 0$, $\alpha^i = x_j\delta\omega^{ji}$, $\beta = x_k\delta\omega^{k0}$, $\beta^i = 0$:

$$\{\mathcal{D}[x_j\delta\omega^{ji}], \mathcal{D}[x_k\delta\omega^{k0}]\} = \mathcal{H}[x_j\delta\omega^{ji}\delta\omega^{k0}\delta_{ik}]. \qquad (A.21)$$

It follows that

$$\delta\omega^{ji}\delta\omega^{k0}\left\{\frac{1}{2}L_{ji}, L_{k0}\right\} = -\delta\omega^{ji}\delta\omega^{k0}\delta_{ik}L_{j0}, \qquad (A.22)$$

so that

$$\{L_{ij}, L_{k0}\} = \delta_{ik}L_{j0} - \delta_{jk}L_{i0}. \qquad (A.23)$$

- Rotations with rotations; $\alpha = 0$, $\alpha^i = x_j\delta\omega^{ji}$, $\beta = 0$, $\beta^i = x_k\delta\bar{\omega}^{ki}$:

$$\{\mathcal{D}[x_k\delta\omega^{ki}], \mathcal{D}[x_l\delta\bar{\omega}^{lj}]\} = \mathcal{D}[x_k\delta\omega^{kj}\delta\bar{\omega}^{li}\delta_{jl} - x_l\delta\bar{\omega}^{lj}\delta\omega^{ki}\delta_{jk}]$$
$$= \mathcal{D}[x_k(\delta\omega^{kj}\delta\bar{\omega}^{li} - \delta\bar{\omega}^{kj}\delta\omega^{li})\delta_{jl}]. \qquad (A.24)$$

It follows that

$$\delta\omega^{ki}\delta\bar{\omega}^{lj}\left\{\frac{1}{2}L_{ki}, \frac{1}{2}L_{lj}\right\} = \frac{1}{2}(\delta\bar{\omega}^{kj}\delta\omega^{li} - \delta\omega^{kj}\delta\bar{\omega}^{li})\delta_{jl}L_{ki}$$
$$= \frac{1}{2}\delta\omega^{ki}\delta\bar{\omega}^{lj}\left(\eta_{jk}L_{li} - \eta_{il}L_{kj}\right). \qquad (A.25)$$

Then,

$$\{L_{ki}, L_{lj}\} = \delta_{jk}L_{li} - \delta_{il}L_{kj} + \delta_{kl}L_{ij} - \delta_{ji}L_{lk}. \qquad (A.26)$$

It is now straightforward to check that Eqs. (A.20), (A.23) and (A.26) are equivalent, for $\theta = 1$, to

$$\{L_{\mu\nu}, L_{\rho\sigma}\} = \eta_{\sigma\mu}L_{\rho\nu} - \eta_{\nu\rho}L_{\mu\sigma} + \eta_{\mu\rho}L_{\nu\sigma} - \eta_{\sigma\nu}L_{\rho\mu}. \qquad (A.27)$$

For $\theta = -1$ we just need to replace $\eta_{\mu\nu} \longrightarrow \delta_{\mu\nu}$ in the equation above.

116

Appendix B

Brief review of on-shell techniques for the evaluation of scattering amplitudes

A key element in the study of the minimally modified theories of gravity of chapter 1 was the spinor helicity formalism used to evaluate the scattering amplitude of gravitons. Let us introduce the main element necessary for our analysis. This appendix is not intended to be an exhaustive review, but rather aims at motivating some basic concepts and results that allow a better understanding of some equations in the main text (and Sec. 1.3 in particular). For in-depth discussions of this interesting subject, we refer the reader to the extensive literature, including the monographs [48, 49, 323] in which most of the relevant references can be found (see also [324] for a shorter introduction starting from the basics).

A basic ingredient that is needed for our discussion are the so-called spinor-helicity variables. These represent a more convenient set of variables (instead of the momenta) in order to describe on-shell massless particles. The starting point for the motivation of these variables is the observation that the algebra of the Lorentz group $SO(1,3)$ is equivalent to the algebra of two $SU(2)$ copies, i.e., at the complex algebra level there is an isomorphism

$$\mathfrak{so}(1,3) \simeq \mathfrak{su}(2) \times \mathfrak{su}(2)^*. \tag{B.1}$$

Furthermore, the Lorentz group is homeomorphic to the group of 2×2 unitary matrix with unit determinant $SL(2,\mathbb{C})$. Therefore, to any Lorentz vector we can associate a 2×2 complex matrix via the map

$$p_\mu \longrightarrow p^{\dot{a}b} = p_\mu (\bar{\sigma}^\mu)^{\dot{a}b}, \tag{B.2}$$

where $\bar{\sigma}^\mu = (\mathbb{1}, -\sigma^i)$ [similarly, let us define $\sigma^\mu = (\mathbb{1}, \sigma^i)$]. Then,

$$\det p^{\dot{a}b} = p_\mu p^\mu. \tag{B.3}$$

Representations of the Lorentz group can be found looking for representations of $SL(2,\mathbb{C})$. These can be labeled using the $SU(2)$ representations. The basic object transforming under the fundamental representation $\mathcal{M}$ is a 2-component spinor $|\psi]_a$ which transforms as

$$|\psi]_a \longrightarrow \mathcal{M}^b{}_a |\psi]_b. \tag{B.4}$$

On the other hand, for the complex conjugate representation one has the transformation rule

$$|\psi\rangle_{\dot{a}} \rightarrow \mathcal{M}^{*\dot{b}}{}_{\dot{a}} |\psi\rangle_{\dot{b}}. \tag{B.5}$$

Dotted indices allow keeping track of the different representations of the SU(2) group, but the notation we are using with angle and square brackets permits us to omit them when convenient. These two representations are

$$|\psi] \sim (1/2, 0), \qquad |\psi\rangle \sim (0, 1/2). \tag{B.6}$$

One can also introduce the additional spinors

$$[\psi|^a = \epsilon^{ab} |\psi]_b, \qquad \langle\psi|^{\dot{a}} = \epsilon^{\dot{a}\dot{b}} |\psi\rangle_{\dot{b}}, \tag{B.7}$$

where

$$\epsilon^{ab} = \begin{pmatrix} 0 & 1 \\ -1 & 0 \end{pmatrix} = \epsilon^{\dot{a}\dot{b}}. \tag{B.8}$$

With these elements, the Dirac equation can be rewritten exploiting the identity[1]

$$\not{p} = \begin{pmatrix} 0 & p_{a\dot{b}} \\ p^{\dot{a}b} & 0 \end{pmatrix}, \tag{B.10}$$

so that $\not{p} = 0$ is equivalent to the Weyl equations

$$p^{\dot{a}b} |p]_b = 0, \qquad p_{a\dot{b}} |p\rangle^{\dot{b}} = 0, \qquad [p|^b p_{b\dot{a}} = 0, \qquad \langle p|_{\dot{b}} p^{\dot{b}a} = 0. \tag{B.11}$$

If we take into account Eq. (B.3), the determinant of these matrices vanishes identically for on-shell massless particles. It follows that one can write

$$p_{a\dot{b}} = -|p]_a \langle p|_{\dot{b}}, \qquad p^{\dot{a}b} = -|p\rangle^{\dot{a}} [p|^b. \tag{B.12}$$

This is one of the main properties that justifies the usefulness of the spinor-helicity variables: we can use the angle and square brackets instead of the momenta in order to write equations that involve the momentum of on-shell massless particles (e.g., scattering particles); note that this is independent of the helicity of these particles. Not only the momentum of an on-shell massless particle can be written in this way, but also other quantities of interest such as polarization vectors of spin-1 particles, namely

$$\epsilon_+^\mu(p, q) = -\frac{\langle q|\gamma^\mu|p]}{\sqrt{2}\langle qp\rangle}, \tag{B.13}$$

which corresponds to the polarization with positive helicity, and the corresponding quantity with negative helicity,

$$\epsilon_-^\mu(p, q) = -\frac{\langle p|\gamma^\mu|q]}{\sqrt{2}[qp]}. \tag{B.14}$$

Eqs. (B.13) and (B.14) are just a particular representation of the usual polarization vectors of photons and gluons in terms of spinor-helicity variables (see, e.g., [49] for a

---

[1]The convention used here for the gamma matrices is

$$\gamma^\mu = \begin{pmatrix} 0 & (\sigma^\mu)_{a\dot{b}} \\ (\bar{\sigma}^\mu)^{\dot{a}b} & 0 \end{pmatrix}. \tag{B.9}$$

very explicit discussion of this point). In these equations, q is a reference spinor that does not have any physical meaning and can be chosen arbitrarily, representing the freedom of choosing a particular gauge.

This construction goes on for particles with higher spin. In particular, the polarization tensors describing the two helicities of the gravitational field (which will be the same for all the theories in which the Fierz-Pauli field equations are recovered at linear order) are given by

$$\epsilon_\pm^{\mu\nu} = \epsilon_\pm^\mu \epsilon_\pm^\nu. \tag{B.15}$$

Complexification of external momenta.

The next ingredient we need to introduce is the complexification of the external momenta. This kind of complexification consist in the shift of the momenta in the complex plane and permits to exploit the analytical structures of scattering amplitudes, which at tree level are rational functions that can only display poles when internal propagating particles (in our case, gravitons) become on-shell; this is what is usually defined as the locality condition. Note that additional poles that do not correspond to physical particles (i.e., the propagating degrees of freedom) may appear in individual Feynman diagrams, but these must cancel in the complete amplitude (these are known as spurious poles). In particular, for the theories analyzed in Sec. 1.2 we know that the only possible complex poles in the amplitudes correspond to physical gravitons on-shell, i.e., satisfying $\hat{p}^2 = 0$.

The complexification used in chapter 1 has the form

$$p_i \longrightarrow \hat{p}_i = p_i + z q_i, \tag{B.16}$$

where $z \in \mathbb{C}$, and the vectors q_i are such to satisfy

$$\sum_{s=1}^n q_s = 0; \tag{B.17}$$

$$q_i \cdot q_j = 0 \qquad \forall i, j; \tag{B.18}$$

$$q_i \cdot p_i = 0 \qquad \forall i. \tag{B.19}$$

This conditions imply

$$\sum_{s=1}^n \hat{p}_i = 0; \tag{B.20}$$

$$\hat{p}_i^2 = 0; \tag{B.21}$$

$$\hat{P}_I^2 := \left(\sum_{i \in I} \hat{p}_i \right)^2 = -\frac{z - z_I}{z_I} P_I^2 \tag{B.22}$$

where I marks a given subset of particles, so that $\hat{P}_I$ and P_I are momenta of internal particles and z_I is a constant whose exact value is irrelevant in this discussion.

In the case of general relativity, and the gravitational theories discussed in this thesis, the optimal choice [53, 54] for the complexification ($N > n/2$ is the number of particles with positive helicity) is given by

$$\hat{p}_s = p_s + z|t\rangle[s|, \qquad \hat{p}_t = p_t - z\sum_{s=1}^{N}|t\rangle[s|. \tag{B.23}$$

where $s \in [1, N]$ labels all the external legs with positive helicity, and t marks a single external leg with negative helicity and the remaining particles are not shifted. In this equation, we have exploited the fact that $\{q_s\}_{s=1}^{N}$ and q_t are null vectors as well by definition, so that these can be decomposed in spinor-helicity variables as in Eq. (B.12). If we decompose in this way the momenta (such that, e.g., $p_s = -|s\rangle[s|$), we can directly write this complexification in terms of spinor-helicity variables as

$$|\hat{s}\rangle = |s\rangle - z|t\rangle, \qquad |\hat{t}] = |t] + z\sum_{s=1}^{N}|s]. \tag{B.24}$$

Validity of the recursion relation

The complexification of the momenta defines a complexified n-point amplitude $A_n(z)$, such that $A_n(0)$ is the original amplitude evaluated on real momenta. Let us consider

$$\oint \frac{A_n(z)}{z}dz, \tag{B.25}$$

where the integration path is a circle of infinite radius. The integrand has a simple pole at the origin whose residue is exactly the scattering amplitude for real momenta that we want to determine. By Eq. (B.22) we know that there are additional simple poles whenever an internal particle goes on shell. Finally, it is possible to prove there are no extra poles. Therefore, by using Cauchy residue theorem to evaluate the integral (B.25), assuming that the the function $A_n(z)$ goes to zero at infinity, we get

$$A_n(z = 0) = -\sum_{z \in z_I} Res\frac{A_n(z)}{z}. \tag{B.26}$$

However, as shown in Fig. B.1, when an internal particle goes on shell, the amplitude is decomposed into two amplitudes with at most $n - 1$ graviton each. Therefore, we can write

$$A_n(z = 0) = \sum A_L\frac{1}{P_I^2}A_R, \tag{B.27}$$

where the sum is intended to run over all the internal particles. Therefore, the n point amplitude can be written in terms of the k points amplitudes with $k \leq n - 1$, implying that scattering amplitudes can be constructed recursively. The only condition to obtain this result was that $A_n(z)$ vanishes at infinity. To ensure that is showing that, a sufficient condition is the individual contributions from all the possible Feynman diagrams contributing to a given amplitude vanish independently. In order to show this, one needs to extract the leading behavior with $|z|$ of all the relevant elements in these
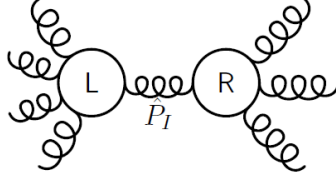
Figure B.1: When an internal particle goes on shell, the amplitude factorize into the product of two amplitudes each of them with at most $n-1$ gravitons.

diagrams. In particular, it will be useful for our arguments in Sec. 1.3 to recall some basic properties of Feynman diagrams with n external particles and k-point vertices, namely the number of vertices v, propagators p and internal vertices i (not stitched to external particles):

- *3-point vertices:* $v = n - 2$, $p = n - 3$ and $i \leq n/2 - 2$.

- *4-point vertices:* $v = n/2 - 1$, $p = n/2 - 2$ and $i \leq n/6 - 1$.

Note that the number of internal vertices i depends on the topology of the particular diagrams considered. We will not need this information for $k \geq 5$, as the corresponding contributions are subleading (which is typically also true for 4-point vertices with respect to 3-point vertices; for instance, considering only vertices quadratic in the momenta, the corresponding powers coming from the vertices are $n - 2$ and $2n - 4$, respectively). In general, the number of vertices and propagators as functions of k are given by

$$v(k) = \frac{n-2}{k-2}, \qquad p(k) = v(k) - 1. \tag{B.28}$$

Appendix C

Regularity conditions for vanishing radius

In Sec. 4.1.1 we have discussed some condition for the absence of curvature singularity in a spherically symmetric and static spacetime in which the area radius can vanish. In this appendix we are going to extend the discuss to the time dependent case. The metric can be written as

$$ds^2 = -e^{-2\phi(v,t)}F(v,t)ds^2 + 2e^{-\phi(v,r)}dvdr + r^2d\Omega^2 \tag{C.1}$$

Let us start assuming that the metric coefficients are either real analytic or finite (which is a weaker assumption) in this open set. Given that the exponential function is real analytic, both functions $F(v,r)$ and $\phi(v,r)$ must be either analytic or finite as well. It follows then that divergences in curvature invariants can be avoided if and only if, for $r = \epsilon \ll 1$,

$$F(v,\epsilon) = 1 + \mathcal{O}(\epsilon^2), \qquad \text{and} \qquad \phi(v,\epsilon) = \Phi_0(v) + \mathcal{O}(\epsilon^2). \tag{C.2}$$

To reach this conclusion, let us start with the following relation satisfied by the Ricci scalar $g^{ab}R_{ab}$:

$$\lim_{r \to 0} r^2 g^{ab}R_{ab} = 2 - 2F(v,0). \tag{C.3}$$

Hence, the condition $F(v,0) = 1 + \mathcal{O}(r^2)$ is necessary to avoid a quadratic divergence. But we are still left with a possible linear divergence, as

$$\lim_{r \to 0} r \, g^{ab}R_{ab} = 4 \, \partial_r\phi(v,r)|_{r=0} \,. \tag{C.4}$$

It is from this equation that the second condition in Eq. (C.2) arises. It is easy to check that if conditions (C.2) are fulfilled, also the curvature invariants $R_{ab}R^{ab}$, $R_{abcd}R^{abcd}$ and $C_{abcd}C^{abcd}$ are finite.

Eq. (C.2) is to be compared with the value $F(v,0) = -\infty$ for standard Schwarzschild and Reissner–Nordström black holes. The different value of $F(v,0)$ translates also into a very different quasi-local structure around $r = 0$, namely that of a future inner trapping horizon or, in other words, a future inner trapped surface for every constant value of v. Indeed, asymptotic flatness and the requirement of existence of a future outer trapping horizon, together with Eq. (C.2), implies that there must be (at least) two radial points in which $F(v,r)$ vanishes for every constant value of v. To see this let us specialize the previously introduced null vectors $\{\boldsymbol{k}, \boldsymbol{l}\}$ to the radial null vector fields

$$\boldsymbol{k} = -e^{\phi(v,r)}\partial_r \,, \qquad \boldsymbol{l} = \partial_v + \frac{1}{2}e^{-\phi(v,r)}F(v,r)\partial_r, \tag{C.5}$$

which satisfy the normalization condition $\boldsymbol{k} \cdot \boldsymbol{l} = -1$. These two linearly independent radial null vector fields correspond to ingoing and outgoing radial null geodesics, respectively. The expansion along outgoing radial null geodesics is then given by

$$\theta^{(l)}(v,r) = \frac{e^{-\phi(v,r)}}{r} F(v,r). \tag{C.6}$$

Asymptotic flatness implies that the expansion is positive in the limit $r \to \infty$. On the other hand, the existence of a future outer marginally trapped surface for each value of v implies that there must exist a function $r_{\text{outer}}(v)$ such that $F(v, r_{\text{outer}}(v)) = 0$ vanishes. Unless the corresponding future outer trapping horizon is extremal, the function $F(v,r)$ will then change sign around $r = r_{\text{outer}}(v)$, being positive just above this value of the radius, and negative just below. It is at this point in the discussion where Eq. (C.2) enters: given that $F(v,0) = 1 > 0$, there must exist another function $r_{\text{innter}}(v)$ such that $F(v, r_{\text{inner}}(v))$. It is straightforward to show that $r = r_{\text{outer}}(v)$ corresponds to a future outer marginally trapped surface, while $r = r_{\text{inner}}(v)$ to a future inner marginally trapped surface; the distinction between outer and inner is provided by the different signs of $\mathcal{L}_{\boldsymbol{k}} \theta^{(l)}$. In fact, from the definitions in Eq. (C.5) follows that

$$\mathcal{L}_{\boldsymbol{k}} \theta^{(l)}(v,r)\big|_{r=r_{\text{outer}}(v)} = -\frac{1}{r} \, \partial_r F(v,r)\big|_{r=r_{\text{outer}}(v)} < 0,$$

$$\mathcal{L}_{\boldsymbol{k}} \theta^{(l)}(v,r)\big|_{r=r_{\text{inner}}(v)} = -\frac{1}{r} \, \partial_r F(v,r)\big|_{r=r_{\text{inner}}(v)} > 0. \tag{C.7}$$

The discussion above relies on both real functions $F(v,r)$ and $\phi(v,r)$ being finite at $r = 0$ (or real analytic, which is stronger). Let us briefly analyze the possibility that these functions are divergent. It is still possible to write down constraints (taking the form of differential equations) to be satisfied by the functions $F(v,r)$ and $\phi(v,r)$ so that each independent curvature invariant remains finite. However, it is not clear that all these constraints are compatible between them and, therefore, whether it is possible to engineer these divergent functions at $r = 0$ to avoid curvature invariants blowing up. Moreover, it is straightforward to see that, if such a geometry exists, it must be characterized by a non-polynomial divergence for $F(v,r)$ and $\phi(v,r)$ at $r = 0$. In fact, assuming for $r = \epsilon \ll 1$ that

$$F(v,\epsilon) = \epsilon^{-\alpha} f(v), \qquad e^{-\phi(v,\epsilon)} = \epsilon^{-\beta} \tilde{\phi}(v), \tag{C.8}$$

with both α and β integers greater than one, it follows that

$$g^{ab} R_{ab}\big|_{r=\epsilon} = \frac{2}{\epsilon^2} - \frac{(\alpha^2 - 3\alpha + 3\alpha\beta + 2\beta^2 - 2\beta + 2) \, f(v)}{\epsilon^{\alpha+2}}. \tag{C.9}$$

The polynomial $\alpha^2 - 3\alpha + 3\alpha\beta + 2\beta^2 - 2\beta + 2 = \alpha^2 + 3(\beta-1)\alpha + \beta^2 + 1 + (\beta-1)^2$ does not have roots in the domain of definition of α and β. Hence, any non-zero α leads to a curvature singularity. A curvature singularity can be avoided if and only if $\alpha = 0$ and

$$f(v) = \frac{1}{\beta^2 - \beta + 1} > 0. \tag{C.10}$$

This would already imply the existence of an inner horizon in complete parallel to our previous discussion. However, computing the Kretschmann scalar shows that

$$\lim_{r \to 0} r^4 R_{abcd} R^{abcd} = \frac{8\beta^2 (\beta^2 + 2)}{(\beta^2 - \beta + 1)^2} \tag{C.11}$$

This implies the necessity of the further condition $\beta = 0$. Hence, even if allowing that $F(v, r)$ and $\phi(v, r)$ diverge polynomially at $r = 0$, in order to avoid that some curvature invariant blows up it is necessary to assume that $F(v, 0) = 1$.

Appendix D

Evaporation time

In this appendix we want to study an interesting aspect of the regular black hole geometries. We have seen in chapter 4 that this type of geometry is associated with an instability of the inner horizon which severely question the viability of the model. If we assume no extra exotic physics and the evolution of a regular black hole simply consist in its evaporation due to Hawking radiation, than the only way to make the model self consistent would be to fine tune the instability time scale to make it longer than the the evaporation timescale. To our knowledge, the evaporation time has not been studied systematically, but its finiteness is always assumed.[1] In order to compute the evaporation timescale, we start from the most conservative viewpoint, which can be summarized in the following two assumptions:

1. *Adiabatic condition.* The only relevant dynamical process during the evaporation is Hawking's radiation which, at each moment of the evaporation, is thermal with temperature given by

$$T = \frac{\kappa_+}{2\pi}. \tag{D.1}$$

2. *Quasi-static condition.* The evaporation is a quasi-static process, meaning that the black hole passes continuously through a sequence of equilibrium states.

We will comment on the validity of these assumptions later on.

According to our hypothesis, the mass loss rate is determined by the Stefan–Boltzmann law,

$$\frac{\mathrm{d}M(v)}{\mathrm{d}v} = -\sigma_{\mathrm{SB}} \, T^4(v) A_+^2(v) = -C\kappa_+^4(v)r_+^2(v), \tag{D.2}$$

where $A_+(v)$ is the area of the outer horizon, σ_{SB} is the Stefan–Boltzman constant and C is a positive constant, whose precise value is for the moment irrelevant. Here M, κ_+ and r_+ have been promoted to dynamical functions of the evaporation time v. Hence, from now on we will be dealing implicitly with geometries of the form

$$\mathrm{d}s^2 = -e^{-2\phi(r,M(v))}F(r,M(v))\mathrm{d}v^2 + 2e^{-\phi(r,M(v))}\mathrm{d}r\mathrm{d}v + r^2(\mathrm{d}\theta^2 + \sin^2\theta\,\mathrm{d}\phi^2). \tag{D.3}$$

We are using the notation $\phi(r,M)$ and $F(r,M)$ in order to emphasize the dependence of these functions on the mass M, and also that these functions can depend on the time v only implicitly, through $M(v)$.

---

[1] The only exception being the "loop black hole" [325], where the evaporation is shown to happen in an infinite time, leaving no remnant.

Integration of Eq. (D.2) requires knowledge of κ_+ and r_+ as functions of M. At the outer horizon we have

$$F(r_+, M) = 0. \tag{D.4}$$

At extremality $r_+ = r_\star$ and $M = M_\star$, so that the condition

$$\left.\frac{\partial F(r, M_\star)}{\partial r}\right|_{r=r_\star} = 0 \tag{D.5}$$

must hold. Since the surface gravity is

$$\kappa_\pm = \frac{e^{-\phi(r_\pm)}}{2} \left.\frac{\partial F(r, M)}{\partial r}\right|_{r=r_\pm}, \tag{D.6}$$

the surface gravity $\kappa_\star$ of the extremal black hole vanishes, unless $\phi(r_\star, M_\star)$ diverges (this specific case is analyzed in Sec. D). This in turn means that the evaporation rate (D.2) vanishes at the end of the evaporation process. An infinitely slow evaporation rate is a clue that the evaporation time may be infinite (in fact, this has been shown to be precisely the case for near-extremal Reissner–Nordström black holes [326]). This would be the worst possible scenario given that, no matter how slow the mass inflation instability grows, its timescale will be trivially smaller than the evaporation time. Let us therefore explore the condition under which this happens.

Computation of the evaporation time

We start by assuming that the evaporation has proceeded adiabatically and quasi-statically up to a point at which the mass is arbitrarily close to the extremal value $M_\star$, $M = M_\star + \Delta M$. Our strategy then consists of integrating Eq. (D.2) from $M_\star + \Delta M$ to $M_\star$, and showing that the corresponding time interval is infinite.

Consider a configuration in which the outer horizon radius is just an arbitrarily small Δr away from $r_\star$

$$r_+ = r_\star + \Delta r = r_\star\left(1 + \epsilon\right), \qquad 0 < \epsilon \ll 1 \tag{D.7}$$

and correspondingly the mass has an arbitrarily small deviation ΔM from $M_\star$

$$M = M_\star + \Delta M = M_\star\left(1 + \beta\epsilon^\sigma\right) + \mathfrak{o}(\epsilon^\sigma), \tag{D.8}$$

where we parametrized ΔM with two real constants β and $\sigma > 0$. These cannot be arbitrarily chosen, because M and r_+ are related to each other by Eq. (D.4). In order to find their relation, let us expand Eq. (D.4) around Δr and ΔM:

$$
\begin{aligned}
0 =& F(r_\star, M_\star) + \left.\frac{\partial F}{\partial r}\right|_{r_\star, M_\star}\Delta r + \left.\frac{\partial F}{\partial M}\right|_{r_\star, M_\star}\Delta M + \\
&+ \frac{1}{2}\left.\frac{\partial^2 F}{\partial r^2}\right|_{r_\star, M_\star}\Delta r^2 + \left.\frac{\partial^2 F}{\partial r \partial M}\right|_{r_\star, M_\star}\Delta r\,\Delta M + \\
&+ \frac{1}{2}\left.\frac{\partial^2 F}{\partial M^2}\right|_{r_\star, M_\star}\Delta M^2 + \dots
\end{aligned}
\tag{D.9}
$$

The first term of Eq. (D.9) vanishes due to Eq. (D.4) evaluated at $r_\star$ and $M_\star$, while the second term vanishes due to Eq. (D.5). Let us start considering the simplest case in which $\partial F/\partial M|_{r_\star,M_\star} \neq 0$. The most general situation is analyzed below. In this case ΔM is of order ϵ^n, where $n \geq 2$ is the first natural number for which

$$\left.\frac{\partial^n F}{\partial r^n}\right|_{r_\star,M_\star} \neq 0, \tag{D.10}$$

so that $\sigma = n$ and

$$\beta = -\frac{1}{n!}\left(\left.\frac{\partial F}{\partial M}\right|_{r_\star,M_\star}\right)^{-1}\left.\frac{\partial^n F}{\partial r^n}\right|_{r_\star,M_\star}. \tag{D.11}$$

From Eq. (D.5), under the assumption that $\phi(r, M)$ is finite, we have $\kappa_\star = 0$ and, therefore,

$$\kappa_+ = \alpha\epsilon^\gamma + \mathfrak{o}(\epsilon^\gamma), \tag{D.12}$$

where we have parametrized the deviation of κ_+ from $\kappa_\star = 0$ with two real constants α and $\gamma > 0$. Plugging Eqs. (D.8) and (D.12) in the Stefan-Boltzmann law (D.2), we can integrate the latter to obtain the evaporation time Δv:

$$\Delta v = -\frac{M_\star}{r_\star^2 C}\frac{\beta\sigma}{\alpha^4}\int_{\epsilon_0}^0 d\epsilon\,\epsilon^{\sigma-4\gamma-1}. \tag{D.13}$$

We see that Δv is finite if and only if

$$\sigma - 4\gamma > 0. \tag{D.14}$$

However,

$$\begin{aligned}
\kappa_+ &= \frac{e^{-\phi(r_+)}}{2}\left.\frac{\partial F}{\partial r}\right|_{r_+} \\
&= \frac{e^{-\phi(r_+)}}{2}\sum_{i,j=0}^\infty \frac{1}{i!j!}\left.\frac{\partial^{(i+j+1)}F}{\partial^{(i+1)}r\partial^{(j)}M}\right|_{r_\star,M_\star} r_\star^i \epsilon^i \Delta M^j,
\end{aligned} \tag{D.15}$$

where in the second line we have used the Taylor expansion of $\partial F/\partial r|_{r_+}$. The leading term in the expansion is

$$\kappa_+ = \frac{e^{-\phi(r_\star)}}{2}\frac{1}{n!}\left.\frac{\partial^n F}{\partial r^n}\right|_{r_\star,M_\star} r_\star^{n-1}\epsilon^{n-1} + \mathfrak{o}(\epsilon^{n-1}), \tag{D.16}$$

where n is the same as in Eq. (D.10). It follows that $\gamma = n - 1$ and $\sigma - 4\gamma = 4 - 3n$. Given that $n \geq 2$, Eq. (D.14) cannot be satisfied.

Let us now relax the assumption $\partial F/\partial M|_{r_\star,M_\star} \neq 0$. Eqs. (D.9), (D.14) and (D.15) are completely generic, and sufficient that the evaporation time is infinite. Indeed, let us distinguish three cases:

Case $\sigma = 1$ Eq. (D.14) becomes $1 - 4\gamma > 0$. But, from Eq. (D.15), γ must be a positive integer. Hence a contradiction.

Case $\sigma < 1$ From Eq. (D.15) there are two subcases. Either γ is a positive integer and Eq. (D.14) is trivially violated, or $\gamma = I + J\sigma$ where $I \geq 0$ and $J > 0$ are appropriate integers. In the last subcase $\gamma \geq \sigma$, hence $\sigma - 4\gamma < -3\sigma < 0$, which contradicts Eq. (D.14).

Case $\sigma > 1$ The term of order $\Delta r^n \sim \epsilon^n$ in Eq. (D.9), where n is defined as in Eq. (D.10), can be canceled only by terms of order $\Delta r^I \Delta M^J \sim \epsilon^{I+J\sigma}$, where $I, J \geq 1$ are appropriate integers such that $n = I + J\sigma$. This implies $\sigma \leq n$. On the other hand, $\gamma = n - 1$ for the same reasoning of Eq. (D.16). Therefore $\sigma - 4\gamma \leq 4 - 3n < 0$, where the last inequality follows from $n \geq 2$. Hence, Eq. (D.14) cannot be satisfied.

Therefore, we conclude that the evaporation time is infinite for analytic spacetime geometries. Intuitively, the result follows from the fact that, in the extremal limit, the surface gravity goes to zero sufficiently fast and makes the evaporation rate indefinitely slow. It is straightforward to realize that a generic, but non-divergent, $\phi(r, M)$ would not change the conclusion. Table D.1 summarizes the properties of several models presented in the literature, and makes explicit that these models have an infinite evaporation time. It may seem surprising that, in all these models, the exponents σ and γ are the same. However, from Eq. (D.9) one can read that these coefficients are in general model independent, unless the function $F(r, M)$ is tuned so that some of its derivatives vanish.

Model	Metric		Inner horizon		Evaporation time		
	$m(r)$	$|\phi(r)|$	r_-	κ_-	σ	γ	Δt
Hayward [109]	$Mr^3(r^3 + 2M\ell^2)$	0	ℓ	$-\frac{1}{\ell}$			
Frolov–Zelnikov [327]	$\frac{Mr^3}{(r^3+2M\ell^2)}$	$< \infty$	ℓ	$-\frac{e^{-\phi(r_-)}}{\ell}$	2	1	∞
Bardeen [103, 108]	$\frac{Mr^3}{\left[r^2+(2M\ell^2)^{2/3}\right]^{3/2}}$	0	$\sqrt{\frac{\ell^3}{2M}}$	$-\frac{1}{\ell}$			
Dymnikova [107, 111]	$M\left[1 - e^{\left(-r^3/2M\ell^2\right)}\right]$	0	ℓ	$-\frac{1}{\ell}$			

Table D.1: The most relevant properties of the examples that we have considered. The parameter ℓ is a length scale, which is usually identified with the Planck length. Only the leading order of r_- and κ_- is provided, so that these quantities must be multiplied by $[1 + \mathcal{O}(\ell/M)]$ terms.

Adiabatic and quasi-static conditions

In this section we rigorously state and we discuss the validity of the adiabatic and the quasi-static conditions.

Adiabatic condition

Hawking radiation is derived assuming that the geometry is static or, at the very least, evolving slow enough in a certain sense. The precise meaning of the word "slow" in this framework was defined in [328, 329]. For the purposes of the present discussion, the thermality of Hawking radiation is guaranteed if the following adiabatic condition is satisfied:

$$\frac{1}{\kappa_+^2}\frac{\mathrm{d}\kappa_+}{\mathrm{d}v} \ll 1. \tag{D.17}$$

For regular black holes, this condition might only fail during the final stages of the evaporation, when both $\mathrm{d}\kappa_+/\mathrm{d}v$ and κ_+^2 go to zero. From Eq. (D.12), it follows that

$$\frac{\mathrm{d}\kappa_+}{\mathrm{d}v} \propto \epsilon^{\gamma-1}\frac{\mathrm{d}\epsilon}{\mathrm{d}v}, \tag{D.18}$$

while taking the derivative in Eq. (D.8) and using the evaporation law (D.2) leads to

$$\epsilon^{\sigma-1}\frac{\mathrm{d}\epsilon}{\mathrm{d}v} \propto \frac{\mathrm{d}M}{\mathrm{d}v} \propto \epsilon^{4\gamma}. \tag{D.19}$$

This permits to solve for $\mathrm{d}\epsilon/\mathrm{d}v$, so that the adiabatic condition becomes

$$\frac{1}{\kappa_+^2}\frac{\mathrm{d}\kappa_+}{\mathrm{d}v} \propto \epsilon^{3\gamma-\sigma}. \tag{D.20}$$

Hence, it follows that the adiabatic condition is satisfied if and only if

$$3\gamma - \sigma > 0. \tag{D.21}$$

Repeating the same analysis performed at the end of Sec. D, one can easily show that this condition is always satisfied for spacetime geometries that are analytic.

Quasi-static condition

We have studied explicitly only the late stages of the evaporation, in which the temperature is arbitrarily small so that the quasi-static approximation is surely valid in this stage. However, we implicitly assumed that the black hole, starting from a macroscopic mass much greater than $M_\star$, reaches a mass $M_\star + \Delta M$ with $\Delta M \ll M_\star$ through an adiabatic and quasi-static process driven by the Hawking radiation.

Since the surface gravity becomes zero both for $M = M_\star$ and at $M \to \infty$, it must have a global maximum for some value M_{peak} of the black hole mass. If the corresponding Hawking temperature T_{peak} is high enough, then the evaporation process can enter in a regime in which most of its mass is emitted in a short time, so that the quasi-static approximation no longer holds. Therefore, we must address whether or not this is the case. For concreteness, we refer to what is probably the simplest regular
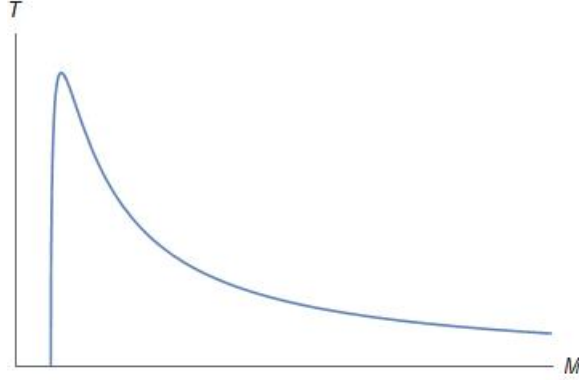
Figure D.1: Qualitative plot of the Hawking temperature as a function of the mass.

black hole model, originally proposed by Hayward [109]. Hayward's metric is specified by

$$F(r, M) = 1 - \frac{2Mr^2}{r^3 + 2M\ell^2}, \qquad \phi(r, M) = 0. \qquad (D.22)$$

The outer and inner horizons $r_\pm$ for a given mass are identified by the relation

$$M = \frac{r_\pm^3}{2\left(r_\pm^2 - \ell^2\right)} \,. \qquad (D.23)$$

When $M \to \infty$, $r_+ \to 2M$ and $r_- \to \ell$. The function (D.23) has a global minimum for $r_\star = \sqrt{3}\ell$ and $M_\star = 3\sqrt{3}\ell/4$, which corresponds to the extremal mass. The surface gravity of the outer horizon is

$$\kappa_+ = \frac{3}{4M} - \frac{1}{r_+} \,. \qquad (D.24)$$

Fig. D.1 shows the dependence of $\kappa_+/2\pi$ on the mass M: We see that there is only one maximum at $M = M_{\rm peak}$. In order to find the exact value of $M_{\rm peak}$ it is sufficient to minimize the function

$$\tilde{F}(r, M) = \frac{\partial F(r, M)}{\partial r} + \tilde{\lambda} F(r, M) \qquad (D.25)$$

with respect to r, M and $\tilde{\lambda}$, finding $r_{\rm peak} = 3\ell$ and $M_{\rm peak} = 27\ell/16$. The corresponding height of the temperature peak is

$$T_{\rm peak} = \frac{\kappa_{\rm peak}}{2\pi} = \frac{1}{18\pi\ell} \approx \frac{10^{-2}}{\ell} \,. \qquad (D.26)$$

Therefore, if we identify ℓ with the Planck length, the peak temperature is two orders of magnitude smaller than the Planck temperature. In order to assess the extent to which this is consistent with the quasi-static condition, let us point that at $M_{\rm peak}$ the system is dominated only by the scale ℓ. Therefore we can roughly estimate the mass loss at the peak by multiplying the peak luminosity

$$\left.\frac{dM}{dt}\right|_{\rm peak} = -\sigma_{\rm SB}\, T_{\rm peak}^4 4\pi r_{\rm peak}^4 \qquad (D.27)$$

by the characteristic timescale at the peak, $t_{\text{peak}} \approx \ell$. Identifying $\ell = L_{\text{planck}}$ we find that the emitted mass is about $10^{-6} M_{\text{peak}}$. We interpret this result as an indication that the system is not much perturbed even at the peak point, implying that the adiabatic approximation is reasonable.

We have numerically computed r_{peak} and M_{peak} for the "Bardeen black hole" [103, 108] and the "Dymnikova black hole" [107], finding that the mass emitted at the peak is $10^{-7} M_{\text{peak}}$ in the former case and $10^{-5} M_{\text{peak}}$ in the latter one. A similar conclusion was reached in [330] in the context of asymptotic safety.

Beyond the quasi-static or adiabatic regimes

Comparing Eqs. (D.14) and (D.21) it is evident that it is not possible to satisfy the adiabatic condition and also have a finite evaporation time (this follows from $\sigma > 0$). Therefore, the only way to build a model with finite evaporation time is going outside either the quasi-static or the adiabatic regimes.

It is possible to go outside the quasi-static approximation by simply picking a $\phi(r, M) \neq 0$ that is very large at the peak mass. In this case the system would enter in a regime that requires beyond semiclassical physics to be addressed (in other words, the effective description in terms of the regular black hole geometry breaks down).

Evading the adiabatic condition is less trivial. One would need to pick a function $\phi(r, M)$ such that it diverges at $r_+ = r_\star$ when $M = M_\star$. Indeed, returning to Eqs. (D.16) and (D.21), it is sufficient for $\sigma - 3\gamma$ to be positive that

$$e^{-\phi(r_\star + \Delta r, M_\star + \Delta M)} \propto \epsilon^{-\delta}, \tag{D.28}$$

where

$$(n-1) - \frac{\sigma}{3} \leq \delta \leq n - 1. \tag{D.29}$$

In particular, the lower bound of δ in Eq. (D.29) ensures that the adiabatic condition is violated, while the upper bound prevents $\kappa_\star$ from diverging. Notice also that, when the upper bound is saturated, $\delta = n - 1$, we are in a special case: $\kappa_\star$ is not zero but it is discontinuous, namely $\lim_{r_+ \to r_\star} \kappa_+ > 0$ while $\lim_{r_- \to r_\star} \kappa_- < 0$.

Let us remark that Eq. (D.29) is not the only constraint that $\phi(r, M)$ must satisfy in order for the scenario to be internally consistent. Obviously the metric should remain non-singular. There are two places in which the metric could become singular, at $r = r_\star$ and at $r = 0$. Computing the Ricci and Kretschmann scalar, one can check that, if Eq. (D.29) holds only when $M = M_\star$, i.e., only when $r_\star$ is an horizon, then the metric is not singular. Additionally, it can be checked that, in order for the metric to not diverge at $r = 0$, we must have that $e^{-\phi(r, M)}$ goes to a constant in the limit $r \to 0$, while its derivative with respect to r must vanish in this limit. Furthermore, we also want the instability timescale of the inner horizon to be much longer than the evaporation time, implying $\exp[-\phi(r_-, M)] \ll 1$. Strictly speaking, this condition is necessary only when the black hole is macroscopic or mesoscopic ($M \gg M_\star$). Indeed $F'(r_-)$ approaches zero in the limit $M \to M_\star$, and, from Eq. (4.10), κ_- might still be small for values of $\exp[-\phi(r_-, M)]$ of order unity or even greater.

If these properties are satisfied, the model can in principle be consistent from a geometric perspective. However, this limits the predictability of the late stages of

evaporation, because one must resort to yet unknown physics beyond the effective description provided by regular black holes. Therefore, that the effective description breaks down just when it would become physically relevant, invalidates the original motivation and limits the scope of these models.

Bibliography

[1] **Virgo, LIGO Scientific** Collaboration, B. P. Abbott *et al.*, "Observation of Gravitational Waves from a Binary Black Hole Merger," *Phys. Rev. Lett.* **116** no. 6, (2016) 061102, `arXiv:1602.03837 [gr-qc]`.

[2] **Virgo, LIGO Scientific** Collaboration, B. P. Abbott *et al.*, "GW151226: Observation of Gravitational Waves from a 22-Solar-Mass Binary Black Hole Coalescence," *Phys. Rev. Lett.* **116** no. 24, (2016) 241103, `arXiv:1606.04855 [gr-qc]`.

[3] **VIRGO, LIGO Scientific** Collaboration, B. P. Abbott *et al.*, "GW170104: Observation of a 50-Solar-Mass Binary Black Hole Coalescence at Redshift 0.2" *Phys. Rev. Lett.* **118** no. 22, (2017) 221101, `arXiv:1706.01812 [gr-qc]`.

[4] **Virgo, LIGO Scientific** Collaboration, B. P. Abbott *et al.*, "GW170608: Observation of a 19-solar-mass Binary Black Hole Coalescence," *Astrophys. J.* **851** no. 2, (2017) L35, `arXiv:1711.05578 [astro-ph.HE]`.

[5] **Virgo, LIGO Scientific** Collaboration, B. P. Abbott *et al.*, "GW170814: A Three-Detector Observation of Gravitational Waves from a Binary Black Hole Coalescence," *Phys. Rev. Lett.* **119** no. 14, (2017) 141101, `arXiv:1709.09660 [gr-qc]`.

[6] **Virgo, LIGO Scientific** Collaboration, B. Abbott *et al.*, "GW170817: Observation of Gravitational Waves from a Binary Neutron Star Inspiral," *Phys. Rev. Lett.* **119** no. 16, (2017) 161101, `arXiv:1710.05832 [gr-qc]`.

[7] **Event Horizon Telescope** Collaboration, K. Akiyama *et al.*, "First M87 Event Horizon Telescope Results. I. The Shadow of the Supermassive Black Hole," *Astrophys. J.* **875** no. 1, (2019) L1, `arXiv:1906.11238 [astro-ph.GA]`.

[8] **Event Horizon Telescope** Collaboration, K. Akiyama *et al.*, "First M87 Event Horizon Telescope Results. II. Array and Instrumentation," *Astrophys. J. Lett.* **875** no. 1, (2019) L2, `arXiv:1906.11239 [astro-ph.IM]`.

[9] **Event Horizon Telescope** Collaboration, K. Akiyama *et al.*, "First M87 Event Horizon Telescope Results. III. Data Processing and Calibration," *Astrophys. J. Lett.* **875** no. 1, (2019) L3, `arXiv:1906.11240 [astro-ph.GA]`.

[10] **Event Horizon Telescope** Collaboration, K. Akiyama *et al.*, "First M87 Event Horizon Telescope Results. IV. Imaging the Central Supermassive Black Hole," *Astrophys. J. Lett.* **875** no. 1, (2019) L4, `arXiv:1906.11241 [astro-ph.GA]`.

[11] **Event Horizon Telescope** Collaboration, K. Akiyama *et al.*, "First M87 Event Horizon Telescope Results. V. Physical Origin of the Asymmetric Ring," *Astrophys. J. Lett.* **875** no. 1, (2019) L5, `arXiv:1906.11242 [astro-ph.GA]`.

[12] **Event Horizon Telescope** Collaboration, K. Akiyama *et al.*, "First M87 Event Horizon Telescope Results. VI. The Shadow and Mass of the Central Black Hole," *Astrophys. J. Lett.* **875** no. 1, (2019) L6, `arXiv:1906.11243 [astro-ph.GA]`.

[13] S. Weinberg, "The Cosmological Constant Problem," *Rev. Mod. Phys.* **61** (1989) 1–23.

[14] J. L. Bernal, L. Verde, and A. G. Riess, "The trouble with H_0," *JCAP* **10** (2016) 019, `arXiv:1607.05617 [astro-ph.CO]`.

[15] J. R. Oppenheimer and G. M. Volkoff, "On Massive neutron cores," *Phys. Rev.* **55** (1939) 374–381.

[16] E. Lifshitz and I. Khalatnikov, "Investigations in relativistic cosmology," *Advances in Physics* **12** no. 46, (1963) 185–249. `https://doi.org/10.1080/00018736300101283`.

[17] R. Penrose, "Gravitational collapse and space-time singularities," *Phys. Rev. Lett.* **14** (1965) 57–59.

[18] S. Hawking, "The occurrence of singularities in cosmology. III. Causality and singularities," *Proc. Roy. Soc. Lond. A* **A300** (1967) 187–201.

[19] S. W. Hawking and R. Penrose, "The Singularities of gravitational collapse and cosmology," *Proc. Roy. Soc. Lond.* **A314** (1970) 529–548.

[20] R. Penrose, "Gravitational collapse: The role of general relativity," *Riv. Nuovo Cim.* **1** (1969) 252–276. [Gen. Rel. Grav.34,1141(2002)].

[21] G. 't Hooft and M. Veltman, "One loop divergencies in the theory of gravitation," *Ann. Inst. H. Poincare Phys. Theor. A* **20** (1974) 69–94.

[22] M. H. Goroff and A. Sagnotti, "Quantum gravity at two loops," *Phys. Lett. B* **160** (1985) 81–86.

[23] A. E. van de Ven, "Two-loop quantum gravity," *Nuclear Physics B* **378** no. 1, (1992) 309 – 366. `http://www.sciencedirect.com/science/article/pii/055032139290011Y`.

[24] S. Weinberg, *Ultravioler divergencer in quantum theories of gravitation,* pp. 790–831. 1, 1980.

[25] A. Bonanno, A. Eichhorn, H. Gies, J. M. Pawlowski, R. Percacci, M. Reuter, F. Saueressig, and G. P. Vacca, "Critical reflections on asymptotically safe gravity," *Front. in Phys.* **8** (2020) 269, `arXiv:2004.06810 [gr-qc]`.

[26] D. Lovelock, "The einstein tensor and its generalizations," *Journal of Mathematical Physics* **12** no. 3, (1971) 498–501. `https://doi.org/10.1063/1.1665613`.

[27] D. v. Glavan and C. Lin, "Einstein-Gauss-Bonnet gravity in 4-dimensional space-time," *Phys. Rev. Lett.* **124** no. 8, (2020) 081301, `arXiv:1905.03601 [gr-qc]`.

[28] K. Aoki, M. A. Gorji, and S. Mukohyama, "A consistent theory of $D \to 4$ Einstein-Gauss-Bonnet gravity," `arXiv:2005.03859 [gr-qc]`.

[29] C. Lin and S. Mukohyama, "A Class of Minimally Modified Gravity Theories," *JCAP* **1710** no. 10, (2017) 033, `arXiv:1708.03757 [gr-qc]`.

[30] T. Thiemann, *Modern Canonical Quantum General Relativity*. Cambridge Monographs on Mathematical Physics. Cambridge University Press, 2008. `https://books.google.it/books?id=LEBIPgAACAAJ`.

[31] M. Bojowald, G. M. Hossain, M. Kagan, and S. Shankaranarayanan, "Anomaly freedom in perturbative loop quantum gravity," *Phys. Rev.* **D78** (2008) 063547, `arXiv:0806.3929 [gr-qc]`.

[32] M. Bojowald and G. M. Paily, "Deformed General Relativity and Effective Actions from Loop Quantum Gravity," *Phys. Rev.* **D86** (2012) 104018, `arXiv:1112.1899 [gr-qc]`.

[33] M. Bojowald and G. M. Paily, "Deformed General Relativity," *Phys. Rev.* **D87** no. 4, (2013) 044044, `arXiv:1212.4773 [gr-qc]`.

[34] M. Bojowald, *Canonical Gravity and Applications: Cosmology, Black Holes, and Quantum Gravity*. Cambridge University Press, 2010. `https://books.google.it/books?id=qGoLVnjDewUC`.

[35] T. Cailleteau, J. Mielczarek, A. Barrau, and J. Grain, "Anomaly-free scalar perturbations with holonomy corrections in loop quantum cosmology," *Class. Quant. Grav.* **29** (2012) 095010, `arXiv:1111.3535 [gr-qc]`.

[36] J. Ben Achour, S. Brahma, and A. Marciano, "Spherically symmetric sector of self dual Ashtekar gravity coupled to matter: Anomaly-free algebra of constraints with holonomy corrections," *Phys. Rev.* **D96** no. 2, (2017) 026002, `arXiv:1608.07314 [gr-qc]`.

[37] M. Bojowald and J. Mielczarek, "Some implications of signature-change in cosmological models of loop quantum gravity," *JCAP* **1508** no. 08, (2015) 052, `arXiv:1503.09154 [gr-qc]`.

[38] M. Bojowald and S. Brahma, "Signature change in loop quantum gravity: Two-dimensional midisuperspace models and dilaton gravity," *Phys. Rev.* **D95** no. 12, (2017) 124014, `arXiv:1610.08840 [gr-qc]`.

[39] S. Brahma and M. Ronco, "Constraining the loop quantum gravity parameter space from phenomenology," *Phys. Lett.* **778** (2018) 184, `arXiv:1801.09417 [hep-th]`.

[40] J. Grain, "The perturbed universe in the deformed algebra approach of Loop Quantum Cosmology," *Int. J. Mod. Phys.* **D25** no. 08, (2016) 1642003, `arXiv:1606.03271 [gr-qc]`.

[41] R. F. Baierlein, D. H. Sharp, and J. A. Wheeler, "Three-Dimensional Geometry as Carrier of Information about Time," *Phys. Rev.* **126** (1962) 1864–1865.

[42] N. O. Murchadha, C. Soo, and H.-L. Yu, "Intrinsic time gravity and the Lichnerowicz-York equation," *Class. Quant. Grav.* **30** (2013) 095016, `arXiv:1208.2525 [gr-qc]`.

[43] R. Percacci, *An Introduction To Covariant Quantum Gravity And Asymptotic Safety*. 100 Years Of General Relativity. World Scientific Publishing Company, 2017. `https://books.google.it/books?id=9fCtDgAAQBAJ`.

[44] N. T. Bishop and L. Rezzolla, "Extraction of Gravitational Waves in Numerical Relativity," *Living Rev. Rel.* **19** (2016) 2, `arXiv:1606.02532 [gr-qc]`.

[45] K. Hinterbichler, "Theoretical Aspects of Massive Gravity," *Rev. Mod. Phys.* **84** (2012) 671–710, `arXiv:1105.3735 [hep-th]`.

[46] T. Ortin, *Gravity and Strings*. Cambridge Monographs on Mathematical Physics. Cambridge University Press, 2015. `http://www.cambridge.org/mw/academic/subjects/physics/theoretical-physics-and-mathematical-physics/gravity-and-strings-2nd-edition`.

[47] A. Zee, "Quantum field theory in a nutshell," *Princeton, UK: Princeton Univ. Pr. (2010) 576 p* (2003) .

[48] H. Elvang and Y. Huang, *Scattering Amplitudes in Gauge Theory and Gravity*. Cambridge University Press, 2015. `https://books.google.it/books?id=MxTRoAEACAAJ`.

[49] H. Elvang and Y.-t. Huang, "Scattering Amplitudes," *arXiv* **1308.1697** (2013) .

[50] E. Witten, "Perturbative gauge theory as a string theory in twistor space," *Commun. Math. Phys.* **252** (2004) 189–258, `arXiv:hep-th/0312171 [hep-th]`.

[51] P. Benincasa and F. Cachazo, "Consistency Conditions on the S-Matrix of Massless Particles," `arXiv:0705.4305 [hep-th]`.

[52] F. Cachazo and P. Svrcek, "Tree level recursion relations in general relativity," `arXiv:hep-th/0502160 [hep-th]`.

[53] P. Benincasa, C. Boucher-Veronneau, and F. Cachazo, "Taming Tree Amplitudes In General Relativity," *JHEP* **11** (2007) 057, `arXiv:hep-th/0702032 [HEP-TH]`.

[54] A. Hall, "On-shell recursion relations for gravity," *Phys. Rev.* **D77** (2008) 124004, `arXiv:0803.0215 [hep-th]`.

[55] N. Arkani-Hamed and J. Kaplan, "On Tree Amplitudes in Gauge Theory and Gravity," *JHEP* **04** (2008) 076, `arXiv:0801.2385 [hep-th]`.

[56] R. Britto, F. Cachazo, and B. Feng, "New recursion relations for tree amplitudes of gluons," *Nucl. Phys.* **B715** (2005) 499–522, `arXiv:hep-th/0412308 [hep-th]`.

[57] R. Britto, F. Cachazo, B. Feng, and E. Witten, "Direct proof of tree-level recursion relation in Yang-Mills theory," *Phys. Rev. Lett.* **94** (2005) 181602, `arXiv:hep-th/0501052 [hep-th]`.

[58] T. Cohen, H. Elvang, and M. Kiermaier, "On-shell constructibility of tree amplitudes in general field theories," *JHEP* **04** (2011) 053, `arXiv:1010.0257 [hep-th]`.

[59] N. E. J. Bjerrum-Bohr, D. C. Dunbar, H. Ita, W. B. Perkins, and K. Risager, "MHV-vertices for gravity amplitudes," *JHEP* **01** (2006) 009, `arXiv:hep-th/0509016 [hep-th]`.

[60] H. Elvang, C. R. T. Jones, and S. G. Naculich, "Soft photon and graviton theorems in effective field theory," *Phys. Rev. Lett.* **118** (Jun, 2017) 231601. `https://link.aps.org/doi/10.1103/PhysRevLett.118.231601`.

[61] D. Comelli, F. Nesti, and L. Pilo, "Nonderivative Modified Gravity: a Classification," *JCAP* **1411** no. 11, (2014) 018, `arXiv:1407.4991 [hep-th]`.

[62] C. Lin, J. Quintin, and R. H. Brandenberger, "Massive gravity and the suppression of anisotropies and gravitational waves in a matter-dominated contracting universe," *Journal of Cosmology and Astroparticle Physics* **2018** no. 01, (2018) 011. `http://stacks.iop.org/1475-7516/2018/i=01/a=011`.

[63] P. Horava, "Quantum Gravity at a Lifshitz Point," *Phys. Rev.* **D79** (2009) 084008, `arXiv:0901.3775 [hep-th]`.

[64] M. Visser, "Status of Horava gravity: A personal perspective," *J. Phys. Conf. Ser.* **314** (2011) 012002, `arXiv:1103.5587 [hep-th]`.

[65] T. P. Sotiriou, "Detecting Lorentz Violations with Gravitational Waves from Black Hole Binaries," *Phys. Rev. Lett.* **120** no. 4, (2018) 041104, `arXiv:1709.00940 [gr-qc]`.

[66] A. Emir, S. Mukohyama, and A. Wang, "General relativity limit of hořava-lifshitz gravity with a scalar field in gradient expansion," *Phys. Rev. D* **85** (Mar, 2012) 064042.

[67] S. Mukohyama, "Horava-lifshitz cosmology: a review," *Classical and Quantum Gravity* **27** no. 22, (2010) 223101.

[68] M. Henneaux and C. Teitelboim, *Quantization of Gauge Systems.* Princeton paperbacks. Princeton University Press, 1994. https://books.google.it/books?id=2FAuAKEKFyYC.

[69] M. Li and Y. Pang, "A Trouble with Horava-Lifshitz Gravity," *JHEP* **08** (2009) 015, arXiv:0905.2751 [hep-th].

[70] D. Blas, O. Pujolas, and S. Sibiryakov, "On the Extra Mode and Inconsistency of Horava Gravity," *JHEP* **10** (2009) 029, arXiv:0906.3046 [hep-th].

[71] C. Lin and Z. Lalak, "Novel matter coupling in Einstein gravity," arXiv:1911.12026 [gr-qc].

[72] K. Aoki, A. De Felice, S. Mukohyama, K. Noui, M. Oliosi, and M. C. Pookkillath, "Minimally Modified Gravity fitting Planck data better than ΛCDM," arXiv:2005.13972 [astro-ph.CO].

[73] R. Wald, *General Relativity.* University of Chicago Press, 1984. https://books.google.it/books?id=ibSdQgAACAAJ.

[74] R. Penrose, *Techniques of Differential Topology in Relativity.* CBMS-NSF Regional Conference Series in Applied Mathematics. Society for Industrial and Applied Mathematics, 1972. https://books.google.it/books?id=k_YiLffd1hsC.

[75] E. Minguzzi and M. Sanchez, "The Causal hierarchy of spacetimes," pp. 299–358. 9, 2006. arXiv:gr-qc/0609119.

[76] M. Sanchez, "Causal hierarchy of spacetimes, temporal functions and smoothness of Geroch's splitting. A Revision," in *13th School of Differential Geometry: Dedicated to the Memory of Jose Fernando Escobar.* 11, 2004. arXiv:gr-qc/0411143.

[77] C. de Rham and G. Gabadadze, "Generalization of the Fierz-Pauli Action," *Phys. Rev.* **D82** (2010) 044020, arXiv:1007.0443 [hep-th].

[78] C. de Rham, G. Gabadadze, and A. J. Tolley, "Resummation of Massive Gravity," *Phys. Rev. Lett.* **106** (2011) 231101, arXiv:1011.1232 [hep-th].

[79] V. Baccetti, P. Martin-Moruno, and M. Visser, "Massive gravity from bimetric gravity," *Class. Quant. Grav.* **30** (2013) 015004, arXiv:1205.2158 [gr-qc].

[80] V. Baccetti, P. Martin-Moruno, and M. Visser, "Gordon and Kerr-Schild ansatze in massive and bimetric gravity," *JHEP* **08** (2012) 108, arXiv:1206.4720 [gr-qc].

[81] M. Visser, "Mass for the graviton," *Gen. Rel. Grav.* **30** (1998) 1717–1728, `arXiv:gr-qc/9705051`.

[82] C. Eling and T. Jacobson, "Black Holes in Einstein-Aether Theory," *Class. Quant. Grav.* **23** (2006) 5643–5660, `arXiv:gr-qc/0604088`. [Erratum: Class.Quant.Grav. 27, 049802 (2010)].

[83] D. Blas and S. Sibiryakov, "Horava gravity versus thermodynamics: The Black hole case," *Phys. Rev. D* **84** (2011) 124043, `arXiv:1110.2195 [hep-th]`.

[84] E. Barausse, T. Jacobson, and T. P. Sotiriou, "Black holes in Einstein-aether and Horava-Lifshitz gravity," *Phys. Rev. D* **83** (2011) 124043, `arXiv:1104.2889 [gr-qc]`.

[85] J. Bhattacharyya, M. Colombo, and T. P. Sotiriou, "Causality and black holes in spacetimes with a preferred foliation," *Class. Quant. Grav.* **33** no. 23, (2016) 235003, `arXiv:1509.01558 [gr-qc]`.

[86] B. Cropp, S. Liberati, A. Mohd, and M. Visser, "Ray tracing Einstein-Æther black holes: Universal versus Killing horizons," *Phys. Rev. D* **89** no. 6, (2014) 064061, `arXiv:1312.0405 [gr-qc]`.

[87] E. Barausse and T. P. Sotiriou, "Slowly rotating black holes in Horava-Lifshitz gravity," *Phys. Rev. D* **87** (2013) 087504, `arXiv:1212.1334 [gr-qc]`.

[88] J. M. M. Senovilla and D. Garfinkle, "The 1965 Penrose singularity theorem," *Class. Quant. Grav.* **32** no. 12, (2015) 124008, `arXiv:1410.5226 [gr-qc]`.

[89] S. W. Hawking and G. F. R. Ellis, *The Large Scale Structure of Space-Time*. Cambridge Monographs on Mathematical Physics. Cambridge University Press, 2011.

[90] G. J. Olmo, D. Rubiera-Garcia, and A. Sanchez-Puente, "Geodesic completeness in a wormhole spacetime with horizons," *Phys. Rev.* **D92** no. 4, (2015) 044047, `arXiv:1508.03272 [hep-th]`.

[91] G. J. Olmo, D. Rubiera-Garcia, and A. Sanchez-Puente, "Impact of curvature divergences on physical observers in a wormhole space-time with horizons," *Class. Quant. Grav.* **33** no. 11, (2016) 115007, `arXiv:1602.01798 [hep-th]`.

[92] C. Bejarano, G. J. Olmo, and D. Rubiera-Garcia, "What is a singular black hole beyond General Relativity?," *Phys. Rev.* **D95** no. 6, (2017) 064043, `arXiv:1702.01292 [hep-th]`.

[93] G. J. Olmo, D. Rubiera-Garcia, and A. Sanchez-Puente, "Accelerated observers and the notion of singular spacetime," *Class. Quant. Grav.* **35** no. 5, (2018) 055010, `arXiv:1710.08712 [gr-qc]`.

[94] W. Kaminski and T. Pawlowski, "Cosmic recall and the scattering picture of Loop Quantum Cosmology," *Phys. Rev.* **D81** (2010) 084027, `arXiv:1001.2663 [gr-qc]`.

[95] A. Ashtekar and P. Singh, "Loop Quantum Cosmology: A Status Report,"
      Class. Quant. Grav. **28** (2011) 213001, `arXiv:1108.0893 [gr-qc]`.

[96] A. Ashtekar and B. Gupt, "Generalized effective description of loop quantum
      cosmology," *Phys. Rev.* **D92** no. 8, (2015) 084060, `arXiv:1509.08899 [gr-qc]`.

[97] A. Bonanno and M. Reuter, "Renormalization group improved black hole
      spacetimes," *Phys. Rev. D* **62** (Jul, 2000) 043008.
      `https://link.aps.org/doi/10.1103/PhysRevD.62.043008`.

[98] A. Adêìféoba, A. Eichhorn, and A. B. Platania, "Towards conditions for
      black-hole singularity-resolution in asymptotically safe quantum gravity,"
      Classical and Quantum Gravity **35** no. 22, (Oct, 2018) 225007.
      `https://doi.org/10.1088%2F1361-6382%2Faae6ef`.

[99] A. Platania, "Dynamical renormalization of black-hole spacetimes," *Eur. Phys.
      J.* **C79** no. 6, (2019) 470, `arXiv:1903.10411 [gr-qc]`.

[100] J. Olmedo, "Brief review on black hole loop quantization," *Universe* **2** no. 2,
      (2016) 12, `arXiv:1606.01429 [gr-qc]`.

[101] M. Campiglia, R. Gambini, J. Olmedo, and J. Pullin, "Quantum self-gravitating
      collapsing matter in a quantum geometry," *Class. Quant. Grav.* **33** no. 18,
      (2016) 18LT01, `arXiv:1601.05688 [gr-qc]`.

[102] E. Alesci, S. Bahrami, and D. Pranzetti, "Quantum evolution of black hole
      initial data sets: Foundations," *Phys. Rev.* **D98** no. 4, (2018) 046014,
      `arXiv:1807.07602 [gr-qc]`.

[103] J. M. Bardeen, "Non-singular general-relativistic gravitational collapse," in
      Proceedings of of International Conference GR5, Tbilisi, USSR, p. 174. 1968.

[104] V. P. Frolov and G. A. Vilkovisky, "Quantum gravity removes classical
      singularities and shortens the life of black holes," in *The Second Marcel
      Grossmann Meeting on the Recent Developments of General Relativity (In
      Honor of Albert Einstein) Trieste, Italy*, p. 0455. 1979.

[105] V. P. Frolov and G. A. Vilkovisky, "Spherically symmetric collapse in quantum
      gravity," *Phys. Lett.* **106B** (1981) 307–313.

[106] T. A. Roman and P. G. Bergmann, "Stellar collapse without singularities?,"
      Phys. Rev. **D28** (1983) 1265–1277.

[107] I. Dymnikova, "Vacuum nonsingular black hole," *Gen. Rel. Grav.* **24** (1992)
      235–242.

[108] A. Borde, "Regular black holes and topology change," *Phys. Rev.* **D55** (1997)
      7615–7617, `arXiv:gr-qc/9612057 [gr-qc]`.

[109] S. A. Hayward, "Formation and evaporation of regular black holes," *Phys. Rev.
      Lett.* **96** (2006) 031103, `arXiv:gr-qc/0506126 [gr-qc]`.

[110] K. A. Bronnikov, V. N. Melnikov, and H. Dehnen, "Regular black holes and black universes," *Gen. Rel. Grav.* **39** (2007) 973–987, `arXiv:gr-qc/0611022 [gr-qc]`.

[111] I. Dymnikova, "Cosmological term as a source of mass," *Class. Quant. Grav.* **19** (2002) 725–740, `arXiv:gr-qc/0112052 [gr-qc]`.

[112] S. Ansoldi, "Spherical black holes with regular center: A Review of existing models including a recent realization with Gaussian sources," in *Conference on Black Holes and Naked Singularities Milan, Italy*. 2008. `arXiv:0802.0330 [gr-qc]`. `https://inspirehep.net/record/778724/files/arXiv:0802.0330.pdf`.

[113] V. P. Frolov, "Information loss problem and a 'black hole' model with a closed apparent horizon," *JHEP* **05** (2014) 049, `arXiv:1402.5446 [hep-th]`.

[114] V. P. Frolov, "Notes on nonsingular models of black holes," *Phys. Rev.* **D94** no. 10, (2016) 104056, `arXiv:1609.01758 [gr-qc]`.

[115] R. Carballo-Rubio, P. Kumar, and W. Lu, "Seeking observational evidence for the formation of trapping horizons in astrophysical black holes," *Phys. Rev.* **D97** no. 12, (2018) 123012, `arXiv:1804.00663 [gr-qc]`.

[116] R. P. Geroch, *Singularities in the Spacetime of General Relativity: Their Definition, Existence, and Local Characterization*. PhD thesis, Princeton University, 1967.

[117] R. P. Geroch, "The domain of dependence," *J. Math. Phys.* **11** (1970) 437–439.

[118] A. Borde, "Topology change in classical general relativity," *ArXiv gr-qc/9406053* (1994) .

[119] P. Hájíček, "Exact models of charged black holes: I. Geometry of totally geodesic null hypersurface," *Communications in Mathematical Physics* **34** (Mar., 1973) 37–52.

[120] S. A. Hayward, "General laws of black hole dynamics," *Phys. Rev.* **D49** (1994) 6467–6474.

[121] A. Ashtekar, C. Beetle, and S. Fairhurst, "Isolated horizons: A Generalization of black hole mechanics," *Class. Quant. Grav.* **16** (1999) L1–L7, `arXiv:gr-qc/9812065 [gr-qc]`.

[122] A. Ashtekar and B. Krishnan, "Dynamical horizons: Energy, angular momentum, fluxes and balance laws," *Phys. Rev. Lett.* **89** (2002) 261101, `arXiv:gr-qc/0207080 [gr-qc]`.

[123] A. Ashtekar and B. Krishnan, "Dynamical horizons and their properties," *Phys. Rev.* **D68** (2003) 104030, `arXiv:gr-qc/0308033 [gr-qc]`.

[124] A. Ashtekar and G. J. Galloway, "Some uniqueness results for dynamical horizons," *Adv. Theor. Math. Phys.* **9** no. 1, (2005) 1–30, `arXiv:gr-qc/0503109 [gr-qc]`.

[125] I. Booth and S. Fairhurst, "The First law for slowly evolving horizons," *Phys. Rev. Lett.* **92** (2004) 011102, `arXiv:gr-qc/0307087 [gr-qc]`.

[126] S. A. Hayward, "Energy and entropy conservation for dynamical black holes," *Phys. Rev.* **D70** (2004) 104027, `arXiv:gr-qc/0408008 [gr-qc]`.

[127] S. A. Hayward, "Angular momentum conservation for dynamical black holes," *Phys. Rev.* **D74** (2006) 104013, `arXiv:gr-qc/0609008 [gr-qc]`.

[128] L. Andersson, M. Mars, and W. Simon, "Local existence of dynamical and trapping horizons," *Phys. Rev. Lett.* **95** (2005) 111102, `arXiv:gr-qc/0506013 [gr-qc]`.

[129] L. Andersson and J. Metzger, "The Area of horizons and the trapped region," *Commun. Math. Phys.* **290** (2009) 941–972, `arXiv:0708.4252 [gr-qc]`.

[130] A. Ashtekar and B. Krishnan, "Isolated and dynamical horizons and their applications," *Living Rev. Rel.* **7** (2004) 10, `arXiv:gr-qc/0407042 [gr-qc]`.

[131] B. Krishnan, "Fundamental properties and applications of quasi-local black hole horizons," *Class. Quant. Grav.* **25** (2008) 114005, `arXiv:0712.1575 [gr-qc]`.

[132] E. Gourgoulhon and J. L. Jaramillo, "New theoretical approaches to black holes," *New Astron. Rev.* **51** (2008) 791–798, `arXiv:0803.2944 [astro-ph]`.

[133] E. Poisson, *A Relativist's Toolkit: The Mathematics of Black-Hole Mechanics*. Cambridge University Press, 2009.

[134] C. Rovelli and F. Vidotto, "Planck stars," *Int. J. Mod. Phys.* **D23** no. 12, (2014) 1442026, `arXiv:1401.6562 [gr-qc]`.

[135] C. Barceló, R. Carballo-Rubio, and L. J. Garay, "Mutiny at the white-hole district," *Int. J. Mod. Phys.* **D23** no. 12, (2014) 1442022, `arXiv:1407.1391 [gr-qc]`.

[136] C. Barceló, R. Carballo-Rubio, L. J. Garay, and G. Jannes, "The lifetime problem of evaporating black holes: mutiny or resignation," *Class. Quant. Grav.* **32** no. 3, (2015) 035012, `arXiv:1409.1501 [gr-qc]`.

[137] H. M. Haggard and C. Rovelli, "Quantum-gravity effects outside the horizon spark black to white hole tunneling," *Phys. Rev.* **D92** no. 10, (2015) 104020, `arXiv:1407.0989 [gr-qc]`.

[138] D. Malafarina, "Classical collapse to black holes and quantum bounces: A review," *Universe* **3** no. 2, (2017) 48, `arXiv:1703.04138 [gr-qc]`.

[139] D. Hochberg and M. Visser, "Geometric structure of the generic static traversable wormhole throat," *Phys. Rev.* **D56** (1997) 4745–4755, `arXiv:gr-qc/9704082 [gr-qc]`.

[140] D. Hochberg and M. Visser, "Dynamic wormholes, anti-trapped surfaces, and energy conditions," *Phys. Rev.* **D58** (1998) 044021, `arXiv:gr-qc/9802046 [gr-qc]`.

[141] C. W. Misner and D. H. Sharp, "Relativistic equations for adiabatic, spherically symmetric gravitational collapse," *Phys. Rev.* **136** (1964) B571–B576.

[142] W. C. Hernandez and C. W. Misner, "Observer Time as a Coordinate in Relativistic Spherical Hydrodynamics," *Astrophys. J.* **143** (1966) 452.

[143] S. A. Hayward, "Gravitational energy in spherical symmetry," *Phys. Rev.* **D53** (1996) 1938–1949, `arXiv:gr-qc/9408002 [gr-qc]`.

[144] M. Simpson and R. Penrose, "Internal instability in a Reissner-Nordstrom black hole," *Int. J. Theor. Phys.* **7** (1973) 183–197.

[145] E. Poisson and W. Israel, "Inner-horizon instability and mass inflation in black holes," *Phys. Rev. Lett.* **63** (1989) 1663–1666.

[146] E. Poisson and W. Israel, "Eschatology of the black hole interior," *Phys. Lett.* **B233** (1989) 74–78.

[147] E. Poisson and W. Israel, "Internal structure of black holes," *Phys. Rev.* **D41** (1990) 1796–1809.

[148] C. Barrabes, W. Israel, and E. Poisson, "Collision of light-like shells and mass inflation in rotating black holes," *Classical and Quantum Gravity* **7** (Dec., 1990) L273–L278.

[149] A. Ori, "Inner structure of a charged black hole: An exact mass-inflation solution," *Phys. Rev. Lett.* **67** (1991) 789–792.

[150] M. Dafermos, "The Interior of charged black holes and the problem of uniqueness in general relativity," *Commun. Pure Appl. Math.* **58** (2005) 0445–0504, `arXiv:gr-qc/0307013 [gr-qc]`.

[151] A. J. S. Hamilton and P. P. Avelino, "The physics of the relativistic counter-streaming instability that drives mass inflation inside black holes," *Phys. Rept.* **495** (2010) 1–32, `arXiv:0811.1926 [gr-qc]`.

[152] D. Markovic and E. Poisson, "Classical stability and quantum instability of black hole Cauchy horizons," *Phys. Rev. Lett.* **74** (1995) 1280–1283, `arXiv:gr-qc/9411002 [gr-qc]`.

[153] T. Dray and G. 't Hooft, "The effect of spherical shells of matter on the schwarzschild black hole," *Comm. Math. Phys.* **99** no. 4, (1985) 613–625. `https://projecteuclid.org:443/euclid.cmp/1103942843`.

[154] I. H. Redmount, "Blue-Sheet Instability of Schwarzschild Wormholes," *Progress of Theoretical Physics* **73** no. 6, (06, 1985) 1401–1426, https://academic.oup.com/ptp/article-pdf/73/6/1401/5338051/73-6-1401.pdf. https://doi.org/10.1143/PTP.73.1401.

[155] E. Poisson, *A Relativist's Toolkit: The Mathematics of Black-Hole Mechanics.* Cambridge University Press, 2004.

[156] R. H. Price, "Nonspherical perturbations of relativistic gravitational collapse. 1. Scalar and gravitational perturbations," *Phys. Rev.* **D5** (1972) 2419–2438.

[157] R. H. Price, "Nonspherical Perturbations of Relativistic Gravitational Collapse. II. Integer-Spin, Zero-Rest-Mass Fields," *Phys. Rev.* **D5** (1972) 2439–2454.

[158] C. Gundlach, R. H. Price, and J. Pullin, "Late time behavior of stellar collapse and explosions: 1. Linearized perturbations," *Phys. Rev.* **D49** (1994) 883–889, arXiv:gr-qc/9307009 [gr-qc].

[159] C. Gundlach, R. H. Price, and J. Pullin, "Late time behavior of stellar collapse and explosions: 2. Nonlinear evolution," *Phys. Rev.* **D49** (1994) 890–899, arXiv:gr-qc/9307010 [gr-qc].

[160] M. Dafermos and I. Rodnianski, "A Proof of Price's law for the collapse of a selfgravitating scalar field," *Invent. Math.* **162** (2005) 381–457, arXiv:gr-qc/0309115 [gr-qc].

[161] V. Cardoso, J. a. L. Costa, K. Destounis, P. Hintz, and A. Jansen, "Quasinormal modes and strong cosmic censorship," *Phys. Rev. Lett.* **120** (Jan, 2018) 031103. https://link.aps.org/doi/10.1103/PhysRevLett.120.031103.

[162] O. J. Dias, F. C. Eperon, H. S. Reall, and J. E. Santos, "Strong cosmic censorship in de Sitter space," *Phys. Rev. D* **97** no. 10, (2018) 104060, arXiv:1801.09694 [gr-qc].

[163] S. Hod, "Strong cosmic censorship in charged black-hole spacetimes: As strong as ever," *Nucl. Phys.* **B941** (2019) 636–645, arXiv:1801.07261 [gr-qc].

[164] V. Cardoso, J. L. Costa, K. Destounis, P. Hintz, and A. Jansen, "Strong cosmic censorship in charged black-hole spacetimes: still subtle," *Phys. Rev.* **D98** no. 10, (2018) 104007, arXiv:1808.03631 [gr-qc].

[165] A. S. Barreto and M. Zworski, "Distribution of resonances for spherical black holes," *Mathematical Research Letters* **4** no. 1, (1997) 103–121.

[166] S. Dyatlov, "Asymptotic distribution of quasi-normal modes for kerr–de sitter black holes," in *Annales Henri Poincaré*, vol. 13, pp. 1101–1166, Springer. 2012.

[167] A. Ashtekar and M. Bojowald, "Black hole evaporation: A paradigm," *Class. Quant. Grav.* **22** (2005) 3349–3362, arXiv:gr-qc/0504029 [gr-qc].

[168] T. De Lorenzo and A. Perez, "Improved Black Hole Fireworks: Asymmetric Black-Hole-to-White-Hole Tunneling Scenario," *Phys. Rev.* **D93** no. 12, (2016) 124018, `arXiv:1512.04566 [gr-qc]`.

[169] E. Bianchi, M. Christodoulou, F. D'Ambrosio, H. M. Haggard, and C. Rovelli, "White Holes as Remnants: A Surprising Scenario for the End of a Black Hole," *Class. Quant. Grav.* **35** no. 22, (2018) 225003, `arXiv:1802.04264 [gr-qc]`.

[170] C. Barceló, R. Carballo-Rubio, and L. J. Garay, "Where does the physics of extreme gravitational collapse reside?," *Universe* **2** no. 2, (2016) 7, `arXiv:1510.04957 [gr-qc]`.

[171] P. Hajicek, "Quantum theory of gravitational collapse: (Lecture notes on quantum conchology)," *Lect. Notes Phys.* **631** (2003) 255–299, `arXiv:gr-qc/0204049 [gr-qc]`. [,255(2002)].

[172] M. Ambrus and P. Hajicek, "Quantum superposition principle and gravitational collapse: Scattering times for spherical shells," *Phys. Rev.* **D72** (2005) 064025, `arXiv:gr-qc/0507017 [gr-qc]`.

[173] C. Barceló, L. J. Garay, and G. Jannes, "Quantum Non-Gravity and Stellar Collapse," *Found. Phys.* **41** (2011) 1532–1541, `arXiv:1002.4651 [gr-qc]`.

[174] A. Ashtekar and M. Bojowald, "Quantum geometry and the Schwarzschild singularity," *Class. Quant. Grav.* **23** (2006) 391–411, `arXiv:gr-qc/0509075 [gr-qc]`.

[175] A. Ashtekar, V. Taveras, and M. Varadarajan, "Information is Not Lost in the Evaporation of 2-dimensional Black Holes," *Phys. Rev. Lett.* **100** (2008) 211302, `arXiv:0801.1811 [gr-qc]`.

[176] A. Corichi and P. Singh, "Loop quantization of the Schwarzschild interior revisited," *Class. Quant. Grav.* **33** no. 5, (2016) 055006, `arXiv:1506.08015 [gr-qc]`.

[177] J. Olmedo, S. Saini, and P. Singh, "From black holes to white holes: a quantum gravitational, symmetric bounce," *Class. Quant. Grav.* **34** no. 22, (2017) 225011, `arXiv:1707.07333 [gr-qc]`.

[178] A. Ashtekar, J. Olmedo, and P. Singh, "Quantum Transfiguration of Kruskal Black Holes," `arXiv:1806.00648 [gr-qc]`.

[179] A. Ashtekar, J. Olmedo, and P. Singh, "Quantum extension of the Kruskal spacetime," *Phys. Rev.* **D98** no. 12, (2018) 126003, `arXiv:1806.02406 [gr-qc]`.

[180] C. Bambi, D. Malafarina, and L. Modesto, "Non-singular quantum-inspired gravitational collapse," *Phys. Rev.* **D88** (2013) 044009, `arXiv:1305.4790 [gr-qc]`.

[181] C. Bambi, D. Malafarina, and L. Modesto, "Black supernovae and black holes in non-local gravity," *JHEP* **04** (2016) 147, arXiv:1603.09592 [gr-qc].

[182] C. Barceló, R. Carballo-Rubio, and L. J. Garay, "Black holes turn white fast, otherwise stay black: no half measures," *JHEP* **01** (2016) 157, arXiv:1511.00633 [gr-qc].

[183] M. Christodoulou, C. Rovelli, S. Speziale, and I. Vilensky, "Planck star tunneling time: An astrophysically relevant observable from background-free quantum gravity," *Phys. Rev.* **D94** no. 8, (2016) 084035, arXiv:1605.05268 [gr-qc].

[184] C. Barceló, R. Carballo-Rubio, and L. J. Garay, "Exponential fading to white of black holes in quantum gravity," *Class. Quant. Grav.* **34** no. 10, (2017) 105007, arXiv:1607.03480 [gr-qc].

[185] A. Barrau, C. Rovelli, and F. Vidotto, "Fast Radio Bursts and White Hole Signals," *Phys. Rev.* **D90** no. 12, (2014) 127503, arXiv:1409.4031 [gr-qc].

[186] A. Barrau, B. Bolliet, F. Vidotto, and C. Weimer, "Phenomenology of bouncing black holes in quantum gravity: a closer look," *JCAP* **1602** no. 02, (2016) 022, arXiv:1507.05424 [gr-qc].

[187] H. A. Buchdahl, "General Relativistic Fluid Spheres," *Phys. Rev.* **116** (1959) 1027.

[188] H. Bondi, "Massive spheres in general relativity," *Proc. Roy. Soc. Lond.* **A282** (1964) 303–317.

[189] C. Cattoen, T. Faber, and M. Visser, "Gravastars must have anisotropic pressures," *Class. Quant. Grav.* **22** (2005) 4189–4202, arXiv:gr-qc/0505137 [gr-qc].

[190] P. O. Mazur and E. Mottola, "Gravitational vacuum condensate stars," *Proc. Nat. Acad. Sci.* **101** (2004) 9545–9550, arXiv:gr-qc/0407075 [gr-qc].

[191] M. Visser, S. Kar, and N. Dadhich, "Traversable wormholes with arbitrarily small energy condition violations," *Phys. Rev. Lett.* **90** (2003) 201102, arXiv:gr-qc/0301003 [gr-qc].

[192] E. Mottola, "New Horizons in Gravity: The Trace Anomaly, Dark Energy and Condensate Stars," *Acta Phys. Polon.* **B41** (2010) 2031–2162, arXiv:1008.5006 [gr-qc].

[193] S. D. Mathur, "The Fuzzball proposal for black holes: An Elementary review," *Fortsch. Phys.* **53** (2005) 793–827, arXiv:hep-th/0502050 [hep-th].

[194] B. Guo, S. Hampton, and S. D. Mathur, "Can we observe fuzzballs or firewalls?," *JHEP* **07** (2018) 162, arXiv:1711.01617 [hep-th].

[195] C. Barceló, S. Liberati, S. Sonego, and M. Visser, "Fate of gravitational collapse in semiclassical gravity," *Phys. Rev.* **D77** (2008) 044032, `arXiv:0712.1130 [gr-qc]`.

[196] C. Barceló, S. Liberati, S. Sonego, and M. Visser, "Black Stars, Not Holes," *Sci. Am.* **301** no. 4, (2009) 38–45.

[197] R. Carballo-Rubio, "Stellar equilibrium in semiclassical gravity," *Phys. Rev. Lett.* **120** no. 6, (2018) 061102, `arXiv:1706.05379 [gr-qc]`.

[198] V. Baccetti, R. B. Mann, and D. R. Terno, "Role of evaporation in gravitational collapse," *Class. Quant. Grav.* **35** no. 18, (2018) 185005, `arXiv:1610.07839 [gr-qc]`.

[199] V. Baccetti, R. B. Mann, and D. R. Terno, "Horizon avoidance in spherically-symmetric collapse," `arXiv:1703.09369 [gr-qc]`.

[200] V. Baccetti, R. B. Mann, and D. R. Terno, "Do event horizons exist?," *Int. J. Mod. Phys.* **D26** no. 12, (2017) 1743008, `arXiv:1706.01180 [gr-qc]`.

[201] H. Kawai, Y. Matsuo, and Y. Yokokura, "A Self-consistent Model of the Black Hole Evaporation," *Int. J. Mod. Phys.* **A28** (2013) 1350050, `arXiv:1302.4733 [hep-th]`.

[202] H. Kawai and Y. Yokokura, "Phenomenological Description of the Interior of the Schwarzschild Black Hole," *Int. J. Mod. Phys.* **A30** (2015) 1550091, `arXiv:1409.5784 [hep-th]`.

[203] H. Kawai and Y. Yokokura, "Interior of Black Holes and Information Recovery," *Phys. Rev.* **D93** no. 4, (2016) 044011, `arXiv:1509.08472 [hep-th]`.

[204] W. G. Unruh and R. M. Wald, "Information Loss," *Rept. Prog. Phys.* **80** no. 9, (2017) 092002, `arXiv:1703.02140 [hep-th]`.

[205] P. Chen, W. G. Unruh, C.-H. Wu, and D.-H. Yeom, "Pre-Hawking radiation cannot prevent the formation of apparent horizon," *Phys. Rev.* **D97** no. 6, (2018) 064045, `arXiv:1710.01533 [gr-qc]`.

[206] B. A. Juárez-Aubry and J. Louko, "Quantum fields during black hole formation: How good an approximation is the Unruh state?," *JHEP* **05** (2018) 140, `arXiv:1804.01228 [gr-qc]`.

[207] V. Cardoso and L. Gualtieri, "Testing the black hole 'no-hair' hypothesis," *Class. Quant. Grav.* **33** no. 17, (2016) 174001, `arXiv:1607.03133 [gr-qc]`.

[208] C. Barceló, R. Carballo-Rubio, and S. Liberati, "Generalized no-hair theorems without horizons," *Class. Quant. Grav.* **36** no. 13, (2019) 13, `arXiv:1901.06388 [gr-qc]`.

[209] G. Raposo, P. Pani, and R. Emparan, "Exotic compact objects with soft hair," *Phys. Rev. D* **99** no. 10, (2019) 104050, `arXiv:1812.07615 [gr-qc]`.

[210] M. Visser, *Lorentzian wormholes: From Einstein to Hawking.* 1995.

[211] M. Visser, "Traversable wormholes: Some simple examples," *Phys. Rev.* **D39** (1989) 3182–3184, `arXiv:0809.0907 [gr-qc]`.

[212] M. Visser, "Traversable wormholes from surgically modified Schwarzschild space-times," *Nucl. Phys.* **B328** (1989) 203–212, `arXiv:0809.0927 [gr-qc]`.

[213] N. Dadhich, S. Kar, S. Mukherji, and M. Visser, "R = 0 space-times and self-dual Lorentzian wormholes," *Phys. Rev.* **D65** (2002) 064004, `arXiv:gr-qc/0109069 [gr-qc]`.

[214] S. Kar, N. Dadhich, and M. Visser, "Quantifying energy condition violations in traversable wormholes," *Pramana* **63** (2004) 859–864, `arXiv:gr-qc/0405103 [gr-qc]`.

[215] M. S. Morris and K. S. Thorne, "Wormholes in space-time and their use for interstellar travel: A tool for teaching general relativity," *Am. J. Phys.* **56** (1988) 395–412.

[216] M. S. Morris, K. S. Thorne, and U. Yurtsever, "Wormholes, Time Machines, and the Weak Energy Condition," *Phys. Rev. Lett.* **61** (1988) 1446–1449.

[217] M. Visser and D. Hochberg, "Generic wormhole throats," *Annals Israel Phys. Soc.* **13** (1997) 249, `arXiv:gr-qc/9710001 [gr-qc]`. [,249(1997)].

[218] V. Cardoso, E. Franzin, and P. Pani, "Is the gravitational-wave ringdown a probe of the event horizon?," *Phys. Rev. Lett.* **116** no. 17, (2016) 171101, `arXiv:1602.07309 [gr-qc]`. [Erratum: Phys. Rev. Lett.117,no.8,089902(2016)].

[219] E. Teo, "Rotating traversable wormholes," *Phys. Rev. D* **58** (Jun, 1998) 024014. `https://link.aps.org/doi/10.1103/PhysRevD.58.024014`.

[220] E. Curiel, "A Primer on Energy Conditions," *Einstein Stud.* **13** (2017) 43–104, `arXiv:1405.0403 [physics.hist-ph]`.

[221] P.-M. Ho and Y. Matsuo, "Static Black Holes With Back Reaction From Vacuum Energy," *Class. Quant. Grav.* **35** no. 6, (2018) 065012, `arXiv:1703.08662 [hep-th]`.

[222] C. Berthiere, D. Sarkar, and S. N. Solodukhin, "The quantum fate of black hole horizons," *Phys. Lett.* **B786** (2018) 21–27, `arXiv:1712.09914 [hep-th]`.

[223] R. P. Kerr, "Gravitational field of a spinning mass as an example of algebraically special metrics," *Phys. Rev. Lett.* **11** (1963) 237–238.

[224] V. Cardoso, *Quasinormal modes and gravitational radiation in black hole spacetimes.* PhD thesis, Lisbon, Tech. U., 2003. `arXiv:gr-qc/0404093 [gr-qc]`.

[225] T. Johannsen and D. Psaltis, "A Metric for Rapidly Spinning Black Holes Suitable for Strong-Field Tests of the No-Hair Theorem," *Phys. Rev.* **D83** (2011) 124015, `arXiv:1105.3191 [gr-qc]`.

[226] S. Chandrasekhar and S. L. Detweiler, "The quasi-normal modes of the Schwarzschild black hole," *Proc. Roy. Soc. Lond.* **A344** (1975) 441–452.

[227] K. D. Kokkotas and B. G. Schmidt, "Quasinormal modes of stars and black holes," *Living Rev. Rel.* **2** (1999) 2, `arXiv:gr-qc/9909058 [gr-qc]`.

[228] M. Elvis, C. G. Page, K. A. Pounds, M. J. Ricketts, and M. J. L. Turner, "Discovery of powerful transient X-ray source A0620-00 with Ariel V Sky Survey Experiment," *nat* **257** (Oct., 1975) 656.

[229] J. E. McClintock and R. A. Remillard, "The black hole binary A0620-00," *apj* **308** (Sept., 1986) 110–122.

[230] J. Casares and P. G. Jonker, "Mass Measurements of Stellar and Intermediate Mass Black-Holes," *Space Sci. Rev.* **183** no. 1-4, (2014) 223–252, `arXiv:1311.5118 [astro-ph.HE]`.

[231] A. G. Cantrell, C. D. Bailyn, J. A. Orosz, J. E. McClintock, R. A. Remillard, C. S. Froning, J. Neilsen, D. M. Gelino, and L. Gou, "The Inclination of the Soft X-Ray Transient A0620-00 and the Mass of its Black Hole," *apj* **710** (Feb., 2010) 1127–1141, `arXiv:1001.0261 [astro-ph.HE]`.

[232] C. E. Rhoades, Jr. and R. Ruffini, "Maximum mass of a neutron star," *Phys. Rev. Lett.* **32** (1974) 324–327.

[233] D. M. Chitre and J. B. Hartle, "Stationary configurations and the upper bound on the mass of nonrotating, causal neutron stars," *apj* **207** (July, 1976) 592–600.

[234] A. Eckart, A. Hüttemann, C. Kiefer, S. Britzen, M. Zajaček, C. Lämmerzahl, M. Stöckler, M. Valencia-S, V. Karas, and M. García-Marín, "The Milky Way's Supermassive Black Hole: How Good a Case Is It?," *Found. Phys.* **47** no. 5, (2017) 553–624, `arXiv:1703.09118 [astro-ph.HE]`.

[235] A. Eckart and R. Genzel, "Observations of stellar proper motions near the Galactic Centre," *Nature* **383** (1996) 415–417.

[236] A. Ghez, M. Morris, E. E. Becklin, T. Kremenek, and A. Tanner, "The Accelerations of stars orbiting the Milky Way's central black hole," *Nature* **407** (2000) 349, `arXiv:astro-ph/0009339 [astro-ph]`.

[237] R. Schodel *et al.*, "A Star in a 15.2 year orbit around the supermassive black hole at the center of the Milky Way," *Nature* (2002) , `arXiv:astro-ph/0210426 [astro-ph]`. [Nature419,694(2002)].

[238] A. M. Ghez *et al.*, "The first measurement of spectral lines in a short - period star bound to the galaxy's central black hole: A paradox of youth," *Astrophys. J.* **586** (2003) L127–L131, `arXiv:astro-ph/0302299 [astro-ph]`.

[239] S. Gillessen, F. Eisenhauer, S. Trippe, T. Alexander, R. Genzel, F. Martins, and T. Ott, "Monitoring stellar orbits around the Massive Black Hole in the Galactic Center," *Astrophys. J.* **692** (2009) 1075–1109, `arXiv:0810.4674 [astro-ph]`.

[240] L. Meyer, A. M. Ghez, R. Schodel, S. Yelda, A. Boehle, J. R. Lu, M. R. Morris, E. E. Becklin, and K. Matthews, "The Shortest Known Period Star Orbiting our Galaxy's Supermassive Black Hole," *Science* **338** (2012) 84–87, `arXiv:1210.1294 [astro-ph.GA]`.

[241] A. Boehle, A. M. Ghez, R. Schödel, L. Meyer, S. Yelda, S. Albers, G. D. Martinez, E. E. Becklin, T. Do, J. R. Lu, K. Matthews, M. R. Morris, B. Sitarski, and G. Witzel, "An Improved Distance and Mass Estimate for Sgr A* from a Multistar Orbit Analysis," *apj* **830** (Oct., 2016) 17, `arXiv:1607.05726`.

[242] M. Parsa, A. Eckart, B. Shahzamanian, V. Karas, M. Zajaček, J. A. Zensus, and C. Straubmeier, "Investigating the Relativistic Motion of the Stars Near the Supermassive Black Hole in the Galactic Center," *apj* **845** (Aug., 2017) 22, `arXiv:1708.03507`.

[243] S. Salim and A. Gould, "Sgr A* "visual binaries": a direct measurement of the galactocentric distance," *Astrophys. J.* **523** (1999) 633, `arXiv:astro-ph/9812292 [astro-ph]`.

[244] C. Francis and E. Anderson, "Two estimates of the distance to the Galactic Centre," *Monthly Notices of the Royal Astronomical Society* **441** (June, 2014) 1105–1114, `arXiv:1309.2629`.

[245] S. Doeleman *et al.*, "Event-horizon-scale structure in the supermassive black hole candidate at the Galactic Centre," *Nature* **455** (2008) 78, `arXiv:0809.2442 [astro-ph]`.

[246] C. M. Will, "Testing the general relativistic no-hair theorems using the Galactic center black hole SgrA*," *Astrophys. J.* **674** (2008) L25–L28, `arXiv:0711.1677 [astro-ph]`.

[247] D. Merritt, T. Alexander, S. Mikkola, and C. M. Will, "Testing Properties of the Galactic Center Black Hole Using Stellar Orbits," *Phys. Rev.* **D81** (2010) 062002, `arXiv:0911.4718 [astro-ph.GA]`.

[248] M. Grould, Z. Meliani, F. H. Vincent, P. Grandclément, and E. Gourgoulhon, "Comparing timelike geodesics around a Kerr black hole and a boson star," *Class. Quant. Grav.* **34** no. 21, (2017) 215007, `arXiv:1709.05938 [astro-ph.HE]`.

[249] GRAVITY Collaboration, Abuter, R., *et al.*, "Detection of the gravitational redshift in the orbit of the star s2 near the galactic centre massive black hole," *A&A* **615** (2018) L15. `https://doi.org/10.1051/0004-6361/201833718`.

[250] S. M. Carroll, *Spacetime and geometry: An introduction to general relativity.*
2004.
http://www.slac.stanford.edu/spires/find/books/www?cl=QC6:C37:2004.

[251] M. A. Abramowicz, W. Kluzniak, and J.-P. Lasota, "No observational proof of
the black hole event-horizon," *Astron. Astrophys.* **396** (2002) L31–L34,
arXiv:astro-ph/0207270 [astro-ph].

[252] V. Cardoso and P. Pani, " from echoes to precision gravitational-wave physics,"
arXiv:1707.03021 [gr-qc].

[253] W. Lu, P. Kumar, and R. Narayan, "Stellar disruption events support the
existence of the black hole event horizon," *Mon. Not. Roy. Astron. Soc.* **468**
no. 1, (2017) 910–919, arXiv:1703.00023 [astro-ph.HE].

[254] M. J. Rees, "Tidal disruption of stars by black holes of $10^6 - 10^8$ solar masses in
nearby galaxies," *Nature* **333** (1988) 523–528.

[255] M. Kesden, "Tidal disruption rate of stars by spinning supermassive black
holes," *Phys. Rev.* **D85** (2012) 024037, arXiv:1109.6329 [astro-ph.CO].

[256] J. Servin and M. Kesden, "Unified treatment of tidal disruption by
Schwarzschild black holes," *Phys. Rev.* **D95** no. 8, (2017) 083001,
arXiv:1611.03036 [astro-ph.HE].

[257] M. MacLeod, J. Guillochon, and E. Ramirez-Ruiz, "The tidal disruption of
giant stars and their contribution to the flaring supermassive black hole
population," *The Astrophysical Journal* **757** no. 2, (2012) 134.
http://stacks.iop.org/0004-637X/757/i=2/a=134.

[258] S. Komossa, "Tidal disruption of stars by supermassive black holes: Status of
observations," *JHEAp* **7** (2015) 148–157, arXiv:1505.01093 [astro-ph.HE].

[259] T. Padmanabhan, *Theoretical Astrophysics: Volume 2, Stars and Stellar
Systems.* Cambridge University Press, 2001.
https://books.google.it/books?id=KRD0uAEACAAJ.

[260] E. A. Magnier, E. Schlafly, D. Finkbeiner, M. Juric, J. L. Tonry, W. S. Burgett,
K. C. Chambers, H. A. Flewelling, N. Kaiser, R.-P. Kudritzki, J. S. Morgan,
P. A. Price, W. E. Sweeney, and C. W. Stubbs, "The Pan-STARRS 1
Photometric Reference Ladder, Release 12.01," *ApJ Supp.* **205** (Apr., 2013) 20,
arXiv:1303.3634 [astro-ph.IM].

[261] E. Quataert, R. Narayan, and M. Reid, "What is the accretion rate in sgr A*?,"
Astrophys. J. **517** (1999) L101, arXiv:astro-ph/9903412 [astro-ph].

[262] J. F. Hawley and S. A. Balbus, "The dynamical structure of nonradiative black
hole accretion flows," *Astrophys. J.* **573** (2002) 738, arXiv:astro-ph/0203309
[astro-ph].

[263] R. Narayan, "Black holes in astrophysics," *New J. Phys.* **7** (2005) 199,
`arXiv:gr-qc/0506078 [gr-qc]`.

[264] A. E. Broderick and R. Narayan, "On the nature of the compact dark mass at
the galactic center," *Astrophys. J.* **638** (2006) L21–L24,
`arXiv:astro-ph/0512211 [astro-ph]`.

[265] A. E. Broderick and R. Narayan, "Where are all the gravastars? Limits upon
the gravastar model from accreting black holes," *Class. Quant. Grav.* **24** (2007)
659–666, `arXiv:gr-qc/0701154 [GR-QC]`.

[266] A. E. Broderick, A. Loeb, and R. Narayan, "The Event Horizon of Sagittarius
A*," *Astrophys. J.* **701** (2009) 1357–1366, `arXiv:0903.1105 [astro-ph.HE]`.

[267] R. Narayan and J. E. McClintock, "Advection-Dominated Accretion and the
Black Hole Event Horizon," *New Astron. Rev.* **51** (2008) 733–751,
`arXiv:0803.0322 [astro-ph]`.

[268] A. E. Broderick, R. Narayan, J. Kormendy, E. S. Perlman, M. J. Rieke, and
S. S. Doeleman, "The Event Horizon of M87," *Astrophys. J.* **805** no. 2, (2015)
179, `arXiv:1503.03873 [astro-ph.HE]`.

[269] V. Cardoso and P. Pani, "Tests for the existence of horizons through
gravitational wave echoes," *Nat. Astron.* **1** (2017) 586–591, `arXiv:1709.01525`
`[gr-qc]`.

[270] M. Visser, "Physical observability of horizons," *Phys. Rev.* **D90** no. 12, (2014)
127502, `arXiv:1407.7295 [gr-qc]`.

[271] L. J. Oldham and M. W. Auger, "Galaxy structure from multiple tracers - II.
M87 from parsec to megaparsec scales," *Monthly Notices of the Royal
Astronomical Society* **457** (Mar., 2016) 421–439, `arXiv:1601.01323`.

[272] A. Zulianello, R. Carballo-Rubio, S. Liberati, and S. Ansoldi, "Electromagnetic
tests of horizonless rotating black hole mimickers," `arXiv:2005.01837 [gr-qc]`.

[273] V. Cardoso, T. Ikeda, C. J. Moore, and C.-M. Yoo, "Remarks on the maximum
luminosity," *Phys. Rev.* **D97** no. 8, (2018) 084013, `arXiv:1803.03271 [gr-qc]`.

[274] J. Eisenstaedt, "Trajectoires et impasses de la solution de Schwarzschild.,"
Archive for History of Exact Sciences **37** (1987) 275–357.

[275] J. M. Bardeen, "Timelike and null geodesics in the Kerr metric," in *Proceedings,
Ecole d'Eté de Physique Théorique: Les Astres Occlus: Les Houches, France,
August, 1972*, pp. 215–240. 1973.

[276] J.-P. Luminet, "Image of a spherical black hole with thin accretion disk,"
Astronomy & Astrophysics **75** (May, 1979) 228–235.

[277] P. V. P. Cunha, C. A. R. Herdeiro, and E. Radu, "Fundamental photon orbits:
black hole shadows and spacetime instabilities," *Phys. Rev.* **D96** no. 2, (2017)
024039, `arXiv:1705.05461 [gr-qc]`.

[278] G. Bisnovatyi-Kogan and O. Tsupko, "Gravitational Lensing in Presence of Plasma: Strong Lens Systems, Black Hole Lensing and Shadow," *Universe* **3** no. 3, (2017) 57.

[279] P. V. P. Cunha and C. A. R. Herdeiro, "Shadows and strong gravitational lensing: a brief review," *Gen. Rel. Grav.* **50** no. 4, (2018) 42, `arXiv:1801.00860 [gr-qc]`.

[280] H. Falcke, F. Melia, and E. Agol, "Viewing the shadow of the black hole at the galactic center," *Astrophys. J.* **528** (2000) L13, `arXiv:astro-ph/9912263 [astro-ph]`.

[281] F. H. Vincent, Z. Meliani, P. Grandclement, E. Gourgoulhon, and O. Straub, "Imaging a boson star at the Galactic center," *Class. Quant. Grav.* **33** no. 10, (2016) 105015, `arXiv:1510.04170 [gr-qc]`.

[282] F. Lamy, E. Gourgoulhon, T. Paumard, and F. H. Vincent, "Imaging a non-singular rotating black hole at the center of the Galaxy," *Class. Quant. Grav.* **35** no. 11, (2018) 115009, `arXiv:1802.01635 [gr-qc]`.

[283] P. V. P. Cunha, C. A. R. Herdeiro, and M. J. Rodriguez, "Does the black hole shadow probe the event horizon geometry?," *Phys. Rev.* **D97** no. 8, (2018) 084020, `arXiv:1802.02675 [gr-qc]`.

[284] R. Shaikh, P. Kocherlakota, R. Narayan, and P. S. Joshi, "Shadows of spherically symmetric black holes and naked singularities," `arXiv:1802.08060 [astro-ph.HE]`.

[285] A. Barrau, B. Bolliet, M. Schutten, and F. Vidotto, "Bouncing black holes in quantum gravity and the Fermi gamma-ray excess," *Phys. Lett.* **B772** (2017) 58–62, `arXiv:1606.08031 [gr-qc]`.

[286] F. Vidotto, "Measuring the last burst of non-singular black holes," *Found. Phys.* **48** no. 10, (2018) 1380–1392, `arXiv:1803.02755 [gr-qc]`.

[287] E. Poisson and C. Will, *Gravity: Newtonian, Post-Newtonian, Relativistic.* Cambridge University Press, 2014. `https://books.google.it/books?id=PZ5cAwAAQBAJ`.

[288] T. Binnington and E. Poisson, "Relativistic theory of tidal love numbers," *Phys. Rev. D* **80** (Oct, 2009) 084018. `https://link.aps.org/doi/10.1103/PhysRevD.80.084018`.

[289] N. Gürlebeck, "No-hair theorem for Black Holes in Astrophysical Environments," *Phys. Rev. Lett.* **114** no. 15, (2015) 151102, `arXiv:1503.03240 [gr-qc]`.

[290] V. Cardoso, E. Franzin, A. Maselli, P. Pani, and G. Raposo, "Testing strong-field gravity with tidal Love numbers," *Phys. Rev.* **D95** no. 8, (2017) 084014, `arXiv:1701.01116 [gr-qc]`. [Addendum: Phys. Rev.D95,no.8,089901(2017)].

[291] J. B. Hartle, "Tidal friction in slowly rotating black holes," *Phys. Rev. D* **8** (Aug, 1973) 1010–1024. https://link.aps.org/doi/10.1103/PhysRevD.8.1010.

[292] S. A. Hughes, "Evolution of circular, nonequatorial orbits of kerr black holes due to gravitational-wave emission. ii. inspiral trajectories and gravitational waveforms," *Phys. Rev. D* **64** (Aug, 2001) 064004. https://link.aps.org/doi/10.1103/PhysRevD.64.064004.

[293] A. Maselli, P. Pani, V. Cardoso, T. Abdelsalhin, L. Gualtieri, and V. Ferrari, "Probing planckian corrections at the horizon scale with lisa binaries," *Phys. Rev. Lett.* **120** (Feb, 2018) 081101. https://link.aps.org/doi/10.1103/PhysRevLett.120.081101.

[294] N. K. Johnson-Mcdaniel, A. Mukherjee, R. Kashyap, P. Ajith, W. Del Pozzo, and S. Vitale, "Constraining black hole mimickers with gravitational wave observations," arXiv:1804.08026 [gr-qc].

[295] S. L. Liebling, M. Lippert, and M. Kavic, "Probing Near-Horizon Fluctuations with Black Hole Binary Mergers," *JHEP* **03** (2018) 176, arXiv:1707.02299 [gr-qc].

[296] M. A. Abramowicz, T. Bulik, G. F. R. Ellis, K. A. Meissner, and M. Wielgus, "The electromagnetic afterglows of gravitational waves as a test for Quantum Gravity," arXiv:1603.07830 [gr-qc].

[297] T. Vachaspati, "Gravitational Waves, Gamma Ray Bursts, and Black Stars," *Int. J. Mod. Phys.* **D25** no. 12, (2016) 1644025, arXiv:1611.03853 [gr-qc].

[298] E. Maggio, L. Buoninfante, A. Mazumdar, and P. Pani, "How does a dark compact object ringdown?," arXiv:2006.14628 [gr-qc].

[299] V. Cardoso, S. Hopper, C. F. B. Macedo, C. Palenzuela, and P. Pani, "Gravitational-wave signatures of exotic compact objects and of quantum corrections at the horizon scale," *Phys. Rev.* **D94** no. 8, (2016) 084031, arXiv:1608.08637 [gr-qc].

[300] Z. Mark, A. Zimmerman, S. M. Du, and Y. Chen, "A recipe for echoes from exotic compact objects," *Phys. Rev.* **D96** no. 8, (2017) 084002, arXiv:1706.06155 [gr-qc].

[301] M. R. Correia and V. Cardoso, "Characterization of echoes: A Dyson-series representation of individual pulses," *Phys. Rev.* **D97** no. 8, (2018) 084030, arXiv:1802.07735 [gr-qc].

[302] A. Testa and P. Pani, "Analytical template for gravitational-wave echoes: signal characterization and prospects of detection with current and future interferometers," *Phys. Rev.* **D98** no. 4, (2018) 044018, arXiv:1806.04253 [gr-qc].

[303] C. P. Burgess, R. Plestid, and M. Rummel, "Effective Field Theory of Black Hole Echoes," arXiv:1808.00847 [gr-qc].

[304] B. Holdom and J. Ren, "Not quite a black hole," *Phys. Rev.* **D95** no. 8, (2017) 084034, arXiv:1612.04889 [gr-qc].

[305] Q. Wang and N. Afshordi, "Black hole echology: The observer's manual," *Phys. Rev.* **D97** no. 12, (2018) 124044, arXiv:1803.02845 [gr-qc].

[306] C. Cutler and K. S. Thorne, "An Overview of gravitational wave sources," in *Proceedings, 16th International Conference on General Relativity and Gravitation: Durban, South Africa, July 15-21, 2001*, pp. 72–111. 2013. arXiv:gr-qc/0204090 [gr-qc].

[307] N. Oshita and N. Afshordi, "Probing microstructure of black hole spacetimes with gravitational wave echoes," arXiv:1807.10287 [gr-qc].

[308] S. M. Du and Y. Chen, "Searching for near-horizon quantum structures in the binary black-hole stochastic gravitational-wave background," *Phys. Rev. Lett.* **121** no. 5, (2018) 051105, arXiv:1803.10947 [gr-qc].

[309] E. Barausse, R. Brito, V. Cardoso, I. Dvorkin, and P. Pani, "The stochastic gravitational-wave background in the absence of horizons," arXiv:1805.08229 [gr-qc].

[310] C. Barceló, R. Carballo-Rubio, and L. J. Garay, "Gravitational wave echoes from macroscopic quantum gravity effects," *JHEP* **05** (2017) 054, arXiv:1701.09156 [gr-qc].

[311] J. Abedi, H. Dykaar, and N. Afshordi, "Echoes from the Abyss: Tentative evidence for Planck-scale structure at black hole horizons," *Phys. Rev.* **D96** no. 8, (2017) 082004, arXiv:1612.00266 [gr-qc].

[312] J. Abedi, H. Dykaar, and N. Afshordi, "Echoes from the Abyss: The Holiday Edition!," arXiv:1701.03485 [gr-qc].

[313] G. Ashton, O. Birnholtz, M. Cabero, C. Capano, T. Dent, B. Krishnan, G. D. Meadors, A. B. Nielsen, A. Nitz, and J. Westerweck, "Comments on: "Echoes from the abyss: Evidence for Planck-scale structure at black hole horizons"," *arXiv* **1612.05625** (2016) .

[314] J. Westerweck, A. Nielsen, O. Fischer-Birnholtz, M. Cabero, C. Capano, T. Dent, B. Krishnan, G. Meadors, and A. H. Nitz, "Low significance of evidence for black hole echoes in gravitational wave data," *Phys. Rev.* **D97** no. 12, (2018) 124037, arXiv:1712.09966 [gr-qc].

[315] R. S. Conklin, B. Holdom, and J. Ren, "Gravitational wave echoes through new windows," *Phys. Rev.* **D98** no. 4, (2018) 044021, arXiv:1712.06517 [gr-qc].

[316] J. Abedi, H. Dykaar, and N. Afshordi, "Comment on: "Low significance of evidence for black hole echoes in gravitational wave data"," `arXiv:1803.08565 [gr-qc]`.

[317] J. Abedi and N. Afshordi, "Echoes from the Abyss: A highly spinning black hole remnant for the binary neutron star merger GW170817," `arXiv:1803.10454 [gr-qc]`.

[318] P. Pani and V. Ferrari, "On gravitational-wave echoes from neutron-star binary coalescences," *Class. Quant. Grav.* **35** (2018) 15, `arXiv:1804.01444 [gr-qc]`.

[319] S. D. Mathur, "Spacetime has a 'thickness'," *Int. J. Mod. Phys.* **D26** no. 12, (2017) 1742002, `arXiv:1705.06407 [hep-th]`.

[320] E. Maggio, P. Pani, and V. Ferrari, "Exotic Compact Objects and How to Quench their Ergoregion Instability," *Phys. Rev. D* **96** no. 10, (2017) 104047, `arXiv:1703.03696 [gr-qc]`.

[321] E. Maggio, V. Cardoso, S. R. Dolan, and P. Pani, "Ergoregion instability of exotic compact objects: electromagnetic and gravitational perturbations and the role of absorption," *Phys. Rev. D* **99** no. 6, (2019) 064007, `arXiv:1807.08840 [gr-qc]`.

[322] H. Yang, A. Zimmerman, and L. Lehner, "Turbulent Black Holes," *Phys. Rev. Lett.* **114** (2015) 081101, `arXiv:1402.4859 [gr-qc]`.

[323] J. M. Henn and J. C. Plefka, "Scattering Amplitudes in Gauge Theories," *Lect. Notes Phys.* **883** (2014) pp.1–195.

[324] D. J. Burger, R. Carballo-Rubio, N. Moynihan, J. Murugan, and A. Weltman, "Amplitudes for astrophysicists: known knowns," *Gen. Rel. Grav.* **50** no. 12, (2018) 156, `arXiv:1704.05067 [astro-ph.HE]`.

[325] E. Alesci and L. Modesto, "Particle Creation by Loop Black Holes," *Gen. Rel. Grav.* **46** (2014) 1656, `arXiv:1101.5792 [gr-qc]`.

[326] A. Fabbri, D. J. Navarro, and J. Navarro-Salas, "Evaporation of near extremal Reissner-Nordstrom black holes," *Phys. Rev. Lett.* **85** (2000) 2434–2437, `arXiv:hep-th/0004027`.

[327] V. P. Frolov and A. Zelnikov, "Quantum radiation from an evaporating nonsingular black hole," *Phys. Rev.* **D95** no. 12, (2017) 124028, `arXiv:1704.03043 [hep-th]`.

[328] C. Barceló, S. Liberati, S. Sonego, and M. Visser, "Minimal conditions for the existence of a Hawking-like flux," *Phys. Rev. D* **83** (2011) 041501, `arXiv:1011.5593 [gr-qc]`.

[329] C. Barceló, S. Liberati, S. Sonego, and M. Visser, "Hawking-like radiation from evolving black holes and compact horizonless objects," *JHEP* **02** (2011) 003, `arXiv:1011.5911 [gr-qc]`.

[330] K. Falls and D. F. Litim, "Black hole thermodynamics under the microscope,"
Phys. Rev. D **89** (2014) 084002, arXiv:1212.1821 [gr-qc].